

The role of bacterial microcompartments  
in *Listeria monocytogenes* growth,  
stress adaptation and virulence

Zhe Zeng

## PROPOSITIONS

1. Linking microcompartment-dependent ethanolamine metabolism to extracellular electron transfer enhances flux through the oxidative branch enabling higher ATP and biomass production. (this thesis)
2. Toxic aldehydes are compartmentalized to support growth and survival of the foodborne pathogen *Listeria monocytogenes*. (this thesis)
3. Scientific breakthroughs require communication of breakthrough quality to outside academia.
4. An entrepreneurial mindset facilitates finalization of a PhD project within the set four years.
5. Cultural differences are shown more prominently in how to face death than in how to face life.
6. Studying abroad will stimulate one's unexpected nostalgic spirit.

Propositions belonging to the thesis, entitled:

The role of bacterial microcompartments in *Listeria monocytogenes* growth, stress adaptation and virulence

Zhe Zeng

Wageningen, 14 December 2021



The role of bacterial microcompartments in *Listeria monocytogenes* growth, stress adaptation and virulence

Zhe Zeng

## **Thesis committee**

### **Promotors**

Prof. Dr T. Abee

Personal chair at the Laboratory of Food Microbiology  
Wageningen University & Research

Prof. Dr E. J. Smid

Personal chair at the Laboratory of Food Microbiology  
Wageningen University & Research

### **Co-promotor**

Dr R. A. Notebaart

Associate professor at the Laboratory of Food Microbiology  
Wageningen University & Research

### **Other members**

Prof. Dr H. Smidt, Wageningen University & Research

Prof. Dr C. Gahan, University College Cork, Ireland

Dr M. H. J. Wells-Bennik, NIZO Food Research, Ede, The Netherlands

Dr A. M. López Contreras, Wageningen University & Research

This research was conducted under the auspices of the Graduate School VLAG  
(Advanced studies in Food Technology, Agrobiotechnology, Nutrition and Health Sciences)

The role of bacterial microcompartments in *Listeria monocytogenes* growth, stress adaptation and virulence

Zhe Zeng

**Thesis**

submitted in fulfilment of the requirements for the degree of doctor  
at Wageningen University  
by the authority of the Rector Magnificus,  
Prof. Dr A.P.J. Mol,  
in the presence of the  
Thesis Committee appointed by the Academic Board  
to be defended in public  
on Tuesday 14 December 2021  
at 1.30 p.m. in the Aula.

**Zhe Zeng**

The role of bacterial microcompartments in *Listeria monocytogenes* growth,  
stress adaptation and virulence

238 pages

PhD thesis, Wageningen University, Wageningen, Netherlands (2021)

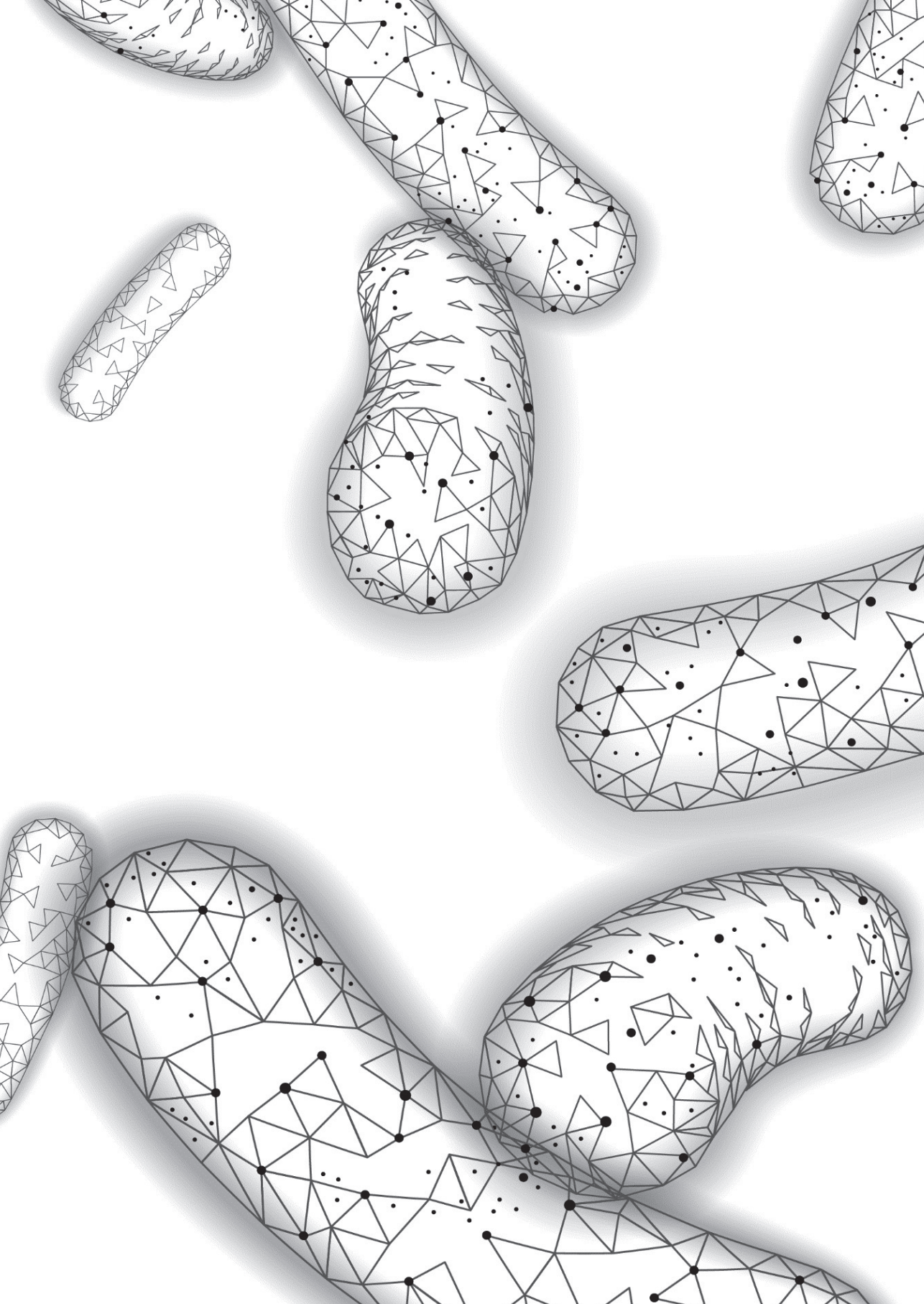
With references, with summary in English

ISBN: 978-94-6395-844-8

DOI: <https://doi.org/10.18174/555299>

# Table of contents

<b>Chapter 1</b>	General introduction	<b>7</b>
<b>Chapter 2</b>	Bacterial microcompartment-dependent 1,2-propanediol utilization stimulates anaerobic growth of <i>Listeria monocytogenes</i> EGDe	<b>35</b>
<b>Chapter 3</b>	Anaerobic growth of <i>Listeria monocytogenes</i> on rhamnose is stimulated by Vitamin B12 and bacterial microcompartment dependent 1,2-propanediol utilization	<b>65</b>
<b>Chapter 4</b>	Bacterial microcompartments coupled with extracellular electron transfer drive the anaerobic utilization of ethanolamine in <i>Listeria monocytogenes</i>	<b>91</b>
<b>Chapter 5</b>	Impact of vitamin B12 on rhamnose metabolism, stress defense and <i>in vitro</i> virulence of <i>Listeria monocytogenes</i>	<b>121</b>
<b>Chapter 6</b>	Impact of bacterial microcompartment-dependent ethanolamine and propanediol metabolism on <i>Listeria monocytogenes</i> interactions with Caco-2 cells	<b>147</b>
<b>Chapter 7</b>	Bacterial microcompartment-dependent 1,2-propanediol utilization of <i>Propionibacterium freudenreichii</i>	<b>183</b>
<b>Chapter 8</b>	General discussion	<b>203</b>
<b>Appendix</b>	Summary Acknowledgements About the author Affiliation of co-authors List of publications Overview of completed training activities	<b>225</b>



# 1

---

## General Introduction

Part of this chapter was submitted for publication:

**Zeng, Z.<sup>#</sup>**, Dank, A<sup>#</sup>, Smid, E. J., Notebaart, R. A., & Abee, T. Bacterial microcompartments in food-related microbes, *Current Opinion in Food Science* (Accepted for publication)

### General Introduction

*Listeria monocytogenes* is a Gram positive foodborne pathogen capable of causing a human infection called listeriosis [1]. Pregnant women, the elderly or individuals with a weakened immune system, are at greatest risk of severe listeriosis and should avoid high risk foods [2, 3]. The foodborne pathogen *L. monocytogenes* has the capacity to grow and survive in a diverse range of natural environments (e.g. soil, water, decaying vegetation and food environment) [4, 5]. The transition of *L. monocytogenes* from foods to the human gastrointestinal (GI) tract, may trigger adaptive responses that support subsequent invasive systemic infections [1, 6]. In recent years it has become clear that so-called Bacterial Microcompartments (BMCs) play a crucial role in the utilization of specific host-derived substrates that result from degradation of phospholipids and metabolism of mucus-derived saccharides, including ethanolamine and 1,2-propanediol. Notably, these compounds are also encountered in a wide range of food products [7-10], and could therefore also contribute to transmission of pathogens to the host [7]. It has been suggested that BMCs also play a role in *L. monocytogenes* ecophysiology and pathogenicity [1, 7, 10-16], but experimental evidence supporting these claims are very scarce. In the following sections, *L. monocytogenes* physiology and virulence determinants will be introduced as well as the composition and functionality of BMC-dependent substrate utilization in context of *L. monocytogenes* physiology. Finally, an outline will be given of the topics addressed in the different research chapters, including a general discussion that summarizes novel insights obtained in *L. monocytogenes* BMCs and perspectives for future research.

### 1.1 The physiology and virulence of *Listeria monocytogenes*

#### 1.1.1 *L. monocytogenes* physiology

*L. monocytogenes* is a Gram positive, non-sporulating, facultative anaerobic foodborne pathogen. *L. monocytogenes* has been discovered in 1926 during an outbreak that affected rabbits and guinea pigs [1, 17]. It was recognized as a food-borne pathogen in the 1980's [1, 17]. Although the number of listeriosis infections per year is moderately low (approximately 23,150 cases were estimated worldwide in 2010), the mortality among elderly, young, pregnant, immunocompromised individuals is very high (20-30%) [1, 3]. Upon ingestion of highly contaminated food (up to  $\sim 10^9$  bacteria), most individuals experience mild to severe gastroenteritis [1, 3]. By contrast, for children, elderly individuals,

immunocompromised individuals and pregnant women, even low levels of food contamination ( $\sim 10^2$ – $10^4$  bacteria) can cause bacterial sepsis, subsequent bacterial meningitis and/or infection of the fetus, resulting in abortion or complications to pregnancy [1, 3].

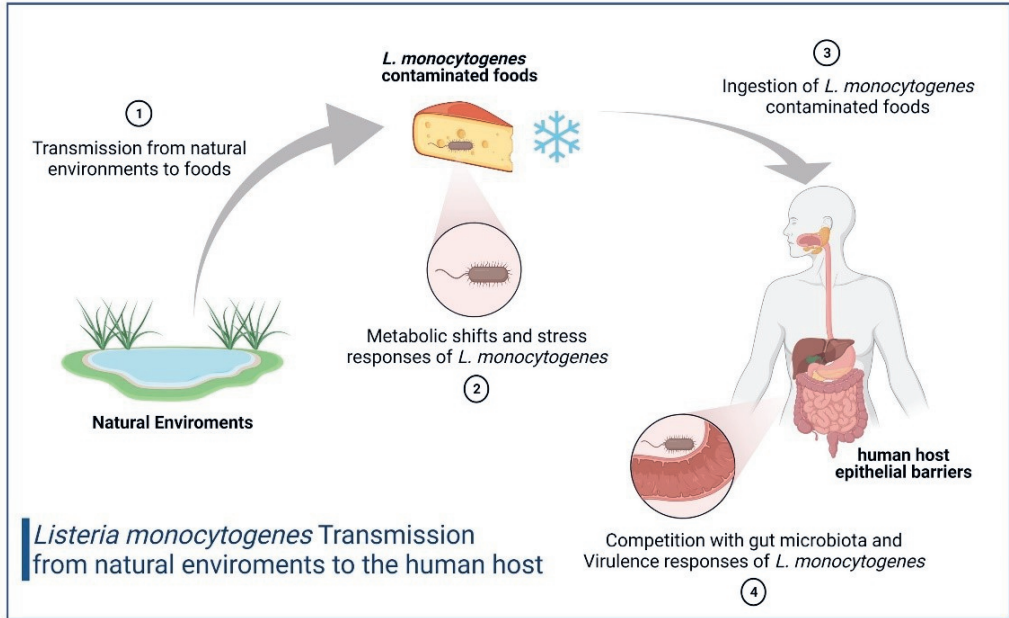


**Figure 1.1 Scheme of *Listeria monocytogenes* transmission from natural environments to the human host.** *L. monocytogenes* is ubiquitous in natural environments. The transmission of *L. monocytogenes* from natural environments to food production facilities and foods can result in contamination with *L. monocytogenes* causing food safety issues. Metabolic versatility and adaptive stress response of *L. monocytogenes* may contribute to the competitive fitness and survival of this pathogen outside and inside the host, in a range of stress conditions, such as low temperature, low pH and nutrient limitation. After the ingestion of high doses of *L. monocytogenes* via contaminated foods, and following stomach passage, it may adhere and subsequently invade intestinal epithelial barrier in immune-compromised hosts and cause listeriosis following transfer to other organs including the brain.

*L. monocytogenes* is well-known for its ability to grow at low temperatures including a range of foods stored at refrigeration temperature, offering a challenge for food manufacturers. *L. monocytogenes* has been shown to grow at temperatures ranging from  $-0.4$  to  $45^{\circ}\text{C}$  [18]. While *L. monocytogenes* has been reported to survive and even duplicate at temperatures as low as  $-0.4^{\circ}\text{C}$ , *L. monocytogenes* growth at temperatures below  $4^{\circ}\text{C}$  is generally quite slow (usually with doubling times of at least 12 h) [18, 19]. Cold stress adaptation mechanisms [15, 18], such as the activation of general stress sigma factor SigB and stress

defence proteins including heat and cold shock proteins, are therefore an important attribute of *L. monocytogenes*, enabling this food pathogen to survive and proliferate in refrigerated foods, including ready-to-eat (RTE) foods [2], such as deli meats, smoked fish, and milk. Additionally, composition of foods including availability of nutrients and storage under modified atmosphere or under vacuum, i.e., in absence of oxygen, can affect growth performance of *L. monocytogenes*. Noteworthy, one of the factors that attenuated growth of *L. monocytogenes* at low temperatures was identified as *eutV*, that together with *eutW*, constitutes a so-called two-component sensor-regulator system, involved in the activation of the ethanolamine utilization (*eut*) gene cluster [15], which aligned with a recent study that reported increased expression of 17 genes of the *eut* operon in *L. monocytogenes* grown at 4°C [20]. The *eut* operon encodes one of the different types of Bacterial Microcompartment-dependent metabolic pathways [21], that is reported to contribute also to *L. monocytogenes* virulence, and both aspects are discussed in more detail in the next sections.

### 1.1.2 *L. monocytogenes* virulence

*L. monocytogenes* has evolved various mechanisms for carbon source utilization, stress adaptation and virulence factors that allow for transmission from the food environment to the human GI tract. The mechanisms of carbon sources utilization and stress adaptation discovered in this bacterium include numerous catabolic enzymes, transporter systems and gene expression regulating proteins [1, 6, 12, 22, 23]. Activation of *L. monocytogenes* virulence factors is primarily regulated via transcription regulator PrfA (positive regulatory factor A) [1, 3, 24]. The activity of PrfA is modulated by selected environmental signals at the transcriptional and post-transcriptional level, including temperature and the availability of efficiently metabolizable carbon sources [1, 24]. For example glycerol and lactose, resulted in differential activation of SigB and stress resistance in *L. monocytogenes* [25]. PrfA expression is also controlled through stress response regulatory proteins such as Sigma B [24, 26]. Therefore, the impact of carbon source utilization on stress resistance activation and virulence of *L. monocytogenes* deserves more detailed analysis.

*L. monocytogenes* is a well-studied model for intracellular infection [1, 3]. *L. monocytogenes* binds to epithelial host cells and promotes invasion in a process mediated by InlA (Internalin A) [1, 27-29] and InlB (Internalin B) [26, 28, 29], but also other factors have been reported to contribute to the process, including Listeria Adhesion Protein (LAP) [1, 30, 31] and other host cell surface modulation

interactions [1, 3]. Next steps in *L. monocytogenes* infection include activation of Listeriolysin O (LLO) [1, 32-34], phospholipase A (PlcA) [1, 35], phospholipase B (PlcB) [1, 36, 37] and actin assembly-inducing protein (ActA) [38, 39]. LLO, together with PlcA and PlcB and possibly ActA promote vacuolar rupture and bacterial escape to the cytoplasm [1, 3]. LLO can also lead to changes in histone modification, desumoylation, mitochondrial fission, endoplasmic reticulum stress and lysosomal permeabilization, all of which apparently linked to its pore-forming activity [1, 32-34]. ActA induces actin polymerization and generates actin comet tails that propel *L. monocytogenes* within the cytoplasm and within membrane protrusions into neighbouring cells via InlC (Internalin C) [1, 36, 40, 41]. There, bacteria localize in a double membrane vacuole, which can be lysed by LLO, PlcA, PlcB and possibly ActA to start a new infection cycle (Figure 1.2) [1].

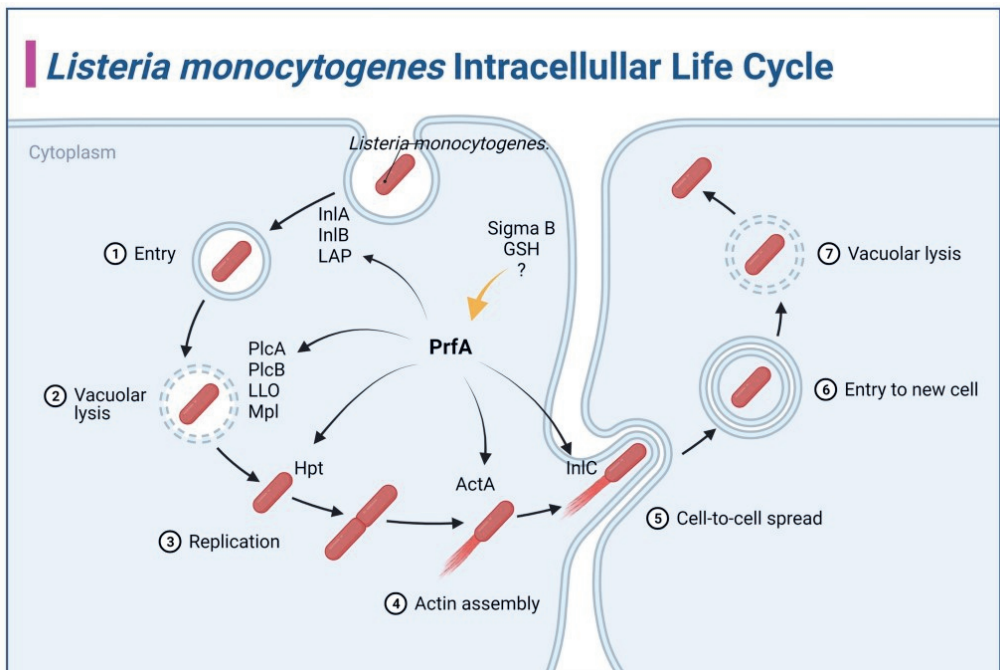


**Figure 1.2. *Listeria monocytogenes* Intracellular Life Cycle and PrfA-mediated regulation.**

(Adapted from D.A. Portnoy [42] and P. Cossart [1]) PrfA (positive regulatory factor A), host cell invasion (internalin InlA and InlB), phagosome lysis: listeriolysin O (LLO), phospholipase A (PlcA), phospholipase B (PlcB) and cell-to-cell spread (actin assembly-inducing protein (ActA), intracellular growth (hexose-6-phosphate supplied by transporter, Hpt), cell-to-cell spread (internalin InlC), and Glutathione (GSH). See text for details

PrfA, a regulatory protein, senses a number of environmental signals and upon activation it triggers a set of key virulence factors during host infection [24, 43]. An

additional set of genes (~145) has been identified that were reported to be regulated by PrfA based on transcriptome profiling [43-45]. PrfA-dependent genes are repressed by some sugars transported through the phosphoenolpyruvate-sugar phosphotransferase system (PTS) [24], such as glucose [44], which indicate that non-PTS carbon sources may not repress the expression of PrfA-dependent genes. Transcriptome profiling experiments with  $\Delta sigB$  and  $\Delta prfA$  mutants suggest regulatory overlap between the stress response mediated by Sigma B and virulence transcriptional networks [1, 24, 26]. Furthermore, *in vitro* studies suggest that PrfA activation is tightly linked to intracellular levels of GSH (Glutathione), as a glutathione synthase mutant ( $\Delta gshF$ ) is activated by exogenous GSH, but not by other reducing agents [46, 47]. These data point to a range of signals that regulate the activation of PrfA, conceivably to optimize signal integration in *L. monocytogenes* to finetune activation of its virulence repertoire in selected environmental conditions. In recent years it has become apparent that so-called Bacterial Microcompartments play a crucial role in specific substrate utilization pathways in *L. monocytogenes* including metabolism of host-derived phospholipid and mucus degradation products [11, 15, 16, 20], and it has been suggested that these BMCs play a role in *L. monocytogenes* transmission in foods and competitive fitness in the human intestine [7, 10].

## 1.2 Bacterial Microcompartments

Bacterial microcompartments (BMCs) are self-assembling organelles that consist of an enzymatic core that is encapsulated by a selectively permeable protein shell [48, 49]. BMCs encasing specific metabolic pathways that involve transient production of toxic volatile metabolites such as aldehydes, are referred to as metabolosomes [48, 49]. Bioinformatics analysis [50, 51] predicted the presence of BMCs in 23 bacterial phyla, and gene clusters for the utilization of host-derived substrates such as 1,2-propanediol and ethanolamine were identified in *L. monocytogenes* [48, 49].

### 1.2.1 Shell Proteins of BMCs

BMCs are typically about 40-200 nm in diameter and are made of three types of shell proteins: hexamers (BMC-H), pseudohexamers (BMC-T), and pentamers (BMC-P) [52-54]. Hexamers and pseudohexamers are formed by the classical BMC shell proteins containing the Pf00936 domain, while pentamers are formed by the non-classical BMC shell proteins containing the Pf03319 domain [50, 55].

Whereas BMC-H and BMC-T proteins constitute the facets of the shells, pentameric proteins are required to cap the vertices of the polyhedral shell in Figure 1.3 [52-54, 56]. This role is served by the third conserved building block, the BMC-P proteins, which contain a single Pfam03319 domain and assemble into cyclical pentamers [52-54, 56]. As icosahedra have only 12 vertices, regardless of their size, the BMC-P proteins are minor components and yet are essential to the diffusive barrier provided by a completely closed shell [52, 54]. These shell proteins are highly conserved across different bacterial phyla allowing accurate bioinformatics analysis-based prediction of BMCs and associated functions of encapsulated enzymes [50, 51, 55].

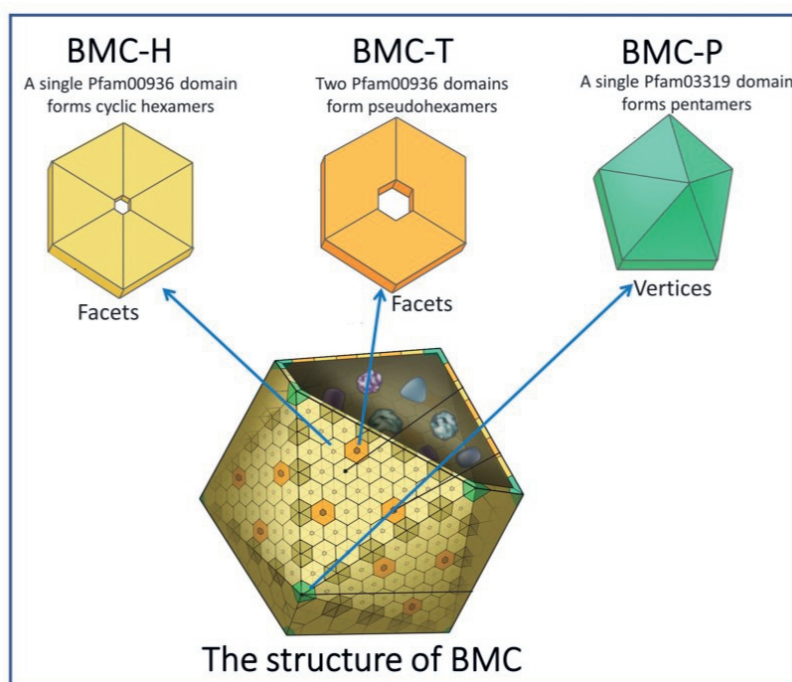


**Figure 1.3 Structures of BMC and BMC shell proteins.** (Adapted from Thom Graves and Cheryl A. Kerfeld [48]) These hexagon-shape (BMC-H and BMC-T) or pentagon-shape (BMC-P) components constitute the icosahedron-shape BMC. The hexagon-shape has a central pore that allows substrates in and products out.

The structure of an intact shell composed of five different proteins from *Haliangium ochraceum* provided atomic resolution detail of the protein-protein interactions  $\sim 400$  Å in diameter[52]. And the protein shell is formed by 540 individual protein chains, constituting a mass of about 6.5 MDa [52]. More recent studies unveiled that the structural variations of BMCs and flexible protein-protein

interactions may enable fine tuning of BMC assembly and shell permeability in response to a varying environment (Reviewed by Lu-Ning Liu et. al [54]). The absence of specific building blocks could also result in BMC structural remodeling, such as the elongated BMCs which lack BMC-P at the vertices [57]. In the *pdu* BMC, deleting the major shell protein PduA resulted in an increased content of the shell protein PduJ and altered metabolic activity [58]. These studies pointed to opportunities for bioengineering of BMCs. Taking advantage of the self-assembly process, BMC shells can be generated by expressing the shell proteins without the cargo proteins [59, 60], and thus be used for “bottom up” approaches to construct synthetic BMCs carrying out novel functions [48, 49, 60]. There are many potential applications for engineered BMCs, including serving as nano-factories to increase metabolic efficiency for synthetic biology or as novel nanoparticles to serve as drug-delivery systems and platforms for designer vaccines [48, 49, 60, 61]. However, novel methods need to be developed that enable the modification of every aspect of the shell, like loading heterologous cargo, engineering the permeability of the pores, and controlling the assembly process [60].

### 1.2.2 The Distribution of BMCs

Recent bioinformatic analysis predicted 23 types of BMC genetic loci, which are present in up to 80% of the bacterial phyla [50]. The greatest diversity of BMC locus types is in the Firmicutes and Gammaproteobacteria [50]. Many of these (sub)types also appear in distantly related phyla which suggests that BMC loci are frequently horizontally transferred [62]. Following the BMC LoClass algorithm [50] to search in Uniprot proteomes database, we unveil a large BMC functional diversity in certain phyla, such as Proteobacteria, Actinobacteria, and Firmicutes (Figure 1.4), reflecting the importance of metabolic flexibility across disparate niches. As shown in Figure 1.4, selected BMCs include previously known ones for the utilization of ethanolamine (EUT BMC), 1,2-propanediol (PDU BMC), choline (GRM BMC), fucose/rhamnose (PVM BMC) and other variants (mainly for the utilization of amino alcohols). Experimental evidence of visual BMC structures aligned with bioinformatics analysis of BMCs has been reported for a number of species including *Salmonella enterica* Serovar Typhimurium, *Escherichia coli*, *Enterococcus faecalis* and *Clostridium* spp., that concerned utilization of ethanolamine and 1,2-propanediol, while for *E. coli* and *Klebsiella pneumoniae* utilization of choline and for *Clostridium* spp. utilization of fucose/rhamnose was studied [7, 48, 49, 63-67]. More recently, comparative genome analysis revealed BMC-dependent metabolic pathways in the uncultured human gut microbiome

[68], which suggests that BMCs play a significant role in uncultured organisms of the human gut microbiome, next to their reported role in enteric pathogens.

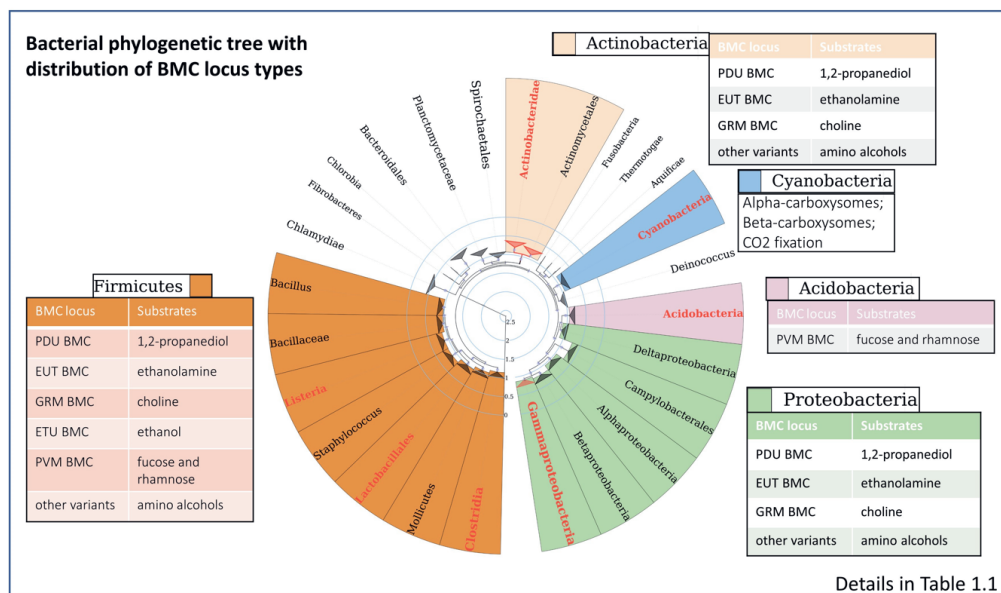


**Figure 1.4 Bacterial phylogenetic tree with distribution of BMC locus types** (based on UniProt reference proteomes database). Bacterial phylogenetic tree was based on Christian Rinke et al. [69] and adapted via online server iTOL [70] by Zhe Zeng. Bacteria phylum with predicted BMCs and published experimental evidences in the same phylum are presented with different colours: Orange represents Firmicutes with predicted types of BMCs attached in chart, Green represents Proteobacteria with predicted types of BMCs attached in chart, Pink represents Acidobacteria with predicted types of BMCs attached in chart, Blue represents Cyanobacteria with carboxysomes loci, Light green represents Actinobacteria with predicted types of BMCs attached in chart. See details of selected species in Table 1.1 in Supplementary Materials, page 16).

### 1.2.3 BMC-dependent 1,2-Propanediol and Ethanolamine Metabolism

1,2-propanediol and ethanolamine are the most widely distributed substrates being metabolized in BMCs [7, 48, 49, 54, 71-74]. The ability to utilize 1,2-propanediol and ethanolamine, and possible impacts on pathogenicity, has been widely studied in enteric pathogens such as *Salmonella enterica* Serovar Typhimurium, Enterohaemorrhagic *E. coli*, *Citrobacter rodentium*, *Clostridium difficile* and *Yersinia enterocolitica* [7].

Notably, 1,2-propanediol is present in foods, as it is used as a food additive in biscuits, cakes and flavored drinks [9]. And 1,2-propanediol is also abundant in the human GI tract where it is derived from anaerobic degradation of rhamnose

or fucose by the human intestinal microbiota [7], including *Bacteroides thetaiotamicron* [75], *Anaerostipes rhamnosivorans* [76], *Bifidobacterium longum* [77] and mucus-colonizing *Akkermansia mucinophila* [78]. The BMC-dependent utilization of 1,2-propanediol (*pdu*) in *S. enterica* includes 23 genes: *pocR*, *pduF*, *pdu*ABCDEFGHIJKLMNOQSTUVWX [57, 79]. Metabolism of 1,2-propanediol starts with the conversion of 1,2-propanediol to propionaldehyde by vitamin B12-dependent diol dehydratase PduCDE [79-81]. The toxic propionaldehyde is then converted to propionate by the enzyme CoA-dependent propionaldehyde dehydrogenase PduP, followed by action of phosphate propanoyltransferase PduL, and propionate kinase PduW located in the cytoplasm, resulting in the end product propionate and the production of ATP. The other end product is produced following conversion of propionaldehyde by propanol dehydrogenase PduQ into 1-propanol. PduQ is thought to be inside BMCs because of the potential association with PduP [82]. The diol dehydratase reactivase PduGH, corrinoid adenosyltransferase PduO and cobalamin reductase PduS are linked to the supply and recycling of vitamin B12. The shell proteins PduTUABKJMN form the hexamer and pentamer building units of the icosahedron shaped BMCs for 1,2-propanediol catabolism shielding the cell constituents against toxicity of the volatile intermediate propionaldehyde and supporting efficient recycling of the CoA cofactor pool [7, 48, 49, 74]. In *Salmonella*, PocR is a transcription factor that is activated by 1,2-propanediol, and subsequently activates expression of the *pdu* operon. In *L. monocytogenes* a vitamin B12-binding riboswitch was identified to control the activation of PocR and the *pdu* operon [83].

Ethanolamine, a product of the breakdown of phosphatidylethanolamine from bacterial and eukaryotic cell membranes, is abundant in the human GI tract [21, 84]. Lipid rich foods such as egg yolk and milk including human milk contain large amounts of phosphatidylethanolamine [7]. It has been shown that some species in the GI tract like *S. enterica*, *E. faecalis*, *C. perfringens* can use ethanolamine as carbon source while for some other human pathogens including *L. monocytogenes*, the putative use of ethanolamine as a substrate was postulated based on the presence of a similar gene cluster [21, 84, 85]. The capability to utilize ethanolamine is encoded by the ethanolamine utilization (*eut*) operon [21, 85, 86]. Ethanolamine is converted to acetaldehyde and ammonia by ethanolamine ammonia lyase EutBC [21, 87, 88]. Acetaldehyde can be catabolized to ethanol by the alcohol dehydrogenase EutG [86] or to acetyl-CoA, by acetaldehyde dehydrogenase EutE [21, 89]. Acetyl-CoA can be degraded to

acetate with ATP production by the phosphotransacetylase EutD [90] and an alternative acetate kinase EutQ [91]. Alternatively, acetyl-CoA can be catabolized in the tricarboxylic acid cycle or the glyoxylate cycle, or used for lipid biosynthesis [21]. The regulation of *eut* gene expression is a bit diverse and can be classified into three characterized systems [21]: (A) EutR regulator in *S. Typhimurium* [92], (B) EutV/W two component regulators in *E. faecalis* and *L. monocytogenes* [93, 94], (C) EatR regulator in *P. aeruginosa* [95]. Furthermore, a vitamin B12-binding riboswitch was identified to control the activation of EutV/W regulators and the *eut* operon [94]. Overall, there is a global association of GI pathogens with BMC-dependent ethanolamine utilization, including a diversity of pathogens including *Salmonella enterica*, enterohemorrhagic *E. coli*, *E. faecalis*, *Clostridium perfringens* and *L. monocytogenes* [21, 86, 89, 96-98]. As mentioned, the GI tract provides a rich source of ethanolamine; ethanolamine concentrations over 2 mM were measured from bovine intestinal content [99], which confer a growth benefit for the bacteria capable of ethanolamine utilization and conceivably affects pathogen virulence, but underlying molecular mechanisms remain to be characterized in more detail [21, 84].

### 1.3 Implications of BMC-dependent Metabolism to *Listeria monocytogenes*

A number of studies showed that BMC-dependent metabolism contributes to the survival of foodborne pathogens in food and food production environments [7, 10, 21, 48], but functional characterizations of the *Listeria monocytogenes* BMC-dependent 1,2-propanediol and ethanolamine metabolism has not been reported up to now. Previous RNAseq studies on *L. monocytogenes* grown on vacuum-packed cold smoked salmon showed increased expression of the *pdu* and *eut* genes [11], conceivably supporting utilization of 1,2-propanediol and ethanolamine and growth in this product [12]. *L. monocytogenes* also increased expression of the *pdu* gene cluster in co-culture biofilms with *Bacillus subtilis* as well as in co-culture with *Brevibacterium* spp. isolated from cheese [100, 101]. *L. monocytogenes* is most likely scavenging the environment for alternative nutrients supporting its establishment in respective niches, that may benefit from co-microbiota activity including lipases and glycosidases that degrade polysaccharides [10]. Another study found that at 4°C *L. monocytogenes* increased expression of 17 genes of the *eut* pathway, while in contrast, many of the *pdu* genes and almost the entire operon for *de novo* synthesis of cobalamin was downregulated [20]. Another study showed that

deletion of *eutV*, one of the two-component regulators of the *eut* operon, also showed reduced growth at 4°C [15]. Furthermore, a study of the regulators of *pdu/eut* found that *pocR* and *eutV/eutW* were highly induced during lactic acid exposure at pH 3.4, suggesting that the induction of the *pdu* and *eut* is dependent on multiple factors and conditions [102].

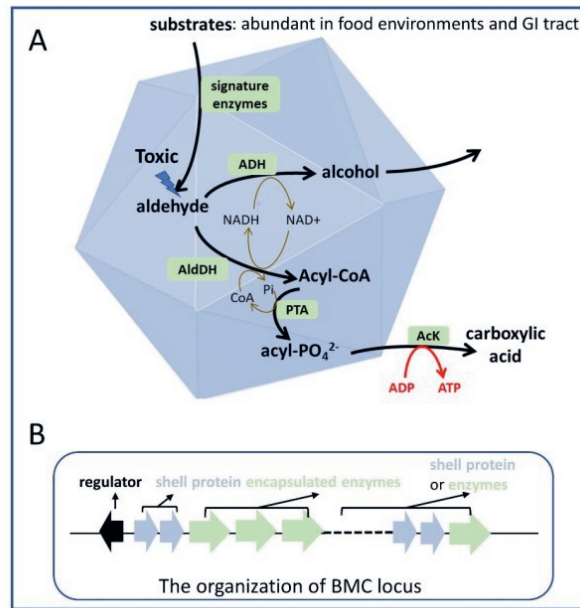


**Figure 1.5 Overview of BMC core reactions and the classical organization of BMC locus. (A)** BMC typically share a common core biochemistry that is based on a signature enzyme, an aldehyde dehydrogenase (AldDH), an alcohol dehydrogenase (ADH) and a phosphotransacylase (PTA). The signature enzyme generates the aldehyde that is then converted to a product alcohol by the ADH. This reaction uses CoA and NAD<sup>+</sup>, which are recycled in a separate reaction branch that uses AldDH and PTAC to produce a phosphorylated product. This product is then dephosphorylated by an acetyl kinase (AcK) in a reaction that generates ATP. **(B)** Typical BMC locus consisting of genes for shell proteins in blue, encapsulated enzymes in green, regulator of BMC locus in black.

Recent research highlight the importance of the *pdu* and *eut* operons for *L. monocytogenes* pathogenicity [10]. The *pdu* and *eut* operons are highly conserved within a single large locus among *Listeria sensu strictu* species representing *Listeria* species more close to pathogenic *L. monocytogenes* but absent in *Listeria sensu lato* species which are exclusively environmental isolates [13, 55]. A transcriptomic study showed that the *pdu* and *eut* genes were significantly upregulated by *L. monocytogenes* in the GI tract and blood of mice [22]. *L. monocytogenes* EGDe virulence in a mouse infection model is reduced by

knockout of *eutB* (encoding the ethanolamine ammonia-lyase subunit) [14] and its persistence in stool and ileal colonisation of female BALB/c mice is reduced in a *pduD* (subunit of propanediol dehydratase) deletion mutant [16].

## 1.4 Objective and outline of this thesis

A detailed outline of the thesis is presented below and in figure 1.6.

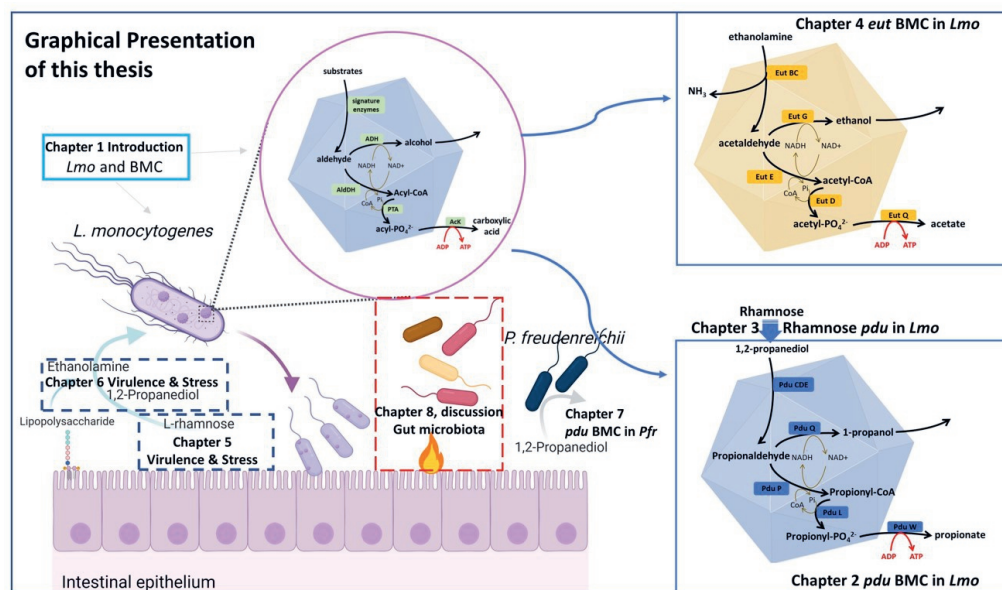


**Figure 1.6 Graphical presentation of the thesis outline**

**Chapter 1** provides an introduction to *L. monocytogenes* ecophysiology, transmission in foods and interaction with the human host, an overview of BMCs composition and functionality, and implication of BMCs to *L. monocytogenes*.

**Chapter 2** describes 1,2-propanediol utilization in *L. monocytogenes* during anaerobic growth and the role of BMCs in this metabolic process. Multiple methods have been integrated including a systematic bioinformatics analysis, metabolic phenotyping, transcriptional analysis, proteomics, TEM (Transmission Electron Microscopy) visualization, and experimental verification in defined medium.

**Chapter 3** extends the study to rhamnose metabolism and rhamnose-derived 1,2-propanediol utilization of *L. monocytogenes* anaerobic growth and the role of BMCs in this process.

**Chapter 4** examines the utilization of ethanolamine and verifies the formation of BMCs for ethanolamine utilization of *L. monocytogenes* supporting anaerobic growth. Again, multiple methods have been integrated including bioinformatics, metabolic phenotyping, comparative proteome analysis, TEM visualization, ferrozine assay for extracellular electron transfer and experimental verification in defined medium.

**Chapter 5** examines the impact of vitamin B12 on rhamnose metabolism, stress defense and in-vitro virulence of *L. monocytogenes* following Chapter 3. Comparative analysis of metabolic phenotyping, proteomics, and in-vitro virulence assays of *L. monocytogenes* grown in aerobic and anaerobic conditions with or without vitamin B12, showed metabolic shifts, activation of stress defense proteins and impact on Caco-2 cell translocation. Possible impact of anaerobic BMC-dependent rhamnose metabolism on *L. monocytogenes* competitive fitness and virulence is discussed.

**Chapter 6.** Following Chapter 2 and Chapter 4, impact of BMC-dependent ethanolamine and propanediol metabolism on *L. monocytogenes* interactions with Caco-2 cells is studied based on comparative proteomics analysis and in-vitro virulence assays of *pdu/eut* induced compared to *pdu/eut* non-induced *L. monocytogenes* cells. Impact of *pdu* and *eut* BMCs activation on adhesion, invasion and translocation efficacy is linked to possible interactions with the host.

**Chapter 7** presents evidence for BMC-dependent anaerobic growth of the probiotic bacterium *Propionibacterium freudenreichii* on 1,2-propanediol. The presence of *pdu* BMCs in *P. freudenreichii* has been confirmed via TEM visualization, metabolic phenotyping and proteomics analysis. This novel finding further extends a role for BMCs in beneficial bacteria, next to pathogenic bacteria, a topic that is further addressed in chapter 8.

**Chapter 8** provides a general discussion of all the results in this thesis and summarizes the functional characterizations of BMCs and their contributions to metabolism, stress response and virulence in *L. monocytogenes* and growth and metabolic versatility of *P. freudenreichii*. I extensively discuss the functionality and potential applications of BMCs as nano-factories to increase metabolic efficiency for synthetic biology, or, as nanoparticles to serve as drug-delivery systems and platforms for designer vaccines.

## 1.5 Supplementary Materials

**Table 1.1 Selected species based on UniProt reference proteomes database with predicted BMC shell proteins hits** ( in total 5181 matched hits, full list are not shown here)

UniProt Protein IDs	Description	Phylum	Species	E-value
H5XTP5	Carboxysome shell protein	Firmicutes	Desulfosporosinus youngiae DSM 17734	3.80E-41
H5XXY4	Carboxysome shell protein	Firmicutes	Desulfosporosinus youngiae DSM 17734	1.90E-40
H5Y076	Carboxysome shell protein	Firmicutes	Desulfosporosinus youngiae DSM 17734	2.90E-38
Q8Y7X6	Lmo1143 protein	Firmicutes	Listeria monocytogenes EGD-e	1.80E-37
Q8XLY2	Propanediol utilization protein	Firmicutes	Clostridium perfringens 13	1.40E-32
L1QMQ0	BMC domain protein	Firmicutes	Clostridium celatum DSM 1785	1.50E-31
Q8Y7T6	Lmo1185 protein	Firmicutes	Listeria monocytogenes EGD-e	3.80E-31
Q8Y7W7	Lmo1152 protein	Firmicutes	Listeria monocytogenes EGD-e	8.70E-30
A3CLC4	Propanediol utilization protein PduB	Firmicutes	Streptococcus sanguinis (strain SK36)	2.70E-29
A0A0R2DBH6	Propanediol utilization protein PduB	Firmicutes	Lactobacillus rennini DSM 20253	1.20E-28
A0A151APE2	Propanediol utilization protein PduB	Firmicutes	Clostridium colicanis DSM 13634	1.20E-27
A0A0R1RS52	Propanediol utilization protein PduB	Firmicutes	Lactobacillus rossiae DSM 15814	6.50E-26
A0A0R2D124	Propanediol utilization protein PduB	Firmicutes	Lactobacillus rennini DSM 20253	4.00E-25
A0A0R1RLZ8	Microcompartments protein	Firmicutes	Lactobacillus rossiae DSM 15814	3.60E-24
A0A0R2D078	Propanediol utilization protein	Firmicutes	Lactobacillus rennini DSM 20253	3.90E-24
A0A0R1RHD9	Major carboxysome shell protein 1A	Firmicutes	Lactobacillus rossiae DSM 15814	7.40E-24
A0A0R2D1T8	Microcompartments protein	Firmicutes	Lactobacillus rennini DSM 20253	7.90E-24
Q8XLY7	Propanediol utilization protein	Firmicutes	Clostridium perfringens 13	2.10E-23
Q8Y7W8	Lmo1151 protein	Firmicutes	Listeria monocytogenes EGD-e	2.90E-23
H5XTN8	Ethanolamine utilization protein	Firmicutes	Desulfosporosinus youngiae DSM 17734	6.30E-23
Q834M2	Microcompartment protein	Firmicutes	Enterococcus faecalis ATCC 700802	7.50E-23
H5Y071	Carboxysome shell protein	Firmicutes	Desulfosporosinus youngiae DSM 17734	7.60E-23
Q8Y7U3	Lmo1177 protein	Firmicutes	Listeria monocytogenes EGD-e	9.50E-23
Q8Y7W0	Lmo1159 protein	Firmicutes	Listeria monocytogenes EGD-e	1.10E-22
A0A151APG0	Propanediol utilization protein PduA	Firmicutes	Clostridium colicanis DSM 13634	1.50E-22
Q92CM7	Lmo1180 protein	Firmicutes	Listeria monocytogenes EGD-e	1.80E-22
A3CLB6	Microcompartment protein, putative	Firmicutes	Streptococcus sanguinis (strain SK36)	3.30E-22
A3CLB3	Ethanolamine utilization protein EutL, putative	Firmicutes	Streptococcus sanguinis (strain SK36)	3.30E-22
A0A0R1RS13	BMC domain-containing protein	Firmicutes	Lactobacillus rossiae DSM 15814	5.50E-22
A0A448FF77	Microcompartments protein	Firmicutes	Bacillus freudenreichii	5.80E-22
L1QMP5	BMC domain protein	Firmicutes	Clostridium celatum DSM 1785	5.90E-22
A3CLB7	Microcompartment protein, putative	Firmicutes	Streptococcus sanguinis (strain SK36)	8.00E-22
H5XTP0	Carboxysome shell protein	Firmicutes	Desulfosporosinus youngiae DSM 17734	8.80E-22
H5XXY7	Carboxysome shell protein	Firmicutes	Desulfosporosinus youngiae DSM 17734	1.30E-21
A0A0R1RHA7	Uncharacterized protein	Firmicutes	Lactobacillus rossiae DSM 15814	1.60E-21
Q8XLZ0	Ethanolamine utilization protein	Firmicutes	Clostridium perfringens 13	2.40E-21
Q8Y7U2	Lmo1178 protein	Firmicutes	Listeria monocytogenes EGD-e	2.50E-21
H5XXY6	Carboxysome shell protein	Firmicutes	Desulfosporosinus youngiae DSM 17734	3.50E-21
Q834L9	Ethanolamine utilization protein EutL	Firmicutes	Enterococcus faecalis ATCC 700802	3.80E-21

## Chapter 1

H5Y074	Carboxysome shell protein	Firmicutes	Desulfosporosinus youngiae DSM 17734	3.80E-21
H5XTN7	Carboxysome shell protein	Firmicutes	Desulfosporosinus youngiae DSM 17734	4.10E-21
H5XXY8	Carboxysome shell protein	Firmicutes	Desulfosporosinus youngiae DSM 17734	4.80E-21
L1QNW9	Putative carboxysome shell protein 1A	Firmicutes	Clostridium celatum DSM 1785	6.90E-21
H5Y090	Carboxysome shell protein	Firmicutes	Desulfosporosinus youngiae DSM 17734	3.40E-20
A0A0R2CZT6	Uncharacterized protein	Firmicutes	Lactobacillus rennini DSM 20253	3.80E-20
H5Y089	Carboxysome shell protein	Firmicutes	Desulfosporosinus youngiae DSM 17734	4.50E-20
A3CLB4	Ethanolamine utilization protein	Firmicutes	Streptococcus sanguinis (strain SK36)	3.20E-19
Q8XLY9	Propanediol utilization protein	Firmicutes	Clostridium perfringens 13	3.60E-19
A0A448FF78	Microcompartments protein	Firmicutes	Bacillus freudenreichii	7.10E-19
A0A0R2D0U3	BMC domain-containing protein	Firmicutes	Lactobacillus rennini DSM 20253	8.90E-19
Q834M0	Microcompartment protein family	Firmicutes	Enterococcus faecalis ATCC 700802	1.70E-18
Q8Y7W1	Lmo1158 protein	Firmicutes	Listeria monocytogenes EGD-e	2.70E-18
A0A0R1RQA5	BMC domain-containing protein	Firmicutes	Lactobacillus rossiae DSM 15814	1.10E-17
A0A151API3	Propanediol utilization protein PduA	Firmicutes	Clostridium colicanis DSM 13634	2.70E-17
A3CLA7	Propanediol utilization protein PduU	Firmicutes	Streptococcus sanguinis (strain SK36)	5.20E-17
Q834L4	Propanediol utilization protein PduU	Firmicutes	Enterococcus faecalis ATCC 700802	2.30E-16
A0A0R2DAB9	Microcompartments protein	Firmicutes	Lactobacillus rennini DSM 20253	2.70E-16
Q8XLZ7	Propanediol utilization protein	Firmicutes	Clostridium perfringens 13	8.30E-16
A0A448FF98	Microcompartments protein	Firmicutes	Bacillus freudenreichii	1.00E-15
L1QMU4	BMC domain protein	Firmicutes	Clostridium celatum DSM 1785	1.40E-15
H5Y083	Ethanolamine utilization protein	Firmicutes	Desulfosporosinus youngiae DSM 17734	4.10E-15
A0A0R2D132	Propanediol utilization protein PduU	Firmicutes	Lactobacillus rennini DSM 20253	2.10E-14
Q8Y7X5	Lmo1144 protein	Firmicutes	Listeria monocytogenes EGD-e	2.80E-14
A0A0R2D042	BMC domain-containing protein	Firmicutes	Lactobacillus rennini DSM 20253	3.50E-14
L1QM02	BMC domain protein	Firmicutes	Clostridium celatum DSM 1785	4.10E-14
A0A0R2CZ93	BMC domain-containing protein	Firmicutes	Lactobacillus rennini DSM 20253	1.10E-13
L1QNJ1	BMC domain protein	Firmicutes	Clostridium celatum DSM 1785	1.80E-13
A0A0R1RIF8	BMC domain-containing protein	Firmicutes	Lactobacillus rossiae DSM 15814	1.70E-12
A0A0R1RIJ7	BMC domain-containing protein	Firmicutes	Lactobacillus rossiae DSM 15814	5.50E-12
H5Y079	BMC domain-containing protein	Firmicutes	Desulfosporosinus youngiae DSM 17734	2.10E-05
Q02B57	Microcompartments protein	Acidobacteria	Solibacter usitatus (strain Ellin6076)	2.40E-41
Q029G2	Microcompartments protein	Acidobacteria	Solibacter usitatus (strain Ellin6076)	2.10E-36
Q025S2	Microcompartments protein	Acidobacteria	Solibacter usitatus (strain Ellin6076)	3.10E-30
A0A0B6X1Q4	Carboxysome shell protein	Acidobacteria	Pyrinomonas methylaliphatogenes	5.80E-24
A0A0B6X4B3	Carboxysome shell protein	Acidobacteria	Pyrinomonas methylaliphatogenes	2.60E-23
A0A143PG95	Ethanolamine utilization protein EutM	Acidobacteria	Luteitalea pratensis	1.70E-22
A0A0B6X296	Carboxysome shell protein	Acidobacteria	Pyrinomonas methylaliphatogenes	2.60E-21
A0A143PYA9	Ethanolamine utilization protein EutM	Acidobacteria	Luteitalea pratensis	2.60E-20
Q02C23	Microcompartments protein	Acidobacteria	Solibacter usitatus (strain Ellin6076)	3.40E-20
A0A143PPE2	Propanediol utilization protein PduA	Acidobacteria	Luteitalea pratensis	5.30E-20
Q02C83	Microcompartments protein	Acidobacteria	Solibacter usitatus (strain Ellin6076)	7.40E-20
Q029G1	Microcompartments protein	Acidobacteria	Solibacter usitatus (strain Ellin6076)	4.40E-18
A8AEM1	Uncharacterized protein	Proteobacteria	Citrobacter koseri ATCC BAA-895	2.10E-40
D2TPS2	Propanediol utilization protein PduT	Proteobacteria	Citrobacter rodentium (strain ICC168)	3.60E-40
A0A1T4W4Z8	Shell CcmL/EutN	Proteobacteria	Desulfovibrio bizertensis DSM 18034	4.70E-40

A0A2X4T9C3	BMC domain-containing protein	Proteobacteria	Salmonella enterica subsp. arizonae	9.30E-40
Q9XDM8	Propanediol utilization protein	Proteobacteria	Salmonella typhimurium strain LT2	1.80E-38
A0A1T4W4K2	Shell CcmL/EutN	Proteobacteria	Desulfovibrio bizertensis DSM 18034	1.70E-37
A0A1T4W614	Shell CcmL/EutN	Proteobacteria	Desulfovibrio bizertensis DSM 18034	2.50E-36
P37449	Propanediol utilization protein PduB	Proteobacteria	Salmonella typhimurium strain LT2	2.80E-29
A8AEN6	Uncharacterized protein	Proteobacteria	Citrobacter koseri ATCC BAA-895	2.10E-28
W1FQT3	Propanediol utilization protein PduB	Proteobacteria	Escherichia coli ISC11	2.10E-28
A0A2X4T711	Propanediol utilization protein PduB	Proteobacteria	Salmonella enterica subsp. arizonae	9.90E-28
D2TPQ7	Propanediol utilization protein PduB	Proteobacteria	Citrobacter rodentium (strain ICC168)	1.10E-27
W1HYR8	Propanediol utilization protein PduB	Proteobacteria	Klebsiella pneumoniae IS39	3.90E-26
W1FQ60	Propanediol utilization protein PduT	Proteobacteria	Escherichia coli ISC11	1.90E-24
A0A370QTV0	BMC domain-containing protein	Proteobacteria	Enterobacillus tribolii	8.30E-23
D2TPR3	Propanediol utilization protein	Proteobacteria	Citrobacter rodentium (strain ICC168)	1.20E-22
A8AEN0	BMC domain-containing protein	Proteobacteria	Citrobacter koseri ATCC BAA-895	1.20E-22
H9L478	Propanediol utilization protein	Proteobacteria	Salmonella typhimurium strain LT2	1.70E-22
W1FTR8	Propanediol utilization protein PduJ	Proteobacteria	Escherichia coli ISC11	2.40E-22
F0LQG4	Carboxysome shell protein	Proteobacteria	Vibrio furnissii DSM 14383	2.70E-22
A0A0J1GXF9	BMC domain-containing protein	Proteobacteria	Photobacterium ganghwense	3.00E-22
A0A0J1GY18	BMC domain-containing protein	Proteobacteria	Photobacterium ganghwense	3.10E-22
A0A1T4W551	Ethanolamine utilization protein EutM	Proteobacteria	Desulfovibrio bizertensis DSM 18034	3.80E-22
A0A370QTT7	BMC domain-containing protein	Proteobacteria	Enterobacillus tribolii	5.60E-22
F0LQG5	Carboxysome shell protein	Proteobacteria	Vibrio furnissii DSM 14383	6.90E-22
A0A2X4WH89	Carboxysome shell protein	Proteobacteria	Salmonella enterica subsp. arizonae	7.50E-22
P0A1C7	Propanediol utilization protein PduA	Proteobacteria	Salmonella typhimurium strain LT2	7.60E-22
A8AEN7	BMC domain-containing protein	Proteobacteria	Citrobacter koseri ATCC BAA-895	7.60E-22
D2TPQ6	Propanediol utilisation protein PduA	Proteobacteria	Citrobacter rodentium (strain ICC168)	7.60E-22
A0A0J1GXG1	BMC domain-containing protein	Proteobacteria	Photobacterium ganghwense	1.30E-21
A0A370QU19	BMC domain-containing protein	Proteobacteria	Enterobacillus tribolii	1.40E-21
A0A1T4W563	BMC domain-containing protein	Proteobacteria	Desulfovibrio bizertensis DSM 18034	1.60E-21
P41791	Ethanolamine utilization protein EutM	Proteobacteria	Salmonella typhimurium strain LT2	2.40E-21
P0ABF4	Ethanolamine utilization protein EutM	Proteobacteria	Escherichia coli (strain K12)	2.40E-21
L0M1P0	Carboxysome shell protein	Proteobacteria	Enterobacteriaceae bacterium FGI 57	2.40E-21
A8ADD8	BMC domain-containing protein	Proteobacteria	Citrobacter koseri ATCC BAA-895	3.10E-21
D2TT92	Ethanolamine utilization protein	Proteobacteria	Citrobacter rodentium (strain ICC168)	3.20E-21
W1G391	Ethanolamine utilization protein EutM	Proteobacteria	Escherichia coli ISC11	3.20E-21
Q32DB4	Uncharacterized protein	Proteobacteria	Shigella dysenteriae Sd197	3.40E-21
Q8XBG4	Ethanolamine utilization protein	Proteobacteria	Escherichia coli O157:H7	3.70E-21
Q8XBI1	Ethanol utilization carboxysome structural protein	Proteobacteria	Escherichia coli O157:H7	4.90E-21
F0LQG6	Carboxysome shell protein	Proteobacteria	Vibrio furnissii DSM 14383	4.90E-21
A0A2X4TJ81	Carboxysome shell protein	Proteobacteria	Salmonella enterica subsp. arizonae	5.00E-21
P0A1C9	Ethanolamine utilization protein EutL	Proteobacteria	Salmonella typhimurium strain LT2	5.80E-21
A0A2X4T411	Ethanolamine utilization protein EutL	Proteobacteria	Salmonella enterica subsp. arizonae	6.10E-21
D2TT83	Ethanolamine utilization protein	Proteobacteria	Citrobacter rodentium (strain ICC168)	6.60E-21
L0M3D1	Ethanolamine utilization protein	Proteobacteria	Enterobacteriaceae bacterium FGI 57	7.70E-21

## Chapter 1

W1FSJ5	Ethanolamine utilization protein EutL	Proteobacteria	Escherichia coli ISC11	8.00E-21
A8ADE7	Uncharacterized protein	Proteobacteria	Citrobacter koseri ATCC BAA-895	3.90E-20
P76541	Ethanolamine utilization protein EutL	Proteobacteria	Escherichia coli (strain K12)	4.30E-20
F9ZLQ9	BMC domain-containing protein	Proteobacteria	Acidithiobacillus caldus (strain SM-1)	5.30E-20
O84926	Carboxysome structural polypeptide	Proteobacteria	Thiomonas intermedia (strain K12)	1.60E-19
A0A4R3JW17	BMC domain-containing protein	Proteobacteria	Sulfuritortus calidifontis	1.80E-19
A0A4R3JZ71	BMC domain-containing protein	Proteobacteria	Sulfuritortus calidifontis	2.20E-19
O84927	Carboxysome structural polypeptide	Proteobacteria	Thiomonas intermedia (strain K12)	4.20E-19
D5X338	Microcompartments protein	Proteobacteria	Thiomonas intermedia (strain K12)	6.10E-19
F9ZLP6	Carboxysome shell protein CsoS1	Proteobacteria	Acidithiobacillus caldus (strain SM-1)	6.50E-19
A0A4V2UQS3	BMC domain-containing protein	Proteobacteria	Sulfuritortus calidifontis	6.50E-19
W1GLG2	Propanediol utilization protein PduA	Proteobacteria	Klebsiella pneumoniae ISC21	6.80E-19
A0A0J9E953	Ethanolamine utilization protein	Proteobacteria	Candidatus Rhodobacter lobularis	7.20E-19
A0A1U7DJ28	BMC domain-containing protein	Proteobacteria	Brevihabduis pacifica	8.80E-19
D2TT82	Ethanolamine utilization protein	Proteobacteria	Citrobacter rodentium (strain ICC168)	1.10E-18
W1GLP1	Propanediol utilization protein PduB	Proteobacteria	Klebsiella pneumoniae ISC21	2.50E-18
A0A370QTW0	BMC domain-containing protein	Proteobacteria	Enterobacillus tribolii	2.80E-18
P76540	Ethanolamine utilization protein EutK	Proteobacteria	Escherichia coli (strain K12)	1.40E-17
A0A1T4W4M6	Shell CcmL/EutN	Proteobacteria	Desulfovibrio bizertensis DSM 18034	1.40E-17
Q32DB5	BMC domain-containing protein	Proteobacteria	Shigella dysenteriae Sd197	1.40E-17
Q8XB12	Ethanol utilization structural protein	Proteobacteria	Escherichia coli O157:H7	2.50E-17
W1HRP2	Propanediol utilization protein PduT	Proteobacteria	Klebsiella pneumoniae IS39	2.60E-17
A8ADE8	BMC domain-containing protein	Proteobacteria	Citrobacter koseri ATCC BAA-895	3.00E-17
Q9ZFU8	Ethanolamine utilization protein EutK	Proteobacteria	Salmonella typhimurium strain LT2	5.50E-17
F9ZLP7	Carboxysome shell protein CsoS1	Proteobacteria	Acidithiobacillus caldus (strain SM-1)	7.60E-17
L0M1P9	Carboxysome shell protein	Proteobacteria	Enterobacteriaceae bacterium FGI 57	8.50E-17
A0A0J9EC93	BMC domain-containing protein	Proteobacteria	Candidatus Rhodobacter lobularis	8.70E-17
D2TPR4	Propanediol utilization protein PduK	Proteobacteria	Citrobacter rodentium (strain ICC168)	9.60E-17
W1FU64	Ethanolamine utilization protein EutK	Proteobacteria	Escherichia coli ISC11	9.70E-17
A0A1T4W531	Ethanolamine utilization protein EutS	Proteobacteria	Desulfovibrio bizertensis DSM 18034	9.90E-17
W1FS57	Propanediol utilization protein PduK	Proteobacteria	Escherichia coli ISC11	1.60E-16
Q9XDN6	Propanediol utilization protein	Proteobacteria	Salmonella typhimurium strain LT2	1.40E-15
D5X345	Microcompartments protein	Proteobacteria	Thiomonas intermedia (strain K12)	1.50E-15
W1GVQ7	Propanediol utilization protein PduU	Proteobacteria	Klebsiella pneumoniae ISC21	1.60E-14
W1HNX8	Propanediol utilization protein PduU	Proteobacteria	Klebsiella pneumoniae IS39	1.60E-14
W1FRV2	Propanediol utilization protein PduU	Proteobacteria	Escherichia coli ISC11	3.20E-14
P0A1D1	Propanediol utilization protein PduU	Proteobacteria	Salmonella typhimurium strain LT2	3.60E-14
P63746	Ethanolamine utilization protein EutS	Proteobacteria	Escherichia coli (strain K12)	5.60E-14
Q8XBF5	Ethanol utilization structural protein	Proteobacteria	Escherichia coli O157:H7	5.60E-14
A0A2X4TKU5	Propanediol utilization protein PduU	Proteobacteria	Salmonella enterica subsp. arizonae	6.50E-14
D2TPS3	Propanediol utilization protein PduU	Proteobacteria	Citrobacter rodentium (strain ICC168)	6.90E-14
A8AEM0	BMC domain-containing protein	Proteobacteria	Citrobacter koseri ATCC BAA-895	7.10E-14

W1GY50	Propanediol utilization protein PduT	Proteobacteria	Klebsiella pneumoniae ISC21	2.70E-13
L0M1N5	Ethanolamine utilization protein	Proteobacteria	Enterobacteriaceae bacterium FGI 57	2.80E-13
D2TT97	Ethanolamine utilization protein	Proteobacteria	Citrobacter rodentium (strain ICC168)	4.00E-13
A8ADD3	BMC domain-containing protein	Proteobacteria	Citrobacter koseri ATCC BAA-895	5.10E-13
Q9ZFV7	Ethanolamine utilization protein EutS	Proteobacteria	Salmonella typhimurium strain LT2	1.00E-12
W1HX23	Ethanolamine utilization protein EutS	Proteobacteria	Klebsiella pneumoniae IS39	1.20E-12
A0A2X4TJ98	Carboxysome shell protein	Proteobacteria	Salmonella enterica subsp. arizonae	4.60E-12
Q32DB0	BMC domain-containing protein	Proteobacteria	Shigella dysenteriae Sd197	1.50E-11
F0LQF8	Carboxysome shell protein	Proteobacteria	Vibrio furnissii DSM 14383	2.20E-11
A0A2X4T7H3	Carboxysome shell protein	Proteobacteria	Salmonella enterica subsp. arizonae	3.40E-10
W1GVT7	Ethanolamine utilization protein EutS	Proteobacteria	Klebsiella pneumoniae ISC21	3.50E-10
A8AEM9	BMC domain-containing protein	Proteobacteria	Citrobacter koseri ATCC BAA-895	4.90E-09
W1FS66	Propanediol utilization protein PduT	Proteobacteria	Escherichia coli ISC11	3.30E-08
W1G6Z1	Ethanolamine utilization protein EutS	Proteobacteria	Escherichia coli ISC11	5.00E-08
A0A2X4T5C5	Carboxysome shell protein	Proteobacteria	Salmonella enterica subsp. arizonae	1.00E-07
A0A2X4TMR0	Propanediol utilization protein	Proteobacteria	Salmonella enterica subsp. arizonae	7.50E-06
A0A1H2EZT4	Malonyl CoA-acyl carrier protein	Proteobacteria	Pseudomonas salegens	0.25
X5KUJ0	Microcompartments protein	Actinobacteria	Mycolicibacterium mageritense DSM 44476	5.60E-22
D7GD15	Propanediol utilization protein PduA	Actinobacteria	Propionibacterium freudenreichii ATCC 9614	1.90E-21
D7GD23	Propanediol utilization protein PduJ	Actinobacteria	Propionibacterium freudenreichii ATCC 9614	3.10E-21
D7GD16	Propanediol utilization protein PduB	Actinobacteria	Propionibacterium freudenreichii ATCC 9614	4.10E-21
A0A132MTN 2	Uncharacterized protein	Actinobacteria	Streptomyces thermoautotrophicus	6.40E-21
A0A2U1FF58	Ethanolamine utilization protein EutM	Actinobacteria	Actinomycetospira cinnamomea	9.20E-21
A0A1C6UM6 2	Ethanolamine utilization protein EutM	Actinobacteria	Micromonospora yangpuensis	2.40E-20
A0A2U1FF89	Ethanolamine utilization protein EutM	Actinobacteria	Actinomycetospira cinnamomea	2.70E-20
D7GD22	Propanediol utilization protein PduK	Actinobacteria	Propionibacterium freudenreichii ATCC 9614	2.40E-19
A0A2U1FFA4	BMC domain-containing protein	Actinobacteria	Actinomycetospira cinnamomea	4.20E-19
C7M1Z5	Microcompartments protein	Actinobacteria	Acidimicrobium ferrooxidans DSM 10331	4.50E-19
C7M1Z6	Microcompartments protein	Actinobacteria	Acidimicrobium ferrooxidans DSM 10331	4.50E-19
C7M1Z7	Microcompartments protein	Actinobacteria	Acidimicrobium ferrooxidans DSM 10331	4.90E-19
A0A132N6B4	Carboxysome structural protein EutM	Actinobacteria	Streptomyces thermoautotrophicus	7.80E-19
X5KYQ9	Microcompartments protein	Actinobacteria	Mycolicibacterium mageritense DSM 44476	9.50E-19
A0A1C6UM2 1	BMC domain-containing protein	Actinobacteria	Micromonospora yangpuensis	5.30E-15
A0A1C6ULW 8	BMC domain-containing protein	Actinobacteria	Micromonospora yangpuensis	4.10E-13
D7GD14	Propanediol utilization protein PduU	Actinobacteria	Propionibacterium freudenreichii ATCC 9614	6.50E-13
X5KN18	Microcompartments protein family protein	Actinobacteria	Mycolicibacterium mageritense DSM 44476	7.00E-12
A0A2U1FIM5	Ethanolamine utilization protein EutM	Actinobacteria	Actinomycetospira cinnamomea	8.60E-12
F4FAP9	Microcompartments protein	Actinobacteria	Verrucosipora maris (strain AB-18-032)	2.50E-11
A0A2U1FJ45	CcmK	Actinobacteria	Actinomycetospira cinnamomea	4.10E-11
F4FAQ0	Microcompartments protein	Actinobacteria	Verrucosipora maris (strain AB-18-032)	9.40E-11
A0A132MTN 0	Uncharacterized protein	Actinobacteria	Streptomyces thermoautotrophicus	1.80E-09

## Chapter 1

B4WNX3	Bacterial microcompartments protein family	Cyanobacteria	Synechococcus sp. ATCC 29403	3.70E-39
K9RT81	Carboxysome shell protein	Cyanobacteria	Synechococcus sp. ATCC 27167	1.90E-30
K9RSK4	Carboxysome shell protein	Cyanobacteria	Synechococcus sp. ATCC 27167	1.10E-22
K9RUF7	Carboxysome shell protein	Cyanobacteria	Synechococcus sp. ATCC 27167	5.80E-22
B4WNW9	Bacterial microcompartments protein	Cyanobacteria	Synechococcus sp. ATCC 29403	1.00E-21
B4WGP7	Bacterial microcompartments protein	Cyanobacteria	Synechococcus sp. ATCC 29403	6.90E-20
C7M1Z5	Microcompartments protein	Actinobacteria	Acidimicrobium ferrooxidans DSM 10331	4.50E-19
C7M1Z6	Microcompartments protein	Actinobacteria	Acidimicrobium ferrooxidans DSM 10331	4.50E-19
C7M1Z7	Microcompartments protein	Actinobacteria	Acidimicrobium ferrooxidans DSM 10331	4.90E-19
K9RZT0	Carboxysome shell protein	Cyanobacteria	Synechococcus sp. ATCC 27167	1.80E-18
B4WJ85	Bacterial microcompartments protein	Cyanobacteria	Synechococcus sp. ATCC 29403	5.30E-18
B4WNW7	Bacterial microcompartments protein	Cyanobacteria	Synechococcus sp. ATCC 29403	1.70E-17
K9RY52	BMC domain-containing protein	Cyanobacteria	Synechococcus sp. ATCC 27167	5.50E-17
K9RTC4	Carboxysome shell protein	Cyanobacteria	Synechococcus sp. ATCC 27167	4.10E-15
B4WJ87	Shell protein family	Cyanobacteria	Synechococcus sp. ATCC 29403	2.20E-11

## 1.6 References

1. Radoshevich, L. and P. Cossart, *Listeria monocytogenes: towards a complete picture of its physiology and pathogenesis*. Nature Reviews Microbiology, 2018. **16**(1): p. 32-46.
2. Prevention, C.f.D.C.a., *Quantitative assessment of the relative risk to public health from foodborne Listeria monocytogenes among selected categories of ready-to-eat foods*. 2003, US Department of Agriculture-Food Safety and Inspection Service Washington, DC.
3. Freitag, N.E., G.C. Port, and M.D. Miner, *Listeria monocytogenes—from saprophyte to intracellular pathogen*. Nature Reviews Microbiology, 2009. **7**(9): p. 623-628.
4. Sauders, B.D., et al., *Diversity of Listeria species in urban and natural environments*. Applied and environmental microbiology, 2012. **78**(12): p. 4420-4433.
5. Haase, J.K., et al., *The ubiquitous nature of Listeria monocytogenes clones: a large-scale Multilocus Sequence Typing study*. Environmental microbiology, 2014. **16**(2): p. 405-416.
6. NicAogáin, K. and C.P. O'Byrne, *The role of stress and stress adaptations in determining the fate of the bacterial pathogen Listeria monocytogenes in the food chain*. Frontiers in microbiology, 2016. **7**: p. 1865.
7. Prentice, M.B., *Bacterial microcompartments and their role in pathogenicity*. Current Opinion in Microbiology, 2021. **63**: p. 19-28.
8. Authority, E.F.S., E.C.f.D. Prevention, and Control, *The European Union summary report on trends and sources of zoonoses, zoonotic agents and food-borne outbreaks in 2017*. EFSA Journal, 2018. **16**(12): p. e05500.
9. Younes, M., et al., *Re-evaluation of propane-1,2-diol alginate (E 405) as a food additive*. Efsa Journal, 2018. **16**(7).
10. Anast, J.M., T.A. Bobik, and S. Schmitz-Esser, *The Cobalamin-dependent gene cluster of Listeria monocytogenes: implications for virulence, stress response, and food safety*. Frontiers in microbiology, 2020. **11**.
11. Tang, S., et al., *Transcriptomic analysis of the adaptation of Listeria monocytogenes to growth on vacuum-packed cold smoked salmon*. Appl. Environ. Microbiol., 2015. **81**(19): p. 6812-6824.
12. Schmid, B., et al., *Role of cold shock proteins in growth of Listeria monocytogenes under cold and osmotic stress conditions*. Applied and environmental microbiology, 2009. **75**(6): p. 1621-1627.
13. Chiara, M., et al., *Comparative genomics of Listeria sensu lato: genus-wide differences in evolutionary dynamics and the progressive gain of complex, potentially pathogenicity-related traits through lateral gene transfer*. Genome biology and evolution, 2015. **7**(8): p. 2154-2172.
14. Joseph, B., et al., *Identification of Listeria monocytogenes genes contributing to intracellular replication by expression profiling and mutant screening*. Journal of bacteriology, 2006. **188**(2): p. 556-568.
15. Chan, Y.C., et al., *Contributions of two-component regulatory systems, alternative  $\sigma$  factors, and negative regulators to Listeria monocytogenes*

- cold adaptation and cold growth*. Journal of food protection, 2008. **71**(2): p. 420-425.
16. Schardt, J., et al., *Comparison between Listeria sensu stricto and Listeria sensu lato strains identifies novel determinants involved in infection*. Scientific reports, 2017. **7**(1): p. 17821.
17. Schlech III, W.F., et al., *Epidemic listeriosis—evidence for transmission by food*. New England journal of medicine, 1983. **308**(4): p. 203-206.
18. Chan, Y.C. and M. Wiedmann, *Physiology and genetics of Listeria monocytogenes survival and growth at cold temperatures*. Critical reviews in food science and nutrition, 2008. **49**(3): p. 237-253.
19. Yousef, A.E. and Y. Lou, *Characteristics of Listeria monocytogenes important to food processors*. Listeria: listeriosis, and food safety, 1999. **131**.
20. Hingston, P., et al., *Strand specific RNA-sequencing and membrane lipid profiling reveals growth phase-dependent cold stress response mechanisms in Listeria monocytogenes*. PLoS One, 2017. **12**(6): p. e0180123.
21. Kaval, K.G. and D.A. Garsin, *Ethanolamine utilization in bacteria*. mBio, 2018. **9**(1): p. e00066-18.
22. Toledo-Arana, A., et al., *The Listeria transcriptional landscape from saprophytism to virulence*. Nature, 2009. **459**(7249): p. 950-956.
23. Chen, G.Y., D.A. Pensinger, and J.D. Sauer, *Listeria monocytogenes cytosolic metabolism promotes replication, survival, and evasion of innate immunity*. Cellular microbiology, 2017. **19**(10): p. e12762.
24. de las Heras, A., et al., *Regulation of Listeria virulence: PrfA master and commander*. Current opinion in microbiology, 2011. **14**(2): p. 118-127.
25. Tapia, N.C., et al., *Different carbon sources result in differential activation of sigma B and stress resistance in Listeria monocytogenes*. International journal of food microbiology, 2020. **320**: p. 108504.
26. Nadon, C.A., et al., *Sigma B contributes to PrfA-mediated virulence in Listeria monocytogenes*. Infection and immunity, 2002. **70**(7): p. 3948-3952.
27. Bonazzi, M., et al., *Successive post-translational modifications of E-cadherin are required for InlA-mediated internalization of Listeria monocytogenes*. Cellular microbiology, 2008. **10**(11): p. 2208-2222.
28. Phelps, C.C., et al., *Relative roles of listeriolysin O, InlA, and InlB in Listeria monocytogenes uptake by host cells*. Infection and immunity, 2018. **86**(10): p. e00555-18.
29. Lingnau, A., et al., *Expression of the Listeria monocytogenes EGD inlA and inlB genes, whose products mediate bacterial entry into tissue culture cell lines, by PrfA-dependent and-independent mechanisms*. Infection and immunity, 1995. **63**(10): p. 3896-3903.
30. Kim, H. and A.K. Bhunia, *Secreted Listeria adhesion protein (Lap) influences Lap-mediated Listeria monocytogenes paracellular translocation through epithelial barrier*. Gut pathogens, 2013. **5**(1): p. 1-11.

31. Burkholder, K.M. and A.K. Bhunia, *Listeria monocytogenes* uses *Listeria* adhesion protein (LAP) to promote bacterial transepithelial translocation and induces expression of LAP receptor Hsp60. *Infection and immunity*, 2010. **78**(12): p. 5062-5073.
32. Hamon, M.A., et al., *Listeriolysin O: the Swiss army knife of Listeria*. *Trends in microbiology*, 2012. **20**(8): p. 360-368.
33. Decatur, A.L. and D.A. Portnoy, A PEST-like sequence in listeriolysin O essential for *Listeria monocytogenes* pathogenicity. *Science*, 2000. **290**(5493): p. 992-995.
34. Safley, S., et al., Role of listeriolysin-O (LLO) in the T lymphocyte response to infection with *Listeria monocytogenes*. Identification of T cell epitopes of LLO. *The Journal of Immunology*, 1991. **146**(10): p. 3604-3616.
35. Camilli, A., L.G. Tilney, and D.A. Portnoy, Dual roles of *plcA* in *Listeria monocytogenes* pathogenesis. *Molecular microbiology*, 1993. **8**(1): p. 143-157.
36. Mitchell, G., et al., Avoidance of autophagy mediated by *PlcA* or *ActA* is required for *Listeria monocytogenes* growth in macrophages. *Infection and immunity*, 2015. **83**(5): p. 2175-2184.
37. Portnoy, D.A., et al., Molecular determinants of *Listeria monocytogenes* pathogenesis. *Infection and immunity*, 1992. **60**(4): p. 1263-1267.
38. Yoshikawa, Y., et al., *Listeria monocytogenes* ActA-mediated escape from autophagic recognition. *Nature cell biology*, 2009. **11**(10): p. 1233-1240.
39. Brundage, R.A., et al., Expression and phosphorylation of the *Listeria monocytogenes* ActA protein in mammalian cells. *Proceedings of the National Academy of Sciences*, 1993. **90**(24): p. 11890-11894.
40. Travier, L. and M. Lecuit, *Listeria monocytogenes* ActA: a new function for a 'classic' virulence factor. *Current opinion in microbiology*, 2014. **17**: p. 53-60.
41. Rajabian, T., et al., The bacterial virulence factor *InlC* perturbs apical cell junctions and promotes cell-to-cell spread of *Listeria*. *Nature cell biology*, 2009. **11**(10): p. 1212-1218.
42. Tilney, L.G. and D.A. Portnoy, Actin filaments and the growth, movement, and spread of the intracellular bacterial parasite, *Listeria monocytogenes*. *Journal of cell Biology*, 1989. **109**(4): p. 1597-1608.
43. Scortti, M., et al., The *PrfA* virulence regulon. *Microbes and Infection*, 2007. **9**(10): p. 1196-1207.
44. Marr, A., et al., Overexpression of *PrfA* leads to growth inhibition of *Listeria monocytogenes* in glucose-containing culture media by interfering with glucose uptake. *Journal of bacteriology*, 2006. **188**(11): p. 3887-3901.
45. Milohanic, E., et al., Transcriptome analysis of *Listeria monocytogenes* identifies three groups of genes differently regulated by *PrfA*. *Molecular microbiology*, 2003. **47**(6): p. 1613-1625.
46. Portman, J.L., et al., Activation of the *Listeria monocytogenes* virulence program by a reducing environment. *MBio*, 2017. **8**(5): p. e01595-17.
47. Reniere, M.L., A.T. Whiteley, and D.A. Portnoy, An *in vivo* selection identifies *Listeria monocytogenes* genes required to sense the intracellular

- environment and activate virulence factor expression. *PLoS pathogens*, 2016. **12**(7): p. e1005741.
48. Kerfeld, C.A., et al., *Bacterial microcompartments*. *Nature Reviews Microbiology*, 2018.
49. Yeates, T.O., et al., *Protein-based organelles in bacteria: carboxysomes and related microcompartments*. *Nature Reviews Microbiology*, 2008. **6**(9): p. 681.
50. Axen, S.D., O. Erbilgin, and C.A. Kerfeld, *A taxonomy of bacterial microcompartment loci constructed by a novel scoring method*. *PLoS computational biology*, 2014. **10**(10): p. e1003898.
51. Sutter, M., et al., *A catalog of the diversity and ubiquity of bacterial microcompartments*. *Nature Communications*, 2021. **12**(1): p. 1-12.
52. Sutter, M., et al., *Assembly principles and structure of a 6.5-MDa bacterial microcompartment shell*. *Science*, 2017. **356**(6344): p. 1293-1297.
53. Kerfeld, C.A., et al., *Protein structures forming the shell of primitive bacterial organelles*. *Science*, 2005. **309**(5736): p. 936-938.
54. Liu, L.-N., et al., *Protein stoichiometry, structural plasticity and regulation of bacterial microcompartments*. *Current Opinion in Microbiology*, 2021. **63**: p. 133-141.
55. Zeng, Z., et al., *Bacterial microcompartment-dependent 1, 2-propanediol utilization stimulates anaerobic growth of Listeria monocytogenes EGDe*. *Frontiers in Microbiology*, 2019. **10**: p. 2660.
56. Tanaka, S., et al., *Atomic-level models of the bacterial carboxysome shell*. *Science*, 2008. **319**(5866): p. 1083-1086.
57. Cheng, S., et al., *Genetic analysis of the protein shell of the microcompartments involved in coenzyme B<sub>12</sub>-dependent 1, 2-propanediol degradation by Salmonella*. *Journal of bacteriology*, 2011. **193**(6): p. 1385-1392.
58. Kennedy, N.W., et al., *Self-assembling shell proteins PduA and PduJ have essential and redundant roles in bacterial microcompartment assembly*. *Journal of Molecular Biology*, 2021. **433**(2): p. 166721.
59. Parsons, J.B., et al., *Synthesis of Empty Bacterial Microcompartments, Directed Organelle Protein Incorporation, and Evidence of Filament-Associated Organelle Movement*. *Molecular Cell*, 2010. **38**(2): p. 305-315.
60. Kirst, H. and C.A. Kerfeld, *Bacterial microcompartments: catalysis-enhancing metabolic modules for next generation metabolic and biomedical engineering*. *Bmc Biology*, 2019. **17**(1).
61. Shen, Y.B., et al., *Applications and perspectives of nanomaterials in novel vaccine development*. *Medchemcomm*, 2018. **9**(2): p. 226-238.
62. Ravcheev, D.A., et al., *Comparative genomic analysis reveals novel microcompartment-associated metabolic pathways in the human gut microbiome*. *Frontiers in genetics*, 2019. **10**: p. 636.
63. Kaval, K.G., et al., *Ethanolamine utilization and bacterial microcompartment formation are subject to carbon catabolite repression*. *Journal of bacteriology*, 2019. **201**(10): p. e00703-18.

64. Pitts, A.C., et al., *Structural insight into the Clostridium difficile ethanolamine utilisation microcompartment*. PLoS one, 2012. **7**(10): p. e48360.
65. Petit, E., et al., *Involvement of a bacterial microcompartment in the metabolism of fucose and rhamnose by Clostridium phytofermentans*. PLoS One, 2013. **8**(1): p. e54337.
66. Crowley, C.S., et al., *Structural insight into the mechanisms of transport across the Salmonella enterica Pdu microcompartment shell*. Journal of Biological Chemistry, 2010. **285**(48): p. 37838-37846.
67. Herring, T.I., et al., *A bacterial microcompartment is used for choline fermentation by Escherichia coli 536*. Journal of bacteriology, 2018. **200**(10): p. e00764-17.
68. Ravcheev, D.A., et al., *Comparative Genomic Analysis Reveals Novel Microcompartment-Associated Metabolic Pathways in the Human Gut Microbiome*. Frontiers in Genetics, 2019. **10**.
69. Rinke, C., et al., *Insights into the phylogeny and coding potential of microbial dark matter*. Nature, 2013. **499**(7459): p. 431-437.
70. Letunic, I. and P. Bork, *Interactive Tree Of Life (iTOL) v5: an online tool for phylogenetic tree display and annotation*. Nucleic acids research, 2021. **49**(W1): p. W293-W296.
71. Stewart, A.M., et al., *Advances in the World of Bacterial Microcompartments*. Trends in Biochemical Sciences, 2021.
72. Wilson, J.W., *Manipulating microcompartment operons to study mechanism and function*. Current Opinion in Microbiology, 2021. **60**: p. 66-72.
73. Ochoa, J.M. and T.O. Yeates, *Recent structural insights into bacterial microcompartment shells*. Current Opinion in Microbiology, 2021. **62**: p. 51-60.
74. Kennedy, N.W., et al., *Bacterial microcompartments: tiny organelles with big potential*. Current Opinion in Microbiology, 2021. **63**: p. 36-42.
75. Ng, K.M., et al., *Microbiota-liberated host sugars facilitate post-antibiotic expansion of enteric pathogens*. Nature, 2013. **502**(7469): p. 96-+.
76. Louis, P. and H.J. Flint, *Formation of propionate and butyrate by the human colonic microbiota*. Environmental Microbiology, 2017. **19**(1): p. 29-41.
77. Bunesova, V., C. Lacroix, and C. Schwab, *Fucosyllactose and L-fucose utilization of infant Bifidobacterium longum and Bifidobacterium kashiwanohense*. BMC Microbiology, 2016. **16**.
78. Belzer, C., et al., *Microbial Metabolic Networks at the Mucus Layer Lead to Diet-Independent Butyrate and Vitamin B-12 Production by Intestinal Symbionts*. Mbio, 2017. **8**(5).
79. Sinha, S., et al., *The PduM protein is a structural component of the microcompartments involved in coenzyme B12-dependent 1, 2-propanediol degradation by Salmonella enterica*. Journal of bacteriology, 2012. **194**(8): p. 1912-1918.
80. Sampson, E.M. and T.A. Bobik, *Microcompartments for B12-dependent 1, 2-propanediol degradation provide protection from DNA and cellular*

- damage by a reactive metabolic intermediate. *Journal of bacteriology*, 2008. **190**(8): p. 2966-2971.
81. Xue, J., et al., *Exogenous or L-rhamnose-derived 1, 2-propanediol is metabolized via a pduD-dependent pathway in Listeria innocua*. *Appl. Environ. Microbiol.*, 2008. **74**(22): p. 7073-7079.
82. Cheng, S., et al., *The PduQ enzyme is an alcohol dehydrogenase used to recycle NAD<sup>+</sup> internally within the Pdu microcompartment of Salmonella enterica*. *PLoS One*, 2012. **7**(10): p. e47144.
83. Mellin, J., et al., *A riboswitch-regulated antisense RNA in Listeria monocytogenes*. *Proceedings of the National Academy of Sciences*, 2013. **110**(32): p. 13132-13137.
84. Garsin, D.A., *Ethanolamine utilization in bacterial pathogens: roles and regulation*. *Nature Reviews Microbiology*, 2010. **8**(4): p. 290-295.
85. Tsoy, O., D. Ravcheev, and A. Mushegian, *Comparative genomics of ethanolamine utilization*. *Journal of bacteriology*, 2009. **191**(23): p. 7157-7164.
86. Stojiljkovic, I., A.J. Bäumler, and F. Heffron, *Ethanolamine utilization in Salmonella typhimurium: nucleotide sequence, protein expression, and mutational analysis of the cchA cchB eutE eutJ eutG eutH gene cluster*. *Journal of bacteriology*, 1995. **177**(5): p. 1357-1366.
87. Chang, G.W. and J.T. Chang, *Evidence for the B12-dependent enzyme ethanolamine deaminase in Salmonella*. *Nature*, 1975. **254**(5496): p. 150-151.
88. Blackwell, C.M. and J.M. Turner, *Microbial metabolism of amino alcohols. Formation of coenzyme B12-dependent ethanolamine ammonia-lyase and its concerted induction in Escherichia coli*. *Biochemical Journal*, 1978. **176**(3): p. 751-757.
89. Roof, D.M. and J.R. Roth, *Ethanolamine utilization in Salmonella typhimurium*. *Journal of bacteriology*, 1988. **170**(9): p. 3855-3863.
90. Brinsmade, S.R. and J.C. Escalante-Semerena, *The eutD gene of Salmonella enterica encodes a protein with phosphotransacetylase enzyme activity*. *Journal of bacteriology*, 2004. **186**(6): p. 1890-1892.
91. Moore, T.C. and J.C. Escalante-Semerena, *The EutQ and EutP proteins are novel acetate kinases involved in ethanolamine catabolism: physiological implications for the function of the ethanolamine metabolosome in S almonella enterica*. *Molecular microbiology*, 2016. **99**(3): p. 497-511.
92. Roof, D.M. and J.R. Roth, *Functions required for vitamin B12-dependent ethanolamine utilization in Salmonella typhimurium*. *Journal of Bacteriology*, 1989. **171**(6): p. 3316-3323.
93. Fox, K.A., et al., *Multiple posttranscriptional regulatory mechanisms partner to control ethanolamine utilization in Enterococcus faecalis*. *Proceedings of the National Academy of Sciences*, 2009. **106**(11): p. 4435-4440.
94. Mellin, J., et al., *Sequestration of a two-component response regulator by a riboswitch-regulated noncoding RNA*. *Science*, 2014. **345**(6199): p. 940-943.

95. Lundgren, B.R., et al., *Ethanolamine catabolism in Pseudomonas aeruginosa PAO1 is regulated by the enhancer-binding protein EatR (PA4021) and the alternative sigma factor RpoN*. Journal of bacteriology, 2016. **198**(17): p. 2318-2329.
96. Anderson, C.J., et al., *Ethanolamine signaling promotes Salmonella niche recognition and adaptation during infection*. PLoS pathogens, 2015. **11**(11): p. e1005278.
97. Kendall, M.M., et al., *Ethanolamine controls expression of genes encoding components involved in interkingdom signaling and virulence in enterohemorrhagic Escherichia coli O157: H7*. mBio, 2012. **3**(3): p. e00050-12.
98. Kaval, K.G., et al., *Loss of ethanolamine utilization in Enterococcus faecalis increases gastrointestinal tract colonization*. mBio, 2018. **9**(3): p. e00790-18.
99. Bertin, Y., et al., *Enterohaemorrhagic Escherichia coli gains a competitive advantage by using ethanolamine as a nitrogen source in the bovine intestinal content*. Environmental microbiology, 2011. **13**(2): p. 365-377.
100. Anast, J.M. and S. Schmitz-Esser, *The transcriptome of Listeria monocytogenes during co-cultivation with cheese rind bacteria suggests adaptation by induction of ethanolamine and 1, 2-propanediol catabolism pathway genes*. PloS one, 2020. **15**(7): p. e0233945.
101. Tirumalai, P.S., *Metabolic gene expression shift by Listeria monocytogenes in coculture biofilms*. Canadian journal of microbiology, 2015. **61**(5): p. 327-334.
102. Cortes, B.W., et al., *Transcriptome sequencing of Listeria monocytogenes reveals major gene expression changes in response to lactic acid stress exposure but a less pronounced response to oxidative stress*. Frontiers in microbiology, 2020. **10**: p. 3110.



# 2

---

## **Bacterial microcompartment-dependent 1,2-propanediol utilization stimulates anaerobic growth of *Listeria monocytogenes* EGDe**

Published as:

**Zeng, Z.**, Smid, E. J., Boeren, S., Notebaart, R. A., & Abee, T. (2019). Bacterial microcompartment-dependent 1, 2-propanediol utilization stimulates anaerobic growth of *Listeria monocytogenes* EGDe. *Frontiers in microbiology*, 10, 2660.

### Abstract

Bacterial microcompartments (BMCs) are proteinaceous organelles that optimize specific metabolic pathways referred to as metabolosomes involving transient production of toxic volatile metabolites such as aldehydes. Previous bioinformatics analysis predicted the presence of BMCs in 23 bacterial phyla including foodborne pathogens and a link with gene clusters for the utilization of host-derived substrates such as 1,2-propanediol, i.e., the Pdu cluster. Although transcriptional regulation of the Pdu cluster and its role in *Listeria monocytogenes* virulence in animal models have recently been reported, the experimental identification and the physiological role of BMCs in *L. monocytogenes* is still unexplored. Here, we ask whether BMCs could enable utilization of 1,2-propanediol (Pd) in *L. monocytogenes* under anaerobic conditions. Using *L. monocytogenes* EGDe as a model strain, we could demonstrate efficient utilization of Pd with concomitant production of 1-propanol and propionate after 24 hours of anaerobic growth, while the utilization was significantly reduced in aerobic conditions. In line with this, expression of genes encoding predicted shell proteins and the signature enzyme propanediol dehydratase is upregulated more than 20-fold in cells anaerobically grown in Pdu-induced versus non-induced control conditions. Additional proteomics analysis confirmed the presence of BMC shell proteins and Pdu enzymes in cells that show active degradation of Pd. Furthermore, using transmission electron microscopy, BMC structures have been detected in these cells linking gene expression, protein composition and BMCs to activation of the Pdu cluster in anaerobic growth of *L. monocytogenes*. Studies in defined minimal medium with Pd as an energy source showed a significant increase in cell numbers, indicating that Pdu and the predicted generation of ATP in the conversion of propionyl-phosphate to the end product propionate can support anaerobic growth of *L. monocytogenes*. Our findings may suggest a role for BMC-dependent utilization of Pd in *L. monocytogenes* growth, transmission and interaction with the human host.

## 2.1 Introduction

Cellular organelles play crucial roles in establishing physical boundaries for biological processes [1]. Although bacteria lack the classic double membrane-enclosed organelles of eukaryotes, they were found to contain semi-permeable protein compartments known as bacterial microcompartments (BMCs) [2, 3]. BMCs are self-assembling organelles that consist of the encapsulated enzymes and the semi-permeable protein shell playing important roles in metabolic pathways with volatile toxic intermediates [4]. A comparative genomic survey previously identified 23 different loci encoding up to 10 functionally distinct BMCs across 23 bacterial phyla [5]. BMCs may be involved in a range of biological conversions varying from carbon fixation [6] to degradation of specific organic compounds such as 1,2-propanediol (Pd) [7, 8] and ethanolamine [9]. BMCs are typically about 40–200 nanometers in diameter and are made of three types of shell proteins: hexamers, pseudohexamers, and pentamers [4, 10]. Hexamers and pseudohexamers are formed by the classical BMC shell proteins containing the Pf00936 domain, while pentamers are formed by the non-classical BMC shell proteins containing the Pf03319 domain [4, 5]. These shell proteins are highly conserved across different bacterial phyla allowing accurate bioinformatics analysis-based prediction of BMCs and associated functions of encapsulated enzymes. Recent evidence has been presented that targeting the encapsulated enzymes to BMCs interior involves the presence of hydrophobic  $\alpha$ -helices at the N terminus mediating the interaction with shell proteins [11–13]. Notably, the BMCs that have been characterized and that participate in the heterotrophic metabolism via short-chain aldehydes are collectively termed metabolosomes [2, 4, 11, 14]. These BMCs share a common encapsulated chemistry driven by three core enzymes: aldehyde dehydrogenase, alcohol dehydrogenase and phosphotransacylase, and their functions have been studied mostly in Gammaproteobacteria including BMCs for the utilization of Pd and ethanolamine in *Salmonella enterica* and *Escherichia coli*, and for choline metabolism in *Desulfovibrio desulfuricans* [2, 7, 9, 15]. Notably, Pd is a major end product from the anaerobic degradation of rhamnose or fucose by human intestinal microbiota, and it is thought to be an important energy source for Pd utilizing bacteria including pathogens such as *Salmonella* spp. and *L. monocytogenes* [16, 17]. BMC-dependent utilization of Pd in *S. enterica* is encoded on the genome within the Pdu cluster which includes 23 genes: *pocR*, *pduF*, *pduABCDEFGHIJKLMNPOQSTUVWX* [16, 18]. Pd is converted into propionaldehyde by coenzyme B12-dependent diol dehydratase (*pduCDE*),

followed by a conversion into 1-propanol and propionate [18]. Furthermore, BMC-dependent Pdu in *S. enterica* serovar Typhimurium was found to support its expansion in the murine large intestine [17, 19]. BMC-dependent utilization of Pd by *Listeria* species including the foodborne human pathogen *L. monocytogenes* has gained attention in recent years due to its possible role in pathogenicity [20-22]. Preliminary bioinformatics analysis indicated that the Pdu cluster in *L. monocytogenes* is mixed with genes encoding enzymes involved in vitamin B12 synthesis and ethanolamine metabolism [23, 24]. Subsequent studies on transcription regulation identified an important role for a vitamin B12-dependent riboswitch in *L. monocytogenes* [24]. Furthermore, a comparative analysis of the virulence characteristics of *L. monocytogenes* EGDe and its PduD knock-out mutant showed that deletion of *pduD* leads to faster clearance in a mouse model of infection [22]. This study suggested that Pd metabolism could contribute to competitive fitness of *L. monocytogenes* in the human gastrointestinal (GI) tract and host invasion. Interestingly, transcriptional analysis of *L. monocytogenes* H7858 grown in vacuum-packaged salmon stored at refrigeration temperature revealed activation of genes in the Pdu cluster suggesting that it can support the growth of this pathogen in specific conditions along the food chain thereby contributing to its transmission from soil to host [20]. However, no experimental evidence has been presented to confirm the synthesis of BMCs in *L. monocytogenes* and to assess their role in Pd metabolism and growth.

Here, we first use a bioinformatics approach to predict and align genes encoding putative BMC shell proteins of the genus *Listeria* and to identify the distribution of the involved Pdu cluster between *Listeria sensu stricto* and *Listeria sensu lato* clades. Using *L. monocytogenes* EGDe as a model, we present evidence for Pd and vitamin B12-induced activation of the genes in the Pdu cluster, Pd metabolism and production of BMCs using transmission electron microscopy combined with proteomics. In addition, we show that anaerobic growth of *L. monocytogenes* EGDe in defined medium is supported by BMC-dependent utilization of Pd acting as an energy source. Finally, we discuss the possible role of BMC-dependent anaerobic metabolism of Pd in *L. monocytogenes* transmission from soil to host.

## 2.2 Materials and Methods

### 2.2.1 Strains, culture conditions and growth measurements

All experiments in this study were carried out with *L. monocytogenes* EGDe and *Listeria grayi* DSM20601. *L. monocytogenes* EGDe and *L. grayi* DSM20601 were grown in Luria Broth (LB) medium and defined medium MWB [25]. LB and MWB were supplemented with Pd and/or vitamin B12 (cobalamin; B12) at final concentrations of 50 mM and 20 nM, respectively [24]. Overnight grown cells in LB with or without Pd and vitamin B12, were washed three times in PBS before inoculation into MWB. LB with 50 mM Pd and 20 nM vitamin B12 was defined as Pdu-induced condition while LB with 50 mM Pd was defined as non-induced control condition. Cultures were incubated at 30°C under aerobic (constantly shaking at 160 rpm) or anaerobic conditions (Anoxomat modified atmosphere, MART; 0% O<sub>2</sub>, 10% CO<sub>2</sub>, 5% H<sub>2</sub>, 85% N<sub>2</sub>) for up to 36 h. OD<sub>600</sub> measurements were performed every 2 h during the first 12 h of incubation, and at 24 and 36 h. Plate counting to quantify Colony Forming Units (CFUs) were performed at 0 h and 36 h for experiments performed in defined medium MWB. All growth measurements were performed in three biological replicates with three technical replicates.

### 2.2.2 Analysis of Pd metabolism using High Pressure Liquid Chromatography (HPLC)

Samples were taken from the cultures at 0, 12, 24 and 36 h. After centrifugation, the supernatant was collected for the HPLC measurements of Pd, 1-propanol and propionate. The experiment was performed twice with three technical replicates per experiment. Additionally, the standard curves of Pd, 1-propanol and propionate were measured in the concentration range of 0.1 mM, 1 mM, 10 mM, 50 mM and 100 mM. HPLC was performed using an Ultimate 3000 HPLC (Dionex) equipped with an RI-101 refractive index detector (Shodex, Kawasaki, Japan), an autosampler and an ion-exclusion Aminex HPX-87H column (7.8 × 300 mm) with a guard column (Bio-Rad, Hercules, CA). As the mobile phase 5 mM H<sub>2</sub>SO<sub>4</sub> was used at a flow rate of 0.6 mL/min, and the column was kept at 40°C. The total run time was 30 min and the injection volume was 10 µL.

### 2.2.3 RNA isolation, cDNA synthesis and Quantitative Real-Time PCR (qRT-PCR)

*L. monocytogenes* cultures were grown anaerobically at 30°C in Pdu-induced or non-induced control conditions. Samples for RNA extraction were taken at 8 h of incubation (late exponential phase). RNA isolation was performed with RNeasy

Mini Kit (Qiagen). cDNA synthesis was performed with the Superscript III inverse transcriptase (Invitrogen). Supplementary Information (SI) Table 1 lists all primers used in this study. The primers were designed with the Primer3 online software, and their specificity was checked by gel electrophoresis of the PCR products. Primer efficiency was checked by the standard curve method. The efficiencies of all primers ranged from 1.99 to 1.89 ( $R^2$  above 0.99). The qRT-PCR was performed using SYBRgreen PCR MasterMix (Applied Biosystems) in a Bio-Rad CFX96 RT-PCR as described before[26]. Relative expression of the target genes in Pdu-induced versus non-induced control conditions was analysed with the  $\Delta\Delta C_t$  method, and expression levels were normalized with the reference gene *rpoB* [24]. Samples were evaluated in triplicate and results represent three independent experiments. Statistically significant differences were calculated by using log2 transformed values evaluated by paired T test.

### 2.2.4 Transmission Electron Microscopy (TEM)

*L. monocytogenes* cultures were grown anaerobically at 30 °C in Pdu-induced or non-induced control conditions. Samples were collected at 12 h of incubation (early stationary phase) About 10  $\mu$ g dry cells were fixed for 2 h in 2.5% (v/v) glutaraldehyde in 0.1 M sodium cacodylate buffer (pH 7.2). After rinsing in the same buffer, a post-fixation was done in 1% (w/v)  $OsO_4$  and 2.5% (w/v)  $K_2Cr_2O_7$  for 1 h at room temperature. The samples were dehydrated by ethanol and were then embedded in resin overnight at 70°C. Thin sections (<100 nm) of polymerized resin samples were obtained with microtomes. After staining with 2% (w/v) aqueous uranyl acetate, the samples were analysed with a Jeol 1400 plus TEM.

### 2.2.5 Proteomics

*L. monocytogenes* cultures were anaerobically grown at 30 °C in Pdu-induced and in non-induced control conditions. Samples were collected at 12 h of incubation and then washed twice with 100 mM Tris (pH 8). About 10 mg wet weight cells in 100  $\mu$ l 100 mM Tris was sonicated for 30s twice to lyse the cells. Samples were prepared according the filter assisted sample preparation protocol (FASP) [27] with the following steps: reduction with 15 mM dithiothreitol, alkylation with 20 mM acrylamide, and digestion with sequencing grade trypsin overnight. Each prepared peptide sample was analysed by injecting (18  $\mu$ l) into a nanoLC-MS/MS (Thermo nLC1000 connected to a LTQ-Orbitrap XL) as described previously [28, 29]. LCMS data with all MS/MS spectra were analysed with the MaxQuant quantitative proteomics software package [30] as described before [28, 31]. A protein database with the protein sequences of *L. monocytogenes* EGDe (ID:

UP000000817) was downloaded from UniProt. Filtering and further bioinformatics and statistical analysis of the MaxQuant ProteinGroups file were performed with Perseus [32]. Reverse hits and contaminants were filtered out. Protein groups were filtered to contain minimally 2 peptides for protein identification of which at least one is unique and at least one is unmodified. Also, each group (Pdu-induced and non-induced control) required three valid values in at least one of the two experimental groups. The volcano plot was prepared based on the student's T-test difference of Pdu-induced/non-induced control.

### 2.2.6 Bioinformatics analysis

#### *Comparative genomics of BMC shell protein domains and the Pdu cluster*

The Hidden Markov Models (HMMs) of two BMC shell protein domains listed as Pf00936 and Pf03319 were retrieved from the Pfam database to predict BMC shell proteins in *Listeria* species. The genus *Listeria* is currently comprised of 17 species [33]. Shell proteins were predicted across 17 *Listeria* species by a HMM search using the hmmer package and a local protein database of *Listeria* genomes [34]. All hits with an e-value less than or equal to 1e-05 that correspond to a genomic record from Genbank, RefSeq, EMBL, or DDBJ databases were accepted as BMC shell protein homologs.

To determine which genes from the Pdu cluster are present and which ones are absent in 17 *Listeria* species, we performed BLASTp using the MultiGeneBlast local programme [35]. In order to obtain the phylogeny of the *Listeria* species, we used a maximum likelihood phylogenetic tree that is based on a concatenated amino acid sequence of 325 single copy genes present in all *Listeria* species [36]. The heat map visualizing the presence/absence of the Pdu proteins across the tree has been generated with Heatmapper [33] using the similarity values of the protein sequences (expressed in %).

#### *Secondary structure of N terminal peptides*

The N terminal secondary structures of all Pdu genes were determined by a neural network secondary structure prediction called Jpred 4 [37]. The input to the Jpred 4 online server (<http://www.compbio.dundee.ac.uk/jpred4/>), were the 40 N terminal amino acids of each protein. Jnetconf: confidence estimation for the prediction with high scores indicating high confidence. Jnetsol25: solvent accessibility, where B means buried and '-' means non-buried at 25% cut-off.



presented in black and non-Pdu genes (others) presented in grey. See SI Table 3 for additional information of the genes in the Pdu cluster. **B)** Phylogenetic tree and corresponding similarity heat map of the *pdu* cluster in 17 *Listeria* species; orange lines represent *Listeria sensu stricto*, black lines represent *Listeria sensu lato* species. Values on branches represent bootstrap values (>70 %) based on 250 bootstrap replicates; Bar, 0.1 amino acid substitutions per site. Protein similarity percentages (%) of the *pdu* genes are indicated by blue colour intensity according to the scale presented to the right. Species with their names in bold are used in subsequent experiments. Modified from Weller et al.

Next, we analysed the genomes of 17 *Listeria* species and the phylogenetic tree was modified from Weller et al. [36] to include *Listeria sensu stricto* and *Listeria sensu lato* (Figure 1B). The genome similarity heat map illustrates the evolutionary dynamics of the *pdu* cluster and reveals that except for the loss of *pduJ* in *L. marthii* FSL S4-120, the *pdu* cluster is highly conserved in *Listeria sensu stricto* species but absent in *Listeria sensu lato* species, in line with previous studies of *Listeria sensu stricto* and *Listeria sensu lato* species [22, 23]. Furthermore, the presence of two essential types of BMC shell proteins with Pf00936 and Pf03319 domains in the *pdu* cluster of *Listeria sensu stricto* species indicates that all these species including *L. monocytogenes* contain the genetic information to produce BMCs and to metabolize Pd.

### 2.3.2 Impact of Pd on growth

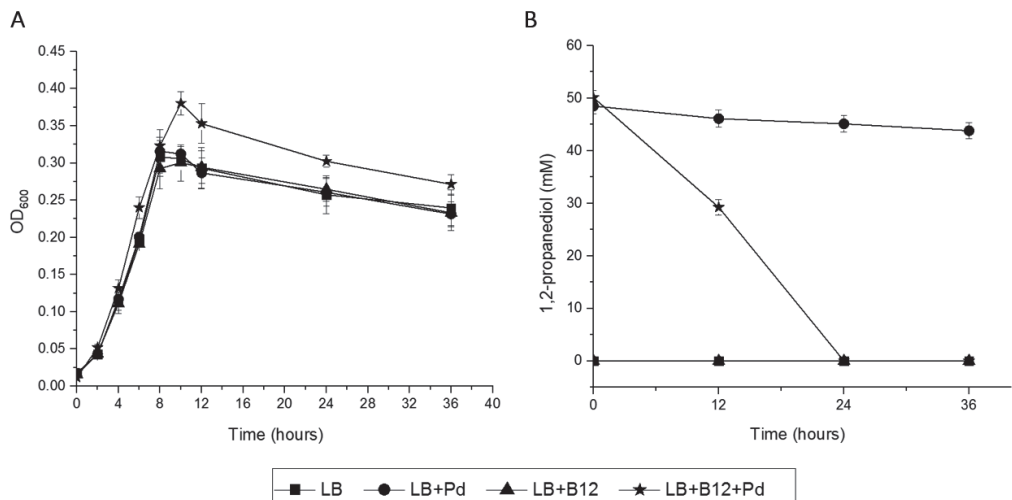


**Figure 2. Anaerobic growth and utilization of Pd in *L. monocytogenes* EGDe**

**A)** Impact of Pd and/or vitamin B12 on anaerobic growth of *L. monocytogenes* EGDe in LB medium. Symbols represent different growth conditions; Luria broth without (LB) and with added Pd (LB+Pd), with added vitamin B12 (LB+B12), and with both compounds added (LB+Pd+B12). ANOVA with post-hoc Tukey test, LB+Pd+B12 versus LB+Pd,  $p < 0.001$  in 10h, 24h and 36h. Results from three

independent experiments with three technical repeats expressed as mean  $\pm$  s.e.m. **B)** Utilization of Pd by *L. monocytogenes* EGDe. Symbols used are the same as in Figure 2A. Error bars in A and B indicate three independent experiments with three technical repeats expressed as mean  $\pm$  s.e.m.

We first examined the impact of Pd as an additional energy source during anaerobic and aerobic growth of *L. monocytogenes* EGDe in LB medium using *pdu*-negative *L. grayi* DSM20601 as a control. The culture medium also includes vitamin B12 as it is required for activation of the *pdu* cluster in *L. monocytogenes* [24] and to act as a cofactor [38]. In anaerobic conditions, *L. monocytogenes* EGDe grown in *pdu*-induced condition LB medium with Pd and B12 reached significantly higher OD values compared to that obtained in *pdu* non-induced condition LB medium with Pd (Figure 2A). HPLC analysis revealed that *L. monocytogenes* EGDe grown in LB medium with Pd and B12 fully utilized 50 mM Pd after 24 h of anaerobic incubation, whereas no utilization was observed in the other conditions (Figure 2B). Notably, in aerobic shaken EGDe cultures in LB with added Pd and B12, no growth stimulation was observed, which is in line with the HPLC analysis that revealed no utilization of Pd (SI Figure 1). As expected, *pdu*-negative *L. grayi* DSM20601 showed no stimulation of growth and no utilization of Pd in both anaerobic and aerobic conditions (SI Figure 2 and SI Figure 3).

Next, we addressed the question whether Pd can act as an energy source in *L. monocytogenes*. To this end, we incubated *L. monocytogenes* EGDe in MWB defined medium with 50 mM Pd with and without 20 nM vitamin B12, representing *pdu*-induced and non-induced control conditions, respectively. As shown in SI Figure 4, *pdu*-induced cells containing BMCs support growth with concomitant production of 1-propanol and propionate, while non-induced control cells without BMCs showed no utilization of Pd and no increased growth. We therefore conclude that activation of the *pdu* cluster supports growth of *L. monocytogenes* EGDe with Pd as an energy source.

### 2.3.3 Expression analysis of selected genes in the *pdu* cluster, Pd metabolism and visualization of BMCs

Utilization of Pd by *pdu*-induced cells and non-induced control cells has been analysed by HPLC and revealed the production of propionate and 1-propanol (Figure 3A). After 24 hours anaerobic incubation, *pdu*-induced *L. monocytogenes* EGDe cells produced  $6.8 \pm 0.69$  mM 1-propanol and  $6.2 \pm 0.64$  mM propionate, whereas both compounds were not produced by the non-induced control cells (Figure 3A). Production of these two compounds following degradation of Pd was

also previously described in *L. innocua* [39]. Gene expression analysis using qRT-PCR indicated enhanced transcript levels of the selected *L. monocytogenes* EGDe *pduSTUABDQL* genes in *pdu-induced* cells compared to non-induced control cells. The *pduS* gene is the starting gene of the Pdu cluster, *pduTUAB* encode four of the seven predicted BMCs shell proteins, *pduD* encodes the subunit of B12-dependent diol dehydratase that converts Pd into propionaldehyde, *pduQ* encodes propanol dehydrogenase that converts propionaldehyde into 1-propanol, and *pduL* encodes phosphotransacylase, that converts propionyl-CoA into propionyl-phosphate (Figure 1A). Figure 3B shows that the selected *pdu* genes were upregulated 23 to 91-fold in *pdu-induced* cells compared to non-induced control cells. In order to study whether *pdu* gene cluster expression is also reflected at the proteome level, we conducted a proteomics analysis. Analysis of the complete list of identified proteins (SI Table 2) and subsequent student's T-test difference scores of *pdu-induced* compared to *pdu* non-induced control cells, resulted in a selection of 539 proteins shown in a volcano plot (Figure 3C), with 79 proteins upregulated more than two times in *pdu-induced* cells. Among these 79 upregulated proteins, 14 proteins are encoded in the *pdu* cluster, i.e., PduSTABCDEGKJLOPQ (Figure 3C), and with PduN present, but not significantly different from non-induced control cells. Clearly, the increased expression of proteins of the *pdu* cluster strongly suggests that the catabolism of Pd is correlated to activation of the *pdu* cluster including the synthesis of BMC shell proteins. Additional analysis of the set of proteins with more than 2-fold higher protein expression in *pdu-induced* cells, revealed a range of stress defence proteins including MntA and MntH, components of the divalent metal ion (manganese, Mn) transporter (involved in cytoplasmic transition metal homeostasis and coping with redox stress), LMO2369, general stress protein 13 (cytosolic small ribosomal subunit associated chaperone linked to a range of stresses including oxidative stress defense), UvrABC system protein C (DNA helicase, linked to DNA damage-induced nucleotide excision repair), ATP-dependent DNA helicase (involved in double-strand break repair via homologous recombination), CshB (DEAD-box ATP-dependent RNA helicase linked to oxidative stress response), GbuA and OpuCA (binding proteins of GbuABC and OpuABC ATP-dependent betaine/carnitine uptake systems involved in osmotic stress defence [40-46]. The significant induction of stress defence and DNA damage repair proteins in *pdu-induced L. monocytogenes* cells has not been studied and reported before, but is in line with the previously reported DNA and cellular damage of *S. enterica* cells exposed to Pd [8]. Creation of BMCs with key

metabolic turnover steps of *pdu* encapsulated, thereby creating a protection against the toxic intermediate propionaldehyde, is proposed to occur in a stepwise manner [2, 17]. Our observation may suggest that BMC assembly co-occurs with activation of stress defence proteins, possibly to respond to toxic intermediates and redox stress before BMC production is completed.

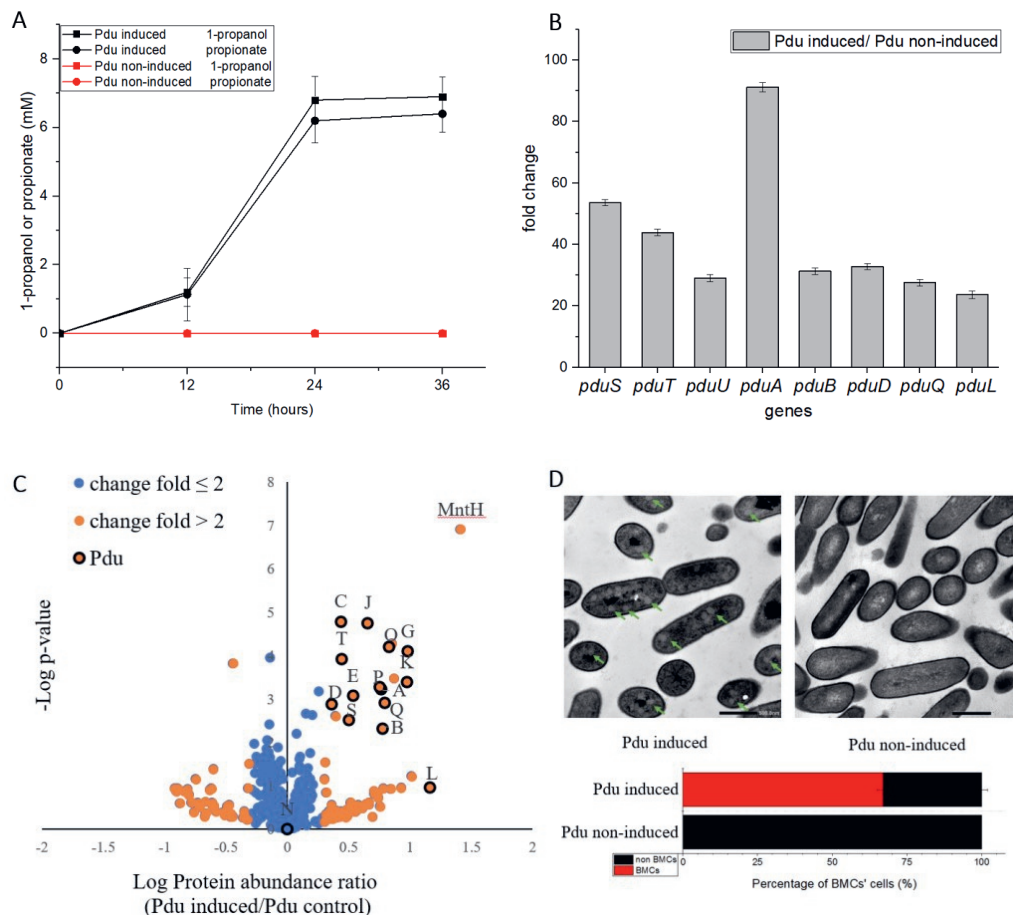


**Figure 3. Comparative analysis of product formation (A), gene expression (B), proteomics (C), and presence of BMCs (D) in *pdu*-induced and non-induced control cells.**

**A**) Production of 1-propanol and propionate in *L. monocytogenes* EGDe *pdu*-induced (in black) and non-induced control cells (in red). Results from three independent experiments with three technical repeats expressed as mean  $\pm$  s.e.m. **B**) Transcription of *pduSTUABDQL* genes. Fold change of selected genes in *pdu*-induced cells versus non-induced control cells. Results from two independent experiments with three technical repeats expressed as mean  $\pm$  s.e.m. **C**) Proteomic volcano plot of *pdu*-induced cells compared to non-induced control cells; Fold change  $\leq 2$  in blue, Fold change  $> 2$  in orange, proteins in the Pdu cluster are indicated by their letter code and black circle. MntH, divalent metal cation transporter. **D**) TEM visualization of BMCs in *pdu*-induced (left) and non-induced control

cells (right) and percentage of BMC-positive cells. Green arrows point to typical BMC structures, with the black scale bars representing 500 nm.

To further confirm the presence of BMCs in *pdu*-induced cells, we used TEM and compared thin sections of both *pdu*-induced and non-induced control cells (Fig 3D). *pdu*-induced cells clearly contain BMC-like structures with an approximate diameter of 60 to 80 nm, which are not present in non-induced control cells. Notably, the identified structures strongly resemble TEM pictures of BMCs in *S. enterica* and *E. coli* [18, 47]. Taken the metabolic, transcriptomic, proteomic and TEM data together, we conclude that the cytosolic BMC-like structures in *L. monocytogenes* EGDe are involved in Pd utilization under anaerobic conditions. From the analysis of 400 cells in *pdu*-induced samples, 268 cells (67%) contained one or more BMCs, whereas no or partial BMC structures could be observed in the other 33% of cells. This observation highlights the need for further studies at subpopulation level to address the question to what extent activation of stress defence and DNA damage repair are linked to initiation and progression of *pdu* BMC assembly and function.

### **2.3.4 Prediction of N terminal encapsulation peptides and the model depicting BMC-dependent conversions in *L. monocytogenes pdu*.**

In order to provide further evidence for the putative location of Pd enzyme-mediated conversions in *L. monocytogenes pdu*-associated BMCs, a comparative analysis of the domains of all the proteins in the *pdu* cluster has been performed, with a special focus on domains mimicking N terminal encapsulation peptides (EPs). We indeed identified a specific hydrophobic  $\alpha$ -helix in the N terminus of the encapsulated enzyme PduP, similar to that of the previously described encapsulated protein PduP in *S. enterica* [12]. Based on this knowledge, we predicted the secondary structure of the 40 amino acids sequence in the N terminal domains of all *L. monocytogenes* EGDe Pdu proteins. In addition to PduP, PduD and PduL were also found to contain the hydrophobic N-terminal  $\alpha$ -helical EP domain (Figure 4A). Interestingly, PduD has been previously confirmed as an encapsulated enzyme in *S. enterica* BMCs [12, 13]. The proposed encapsulation of PduL that converts propionyl-CoA into propionyl-phosphate would support efficient recycling of CoA inside the BMC. Based on our analysis, we propose that the PduDPL enzymes are encapsulated in *L. monocytogenes* EGDe *pdu*-associated BMCs (Figure 4B, and discussion).

## 2.3 Discussion

The proposed model for BMC-dependent *pdu* metabolism in *L. monocytogenes* combines bioinformatics analysis, metabolic phenotyping, transcriptional analysis, proteomics, TEM visualization and experimental verification in defined medium.

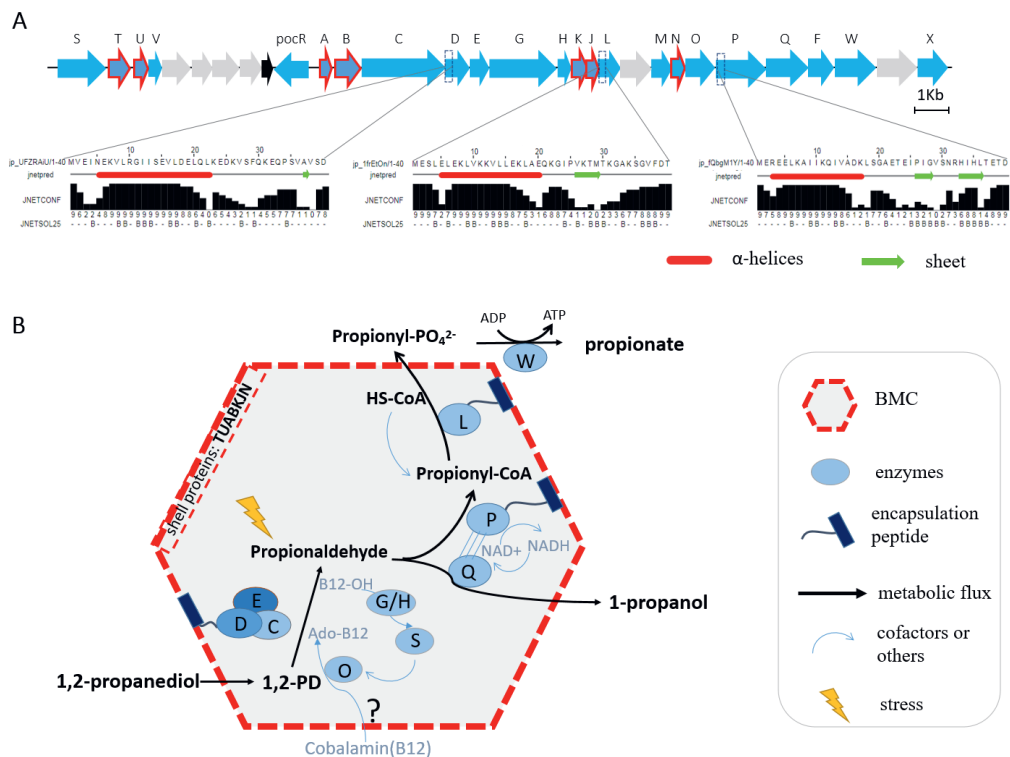


**Figure 4. Prediction of N terminal encapsulation peptides (A) and the corresponding model of BMC-dependent metabolism of Pd catabolism in *Listeria sensu stricto* (B).**

**A)** Pdu enzymes and corresponding reactions, with the predicted N-terminal encapsulation peptides of PduD, PduP and PduL indicated, with alpha helices marked as red tubes and sheets as green arrows. Jnetconf: confidence estimation for the prediction with high scores indicating high confidence. Jnetsol25: solvent accessibility, where B means buried and '-' means non-buried at 25% cut-off. **B)** Model of the proposed BMC-dependent Pd metabolism in *Listeria sensu stricto*. PduCDE, B12-dependent diol dehydratase; PduP, CoA-dependent propionaldehyde dehydrogenase; PduGH, diol dehydratase reactivase; PduO, corrinoid adenosyltransferase; PduS, cobalamin reductase; PduL, phosphate propanoyltransferase; PduW, propionate kinase; PduQ, propanol dehydrogenase.

As illustrated in Figure 4B, the catabolism of Pd starts with the conversion of Pd to propionaldehyde by vitamin B12-dependent diol dehydratase PduCDE [8, 16, 39]. The toxic propionaldehyde is then converted to propionate by the enzyme CoA-dependent propionaldehyde dehydrogenase PduP, followed by action of

phosphate propanoyltransferase PduL, and propionate kinase PduW located in the cytoplasm, resulting in the end product propionate and the production of ATP. The other end product is produced following conversion of propionaldehyde by propanol dehydrogenase PduQ into 1-propanol. PduQ is thought to be inside BMCs because of the potential association with PduP [48]. The diol dehydratase reactivase PduGH, corrinoid adenosyltransferase PduO and cobalamin reductase PduS are linked to the supply and recycling of vitamin B12. Predicted shell proteins PduTUABKJ and PduN form the hexamer and pentamer building units of the icosahedron shaped BMCs for *pdu* catabolism shielding the cell constituents against toxicity of the volatile intermediate propionaldehyde and supporting efficient recycling of the CoA cofactor pool. Based on our *pdu* metabolism studies, gene expression analysis and proteomics data, and in line with their role in Pdu enzyme activity, we locate the vitamin B12 recycling proteins PduGHOS inside the *L. monocytogenes* BMC. It should be noted that the exact mechanisms underlying the entry of vitamin B12 and the encapsulation of vitamin B12 recycling proteins PduGHOS remain to be elucidated [2].

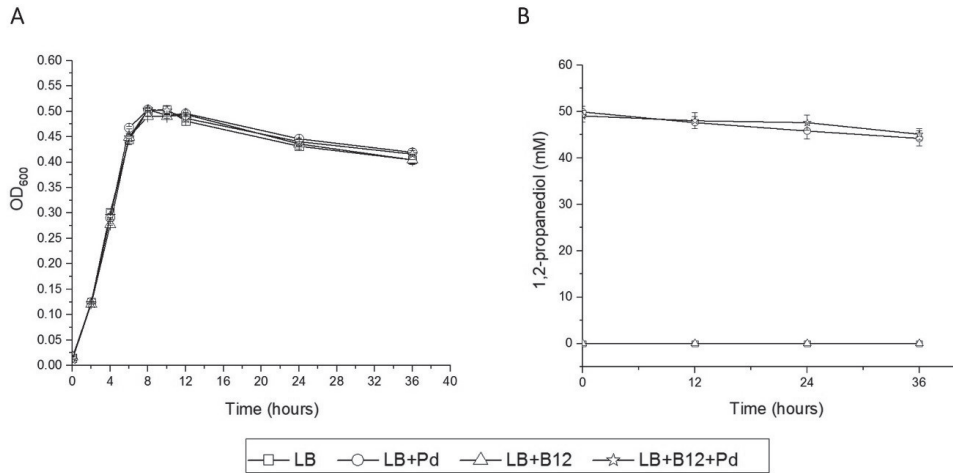
According to the alignment of *pdu* clusters in 17 *Listeria* species and in line with previous genome comparisons [22, 23], we propose that BMC-dependent *pdu* clusters, except for the loss of *pduJ* in *Listeria marthii* FSL S4-120, are present in *Listeria sensu stricto* but absent in *Listeria sensu lato*. Considering the highly conserved *pdu* cluster in *Listeria sensu stricto* and the reported degradation of Pd in another *Listeria sensu stricto* species, *L. innocua* [39], it is conceivable that the presented BMC-dependent *pdu* model also fits Pd metabolism in other *Listeria sensu stricto* species.

Since Pd can be present in processed foods and in the human gut, it is assumed that *pdu* BMCs belong to a subset of BMCs that contribute to the fitness and virulence of some pathogenic bacteria including *S. enterica* and *L. monocytogenes* [17, 19, 22, 38]. The possible contribution of *pdu* BMCs to the pathogenicity of *L. monocytogenes* is however still poorly understood, but a recent study using *L. monocytogenes* EGDe and its PduD knock-out mutant, showed that deletion of *pduD* leads to faster clearance in a mouse model of infection [22]. Notably, our studies demonstrate that Pd utilization indeed stimulates the anaerobic growth of *L. monocytogenes*. Furthermore, studies in defined minimal medium with Pd as an energy source show that the predicted generation of ATP in the conversion of propionyl-phosphate to the end product propionate can support anaerobic growth of *L. monocytogenes*. This suggests

that BMC-dependent *pdu* contributes to competitive fitness of *L. monocytogenes* in the human GI tract and host invasion. Whether BMC-dependent *pdu* contributes to growth of this pathogen in specific conditions along the food chain, as suggested by Tang et al. based on the activation of *pdu* cluster genes in *L. monocytogenes* H7858 grown in vacuum-packaged salmon stored at refrigeration temperature [20], remains to be established.

Strikingly, the impact of *pdu* activation and the timing of BMC assembly on cell physiology and fitness has gained very little attention, although optimization of the process is required to enable enhanced substrate flux and efficient toxicity mitigation [17]. Indeed, our proteomics data reveal significant activation of stress defence proteins, including general stress sigma factor Sigma B-controlled genes *gbuA* and *opuC* encoding transporter binding proteins involved in the uptake of compatible solutes (betaine/carnitine) that have a role in cell turgor homeostasis, but also in maintenance of protein/enzyme and membrane functionality [41, 45, 49, 50], and *uvrAB*, part of the *L. monocytogenes* SOS response, contributing to protection and/or DNA damage repair in the cells [41]. Notably, Liu et al. [51] identified new Sigma B-dependent functions in *L. monocytogenes* including the regulation of genes involved in *pdu*. Combined with our observations, and the previous reported role for a vitamin B12-dependent riboswitch [24], this could point to an integration of signals and responses enabling adequate and timely assembly of *L. monocytogenes pdu* BMCs. Obviously, further work is needed to understand BMC function at population and systems-level, especially considering the observed population heterogeneity in our studies, with an approximate 67% and 33% of BMC positive versus BMC-negative cells. Such future studies should address to what level the activation of stress defence and DNA damage repair are linked to *pdu* BMC assembly and function, and how this affects the role of *pdu* BMCs in *L. monocytogenes* transmission and interaction with the human host.

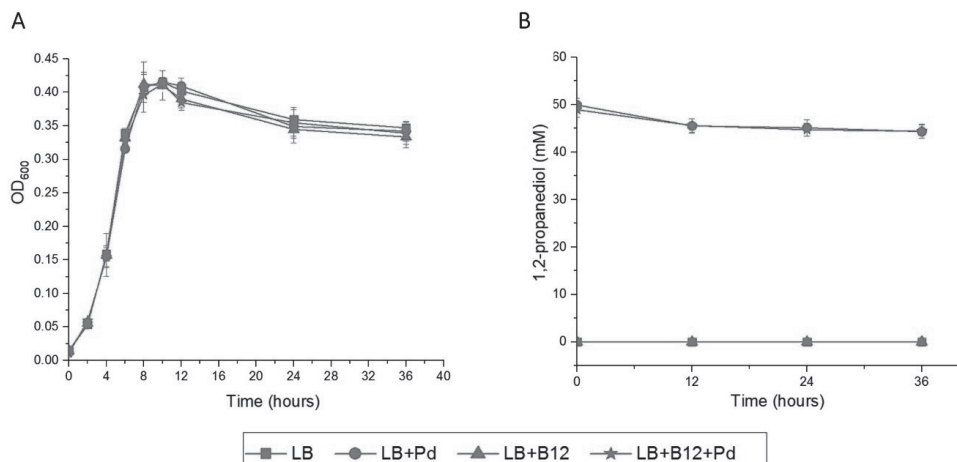
## 2.4 Supplementary Materials



**SI Figure 1. 1,2-propanediol is not utilized and does not support growth of *L. monocytogenes* EGDe in aerobic conditions**

**A)** Impact of Pd and/or B12 on aerobic growth of *L. monocytogenes* EGDe in LB medium. Symbols represent different growth conditions; Luria broth without (LB) and with added 1,2-propanediol (LB+Pd), with added vitamin B12 (LB+B12), and with both compounds added (LB+Pd+B12). ANOVA with Tukey's post-test, no significant differences,  $p > 0.05$ . Results from three independent experiments with three technical repeats expressed as mean  $\pm$  s.e.m.

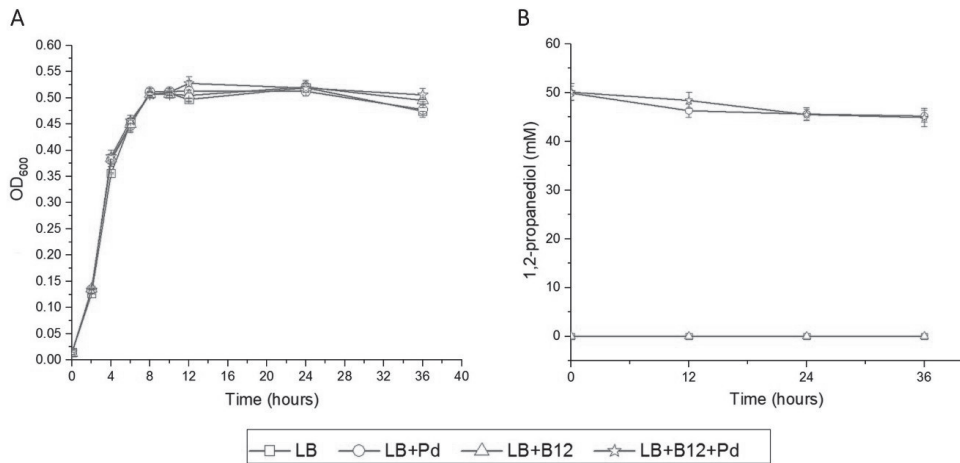
**B)** Utilization of 1,2-propanediol by *L. monocytogenes* EGDe during aerobic growth. Results from three independent experiments with three technical repeats are expressed as mean  $\pm$  s.e.m.



**SI Figure 2. 1,2-propanediol is not utilized and does not support growth of *pdu*-negative *L. grayi* DSM20601 in anaerobic conditions**

**A)** Impact of Pd and/or B12 on anaerobic growth of *L. grayi* DSM20601 in LB medium. Symbols represent different growth conditions; Luria broth without (LB) and with added 1,2-propanediol (LB+Pd), with added vitamin B12 (LB+B12), and with both compounds added (LB+Pd+B12). ANOVA with Tukey's post-test, no significant differences,  $p > 0.05$ . Results from three independent experiments with three technical repeats expressed as mean  $\pm$  s.e.m.

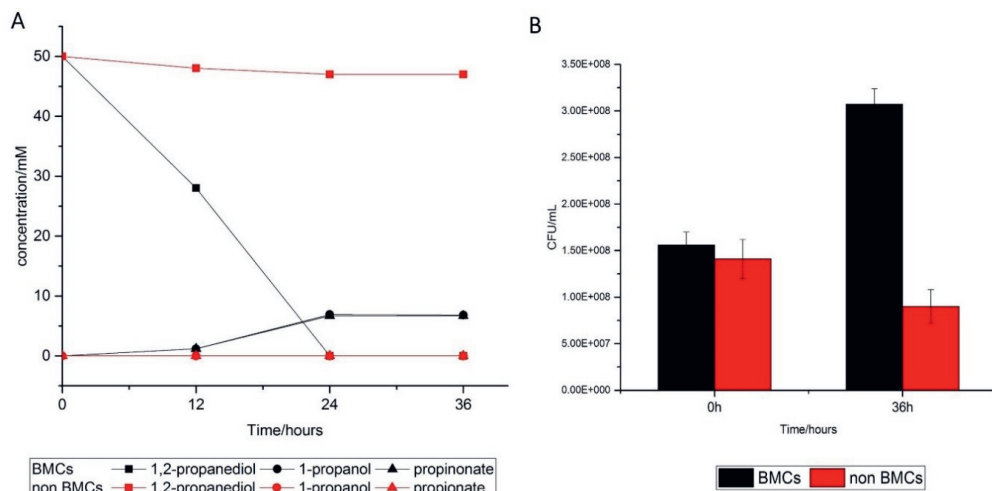
**B)** Utilization of 1,2-propanediol by *L. grayi* DSM20601 during anaerobic growth. Results from three independent experiments with three technical repeats are expressed as mean  $\pm$  s.e.m.



**SI Figure 3. 1,2-propanediol is not utilized and does not support growth of *pdu*-negative *L. grayi* DSM20601 in aerobic conditions**

**A)** Impact of Pd and/or B12 on aerobic growth of *L. grayi* DSM20601 in LB medium. Symbols represent different growth conditions; Luria broth without (LB) and with added 1,2-propanediol (LB+Pd), with added vitamin B12 (LB+B12), and with both compounds added (LB+Pd+B12). ANOVA with Tukey's post-test, no significant differences,  $p > 0.05$ . Results from three independent experiments with three technical repeats expressed as mean  $\pm$  s.e.m.

**B)** Utilisation of 1,2-propanediol by *L. grayi* DSM20601 during aerobic growth. Results from three independent experiments with three technical repeats are expressed as mean  $\pm$  s.e.m.



**SI Figure 4. 1,2-propanediol utilization and product formation (A) and impact on CFUs of *L. monocytogenes* EGDe (B) in MWB defined medium in anaerobic conditions**

Utilization of 1,2-propanediol (squares), production of 1-propanol (circles) and production of propionate (triangles); *pdu* induced (in black) and *pdu* control cells (in red). Results from three independent experiments with three technical repeats are expressed as mean  $\pm$  s.e.m BMCs and non BMCs represent *pdu*-induced cells with BMCs present, and non-induced control cells without BMCs, respectively; indicated p value from two-sided T-test.

SI Table 1 Primers used for RT-PCR

Primer	Sequences (5'-3')
RpoB_F	GCGAACATGCAACGTCAAGCAGTA
RpoB_R	ATGTTTGGCAGTTACAGCAGCACC
PduS_F	GCGGCATTCCACTAATGGTT
PduS_R	TGCCGCTGCTAAACAACTT
PduT_F	GCGGTCGATACGATGCTAAA
PduT_R	TCAGACACACGTGGAATCAC
PduU_F	TTAATCGCCAATCCGAACCG
PduU_R	AAAGCCAATTTCGTACGTCACC
PduA_F	CCGCTGACGCTATGGTTAAA
PduA_R	ATCAGTATGCGGACGAGGAA
PduB_F	GTGAAACGCGCAGTAGAAGT
PduB_R	GCTGGAGCACCAACCATAAG
PduD_F	CGTTGTCCGTGTATTCCGTT
PduD_R	TAGTGGTGCTTTCGGAATA
PduQ_F	TGAGGCAGGCAAAATCCAAC
PduQ_R	TGTAATAACGGTTGCGGCTG
PduW_F	ACGAGCAATCAATGACCACG
PduW_R	CAGTGGTGCAAGGTTTGTC
PduL_F	GTGACCTATCTCAACCGGGT
PduL_R	GTCTCCACTTTCGCGAACTG

Note: F: Forward, R: Reverse

SI Table 2 Protein profiling of *pdu-induced* compared with non-induced *L. monocytogenes* EGDe in. (Only list the top 100 rows, the full table with 539 rows was online in bellowing link)

Protein IDs	Gene	Protein	-Log p-value (Pos/Neg)	Log Protein abundance ratio (Pos/Neg)		
		<b>Pdu and selected stress defence / damage repair proteins highlighted</b>		change fold $\leq 2$	change fold $> 2$	Pdu
Q8Y773	<b>mntH</b>	<b>Divalent metal cation transporter MntH</b>	1.412057241	6.911140637	6.911140637	
Q8Y7V9	<b>Lmo1160 PduL</b>	<b>Phosphate propanoyltransferase</b>	1.16380628	0.95715462	0.95715462	0.95715462
Q8Y7V8	Lmo1161 EutJ	Lmo1161 protein	1.013724963	1.218738113	1.218738113	
Q8Y7W3	<b>Lmo1156 PduG</b>	<b>Lmo1156 protein</b>	0.982607841	4.1034891	4.1034891	4.1034891
Q8Y7W1	<b>Lmo1158 PduK</b>	<b>Lmo1158 protein</b>	0.974250793	3.392154265	3.392154265	3.392154265
Q8Y4R5	<b>Lmo2369</b>	<b>Lmo2369 protein general stress protein 13</b>	0.92863814	0.948567941	0.948567941	
Q8Y8R6	nifJ	Pyruvate-flavodoxin oxidoreductase	0.8725516	3.473027877	3.473027877	
Q8Y7V1	ackA2	Acetate kinase 2	0.854615211	4.276353662	4.276353662	
Q8Y3M5	<b>mnmg</b>	<b>tRNA uridine 5-carboxymethylaminomethyl modification enzyme MnmG</b>	0.844640414	0.92420237	0.92420237	
Q8Y7V5	<b>Lmo1164 PduO</b>	<b>Hyghly similar to Salmonella enterica PduO protein</b>	0.82618173	4.205881273	4.205881273	4.205881273

## Chapter 2

Q8Y7V3	<b>Lmo1166 PduQ</b>	<b>Lmo1166 protein</b>	0.79635032	2.909608039	2.909608039	2.909608039
P0DJL9	dat	D-alanine aminotransferase	0.782444477	0.934677841	0.934677841	
Q8Y7W7	<b>Lmo1152 PduB</b>	<b>Lmo1152 protein</b>	0.774747372	2.311270065	2.311270065	2.311270065
Q8Y7W8	<b>Lmo1151 PduA</b>	<b>Lmo1151 protein</b>	0.762000084	3.220437429	3.220437429	3.220437429
Q8Y7P0	<b>uvrC</b>	<b>UvrABC system protein C</b>	0.756868362	0.517164966	0.517164966	
Q8Y7V4	<b>Lmo1165 PduP</b>	Lmo1165 protein	0.750944455	3.272963367	3.272963367	3.272963367
Q8Y653	<b>mntA</b>	<b>Manganese-binding lipoprotein MntA</b>	0.741460482	0.719932264	0.719932264	
Q7AP63	lmo1467	Lmo1467 protein	0.735934099	0.822004318	0.822004318	
P66144	rpmB	50S ribosomal protein L28	0.711361567	0.807528871	0.807528871	
Q8Y8T0	lmo0814	Lmo0814 protein	0.707129637	0.877600239	0.877600239	
Q8Y9H5	lmo0553	Lmo0553 protein	0.696485996	0.278397109	0.278397109	
Q8Y7N3	lmo1241	Lmo1241 protein	0.667309602	0.612350345	0.612350345	
Q8Y7I9	luxS	S-ribosylhomocysteine lyase	0.66616869	0.560169045	0.560169045	
Q8Y7W0	<b>Lmo1159 PduJ</b>	<b>Lmo1159 protein</b>	0.65601031	4.750827591	4.750827591	4.750827591
Q8Y746	lmo1466	Lmo1466 protein	0.644208749	0.577445149	0.577445149	
Q8Y8K3	lmo0898	Lmo0898 protein	0.612793763	0.480655527	0.480655527	
Q92F34	lmo0241	Lmo0241 protein	0.583139261	0.525254458	0.525254458	
Q8Y8P1	ddl	D-alanine--D-alanine ligase	0.577791691	0.556986165	0.556986165	
Q8YAF6	lmo0170	Lmo0170 protein	0.568366528	0.429401309	0.429401309	
Q8Y6S4	lmo1609	Lmo1609 protein	0.556457678	0.434412639	0.434412639	
P67288	lmo1306	UPF0154 protein lmo1306	0.554160595	0.398844075	0.398844075	
Q8Y6T8	ezrA	Septation ring formation regulator EzrA	0.552096049	0.419686534	0.419686534	
Q8Y776	murB	UDP-N-acetylenolpyruvoylglucosamine reductase	0.546773593	0.495814902	0.495814902	
Q8Y7W4	<b>Lmo1155 PduE</b>	<b>Lmo1155 protein</b>	0.535548846	3.077296858	3.077296858	3.077296858
Q8Y3Y6	tmk	Thymidylate kinase	0.516982079	0.611843181	0.611843181	
Q8Y7Q5	lmo1217	Lmo1217 protein	0.503266493	0.362227909	0.362227909	
Q8Y7X7	<b>Lmo1142 PduS</b>	<b>Lmo1142 protein</b>	0.502383232	2.520463929	2.520463929	2.520463929
Q8Y5W6	cmk	Cytidylate kinase	0.501342614	0.41055257	0.41055257	
Q8Y7D2	lmo1351	Lmo1351 protein	0.501260281	0.428354912	0.428354912	
Q7AP76	<b>gbuA</b>	<b>GbuA protein</b>	0.495570819	0.393127216	0.393127216	
Q8Y8T3	lmo0811	Lmo0811 protein	0.493961493	0.345163859	0.345163859	
Q7AP53	lmo2193	Lmo2193 protein	0.490475019	0.305791557	0.305791557	
Q8Y826	lmo1092	Nicotinate phosphoribosyltransferase	0.488168875	0.406150191	0.406150191	
Q8Y892	lmo1022	Lmo1022 protein	0.484237989	0.447591114	0.447591114	
Q8Y637	lmo1863	DegV domain-containing protein lmo1863	0.480302652	0.273199047	0.273199047	
Q8Y6I5	lmo1699	Lmo1699 protein	0.475537459	0.290144276	0.290144276	
Q8YAT6	lmo0027	Lmo0027 protein	0.457876682	0.304843948	0.304843948	
Q8Y834	lmo1084	dTDP-4-dehydroorhamn e reductase	0.456644217	0.340909311	0.340909311	
Q8Y7X6	<b>Lmo1143 PduT</b>	<b>Lmo1143 protein</b>	0.443217595	3.923813965	3.923813965	3.923813965
Q8Y564	hemE	Uroporphyrinogen decarboxylase	0.443064849	0.294530019	0.294530019	
Q8Y6C9	<b>pcrA</b>	<b>ATP-dependent DNA helicase</b>	0.43773826	0.402003089	0.402003089	
Q8Y7W6	<b>Lmo1153 PduC</b>	<b>Lmo1153 protein</b>	0.436082204	4.786555316	4.786555316	4.786555316
Q8Y782	lmo1414	Lmo1414 protein	0.434776147	0.376036491	0.376036491	
Q8Y7D4	gcvPA	Probable glycine dehydrogenase (decarboxylating) subunit 1	0.434766293	0.305547069	0.305547069	
Q92AJ3	lmo1815	Lmo1815 protein	0.42840306	0.28480583	0.28480583	

P53434	lmo1452	GTP cyclohydrolase 1 type 2 homolog	0.406910102	0.272450708	0.272450708	
Q8Y990	fsa	Transaldolase	0.402746677	0.344976642	0.344976642	
Q8Y672	gmk	Guanylate kinase	0.399747372	0.421612006	0.421612006	
Q8YAC3	cysK	Cysteine synthase	0.393581231	2.606501872	2.606501872	
Q8Y924	lmo0718	Lmo0718 protein	0.377456824	0.299576687	0.299576687	
Q8Y5V9	lmo1946	Lmo1946 protein	0.37380298	0.238822152	0.238822152	
Q8Y755	<b>cshB</b>	<b>DEAD-box ATP-dependent RNA helicase CshB</b>	0.368608316	0.240220785	0.240220785	
Q8YAG3	lmo0163	Lmo0163 protein	0.36579895	0.348331277	0.348331277	
P65770	nadK2	NAD kinase 2	0.361958186	0.294311917	0.294311917	
Q8YA79	lmo0280	Anaerobic ribonucleotide-triphosphate reductase-activating protein	0.361652056	0.552423954	0.552423954	
Q8Y7W5	<b>Lmo1154 PduD</b>	<b>Lmo1154 protein</b>	0.360696157	2.879733915	2.879733915	2.879733915
Q8Y4A5	thrC	Threonine synthase	0.354188919	0.345953329	0.345953329	
Q8Y888	lmo1029	Lmo1029 protein	0.349815369	0.272361902	0.272361902	
Q8Y5L7	rsmH	ribosomal RNA small subunit methyltransferase H	0.349059105	0.407614772	0.407614772	
Q8Y606	aspB	Aminotransferase	0.341557821	0.239094582	0.239094582	
Q93Q55	proA	Gamma-glutamyl Phosphate reductase	0.341506004	0.40641681	0.40641681	
Q8Y763	lmo1438	Lmo1438 protein	0.327092965	0.291876388	0.291876388	
Q8Y4K4	lmo2434	Probable glutamate decarboxylase gamma	0.324357669	0.24881252	0.24881252	
Q92C24	rpsO	30S ribosomal protein S15	0.317585786	0.841445888	0.841445888	
Q8YA82	lmo0277	Lmo0277 protein	0.315716108	0.336902509	0.336902509	
Q8Y8E7	nagB	glucosamine-6-phosphate deaminase	0.312450091	0.209357432	0.209357432	
Q8Y920	lmo0722	Lmo0722 protein	0.310099443	1.53717574	1.53717574	
Q7AP65	<b>opuCA</b>	<b>OpuCA protein</b>	0.303460916	1.146327083	1.146327083	
Q8Y840	lmo1078	UTP--glucose-1-phosphate uridylyltransferase	0.302845478	0.163949445	0.163949445	
Q93Q56	proB	Glutamate 5-kinase	0.289316813	0.260010992		
P0A357	cspLB	Cold shock-like protein CspLB	0.261767228	0.134696456		
Q8Y3Y2	lmo2697	Lmo2697 protein	0.26005729	3.173990005		
Q8Y688	plsX	Phosphate acyltransferase	0.24896733	0.184027602		
Q8Y801	lmo1118	Lmo1118 protein	0.230370363	0.183642109		
Q8Y949	lmo0688	Lmo0688 protein	0.227655888	0.165806668		
Q8Y3Y3	lmo2696	Lmo2696 protein	0.210680962	1.01784516		
Q8Y3P9	kat	Catalase	0.207210541	2.617042056		
P66352	rpsK	30S ribosomal protein S11	0.206027667	0.772190639		
P66103	rplT	50S ribosomal protein L20	0.193598111	0.862202673		
Q8YAM0	lmo0098	Lmo0098 protein	0.191999594	0.686161076		
Q8Y8K6	rsbW	Serine-protein kinase RsbW	0.191599846	0.706850965		
Q927L7	rplN	50S ribosomal protein L14	0.18895181	1.751371085		
Q8Y8I9	lmo0913	Aldehyde dehydrogenase	0.187241236	1.146424878		
P0A491	rpml	50S ribosomal protein L35	0.187007268	0.842705462		
P66611	rpsG	30S ribosomal protein S7	0.186096827	0.476650389		
Q8Y4P6	lmo2389	Lmo2389 protein	0.184452534	1.082139131		
P66484	rpsS	30S ribosomal protein S19	0.181478182	0.830080338		
Q8Y5B0	sepA	SepA protein	0.171952248	1.406645191		

**SI Table 3 Annotation and Pfam domain information of the genes in the *pdu* cluster.**

Gene ID	Gene tag	Gene Name	Pfam Domain
986177	lmo1142	Pdu S	NADH-ubiquinone oxidoreductase 51kDa subunit, FMN-binding domain (IPR011538)
			Soluble ligand binding domain (IPR019554)
			4Fe-4S ferredoxin-type, iron-sulphur binding domain(IPR017896)
			RnfC Barrel sandwich hybrid domain (IPR026902)
986169	lmo1143	Pdu T	Microcompartment protein, bacteria (IPR000249)
			Microcompartment protein, bacteria (IPR000249)
986310	lmo1144	Pdu U	Microcompartment protein, bacteria (IPR000249)
986160	lmo1145	PduV	P-loop containing nucleoside triphosphate hydrolase (IPR027417)
			Ethanolamine/propanediol utilisation protein, EutP/PduV (IPR012381)
986162	lmo1146		
986161	lmo1147	CopB	Cobinamide kinase/cobinamide phosphate guanylttransferase (IPR003203)
986158	lmo1148	CopD	Adenosylcobinamide-GDP ribazoletransferase (IPR003805)
986156	lmo1149	CopE	Histidine phosphatase superfamily, clade-1 (IPR013078)
			Alpha-ribazole phosphatase, CobC (IPR017578)
18245192	rli39	Riboswitch	
986159	lmo1150	PocR	Transcription regulator HTH, AraC- type (IPR020449)
18245193	rliH		
986164	lmo1151	PduA	Homologous superfamily CcmK-like superfamily (IPR037233)
			Domain Microcompartment protein, bacteria (IPR000249)
986154	lmo1152	PduB	Polyhedral organelle shell protein, EutL/PduB type (IPR009193)
			Microcompartment protein PduB (IPR030984)
986155	lmo1153	PduC	Homologous superfamily: Cobalamin (vitamin B12)-dependent enzyme, catalytic (IPR016176)
			Homologous superfamily: Diol/glycerol dehydratase, large subunit superfamily (IPR036999)
986151	lmo1154	PduD	Propanediol/glycerol dehydratase, medium subunit (IPR025541)
986153	lmo1155	PduE	Propanediol/glycerol dehydratase, small subunit (IPR003207)
986150	lmo1156	PduG	Diol dehydratase-reactivating factor alpha subunit (IPR009191)
986152	lmo1157	PduH	Diol/glycerol dehydratase/dehydratase reactivating factor (IPR003208)
			Diol/glycerol dehydratase reactivating factor, small subunit (IPR009192)
986149	lmo1158	PduK	Homologous superfamily CcmK-like superfamily (IPR037233)
			Domain Microcompartment protein, bacteria (IPR000249)
986147	lmo1159	PduJ	Homologous superfamily CcmK-like superfamily (IPR037233)
			Domain Microcompartment protein, bacteria (IPR000249)
986142	lmo1160	PduL	Phosphate propanoyltransferase (IPR008300)
986144	lmo1161	EutJ	Ethanolamine utilisation EutJ (IPR013366)
986141	lmo1162	PduM	Microcompartment protein PduM (IPR030992)
986140	lmo1163	PduN	Ethanolamine utilization protein EutN/carboxysome structural protein CcmI (IPR004992)

986139	Imo1164	PduO	Adenosylcobalamin biosynthesis, ATP:cob(I)alamin adenosyltransferase, bifunctional PduO (IPR009221) Homologous superfamily: GlcG-like domain superfamily (IPR038084)
986133	Imo1165	PduP	Acetaldehyde/propionaldehyde dehydrogenase, EutE/PduP-related (IPR012408)
986134	Imo1166	PduQ	Iron-type alcohol dehydrogenase-like (IPR039697)
986131	Imo1167	PduF	Major intrinsic protein (IPR000425)
986132	Imo1168	PduW	Acetate/propionate kinase (IPR004372)
986129	Imo1169	CobD	L-threonine-O-3-phosphate decarboxylase (IPR005860)
986128	Imo1170	PduX	Propanediol utilisation/coumermycin biosynthesis, PduX-related (IPR012363)

**The Supplementary Materials for this chapter can also be found online at:**

<https://www.frontiersin.org/articles/10.3389/fmicb.2019.02660/full#supplementary-material>



## 2.5 References

1. Yates, J.R., et al., *Proteomics of organelles and large cellular structures*. Nature Reviews Molecular Cell Biology, 2005. **6**(9): p. 702-714.
2. Kerfeld, C.A., et al., *Bacterial microcompartments*. Nature Reviews Microbiology, 2018.
3. Yeates, T.O., et al., *Protein-based organelles in bacteria: carboxysomes and related microcompartments*. Nature Reviews Microbiology, 2008. **6**(9): p. 681.
4. Sutter, M., et al., *Assembly principles and structure of a 6.5-MDa bacterial microcompartment shell*. Science, 2017. **356**(6344): p. 1293-1297.
5. Axen, S.D., O. Erbilgin, and C.A. Kerfeld, *A taxonomy of bacterial microcompartment loci constructed by a novel scoring method*. PLoS computational biology, 2014. **10**(10): p. e1003898.
6. Rae, B.D., et al., *Functions, compositions, and evolution of the two types of carboxysomes: polyhedral microcompartments that facilitate CO<sub>2</sub> fixation in cyanobacteria and some proteobacteria*. Microbiol. Mol. Biol. Rev., 2013. **77**(3): p. 357-379.
7. Bobik, T.A., et al., *The Propanediol Utilization (pdu) Operon of Salmonella enterica Serovar Typhimurium LT2 Includes Genes Necessary for Formation of Polyhedral Organelles Involved in Coenzyme B<sub>12</sub>-Dependent 1, 2-Propanediol Degradation*. Journal of bacteriology, 1999. **181**(19): p. 5967-5975.
8. Sampson, E.M. and T.A. Bobik, *Microcompartments for B<sub>12</sub>-dependent 1, 2-propanediol degradation provide protection from DNA and cellular damage by a reactive metabolic intermediate*. Journal of bacteriology, 2008. **190**(8): p. 2966-2971.
9. Garsin, D.A., *Ethanolamine utilization in bacterial pathogens: roles and regulation*. Nature Reviews Microbiology, 2010. **8**(4): p. 290.
10. Kerfeld, C.A., et al., *Protein structures forming the shell of primitive bacterial organelles*. Science, 2005. **309**(5736): p. 936-938.
11. Aussignargues, C., et al., *Bacterial microcompartment assembly: the key role of encapsulation peptides*. Communicative & integrative biology, 2015. **8**(3): p. e1039755.
12. Fan, C., et al., *Interactions between the termini of lumen enzymes and shell proteins mediate enzyme encapsulation into bacterial microcompartments*. Proceedings of the National Academy of Sciences, 2012. **109**(37): p. 14995-15000.
13. Jakobson, C.M., et al., *Localization of proteins to the 1, 2-propanediol utilization microcompartment by non-native signal sequences is mediated by a common hydrophobic motif*. Journal of Biological Chemistry, 2015. **290**(40): p. 24519-24533.
14. Kerfeld, C.A. and O. Erbilgin, *Bacterial microcompartments and the modular construction of microbial metabolism*. Trends in microbiology, 2015. **23**(1): p. 22-34.

15. Craciun, S. and E.P. Balskus, *Microbial conversion of choline to trimethylamine requires a glycyl radical enzyme*. Proceedings of the National Academy of Sciences, 2012. **109**(52): p. 21307-21312.
16. Sinha, S., et al., *The PduM protein is a structural component of the microcompartments involved in coenzyme B12-dependent 1, 2-propanediol degradation by Salmonella enterica*. Journal of bacteriology, 2012. **194**(8): p. 1912-1918.
17. Jakobson, C.M. and D. Tullman-Ercek, *Dumpster diving in the gut: bacterial microcompartments as part of a host-associated lifestyle*. PLoS pathogens, 2016. **12**(5): p. e1005558.
18. Cheng, S., et al., *Genetic analysis of the protein shell of the microcompartments involved in coenzyme B12-dependent 1, 2-propanediol degradation by Salmonella*. Journal of bacteriology, 2011. **193**(6): p. 1385-1392.
19. Faber, F., et al., *Respiration of microbiota-derived 1, 2-propanediol drives Salmonella expansion during colitis*. PLoS pathogens, 2017. **13**(1): p. e1006129.
20. Tang, S., et al., *Transcriptomic analysis of the adaptation of Listeria monocytogenes to growth on vacuum-packed cold smoked salmon*. Appl. Environ. Microbiol., 2015. **81**(19): p. 6812-6824.
21. Orsi, R.H. and M. Wiedmann, *Characteristics and distribution of Listeria spp., including Listeria species newly described since 2009*. Applied microbiology and biotechnology, 2016. **100**(12): p. 5273-5287.
22. Schardt, J., et al., *Comparison between Listeria sensu stricto and Listeria sensu lato strains identifies novel determinants involved in infection*. Scientific reports, 2017. **7**(1): p. 17821.
23. Chiara, M., et al., *Comparative genomics of Listeria sensu lato: genus-wide differences in evolutionary dynamics and the progressive gain of complex, potentially pathogenicity-related traits through lateral gene transfer*. Genome biology and evolution, 2015. **7**(8): p. 2154-2172.
24. Mellin, J., et al., *A riboswitch-regulated antisense RNA in Listeria monocytogenes*. Proceedings of the National Academy of Sciences, 2013. **110**(32): p. 13132-13137.
25. Tsai, H.-N. and D.A. Hodgson, *Development of a synthetic minimal medium for Listeria monocytogenes*. Appl. Environ. Microbiol., 2003. **69**(11): p. 6943-6945.
26. Metselaar, K.I., et al., *Diversity of acid stress resistant variants of Listeria monocytogenes and the potential role of ribosomal protein S21 encoded by rpsU*. Frontiers in microbiology, 2015. **6**: p. 422.
27. Wiśniewski, J.R., et al., *Universal sample preparation method for proteome analysis*. Nature methods, 2009. **6**(5): p. 359.
28. Wendrich, J.R., et al., *In vivo identification of plant protein complexes using IP-MS/MS*, in *Plant Hormones*. 2017, Springer. p. 147-158.
29. Lu, J., et al., *Filter-aided sample preparation with dimethyl labeling to identify and quantify milk fat globule membrane proteins*. Journal of proteomics, 2011. **75**(1): p. 34-43.

30. Cox, J., et al., *Accurate proteome-wide label-free quantification by delayed normalization and maximal peptide ratio extraction, termed MaxLFQ*. Molecular & cellular proteomics, 2014. **13**(9): p. 2513-2526.
31. Smaczniak, C., et al., *Characterization of MADS-domain transcription factor complexes in Arabidopsis flower development*. Proceedings of the National Academy of Sciences, 2012. **109**(5): p. 1560-1565.
32. Bielow, C., G. Mastrobuoni, and S. Kempa, *Proteomics quality control: quality control software for MaxQuant results*. Journal of proteome research, 2015. **15**(3): p. 777-787.
33. Babicki, S., et al., *Heatmapper: web-enabled heat mapping for all*. Nucleic acids research, 2016. **44**(W1): p. W147-W153.
34. Mistry, J., et al., *Challenges in homology search: HMMER3 and convergent evolution of coiled-coil regions*. Nucleic acids research, 2013. **41**(12): p. e121-e121.
35. Medema, M.H., E. Takano, and R. Breitling, *Detecting sequence homology at the gene cluster level with MultiGeneBlast*. Molecular biology and evolution, 2013. **30**(5): p. 1218-1223.
36. Weller, D., et al., *Listeria booriae* sp. nov. and *Listeria newyorkensis* sp. nov., from food processing environments in the USA. International journal of systematic and evolutionary microbiology, 2015. **65**(1): p. 286-292.
37. Drozdetskiy, A., et al., *JPred4: a protein secondary structure prediction server*. Nucleic acids research, 2015. **43**(W1): p. W389-W394.
38. Staib, L. and T.M. Fuchs, *Regulation of fucose and 1, 2-propanediol utilization by Salmonella enterica serovar Typhimurium*. Frontiers in microbiology, 2015. **6**: p. 1116.
39. Xue, J., et al., *Exogenous or L-rhamnose-derived 1, 2-propanediol is metabolized via a pduD-dependent pathway in Listeria innocua*. Appl. Environ. Microbiol., 2008. **74**(22): p. 7073-7079.
40. van Schaik, W. and T. Abee, *The role of sigma(B) in the stress response of Gram-positive bacteria - targets for food preservation and safety*. Current Opinion in Biotechnology, 2005. **16**(2): p. 218-224.
41. van der Veen, S., et al., *The heat-shock response of Listeria monocytogenes comprises genes involved in heat shock, cell division, cell wall synthesis, and the SOS response*. Microbiology-Sgm, 2007. **153**: p. 3593-3607.
42. Yu, W.Y., et al., *Solution structure of GSP13 from Bacillus subtilis exhibits an S1 domain related to cold shock proteins*. Journal of Biomolecular Nmr, 2009. **43**(4): p. 255-259.
43. Markkula, A., et al., *Roles of Four Putative DEAD-Box RNA Helicase Genes in Growth of Listeria monocytogenes EGD-e under Heat, pH, Osmotic, Ethanol, and Oxidative Stress Conditions*. Applied and Environmental Microbiology, 2012. **78**(19): p. 6875-6882.
44. Begg, S.L., *The role of metal ions in the virulence and viability of bacterial pathogens*. Biochemical Society Transactions, 2019. **47**: p. 77-87.

45. Dorey, A., et al., *Role and regulation of the stress activated sigma factor sigma B ( $\sigma_B$ ) in the saprophytic and host-associated life stages of Listeria monocytogenes*. *Advances in applied microbiology*, 2019. **106**: p. 1-48.
46. Kim, S.H., et al., *Role of uvrA in the growth and survival of Listeria monocytogenes under UV radiation and acid and bile stress*. *Journal of Food Protection*, 2006. **69**(12): p. 3031-3036.
47. Dadswell, K., et al., *Bacterial microcompartment-mediated ethanolamine metabolism in E. coli urinary tract infection*. *Infection and immunity*, 2019: p. IAI. 00211-19.
48. Cheng, S., et al., *The PduQ enzyme is an alcohol dehydrogenase used to recycle NAD<sup>+</sup> internally within the Pdu microcompartment of Salmonella enterica*. *PLoS One*, 2012. **7**(10): p. e47144.
49. Wemekamp-Kamphuis, H.H., et al., *Multiple deletions of the osmolyte transporters BetL, Gbu, and OpuC of Listeria monocytogenes affect virulence and growth at high osmolarity*. *Appl. Environ. Microbiol.*, 2002. **68**(10): p. 4710-4716.
50. Marinho, C.M., et al., *The  $\sigma_B$ -dependent regulatory sRNA Rli47 represses isoleucine biosynthesis in Listeria monocytogenes through a direct interaction with the ilvA transcript*. *RNA biology*, 2019: p. 1-15.
51. Liu, Y., et al., *Systematic review of the Listeria monocytogenes  $\sigma_B$  regulon supports a role in stress response, virulence and metabolism*. *Future microbiology*, 2019(0).



# 3

---

## **Anaerobic growth of *Listeria monocytogenes* on rhamnose is stimulated by Vitamin B12 and bacterial microcompartment dependent 1,2-propanediol utilization**

Published as:

**Zeng Z**, Li S, Boeren S, Smid EJ, Notebaart RA, Abee T. Anaerobic Growth of *Listeria monocytogenes* on Rhamnose Is Stimulated by Vitamin B12 and Bacterial Microcompartment-Dependent 1,2-Propanediol Utilization. *mSphere*. 2021 Jul 21:e0043421.

### Abstract

The food-borne pathogen *Listeria monocytogenes* can form proteinaceous organelles called bacterial microcompartments (BMCs) that optimize the utilization of substrates, such as 1,2-propanediol, and confer an anaerobic growth advantage. Rhamnose is a deoxyhexose sugar abundant in a range of environments including the human intestine, and can be degraded in anaerobic conditions into 1,2-propanediol, next to acetate and lactate. Rhamnose-derived 1,2-propanediol were found to link with BMCs in some human pathogens such as *Salmonella enterica*, but the involvement of BMCs in rhamnose metabolism and potential physiological effects on *L. monocytogenes* are still unknown. In this study, we firstly test the effect of rhamnose uptake and utilization on anaerobic growth of *L. monocytogenes* EGDe without and with added vitamin B12, followed by metabolic analysis. We unveil that the vitamin B12-dependent activation of *pdu* stimulates metabolism and anaerobic growth of *L. monocytogenes* EGDe on rhamnose via 1,2-propanediol degradation into 1-propanol and propionate. Transmission electron microscopy of *pdu*-induced cells shows that BMCs are formed and additional proteomics experiments confirm expression of *pdu* BMC shell proteins and enzymes. Finally, we discuss physiological effects and energy efficiency of *L. monocytogenes pdu* BMC-driven anaerobic rhamnose metabolism and impact on competitive fitness in environments such as the human intestine.

**Importance:** *Listeria monocytogenes* is a foodborne pathogen causing severe illness, and as such, it is crucial to understand the molecular mechanisms contributing to its survival strategy and pathogenicity. Rhamnose is a deoxyhexose sugar abundant in a range of environments including the human intestine, and can be degraded in anaerobic conditions into 1,2-propanediol. In our previous study, the utilization of 1,2-propanediol (*pdu*) in *L. monocytogenes* was proved to be metabolized in bacterial microcompartments (BMCs) which are self-assembling subcellular proteinaceous structures and analogs of eukaryotic organelles. Here, we unveil that the vitamin B12-dependent activation of *pdu* stimulates metabolism and anaerobic growth of *L. monocytogenes* EGDe on rhamnose via BMC-dependent 1,2-propanediol utilization. Combined with metabolic and proteomics analysis, our discussion on physiological effects and energy efficiency of BMC-driven rhamnose metabolism shed new light to understand the impact on *L. monocytogenes* competitive fitness in ecosystems such as the human intestine.

### 3.1 Introduction

*Listeria monocytogenes* is a Gram-positive facultative anaerobe and a food-borne pathogen which causes a severe human infection called listeriosis [1, 2]. The pathogen continues to cause food-borne illness outbreaks characterised by high mortality ranging from 20 to 30% [1, 3]. *L. monocytogenes* is found ubiquitously in natural environments and it can survive a variety of stress conditions leading to the colonization of different niches including a range of food processing environments [1, 3, 4]. To survive in such a variety of niches, *L. monocytogenes* should be able to adapt to environmental stresses and to use a range of nutrients for growth in aerobic and anaerobic conditions [1, 5, 6].

Recent studies on anaerobic growth of *L. monocytogenes* have provided evidence that it has the capacity to form proteinaceous organelles so-called bacterial microcompartments (BMCs) that enable extension of its metabolic repertoire by supporting the utilization of 1,2-propanediol and ethanolamine [7-9]. BMCs are self-assembling organelles that consist of an enzymatic core that is encapsulated by a semi-permeable protein shell [7, 10, 11]. The separation of the encapsulated enzymes from the cytosol is thought to protect the cell from toxic metabolic intermediates such as aldehydes, and prevent unwanted side reactions [7, 10, 11]. In our previous studies, we showed that the *L. monocytogenes* 1,2-propanediol utilization gene cluster (*pdu*) is activated in the presence of 1,2-propanediol and vitamin B12, resulting in stimulation of growth in anaerobic conditions [8]. Vitamin B12 is required for activation of the *pdu* cluster in *L. monocytogenes* [8, 12] and to act as a cofactor of 1,2-propanediol reductase [13]. Activation of BMC-dependent *pdu* supports degradation of 1,2-propanediol via the toxic intermediate propionaldehyde into 1-propanol and propionate via respective reductive and oxidative branches, with the latter resulting in extra ATP generation leading to enhanced anaerobic growth of *L. monocytogenes* [8]. Notably, 1,2-propanediol is a major end product from the anaerobic degradation of mucus-derived rhamnose by human intestinal microbiota and it is thought to be an important energy source supporting intestinal growth of selected pathogens such as *Salmonella* spp. and *L. monocytogenes* [7, 14-16].

Rhamnose is a naturally occurring deoxyhexose sugar abundant in glycans on surfaces of mammalian and bacterial cells and in cell walls of many plant and insect species [14, 17]. Anaerobic metabolism of rhamnose has been studied previously in a range of bacteria including *E. coli*, and rhamnose is parallelly metabolized into lactaldehyde and dihydroxyacetone phosphate (DHAP) [18, 19].

DHAP is converted in the glycolytic pathway leading to a variety of fermentation products, while lactaldehyde is converted to 1,2-propanediol that is subsequently secreted [18, 19]. Notably, for example in *Salmonella spp.* and *Clostridium phytofermentans*, rhamnose-derived 1,2-propanediol can be converted to 1-propanol and propionate via BMC-dependent *pdu* [14, 16]. Although rhamnose-derived 1,2-propanediol was found to be metabolised via a *pduD*-dependent pathway in *Listeria innocua* [20], the possible activation and contribution of BMC-dependent *pdu* to anaerobic metabolism and growth of *L. monocytogenes* on rhamnose remains to be investigated.

In this study, we firstly quantified the effect of rhamnose as sole carbon source on anaerobic growth and metabolism of *L. monocytogenes* in absence and presence of vitamin B12 (cobalamine), an essential co-factor of 1,2-propanediol reductase, the signature enzyme of BMC-dependent *pdu* [13]. Next, we analysed rhamnose utilization and end product formation, and combined with Transmission Electron Microscopy and proteomics, we provide evidence for a B12-dependent *pdu*-induced metabolic shift. We summarize our findings in a model integrating BMC-dependent *pdu* with rhamnose metabolism, and discuss impact on growth and survival of *L. monocytogenes* in anaerobic environments such as the human intestine.

## 3.2 Materials and Methods

### 3.2.1 Strains, Culture Conditions, and Growth Measurements

All experiments in this study were carried out with *L. monocytogenes* EGDe anaerobically grown at 30°C in defined medium MWB (Modified Welshimer's broth) [21]. Overnight grown cells in Luria Broth (LB) were washed three times in PBS before inoculation into MWB. MWB was supplemented with 20mM L-rhamnose as sole carbon source with or without addition of 20nM vitamin B12. Anaerobic conditions were achieved by Anoxomat Anaerobic Culture System with a gas mixture composed of 10% CO<sub>2</sub>, 5% H<sub>2</sub>, 85% N<sub>2</sub>. MWB with 20 mM rhamnose and 20 nM vitamin B12 was defined as rhamnose *pdu*-induced, while MWB with 20 mM rhamnose was defined as rhamnose *pdu* non-induced condition. OD600 measurements in MWB were performed every 12 h for 3 days. Plate counting in MWB to quantify Colony Forming Units (CFUs) was performed every 24 h for 3 days. All growth measurements were performed with three independent experiments with three technical repeats.

### 3.2.2 Analysis of metabolites for Rhamnose metabolism using High Pressure Liquid Chromatography (HPLC)

Samples were taken from the cultures at 0, 24, 48, and 72 h. After centrifugation, the supernatant was collected for the HPLC measurements of rhamnose, acetate, lactate, 1,2-propanediol, 1-propanol and propionate. The experiment was performed with three biological replicates. Additionally, the standard curves of all the metabolites were measured in the concentrations 0.1, 1, 5, 10, and 50 mM. HPLC was performed using an Ultimate 3000 HPLC (Dionex) equipped with an RI-101 refractive index detector (Shodex, Kawasaki, Japan), an autosampler and an ion-exclusion Aminex HPX-87H column (7.8 mm × 300 mm) with a guard column (Bio-Rad, Hercules, CA). As the mobile phase 5 mM H<sub>2</sub>SO<sub>4</sub> was used at a flow rate of 0.6 ml/min, the column was kept at 40°C. The total run time was 30 min and the injection volume was 10 µl. All the HPLC measurements were performed with three independent experiments with three technical repeats.

### 3.2.3 Transmission Electron Microscopy (TEM)

*L. monocytogenes* EGDe cultures were grown anaerobically at 30°C rhamnose *pdu*-induced and rhamnose *pdu* non-induced condition. Samples were collected at 48 h of incubation. About 10 µg dry cells were fixed for 2 h in 2.5% (v/v) glutaraldehyde in 0.1 M sodium cacodylate buffer (pH 7.2). After rinsing in the same buffer, a post-fixation was done in 1% (w/v) OsO<sub>4</sub> for 1 h at room temperature. The samples were dehydrated by ethanol and were then embedded in resin (Spurr HM20) 8 h at 70°C. Thin sections (<100 nm) of polymerized resin samples were obtained with microtomes. After staining with 2% (w/v) aqueous uranyl acetate, the samples were analyzed with a Jeol 1400 plus TEM with 120 kV setting [8, 9]. The observation of BMCs structures was performed within three biological replicates, and determination of the fraction of BMC positive cells was based on the analysis of 300 cells in respective TEM pictures of *pdu*-induced and *pdu* non-induced conditions, as previously described [8].

### 3.2.4 Proteomics

*L. monocytogenes* cultures were anaerobically grown at 30°C in rhamnose *pdu*-induced and rhamnose *pdu* non-induced condition. Samples were collected at 48 h of incubation and then washed twice with 100 mM Tris (pH 8). About 10 mg wet weight cells in 100 µl 100 mM Tris was sonicated for 30 s twice to lyse the cells. Samples were prepared according to the filter assisted sample preparation protocol (FASP) with the following steps: reduction with 15 mM dithiothreitol, alkylation with 20 mM acrylamide, and digestion with sequencing grade trypsin

overnight [22]. Each prepared peptide sample was analyzed by injecting (18 µl) into a nanoLC-MS/MS (Thermo nLC1000 connected to a LTQ-Orbitrap XL) as described previously [8, 9]. LCMS data with all MS/MS spectra were analyzed with the MaxQuant quantitative proteomics software package as described before [8, 9, 23]. A protein database with the protein sequences of *L. monocytogenes* EGDe (ID: UP000000817) was downloaded from UniProt. Filtering and further bioinformatics and statistical analysis of the MaxQuant ProteinGroups file were performed with Perseus [24]. Reverse hits and contaminants were filtered out. Protein groups were filtered to contain minimally two peptides for protein identification of which at least one is unique and at least one is unmodified. The volcano plot was prepared based on the Student's t-test difference of Pdu-induced/non-induced control. The mass spectrometry proteomics data have been deposited to the ProteomeXchange Consortium via the PRIDE[25] partner repository with the dataset identifier PXD025734.

<https://www.ebi.ac.uk/pride/archive/projects/PXD025734> .

### 3.2.5 Bioinformatics and Statistical Analysis

Pathview R package [26] to visualize the proteomics data: The UniProt protein IDs from Supplementary Table 1 were collected and retrieved to Entre IDs. A list of Entrez IDs, protein expression indicated by LFQ intensity (Supplementary Table 2) was mapped to the *L. monocytogenes* EGDe KEGG pathway database using the tool Pathview (R version 3.2.1). The box represent genes and the different color indicates level of expression with default setting.

Statistical analyses were performed in Prism 8.0.1 for Windows (GraphPad Software). As indicated in the figure legend, Statistical significances are shown in \*\*\*,  $P < 0.001$ ; \*,  $P < 0.05$ ; ns,  $P > 0.05$  with Holm-Sidak T-test.

### 3.3 Results

#### 3.3.1 Activation of *pdu* stimulates anaerobic growth of *L. monocytogenes* EGDe on rhamnose

We first examined if rhamnose can function as a sole carbon source to support anaerobic growth of *L. monocytogenes* EGDe in MWB defined medium without and with added vitamin B12 (cobalamin) (Figure 1). In MWB defined medium supplied with 20mM rhamnose OD<sub>600</sub> reaches a maximum of about 0.37 after 48 h, while in MWB supplied with 20mM rhamnose and 20nM B12 OD<sub>600</sub> continues to increase after 48 h, reaching a significant higher OD<sub>600</sub> of 0.51 at 72 h. Enhanced growth on MWB supplied with rhamnose and B12 compared to MWB plus rhamnose, is also evident from plate counts which increase from 6.5 to 8.2 log<sub>10</sub> CFU/ml and from 6.5 to 7.2 log<sub>10</sub> CFU/ml, respectively (figure 1B). There is no significant difference in growth performance of *L. monocytogenes* EGDe on MWB supplied with 20mM glucose and MWB supplied with 20mM glucose and 20 nM B12, and at 48 h final levels of 8.8 log<sub>10</sub> CFU/ml were reached (Supplementary Figure 1). These results suggest that in B12 stimulated anaerobic growth of *L. monocytogenes* EGDe on MWB medium with rhamnose as sole carbon source is linked to activation of *pdu*.

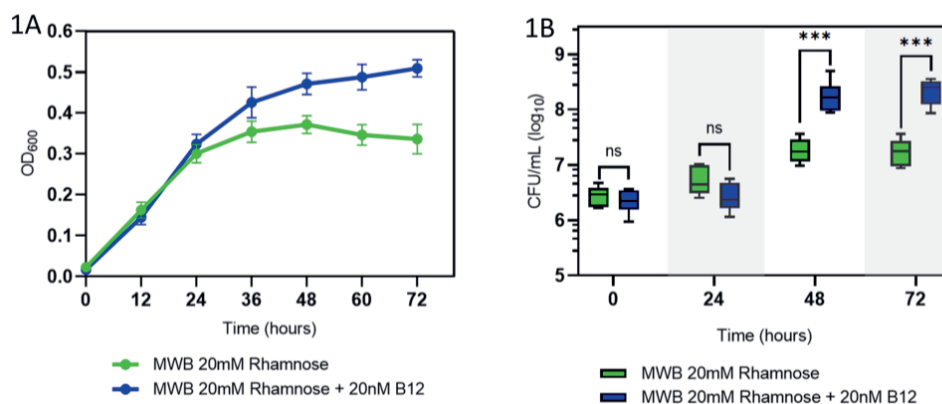


**Figure 1. Impact of L-rhamnose and vitamin B12 on anaerobic growth of *L. monocytogenes* EGDe.**

**(1A)** OD<sub>600</sub> growth curves in MWB defined medium with 20 mM L-rhamnose as sole carbon source (green symbols) and MWB with 20 mM Rhamnose and 20n M B12 (blue symbols). **(1B)** CFUs during growth on MWB 20mM Rhamnose (green symbols) and on MWB 20 mM Rhamnose + 20 nM B12 (blue symbols). Results from three independent experiments with three technical repeats are expressed as mean and standard errors. Statistical significance is indicated (\*\*\*,  $P < 0.001$ ; ns,  $P > 0.05$  Holm-Sidak T-test).

### 3.3.2 Activation of *pdu* supports 1,2-propanediol degradation and stimulates rhamnose metabolism

To confirm possible activation of *pdu*, metabolic analysis via HPLC was conducted to quantify substrate consumption and product formation following anaerobic growth of *L. monocytogenes* EGDe on MWB plus 20mM rhamnose and MWB plus 20mM rhamnose and 20nM B12. As shown in Figure 2A, at 72 h, the initial 20mM rhamnose is completely consumed in *pdu* induced condition, whereas 3.5 mM of rhamnose is retained in *pdu* non-induced condition. Additional end product analysis at 72 h shows accumulation of approximately 6.7 mM of 1,2-propanediol in *pdu* non-induced condition and nearly zero production of propionate and 1-propanol. In *pdu* induced condition a significant lower amount of 1,2-propanediol is found, about 1.4 mM, and higher levels of approximately 3.4 mM propionate and 3.6 mM 1-propanol are produced at 72 h, in line with the expected 1:1 molar stoichiometry of *L. monocytogenes* BMC-dependent *pdu* [9]. Enhanced rhamnose metabolism in *pdu*-induced cells is also evident from production of acetate and lactate. At 72h, 4.1 mM acetate and 2.3 lactate are produced in *pdu* non-induced condition while 7.6 mM acetate and 5.1 mM lactate are produced in *pdu* induced condition.

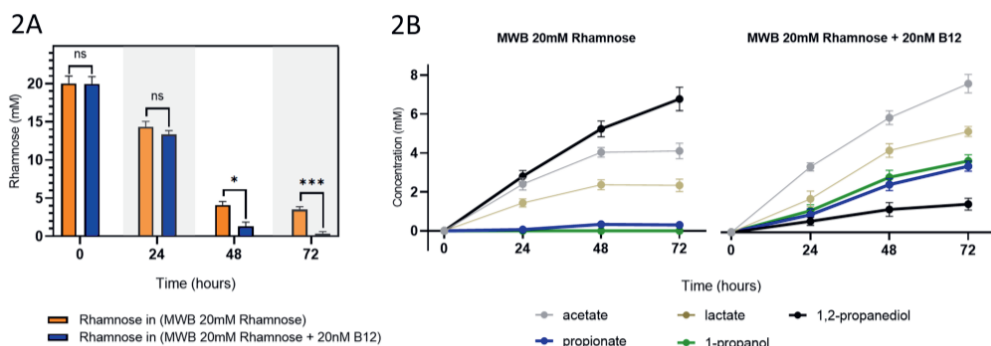


**Figure 2. Impact of vitamin B12 on Rhamnose metabolism of anaerobically grown *L. monocytogenes* EGDe.**

**(2A)** Utilization of Rhamnose by *L. monocytogenes* EGDe anaerobically grown in MWB plus 20 mM Rhamnose (orange bars) and MWB plus 20mM Rhamnose and 20 nM B12 (blue bars). **(2B)** Metabolites from Rhamnose metabolism of *L. monocytogenes* EGDe anaerobically grown in MWB plus 20mM Rhamnose (left) and MWB plus 20 mM Rhamnose and 20 nM B12 (right). Results from three independent experiments are expressed as mean and standard errors. Statistical significance is indicated (\*\*\*,  $P < 0.001$ ; \*,  $P < 0.05$ ; ns,  $P > 0.05$  Holm-Sidak T-test).

### 3.3.3 Visualization of BMCs and expression analysis of BMC shell proteins

To answer the question if BMCs are formed to support the utilization of rhamnose-derived 1,2-propanediol, Transmission Electron Microscopy (TEM) was performed to observe BMCs structures, and proteomics was applied to measure the expression of BMC shell proteins (Figure 3A). The *pdu* induced cells clearly contain BMC-like structures (60 - 70 % of 300 cells BMC positive) with an approximate diameter of 50-80 nm, while similar structures were not observed in *pdu* non-induced cells. Notably, the identified structures strongly resemble TEM pictures of previously reported *pdu* BMCs in *L. monocytogenes* [8, 9] and in *S. enterica* and *E. coli* [13, 27]. Compared to *pdu* non-induced cells, *pdu* induced cells show significant upregulation of 21 measurable Pdu proteins (Figure 3B), including seven proteins annotated as BMCs shell proteins, PduTUABKJN. Notably, *pdu*-induced and *pdu* non-induced rhamnose grown cells show similar expression of proteins in the rhamnose metabolism cluster (*Imo2850*, *rhaA*, *rhaB* and *rhaM*) (Figure 3B), which indicates that the activation of *pdu* BMC does not affect the expression of these enzymes.

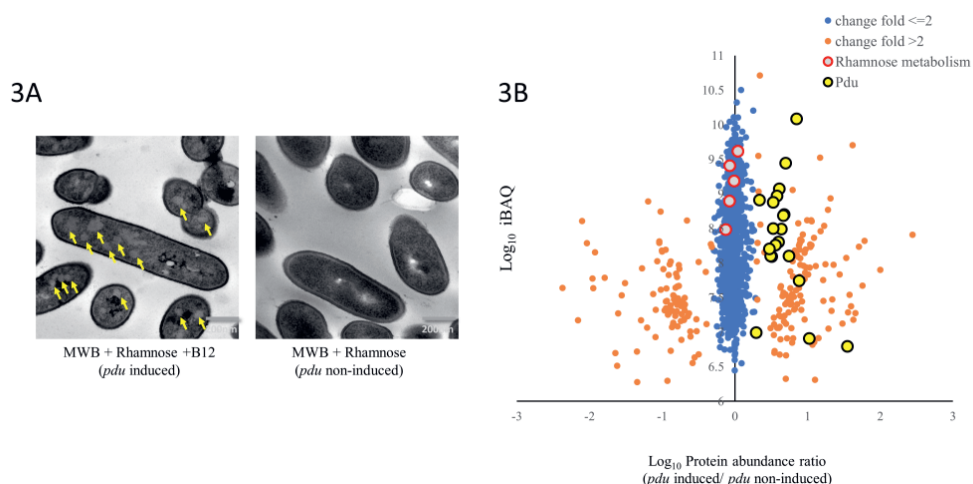


**Figure 3. TEM visualization of BMCs and proteomics analysis of *pdu* induced cells (MWB plus 20 mM Rhamnose and B12) compared to *pdu* non-induced cells (MWB plus 20 mM Rhamnose).**

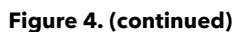
**(3A)** TEM visualization of BMCs in cells grown on MWB plus 20 mM Rhamnose and B12 (left; yellow arrows point to BMCs) and cells grown on MWB with 20mM Rhamnose (right). **(3B)** Proteomic ratio plot of MWB plus 20mM Rhamnose and B12 compared to MWB plus 20 mM Rhamnose grown cells. Fold change  $\leq 2$  in blue, fold change  $> 2$  in orange, proteins in the Pdu cluster are black encircled in yellow, and proteins in the Rhamnose cluster are red-encircled in grey. More details in text and in Supplementary Table 1.

### 3.3.4 Proteomics-based pathway visualization of propanoate metabolism and vitamin B12 metabolism

To visualize the metabolism from 1,2-propanediol to propanoate (propionate) and 1-propanol, the identified proteins and expression levels presented in Supplementary Table 1, are mapped to propanoate metabolic pathways of *L. monocytogenes* EGDe. As shown in Figure 4A, the enzymes involved in degradation of rhamnose-derived 1,2-propanediol into propanoate (propionate) and 1-propanol are all significantly upregulated in *pdu* induced condition compared to *pdu* non-induced condition. The propanediol dehydratase (EC 4.2.1.28) is an enzyme with three subunits encoded by *pduC*, *pduD* and *pduE*, which converts 1,2-propanediol into propanal (propionaldehyde). Propionaldehyde is metabolized to 1-propanol by propanol dehydrogenase PduQ and propanol-CoA by propionaldehyde dehydrogenase PduP (EC 1.2.1.87). Propanol-CoA is converted to propanoyl-phosphate by phosphate propanoyltransferase PduL (EC 2.3.1.222), with propanoyl-phosphate subsequently converted to propanoate by propionate kinase PduW (EC 2.7.2.1). We found that the vitamin B12 biosynthesis pathway that is grouped in porphyrin and chlorophyll metabolism, is significantly downregulated in *pdu* induced condition compared to *pdu* non-induced condition (Proteomics-based pathway visualization of porphyrin and chlorophyll metabolism, Figure 4B), which suggests that supplementation of 20nM B12 represses the expression of proteins required for B12 biosynthesis. This also includes the three enzymes mediating the final steps in B12 biosynthesis, CobU, CobS and CobC, encoded by the respective genes located in the *pdu* cluster (Figure 4B) [8, 28-30]. Apparently, B12 accumulation from the medium supports activation of *pdu* BMCs, whereas despite expression of B12 biosynthesis enzymes, production of B12 and levels reached are not sufficient to induce *pdu* in *L. monocytogenes* EGDe grown in MWB without added B12.

[illegible]

75



### 3.4 Discussion

The presented model of 1,2-propanediol BMCs in rhamnose metabolism is based on growth phenotypes, metabolic analysis, proteomics, TEM visualization and our understanding of 1,2-propanediol BMCs in anaerobic growth of *L. monocytogenes* EGDe. As illustrated in Figure 5, the rhamnose catabolism gene cluster (*rha*) in *L. monocytogenes* EGDe is composed of *lmo2846-lmo2851* [31]. *lmo2850* encodes a secondary transporter which has high similarity with L-rhamnose permease RhaT in *E. coli* [32-34], and is conceivably acting as the transporter of  $\alpha$ -L-rhamnose. L-rhamnose mutarotase RhaM mediates the conversion of  $\alpha$ -L-rhamnose into  $\beta$ -L-rhamnose (also called L-rhamnopyranose) [31, 35].  $\beta$ -L-rhamnose is converted to L-rhamnulose by L-rhamnose isomerase RhaA [31, 36]. L-rhamnose is then phosphorylated to L-rhamnulose 1-phosphate by rhamnulokinase RhaB with one ATP consumption [31, 36]. L-rhamnulose 1-phosphate is split into (S)-lactaldehyde and dihydroxyacetone phosphate (DHAP) by rhamnulose-1-phosphate aldolase RhaD [31, 36]. DHAP can be metabolized to glyceraldehyde 3-phosphate via Triosephosphate isomerase 1 TpiA1 and via the glycolytic pathway [14, 37] and the GABA ( $\gamma$ -aminobutyric acid) shunt in the incomplete TCA cycle in *L. monocytogenes* [38], to the end products acetate and lactate, as confirmed in our metabolic analysis. The observed production of 1,2-propanediol in *pdu* non-induced conditions confirms the predicted anaerobic conversion of lactaldehyde to 1,2-propanediol in *L. monocytogenes* EGDe. The activity of lactaldehyde reductase has not been described in *L. monocytogenes* [39], but protein similarity alignment with lactaldehyde reductase FucO of *Escherichia coli* [39], suggests four putative candidates annotated as alcohol dehydrogenase in *L. monocytogenes* EGDe including *lmo1166*, *lmo1171*, *lmo1634* and *lmo1737*, detected in the proteomes of both *pdu* non-induced and *pdu*-induced cells (for details see Supplementary File 1). Since the discovery of the role of *pdu* BMCs dehydratase in rhamnose (and fucose) utilization, two pathway scenarios have been proposed, one with and one without lactaldehyde reductase encapsulated inside BMCs [31, 35]. In line with previously reported comparative genomic analysis [31, 35], our data now provide evidence for the latter model to be active in *L. monocytogenes* since rhamnose is converted via lactaldehyde to 1,2-propanediol in absence of BMCs in *pdu* non-induced condition, while with added B12 metabolism of 1,2-propanediol proceeds via *pdu* BMCs.

The activation of *pdu* BMCs enhances anaerobic rhamnose metabolism in *L. monocytogenes* and conceivably generates additional energy via the ATP producing propionate branch in *pdu*, and via enhanced flux into the glycolytic pathway resulting in a significant stimulation of growth. At 72 h, 20 mM rhamnose is metabolized into 7.6 mM acetate, 5.1 mM lactate, 1.4mM 1,2-propanediol, 3.4 mM propionate and 3.6 mM 1-propanol in *pdu* induced condition, while 16.5 mM rhamnose is metabolized into 4.1 mM acetate, 2.3 mM lactate, 6.7 mM 1,2-propanediol in *pdu* non-induced condition. Theoretical ATP yield from rhamnose conversion to lactate, acetate and propionate includes production of 1.5 ATP per 1 lactate, 2.5 ATP per 1 acetate and 0.5 ATP per 1 propionate produced (for details of reactions see Supplementary Table 3 ). Based on concentrations of end products at 72h , *pdu* induced cells theoretically generate 1.425 ATP per 1 rhamnose while *pdu* non-induced cells generate 0.830 ATP per 1 rhamnose (for details of calculations see Supplementary Table 3). The theoretical energy gain of *L. monocytogenes* EGDe from anaerobic rhamnose metabolism with the activation of 1,2-propanediol BMCs, could offer an explanation for the 10-fold higher number of CFUs reached (8.2 log<sub>10</sub> CFU/ml) compared to non-*pdu* induced conditions (7.2 log<sub>10</sub>/ml).

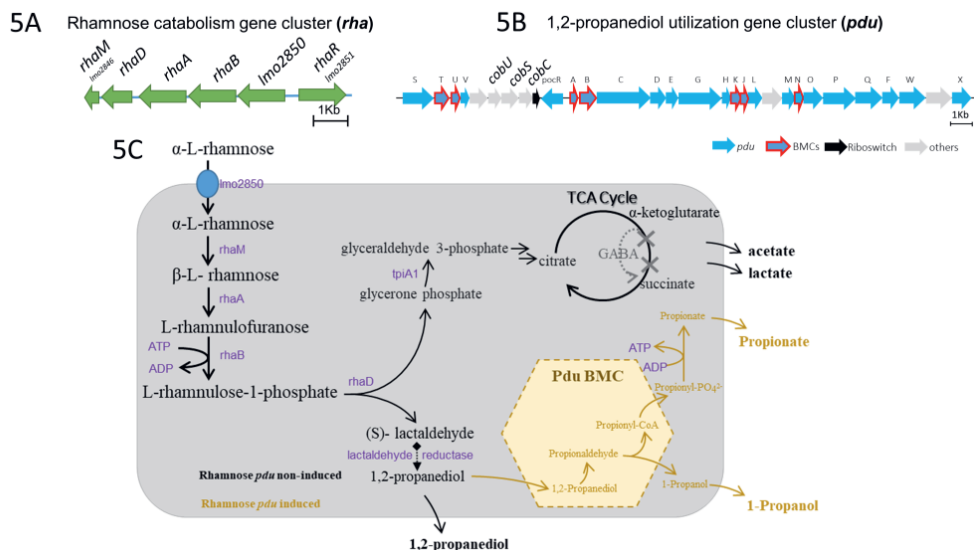
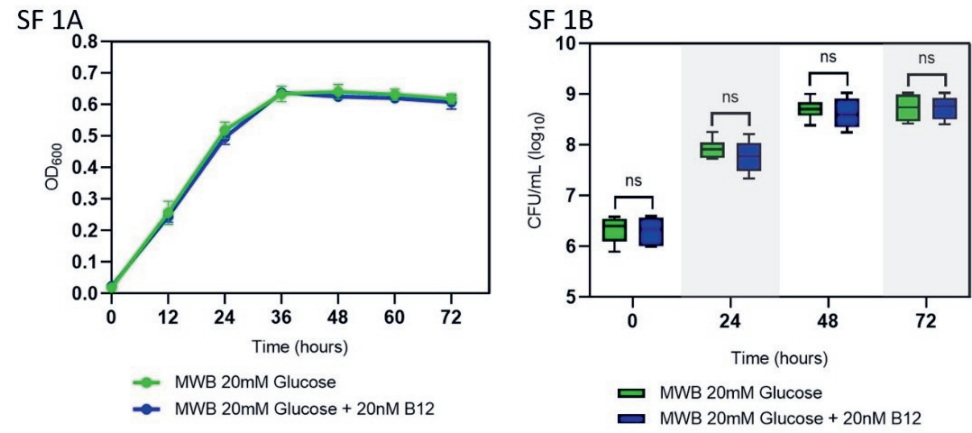


**Figure 5. Overview of rhamnose metabolism with or without 1,2-propanediol BMCs in *L. monocytogenes*.** (5A) Rhamnose catabolism gene cluster, *rha* (5B) 1,2-propanediol utilization gene cluster, *pdu*. Details for (5A) and (5B) are in Supplementary Table 4. (5C) The Proposed rhamnose metabolism model based on this study. Arrows represent reactions and enzymes and compounds indicated in black represent rhamnose metabolism without BMCs, and 1,2-propanediol BMC reactions

activated by B12 and compounds involved are shown in yellow. For details see corresponding sections in results and discussion.

Our data provide evidence for another extension of the BMC-dependent metabolic repertoire of *L. monocytogenes* in anaerobic conditions, that now includes BMC-dependent ethanolamine utilization (*eut*) [9], BMC *pdu* [8], and BMC *pdu*-stimulated rhamnose metabolism. The indicated substrates can be found in a wide range of environments including foods and human gastrointestinal tract. Substrates for microcompartment metabolism like ethanolamine and 1,2-propanediol are constantly produced in the human intestine by bacterial metabolism of food or host cell components. Enteric pathogens such as *Salmonella* spp. gain a competitive advantage in the intestine by utilizing these substrates, an advantage enhanced by the host inflammatory response [15, 40-42]. It is conceivable, that the competitive fitness of *L. monocytogenes* can be enhanced by activation of BMC dependent *eut* and *pdu*, with corresponding substrates provided by enzymatic activities of gut microbiota, such as release of ethanolamine following membrane phospholipid degradation and release of rhamnose following mucus glycan hydrolysis activity, and propanediol as a fermentation product [15]. Notably, despite the presence of a complete vitamin B12 synthesis cluster, we found that *eut* [9], *pdu* [8], and *pdu*-stimulated rhamnose utilization in *L. monocytogenes* in the current study, requires supplementation of B12 to the medium. This points to an important role of B12 in activation of *L. monocytogenes* BMC-mediated metabolic pathways containing B12-dependent signature aldehyde reductases. Vitamin B12 can be found in foods including meat and dairy products [29, 43] and is also found in human intestine, where part of the B12 is derived from gut microbiota that have the capacity to produce B12 [12, 29]. The fact that we observed in the current study induction of the B12 synthesis pathway in cells grown in MWB plus rhamnose but no activation of B12-dependent *pdu*, while activation was found with B12 added to the medium, points to an intricate regulation of the B12 synthesis pathway and its connection to BMCs activation. In addition to earlier studies on transcriptional and translational control of BMC *eut* and *pdu* in *L. monocytogenes* [1, 12, 15, 29, 44], studies are required to assess for example impact of extracellular and intracellular B12 concentrations on activation of BMC pathways and their role in *L. monocytogenes* ecophysiology and virulence.

3.5 Supplementary Materials



**Supplementary Figure 1. Anaerobic growth of *L. monocytogenes* EGDe on MWB plus glucose (green symbols) and MWB plus 20 mM glucose and 20 nM B12 (blue symbols).** (SF 1A) OD<sub>600</sub> growth curves, (SF 1B) CFUs determined at indicated time points during growth on MWB plus 20 mM glucose (green bars) and MWB plus 20 mM glucose and 20 nM B12 (blue bars). Results from three independent experiments with three technical repeats are expressed as mean and standard errors. Statistical significance is indicated (ns, P>0.05 Holm-Sidak T-test)

**Supplementary Table 1.** Protein profiling of *pdu*-induced compared with non-induced *L. monocytogenes* EGDe in MWB medium with Rhamnose. (Only list the top 100 rows, the full table with 1294 rows was online in bellowing link)

X axis : LFQ intensity	Y axis: Total iBAQ	Rha or pdu	Protein IDs	Protein Annotation	Gene Name
log10 (Pos/Neg)	iBAQ				
2.444868565	8.40715287		Q8Y523	Lmo2254 protein	lmo2254
2.001654863	7.898719698		Q8Y7A9	Membrane protein insertase YidC 1	yidC1
1.78644681	8.319189369		Q8Y8G0	Lmo0944 protein	lmo0944
1.756666899	7.671006131		Q8Y985	Lmo0648 protein	lmo0648
1.708023787	8.235679919		Q8Y569	Lmo2207 protein	lmo2207
1.657866478	7.27186483		Q8Y9F9	ATP phosphoribosyltransferase regulatory subunit	hisZ
1.631134987	7.176756667		Q8Y6X0	Chromosome replication initiation / membrane attachment protein DnaB	dnaB
1.619628191	9.703540703		Q92AD0	CspD protein	cspD
1.598968029	7.372672707		Q8Y403	Lmo2675 protein	lmo2675
1.578961134	7.539527731		Q8Y5N5	Lmo2022 protein	lmo2022
1.556344271	7.28302971		Q8Y455	Energy-coupling factor transporter ATP-binding protein EcfA2	ecfA2
1.546034813	6.794348604	pdu	Q8Y7W2	Lmo1157 protein	PduH
1.532580137	8.07081336		Q8Y9C3	Lmo0609 protein	lmo0609
1.482708454	7.121362841		Q8Y8Z0	Lmo0752 protein	lmo0752

1.441064358	7.834585997		Q8Y6C4	Phosphoribosylglycinamide formyltransferase	purN
1.358945608	7.974728095		Q8Y717	ATP-dependent RecD-like DNA helicase	recD2
1.340945005	7.471247692		Q8Y9Q0	Lmo0474 protein	lmo0474
1.32920599	7.308030554		Q8Y7B7	Lmo1369 protein	lmo1369
1.315590143	8.934574194		P0A4Q8	UPF0145 protein lmo0208	lmo0208
1.288183928	7.050843581		Q8Y5F6	Lmo2108 protein	lmo2108
1.281007528	8.768882185		Q92C24	30S ribosomal protein S15	rpsO
1.246596575	7.978782905		Q8Y3R3	Glutathione biosynthesis bifunctional protein GshAB	gshAB
1.228598833	8.536634185		Q8Y6F1	Lmo1736 protein	lmo1736
1.219435215	7.448489892		Q8YAN3	Lmo0084 protein	lmo0084
1.216575861	7.752071507		Q8Y4W0	Lmo2319 protein	lmo2319
1.179326057	8.457306492		Q8Y9W3	Lmo0406 protein	lmo0406
1.171905041	9.523941465	pdu	Q8Y7W8	Lmo1151 protein	PduA
1.152827501	6.912928473		Q8Y3U4	Lmo2737 protein	lmo2737
1.115174055	7.953914252		Q8Y849	Lmo1069 protein	lmo1069
1.105092049	6.307816827		Q8Y6P0	Lmo1644 protein	lmo1644
1.091968298	6.8521688		Q8Y9P2	Probable dual-specificity RNA methyltransferase RlmN	rlmN
1.089939833	8.363066419		Q8Y6K1	Lmo1683 protein	lmo1683
1.068555117	6.817413307		Q8Y4N3	Lmo2403 protein	lmo2403
1.058516741	8.603772075		Q8YAU8	AA3-600 quinol oxidase subunit III	qoxC
1.05541873	8.257102333		Q8Y747	Endoribonuclease YbeY	ybeY
1.051350832	8.617912031		Q9ZIM1	Uncharacterized protein Lmo0216	lmo0216
1.04192996	8.22960506		Q8Y6P1	Lmo1643 protein	lmo1643
1.035909176	8.268086304		Q8Y3V7	Lmo2724 protein	lmo2724
1.031580925	7.932625944		Q8Y4A7	Thymidine kinase	tdk
1.022472382	6.907368359	pdu	Q8Y7W9	Regulatory protein similar to Salmonella typhimurium PcoR protein	PcoR
1.010482788	7.834401627		Q8Y8Q2	Lmo0844 protein	lmo0844
0.99387002	8.6164335		Q92AN7	Phosphoribosylformylglycinamide synthase subunit PurS	purS
0.980150938	7.937141608		Q8Y713	Lmo1513 protein	lmo1513
0.975621223	8.195124423		Q8Y6A2	Ribosome maturation factor RimM	rimM
0.967209101	7.859228391		Q8Y9E9	Lmo0580 protein	lmo0580
0.960325956	8.146778989		Q8Y5Y4	Lmo1919 protein	lmo1919
0.959985971	7.179896333		Q8Y638	Lmo1862 protein	lmo1862
0.958674908	7.766858811		Q8Y8U5	Lmo0797 protein	lmo0797
0.945564508	7.958544772		Q8Y409	Lmo2669 protein	lmo2669
0.936180592	8.409645752		Q8Y8A7	Lmo1001 protein	lmo1001
0.933904648	7.745152895		Q8Y691	Ribonuclease 3	rnc
0.925149918	7.442354323		Q8Y7F3	tRNA pseudouridine synthase B	truB
0.919288158	8.3232521		Q8Y6W9	Transcriptional repressor NrdR	nrdR
0.916373968	7.32130839		Q8Y5S2	Dihydroxy-acid dehydratase	ilvD
0.902123213	7.971572701		Q8YA78	Lmo0281 protein	lmo0281
0.901861429	7.526326352		Q8Y433	Lmo2641 protein	lmo2641
0.901158571	8.33655979		Q8Y9Y0	Lmo0387 protein	lmo0387
0.899579525	8.070555016		Q8YA86	Lmo0273 protein	lmo0273
0.89653945	7.759138816		Q8Y5X1	GTP cyclohydrolase 1	folE
0.894593716	8.283007076		Q8Y7V1	Acetate kinase 2	ackA2
0.892370224	7.801527189		Q8Y8H6	Lmo0927 protein	lmo0927
0.892153263	8.192009593		Q8Y3X2	Lmo2707 protein	lmo2707
0.883132219	7.637079257		Q8Y607	DnaD protein	dnaD
0.882959127	7.743854555	pdu	Q92CN5	Lmo1172 protein	lmo1172

## Chapter 3

0.88265419	8.25161389		Q8Y963	Lmo0670 protein	lmo0670
0.873026371	8.573173413		Q8Y6D8	Shikimate kinase	aroK
0.872084141	7.768171743		Q8Y8A5	Lmo1005 protein	lmo1005
0.864576817	8.089304452		Q8Y5A1	Lmo2168 protein	lmo2168
0.859047174	7.401262648		Q8Y4U6	FruA protein	fruA
0.857785702	8.104760167		Q8Y8L1	Lmo0887 protein	lmo0887
0.84902668	10.08554031	pdu	Q8Y7W0	Lmo1159 protein	PduJ
0.843302965	7.603707183		Q8Y8F4	Lmo0950 protein	lmo0950
0.82746768	8.17773845		Q8Y560	Lmo2216 protein	lmo2216
0.826002836	7.336879816		Q8Y4H9	Lmo2462 protein	lmo2462
0.818063736	7.325515663		Q8YAG4	Lmo0162 protein	lmo0162
0.814146519	7.507950273		Q8Y6E6	Lmo1741 protein	lmo1741
0.804112196	6.907599443		Q8YAQ0	Lmo0067 protein	lmo0067
0.799869061	7.805004432		Q8Y4V4	Lmo2326 protein	lmo2326
0.797634602	8.023005397		Q8Y9L5	Lmo0512 protein	lmo0512
0.796156883	9.056180423		P66144	50S ribosomal protein L28	rpmB
0.789059401	7.549579485		Q8Y6U9	Lmo1582 protein	lmo1582
0.787975311	6.8469059		Q8Y4Z6	Protein gp20 [Bacteriophage A118]	lmo2283
0.785645723	7.535572587		Q8Y4J9	Lmo2439 protein	lmo2439
0.779451132	7.056752441		Q48759	Protein-arginine kinase	mcsB
0.779250622	7.408104227		Q8Y457	tRNA pseudouridine synthase A	truA
0.769850254	7.460597189		Q8Y6X3	Probable GTP-binding protein EngB	engB
0.766243935	7.87653536		Q8Y9G3	Imidazole glycerol phosphate synthase subunit HisH	hisH
0.764287472	7.400123355		Q8YAD1	Peptidyl-tRNA hydrolase	pth
0.763047457	7.635735002		Q8Y6V4	UPF0173 metal-dependent hydrolase lmo1577	lmo1577
0.749732971	7.424342516		Q8Y8R9	3-hydroxy-3-methylglutaryl coenzyme A reductase	lmo0825
0.744203329	8.10233078	pdu	Q8Y7V9	Phosphate propanoyltransferase	PduL
0.739841223	7.28302971		Q8Y7N7	Glutamate racemase	murl
0.739699364	7.427567248		Q8Y6K4	Lmo1680 protein	lmo1680
0.739346743	7.503204876		Q8Y7M3	Lmo1251 protein	lmo1251
0.720335007	6.908050507		Q8YA57	Lmo0304 protein	lmo0304
0.718988895	7.432600545		Q8Y9T7	Lmo0436 protein	lmo0436
0.706874132	7.117470164		Q8Y6N8	Nuclease SbcCD subunit D	sbcD
0.70556736	6.660780128		Q8Y903	Lmo0739 protein	lmo0739

**Supplementary Table 2.** Input to Pathview with Entrez IDs and protein expression indicated by LFO intensity. (Only list the top 100 rows, the full table with 1294 rows was online in bellowing link)

log10 (Anaerobic Pdu induced vs Pdu control)	Protein IDs	Entrez IDs	Change Fold
2.444868565	Q8Y523	984903	278.5278101
2.001654863	Q8Y7A9	987847	100.3817733
1.78644681	Q8Y8G0	986825	61.15708962
1.756666899	Q8Y985	987051	57.1040484
1.708023787	Q8Y569	984638	51.05329614
1.657866478	Q8Y9F9	984506	45.48481975
1.631134987	Q8Y6X0	986991	42.76958014
1.619628191	Q92AD0	985814	41.65126452

1.598968029	Q8Y403	986871	39.71623109
1.578961134	Q8Y5N5	987950	37.92810407
1.556344271	Q8Y455	986309	36.0034626
1.546034813	Q8Y7W2	986152	35.15886226
1.532580137	Q8Y9C3	986403	34.0863216
1.482708454	Q8Y8Z0	985519	30.38844337
1.441064358	Q8Y6C4	985978	27.60986974
1.358945608	Q8Y717	987759	22.85312569
1.340945005	Q8Y9Q0	985208	21.92527279
1.32920599	Q8Y7B7	986887	21.34056876
1.315590143	P0A4Q8	987041	20.68188616
1.288183928	Q8Y5F6	988008	19.41708034
1.281007528	Q92C24	987711	19.09886365
1.246596575	Q8Y3R3	986798	17.64398073
1.228598833	Q8Y6F1	986571	16.92773428
1.219435215	Q8YAN3	986581	16.57430075
1.216575861	Q8Y4W0	984557	16.46553555
1.179326057	Q8Y9W3	987775	15.1121431
1.171905041	Q8Y7W8	986164	14.85610775
1.152827501	Q8Y3U4	987071	14.2176396
1.115174055	Q8Y849	986276	13.03689162
1.105092049	Q8Y6P0	985681	12.73773028
1.091968298	Q8Y9P2	986229	12.35857217
1.089939833	Q8Y6K1	985632	12.30098341
1.068555117	Q8Y4N3	987496	11.70995205
1.058516741	Q8YAU8	984980	11.44238986
1.05541873	Q8Y747	987827	11.36105677
1.051350832	Q9ZIM1	987050	11.2551382
1.04192996	Q8Y6P1	985686	11.01361676
1.035909176	Q8Y3V7	984922	10.86198443
1.031580925	Q8Y4A7	986601	10.75426973
1.022472382	Q8Y7W9	986159	10.53106714
1.010482788	Q8Y8Q2	985332	10.24431179
0.99387002	Q92AN7	985970	9.85984346
0.980150938	Q8Y713	987764	9.553245492
0.975621223	Q8Y6A2	985937	9.45412246
0.967209101	Q8Y9E9	986638	9.272761736
0.960325956	Q8Y5Y4	985763	9.126955989
0.959985971	Q8Y638	985832	9.119813801
0.958674908	Q8Y8U5	985426	9.092324094
0.945564508	Q8Y409	987156	8.821948302
0.936180592	Q8Y8A7	986350	8.633374726
0.933904648	Q8Y691	985924	8.588249402
0.925149918	Q8Y7F3	987709	8.416856397
0.919288158	Q8Y6W9	986952	8.304015639
0.916373968	Q8Y5S2	984864	8.248480806
0.902123213	Q8YA78	987437	7.982211169
0.901861429	Q8Y433	986303	7.977401109
0.901158571	Q8Y9Y0	987643	7.964501002
0.899579525	Q8YA86	987401	7.935595546
0.89653945	Q8Y5X1	987987	7.880240094
0.894593716	Q8Y7V1	986132	7.845013868

0.892370224	Q8Y8H6	986782	7.804951775
0.892153263	Q8Y3X2	984953	7.801053622
0.883132219	Q8Y607	985793	7.640683659
0.882959127	Q92CN5	986126	7.637639004
0.88265419	Q8Y963	985009	7.632278162
0.873026371	Q8Y6D8	986346	7.464940853
0.872084141	Q8Y8A5	986400	7.448762732
0.864576817	Q8Y5A1	984676	7.321108051
0.859047174	Q8Y4U6	984474	7.228483174
0.857785702	Q8Y8L1	986567	7.207517437
0.84902668	Q8Y7W0	986147	7.063609468
0.843302965	Q8Y8F4	987861	6.971126525
0.82746768	Q8Y560	984814	6.721522859
0.826002836	Q8Y4H9	987372	6.698889842
0.818063736	Q8YAG4	986854	6.577543606
0.814146519	Q8Y6E6	985955	6.518482722
0.804112196	Q8YAQ0	986401	6.369600524
0.799869061	Q8Y4V4	984477	6.3076714
0.797634602	Q8Y9L5	985264	6.275301573
0.796156883	P66144	985895	6.253985691
0.789059401	Q8Y6U9	986947	6.152610192
0.787975311	Q8Y4Z6	984481	6.137271151
0.785645723	Q8Y4J9	987411	6.104438509
0.779451132	Q48759	987202	6.017985428
0.779250622	Q8Y457	986311	6.015207617
0.769850254	Q8Y6X3	986915	5.886406554
0.766243935	Q8Y9G3	984852	5.837729059
0.764287472	Q8YAD1	987046	5.811489691
0.763047457	Q8Y6V4	986999	5.794920159
0.749732971	Q8Y8R9	985372	5.619956722
0.744203329	Q8Y7V9	986142	5.548854398
0.739841223	Q8Y7N7	986027	5.493399995
0.739699364	Q8Y6K4	985641	5.49160591
0.739346743	Q8Y7M3	986006	5.487148865
0.720335007	Q8YA57	987515	5.252124432
0.718988895	Q8Y9T7	986537	5.235870487
0.706874132	Q8Y6N8	985682	5.091832774
0.70556736	Q8Y903	985542	5.07653471

**Supplementary Table 3.** Reaction list of Rhamnose metabolism and theoretical ATP yield from rhamnose conversion to lactate, acetate and propionate.

Reaction IDs from BIGG	Reaction from BIGG database	Genes	Description of reaction	ATP production
<b>RMNt</b>	$\alpha$ -L-Rhamnose $\rightleftharpoons$ $\beta$ -L-Rhamnose	rhaM	L-rhamnose mutarotase	0
<b>RMI</b>	$\beta$ -L-Rhamnose $\rightleftharpoons$ L-Rhamnulose	rhaA	L-rhamnose isomerase	0
<b>RMK</b>	ATP + L-rhamnulose $\rightleftharpoons$ ADP + L-rhamnulose 1-phosphate	rhaB	Rhamnulokinase	-1

<b>RMPA</b>	L-rhamnulose 1-phosphate <=> glycerone phosphate + L-lactaldehyde	rhaD	Rhamnulose-1-phosphate aldolase	0
<b>SPPDOy</b>	L-lactaldehyde + NADPH + H+ <=> 1,2-propanediol + NADP+	?	lactaldehyde reductase	0
<b>PPDD</b>	1,2-propanediol <=> propionaldehyde + H <sub>2</sub> O	pduCDE	propanediol dehydratase	0
<b>MMSAD</b>	propionaldehyde + CoA + NAD+ = propanoyl-CoA + NADH + H+	pduP	propanal dehydrogenase	0
<b>PTAB</b>	propanoyl-CoA + phosphate <=> CoA + propanoyl phosphate	pduL	propanoyl-CoA:phosphate propanoyltransferase	0
<b>PPA</b>	ADP + propanoyl phosphate <=> ATP + propionate acid	pduW	Propionate kinase	1
<b>ALCD</b>	propionaldehyde + NADH + H+ = NAD+ + 1-propanol	pduQ	Alcohol dehydrogenase (Propanal)	0
<b>TPI</b>	glycerone phosphate <=> Glyceraldehyde 3-phosphate	tpiA1	Triose-phosphate isomerase	0
<b>GAP</b>	Glyceraldehyde 3-phosphate + NAD+ + Phosphate <=> 3-Phospho-D-glyceroyl phosphate + H+ + NADH	gap	Glyceraldehyde-3-phosphate dehydrogenase	0
<b>PGK</b>	3-Phospho-D-glyceroyl phosphate + ADP <=> 3-Phospho-D-glycerate + ATP	pgk	Phosphoglycerate kinase	1
<b>PGM</b>	3-Phospho-D-glycerate <=> D-Glycerate 2-phosphate	pgm	Phosphoglycerate mutase	0
<b>ENO</b>	D-Glycerate 2-phosphate <=> H <sub>2</sub> O + Phosphoenolpyruvate	eno	Enolase	0
<b>PYK</b>	Phosphoenolpyruvate + ADP + H+ <=> Pyruvate + ATP	pyk	Pyruvate kinase	1
<b>LDH</b>	Pyruvate + NADH + H+ <=> L-Lactate + NADH	ldh	L-lactate dehydrogenase	0
<b>PDH</b>	Pyruvate + NAD+ + CoA <=> Acetyl-CoA + CO <sub>2</sub> + NADH	pdh	Pyruvate dehydrogenase	0
<b>PTAr</b>	Acetyl-CoA + Phosphate <=> Acetyl phosphate + CoA	pta	Phosphotransacetylase	0
<b>ACKr</b>	Acetyl phosphate + ADP <=> Acetate + ATP	ack	Acetate kinase	1

**theoretical ATP yield from rhamnose conversion to lactate: -0.5 ATP from RMK + 1 ATP from PGK + 1 ATP from PYK = 1.5 ATP / 1 lactate**

**theoretical ATP yield from rhamnose conversion to acetate: -0.5 ATP from RMK + 1 ATP from PGK + 1 ATP from PYK + 1 ATP from ACKr = 2.5 ATP / 1 acetate**

**theoretical ATP yield from rhamnose conversion to propionate: -0.5 ATP from RMK + 1 ATP from PAA = 0.5 ATP / 1 propionate**

**Supplementary Table 4.** Annotation and Proteins IDs of *rha* and *pdu* cluster

Rhamnose catabolism gene cluster ( <i>rha</i> )			
UniProt Protein ID	Gene locus ID	Gene Name	Protein Family Membership (InterPro ID)
Q8Y3I9	lmo2846	rhaM	L-rhamnose mutarotase (IPR013448)
Q8Y3I8	lmo2847	rhaD	Rhamnulose-1-phosphate aldolase (IPR013447)
Q8Y3I7	lmo2848	rhaA	Rhamnose isomerase (IPR009308)
Q8Y3I6	lmo2849	rhaB	Rhamnulokinase (IPR013449)
Q926Q9	lmo2850		MFS transporter superfamily (IPR036259)
Q8Y3I5	lmo2851	rhaR	Transcription regulator HTH-like (IPR037923)

1,2-propanediol utilization gene cluster ( <i>pdu</i> )			
UniProt Protein ID	Gene locus ID	Gene Name	Protein Family Membership (InterPro ID)
Q8Y7X7	lmo1142	pduS	Propanediol utilization protein, PduS (IPR017054)
Q8Y7X6	lmo1143	pduT	Polyhedral organelle shell protein, PduT (IPR011238)
Q8Y7X5	lmo1144	pduU	Polyhedral organelle shell protein, PduU (IPR009307)

Q8Y7X4	lmo1145	pduV	Propanediol utilisation protein, PduV (IPR012381)
Q8Y7X3	lmo1146		Unannotated
Q8Y7X2	lmo1147	cobU	Cobinamide kinase/cobinamide phosphate guanyltriferase (IPR003203)
Q8Y7X1	lmo1148	cobS	Adenosylcobinamide-GDP ribazoletransferase (IPR003805)
Q8Y7X0	lmo1149	cobC	Alpha-ribazole phosphatase, CobC (IPR017578)
	rli39	Riboswitch, small RNA	
Q8Y7W9	lmo1150	PocR	Transcription regulator HTH, AraC- type (IPR020449)
	rliH	small RNA	
Q8Y7W8	lmo1151	pduA	Polyhedral organelle shell protein, PduA (IPR011238)
Q8Y7W7	lmo1152	pduB	Polyhedral organelle shell protein, PduB (IPR009193)
Q8Y7W6	lmo1153	pduC	Propanediol/glycerol dehydratase, large subunit superfamily (IPR036999)
Q8Y7W5	lmo1154	pduD	Propanediol/glycerol dehydratase, medium subunit (IPR025541)
Q8Y7W4	lmo1155	pduE	Propanediol/glycerol dehydratase, small subunit (IPR003207)
Q8Y7W3	lmo1156	pduG	Diol dehydratase reactivating factor, alpha subunit (IPR009191)
Q8Y7W2	lmo1157	pduH	Diol dehydratase reactivating factor, small subunit (IPR009192)
Q8Y7W1	lmo1158	pduK	Polyhedral organelle shell protein, PduK (IPR011238)
Q8Y7W0	lmo1159	pduJ	Polyhedral organelle shell protein, PduJ (IPR011238)
Q8Y7V9	lmo1160	pduL	Phosphate propanoyltransferase (IPR008300)
Q8Y7V8	lmo1161	eutJ	Ethanolamine utilization protein EutJ family protein, (TIGR02529)
Q8Y7V7	lmo1162	pduM	Propanediol utilization protein, PduM (IPR030992)
Q8Y7V6	lmo1163	pduN	Polyhedral organelle shell protein, PduN (IPR004992)
Q8Y7V5	lmo1164	pduO	Adenosylcobalamin biosynthesis, ATP:cob(I)alamin adenosyltransferase, bifunctional PduO (IPR009221)
Q8Y7V4	lmo1165	pduP	Propionaldehyde dehydrogenase, PduP-related (IPR012408)
Q8Y7V3	lmo1166	pduQ	Iron-type alcohol dehydrogenase-like (IPR039697)
Q8Y7V2	lmo1167	pduF	Propanediol utilization protein, PduF (IPR000425)
Q8Y7V1	lmo1168	pduW	Acetate/propionate kinase (IPR004372)
Q8Y7V0	lmo1169		L-threonine-O-3-phosphate decarboxylase (IPR005860)
Q8Y7U9	lmo1170	pduX	Propanediol utilisation protein, PduX-related (IPR012363)

**Supplementary File 1.** Protein similarity alignment with lactaldehyde reductase FucO of *Escherichia coli* against *L. monocytogenes* EGDe

**The Supplementary Materials for this article can also be found online at:**

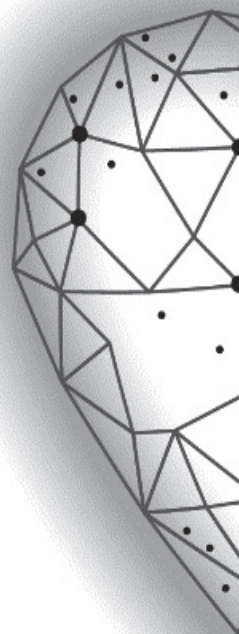
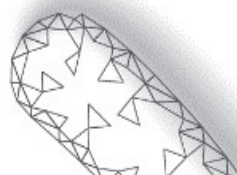
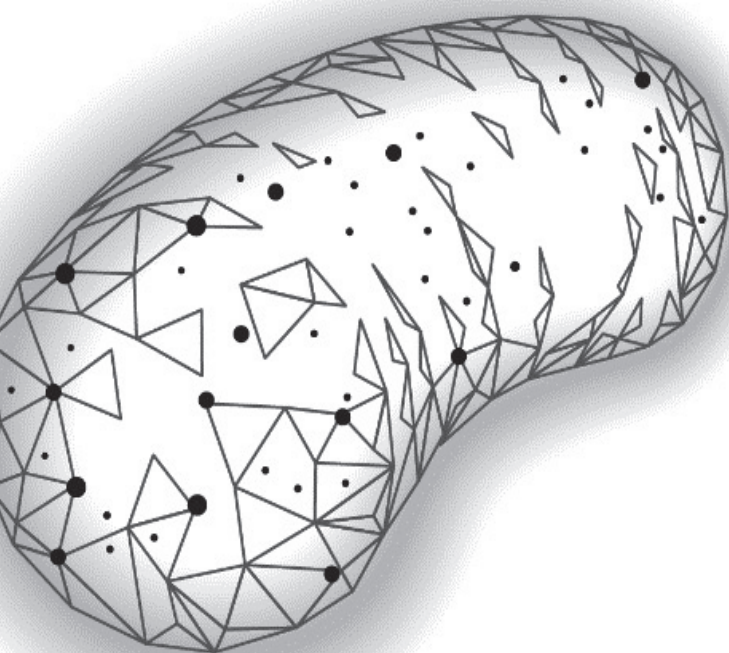
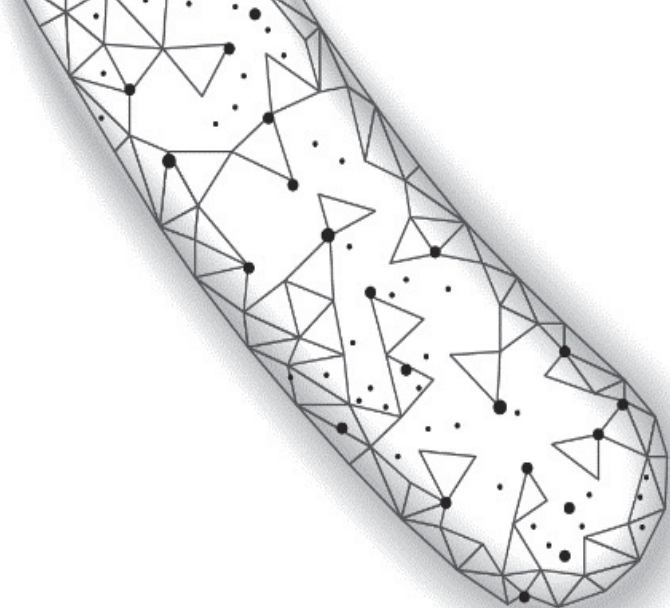
<https://doi.org/10.1128/mSphere.00434-21>

### 3.6 References

1. Radoshevich, L. and P. Cossart, *Listeria monocytogenes: towards a complete picture of its physiology and pathogenesis*. Nature Reviews Microbiology, 2018. **16**(1): p. 32-46.
2. Jemmi, T. and R. Stephan, *Listeria monocytogenes: food-borne pathogen and hygiene indicator*. Rev Sci Tech, 2006. **25**(2): p. 571-80.
3. Gahan, C.G. and C. Hill, *Listeria monocytogenes: survival and adaptation in the gastrointestinal tract*. Frontiers in cellular and infection microbiology, 2014. **4**: p. 9.
4. NicAogáin, K. and C.P. O'Byrne, *The role of stress and stress adaptations in determining the fate of the bacterial pathogen Listeria monocytogenes in the food chain*. Frontiers in microbiology, 2016. **7**: p. 1865.
5. Tompkin, R., *Control of Listeria monocytogenes in the food-processing environment*. Journal of food protection, 2002. **65**(4): p. 709-725.
6. Portman, J.L., et al., *Activation of the Listeria monocytogenes virulence program by a reducing environment*. MBio, 2017. **8**(5).
7. Kerfeld, C.A., et al., *Bacterial microcompartments*. Nature Reviews Microbiology, 2018.
8. Zeng, Z., et al., *Bacterial microcompartment-dependent 1, 2-propanediol utilization stimulates anaerobic growth of Listeria monocytogenes EGDe*. Frontiers in Microbiology, 2019. **10**: p. 2660.
9. Zeng, Z., et al., *Bacterial Microcompartments Coupled with Extracellular Electron Transfer Drive the Anaerobic Utilization of Ethanolamine in Listeria monocytogenes*. mSystems, 2021. **6**(2).
10. Yeates, T.O., C.S. Crowley, and S. Tanaka, *Bacterial microcompartment organelles: protein shell structure and evolution*. Annual review of biophysics, 2010. **39**: p. 185-205.
11. Liu, L.N., *Bacterial metabolosomes: new insights into their structure and bioengineering*. Microbial Biotechnology, 2021. **14**(1): p. 88-93.
12. Mellin, J., et al., *A riboswitch-regulated antisense RNA in Listeria monocytogenes*. Proceedings of the National Academy of Sciences, 2013. **110**(32): p. 13132-13137.
13. Cheng, S., et al., *Genetic analysis of the protein shell of the microcompartments involved in coenzyme B12-dependent 1, 2-propanediol degradation by Salmonella*. Journal of bacteriology, 2011. **193**(6): p. 1385-1392.
14. Petit, E., et al., *Involvement of a bacterial microcompartment in the metabolism of fucose and rhamnose by Clostridium phytofermentans*. PLoS One, 2013. **8**(1): p. e54337.
15. Jakobson, C.M. and D. Tullman-Ercek, *Dumpster diving in the gut: bacterial microcompartments as part of a host-associated lifestyle*. PLoS pathogens, 2016. **12**(5): p. e1005558.
16. Obradors, N., et al., *Anaerobic metabolism of the L-rhamnose fermentation product 1, 2-propanediol in Salmonella typhimurium*. Journal of bacteriology, 1988. **170**(5): p. 2159-2162.

17. Tonetti, M., et al., *The metabolism of 6-deoxyhexoses in bacterial and animal cells*. Biochimie, 1998. **80**(11): p. 923-931.
18. Chen, Y., et al., *Cross-induction of the L-fucose system by L-rhamnose in Escherichia coli*. Journal of bacteriology, 1987. **169**(8): p. 3712-3719.
19. Giraud, M.-F. and J.H. Naismith, *The rhamnose pathway*. Current opinion in structural biology, 2000. **10**(6): p. 687-696.
20. Xue, J., et al., *Exogenous or L-rhamnose-derived 1, 2-propanediol is metabolized via a pduD-dependent pathway in Listeria innocua*. Appl. Environ. Microbiol., 2008. **74**(22): p. 7073-7079.
21. Schneebeli, R. and T. Egli, *A defined, glucose-limited mineral medium for the cultivation of Listeria*. Applied and environmental microbiology, 2013: p. AEM. 03538-12.
22. Wiśniewski, J.R., et al., *Universal sample preparation method for proteome analysis*. Nature methods, 2009. **6**(5): p. 359.
23. Cox, J., et al., *Accurate proteome-wide label-free quantification by delayed normalization and maximal peptide ratio extraction, termed MaxLFQ*. Molecular & cellular proteomics, 2014. **13**(9): p. 2513-2526.
24. Bielow, C., G. Mastrobuoni, and S. Kempa, *Proteomics quality control: quality control software for MaxQuant results*. Journal of proteome research, 2015. **15**(3): p. 777-787.
25. Vizcaino, J.A., et al., *2016 update of the PRIDE database and its related tools (vol 44, pg D447, 2016)*. Nucleic Acids Research, 2016. **44**(22): p. 11033-11033.
26. Luo, W. and C. Brouwer, *Pathview: an R/Bioconductor package for pathway-based data integration and visualization*. Bioinformatics, 2013. **29**(14): p. 1830-1831.
27. Dadswell, K., et al., *Bacterial microcompartment-mediated ethanolamine metabolism in E. coli urinary tract infection*. Infection and immunity, 2019: p. IAI. 00211-19.
28. Fang, H., J. Kang, and D. Zhang, *Microbial production of vitamin B 12: a review and future perspectives*. Microbial cell factories, 2017. **16**(1): p. 1-14.
29. Rowley, C.A. and M.M. Kendall, *To B12 or not to B12: Five questions on the role of cobalamin in host-microbial interactions*. PLoS pathogens, 2019. **15**(1): p. e1007479.
30. Buchrieser, C., et al., *Comparison of the genome sequences of Listeria monocytogenes and Listeria innocua: clues for evolution and pathogenicity*. FEMS Immunology & Medical Microbiology, 2003. **35**(3): p. 207-213.
31. Fieseler, L., et al., *Rhamnose-inducible gene expression in Listeria monocytogenes*. PLoS One, 2012. **7**(8): p. e43444.
32. Muir, J., et al., *Proton-linked L-rhamnose transport, and its comparison with L-fucose transport in Enterobacteriaceae*. Biochemical Journal, 1993. **290**(3): p. 833-842.
33. Glaser, P., et al., *Comparative genomics of Listeria species*. Science, 2001. **294**(5543): p. 849-852.

34. Rodionova, I.A., et al., *Comparative genomics and functional analysis of rhamnose catabolic pathways and regulons in bacteria*. Frontiers in microbiology, 2013. **4**: p. 407.
35. Ryu, K.-S., et al., *Structural insights into the monosaccharide specificity of Escherichia coli rhamnose mutarotase*. Journal of molecular biology, 2005. **349**(1): p. 153-162.
36. Badía, J., et al., *Identification of the rhaA, rhaB and rhaD gene products from Escherichia coli K-12*. FEMS microbiology letters, 1989. **65**(3): p. 253-257.
37. Misra, S.K., et al., *Analysis of the serine/threonine/tyrosine phosphoproteome of the pathogenic bacterium Listeria monocytogenes reveals phosphorylated proteins related to virulence*. Proteomics, 2011. **11**(21): p. 4155-4165.
38. Feehily, C., C.P. O'Byrne, and K.A.G. Karatzas, *Functional  $\gamma$ -aminobutyrate shunt in Listeria monocytogenes: role in acid tolerance and succinate biosynthesis*. Applied and environmental microbiology, 2013. **79**(1): p. 74-80.
39. Cocks, G., J. Aguilar, and E. Lin, *Evolution of L-1, 2-propanediol catabolism in Escherichia coli by recruitment of enzymes for L-fucose and L-lactate metabolism*. Journal of Bacteriology, 1974. **118**(1): p. 83-88.
40. Thiennimitr, P., et al., *Intestinal inflammation allows Salmonella to use ethanolamine to compete with the microbiota*. Proceedings of the National Academy of Sciences, 2011. **108**(42): p. 17480-17485.
41. Sperandio, V., *Pathogens' adaptation to the human host*. Proceedings of the National Academy of Sciences, 2018. **115**(38): p. 9342-9343.
42. Prentice, M.B., *Bacterial microcompartments and their role in pathogenicity*. Current Opinion in Microbiology, 2021. **63**: p. 19-28.
43. Watanabe, F., et al., *Biologically active vitamin B12 compounds in foods for preventing deficiency among vegetarians and elderly subjects*. Journal of agricultural and food chemistry, 2013. **61**(28): p. 6769-6775.
44. Mellin, J., et al., *Sequestration of a two-component response regulator by a riboswitch-regulated noncoding RNA*. Science, 2014. **345**(6199): p. 940-943.



# 4

---

## **Bacterial microcompartments coupled with extracellular electron transfer drive the anaerobic utilization of ethanolamine in *Listeria monocytogenes***

Published as:

**Zeng, Z.**, Boeren, S., Bhandula, V., Light, S. H., Smid, E. J., Notebaart, R. A., & Abee, T. (2021). Bacterial microcompartments coupled with extracellular electron transfer drive the anaerobic utilization of ethanolamine in *Listeria monocytogenes*. *mSystems*, 6(2), e01349-20

## Abstract

Ethanolamine (EA) is a valuable microbial carbon and nitrogen source derived from cell membranes. EA catabolism is suggested to occur in a cellular metabolic subsystem called bacterial microcompartment (BMC) and activation of EA utilization (*eut*) genes is linked to bacterial pathogenesis. Despite reports showing that activation of *eut* is regulated by a vitamin B12-binding riboswitch and that upregulation of *eut* genes occurs in mice, it remains unknown whether EA catabolism is BMC dependent in *Listeria monocytogenes*. Here, we provide evidence for BMC-dependent anaerobic EA utilization via metabolic analysis, proteomics and electron microscopy. First, we show B12-induced activation of the *eut* operon in *L. monocytogenes* coupled to the utilization of EA thereby enabling growth. Next, we demonstrate BMC formation connected with EA catabolism with the production of acetate and ethanol in a molar ratio of 2:1. Flux via the ATP generating acetate branch causes an apparent redox imbalance due to reduced regeneration of NAD<sup>+</sup> in the ethanol branch resulting in a surplus of NADH. We hypothesize that the redox imbalance is compensated by linking *eut* BMC to anaerobic flavin-based extracellular electron transfer (EET). Using *L. monocytogenes* wild type, a BMC mutant and an EET mutant, we demonstrate an interaction between BMC and EET and provide evidence for a role of Fe<sup>3+</sup> as an electron acceptor. Taken together, our results suggest an important role of BMC-dependent EA catabolism in *L. monocytogenes* growth in anaerobic environments like the human gastrointestinal tract, with a crucial role for the flavin-based EET system in redox balancing.

**IMPORTANCE:** *Listeria monocytogenes* is a food-borne pathogen causing severe illness and, as such, it is crucial to understand the molecular mechanisms contributing to pathogenicity. One carbon source that allows *L. monocytogenes* to grow in humans is ethanolamine (EA), which is derived from phospholipids present in eukaryotic cell membranes. It is hypothesized that EA utilization occurs in bacterial microcompartments (BMCs), self-assembling subcellular proteinaceous structures and analogs of eukaryotic organelles. Here, we demonstrate that BMC-driven utilization of EA in *L. monocytogenes* results in increased energy production essential for anaerobic growth. However, exploiting BMCs and the encapsulated metabolic pathways also requires balancing of oxidative and reductive pathways. We now provide evidence that *L. monocytogenes* copes with this by linking BMC activity to flavin-based extracellular electron transfer (EET) using iron as an electron acceptor. Our results shed new light on an important molecular mechanism that enables *L. monocytogenes* to grow using host-derived phospholipid degradation products.

## 4.1 Introduction

Pathogens have evolved mechanisms to utilize specific metabolites as carbon-sources to sidestep nutritional competition with commensal bacteria in the human gastrointestinal (GI) tract [1-4]. Ethanolamine(EA), a product of the breakdown of phosphatidylethanolamine from eukaryotic cell membranes, is such a metabolite and is abundant in the human GI tract [5, 6]. It has been shown that some species in the GI tract like *Salmonella enterica*, *Enterococcus faecalis*, *Clostridium perfringens* can use EA as carbon source while for some other human pathogens including *Listeria monocytogenes*, the putative use of EA as a substrate was postulated based on the presence of a similar gene cluster [5-7]. The capability to utilize EA is encoded by the ethanolamine utilization (*eut*) operon [6-8]. EA is converted to acetaldehyde and ammonia by ethanolamine ammonia lyase EutBC [6, 9, 10]. Acetaldehyde can be catabolized to ethanol by the alcohol dehydrogenase EutG [8] or to acetyl-CoA, by acetaldehyde dehydrogenase EutE [6, 11]. Acetyl-CoA can be degraded to acetate with ATP production by the phosphotransacetylase EutD [12] and an alternative acetate kinase EutQ [13]. Alternatively, acetyl-CoA can be catabolized in the tricarboxylic acid cycle or the glyoxylate cycle, or used for lipid biosynthesis [6]. According to current models, EA is catabolized to acetate and ethanol in a molar ratio 1:1, via oxidative ATP-producing branch and reductive NAD<sup>+</sup>-regenerating branch [6]. Interestingly, previous studies showed that EA only confers a marked anaerobic growth advantage on *Salmonella enterica* serovar *Typhimurium* (*S. Typhimurium*) in the presence of tetrathionate, acting as an alternative electron acceptor via tetrathionate reductase [6, 14-16]. And the mutant lacking the tetrathionate reductase showed a decreasing colonization capacity in a mouse colitis model, which points to a role for anaerobic electron transfer in EA catabolism contributing to growth of *S. Typhimurium* in the lumen of the inflamed intestine [15]. Anaerobic EA catabolism in *L. monocytogenes*, including possible roles for anaerobic respiration, has not been studied. Notably, *L. monocytogenes* lacks tetrathionate reductase, but anaerobic electron transfer with fumarate reduction via membrane-bound fumarate reductase [17] and recently described flavin-based extracellular electron transfer (EET) with Fe<sup>3+</sup> as an electron acceptor [18], could act as substitutes in BMC-dependent EA catabolism.

The enzymes of the indicated EA pathway are present in a bacterial microcompartment (BMC), and structural shell proteins that constitute the BMC building blocks are encoded by genes in the *eut* cluster [19]. BMCs consist of a

capsule of semi-permeable shell proteins and encapsulated enzymes of metabolic pathways that liberate toxic intermediates in the lumen of the capsules [19-21]. In the formation of BMCs, so-called encapsulation peptides, 10-20 residue-long hydrophobic  $\alpha$ -helices in the N-terminal of some core enzymes, play a key role in the encapsulation mechanism [22, 23]. In our previous study, evidence was provided for a role of BMC-dependent utilization of 1,2-propanediol in *L. monocytogenes* supporting anaerobic growth and metabolism, and encapsulated enzymes PduD PduL and PduP were found to contain encapsulation peptides [24]. Expression of the *eut* operon in *L. monocytogenes* is under the regulation of the two-component regulators EutVW sequestered by a B12-binding riboswitch [25, 26]. Upregulation of the *eut* operon has been found in *L. monocytogenes* grown on vacuum-packed cold smoked salmon and in co-cultures with cheese rind bacteria, which suggests a possible role of *eut* operon in the adaptation of *L. monocytogenes* to available nutrient sources [27, 28]. The *L. monocytogenes eut* operon exhibited increased expression inside the host cell, and loss of one of the key enzymes, ethanolamine ammonia lyase (EutB), caused a defect in intracellular growth [29].

Here we show by using metabolic analysis, transmission electron microscopy and proteomics, that *L. monocytogenes* forms *eut* BMCs and utilizes EA as a carbon source in anaerobic conditions with end products acetate and ethanol in a molar ratio 2:1. We demonstrate that the resulting redox imbalance is compensated by the flavin-based EET system by comparative growth and metabolic analysis of *L. monocytogenes* wild type, a BMC mutant and a EET mutant. Our results suggest an important role of anaerobic BMC-dependent EA catabolism in the physiology of *L. monocytogenes*, with a crucial role for the flavin-based EET system in redox balancing.

## 4.2 Materials and Methods

### 4.2.1 Strains, Culture Conditions, and Growth Measurements

All *L. monocytogenes* strains used in this study were shown in (Supplementary Table 6). *L. monocytogenes* strains were anaerobically grown at 30°C in Luria Broth (LB) medium and defined medium MWB[31]. LB and MWB were supplemented with 15mM EA and/or 20nM vitamin B12 [25]. Anaerobic conditions were achieved by Anoxomat Anaerobic Culture System with the environment 10% CO<sub>2</sub>, 5% H<sub>2</sub>, 85% N<sub>2</sub>. LB and MWB with 15 mM EA and 20 nM vitamin B12 were defined as *eut*-induced condition, while LB and MWB with 15

mM EA were defined as non-induced condition. OD<sub>600</sub> measurements in LB were performed every 2 h during the first 12 h of incubation and at 24 and 36 h. Plate counting in MWB to quantify Colony Forming Units (CFUs) was performed every 12 h from 0h to 36h.

#### 4.2.2 Construction of strain *L. monocytogenes* 10403S $\Delta$ *eutB*

*L. monocytogenes*  $\Delta$ *eutB* strain was derived from wild-type 10403S (DP-L6253). Gene deletions were generated by allelic exchange using the plasmid pKSV7 [44] with chloramphenicol resistance gene. Primers used for  $\Delta$ *eutB* fragment construction and validation of deletion are given in (Supplementary Table 7). Fragment A and fragment B flanking *eutB* gene were ligated into plasmid using Gibson assembly and cloned in Top10 *E. coli*. Plasmid construct was verified by Sanger sequencing. Plasmid was then transformed into SM10 *E. Coli*. Transconjugation was performed to integrate plasmid using restrictive temperature of 42°C and colonies that were resistant to streptomycin (200 µg/mL) and chloramphenicol (7.5 µg/mL) were selected. This was followed by passaging in Brain-Heart Infusion at 37°C with shaking, diluting 1:1000 every 8 h. Mutant was obtained by screening for chloramphenicol sensitive colonies followed by colony PCR using validation primers.

#### 4.2.3 Analysis of metabolites for EA catabolism

After centrifugation, the supernatants of the cultures were collected and filtered with 0.45 µm syringe filter for the measurements. EA(mono-ethanolamine) with 1:1 dilution in ethanol was measured by Gas Chromatography with Flame Ionization Detection (GC-FID) while ethanol and acetate were directly measured by High Pressure Liquid Chromatography (HPLC). The experiment was performed twice with three technical replicates per experiment. Additionally, the standard curves of EA, ethanol and acetate were measured in the concentration range of 0.1, 1, 5, 10, 15mM. HPLC was performed as described before[24]. GC-FID conditions for the final method were as follows: 0.3-µL injection, 260 °C injector temperature, 1177 injector, SGE focus liner, 1:10 split, 335 °C detector temperature, and electronic flow controller delivering 2.8 mL/min helium carrier gas with a 2.0 psi pressure pulse for 0.25 min after injection. The retention time of EA was at 11 min, and the total run time was 50 min [45].

#### 4.2.4 Proteomics

*L. monocytogenes* EGDe cultures were anaerobically grown at 30°C in *eut* induced and in non-induced conditions. Samples were collected at 12 h for LB

and 24 h for MWB. Then samples were washed twice with 100 mM Tris (pH 8). About 10 mg wet weight cells in 100  $\mu$ l 100 mM Tris was sonicated for 30 s twice to lyse the cells. Samples were prepared according to the filter assisted sample preparation protocol (FASP) [46]. Each prepared peptide sample was analyzed by injecting (18  $\mu$ l) into a nanoLC-MS/MS (Thermo nLC1000 connected to a LTQ-Orbitrap XL) [24]. LCMS data with all MS/MS spectra were analyzed with the MaxQuant quantitative proteomics software package as described before [47]. A protein database with the protein sequences of *L. monocytogenes* EGDe (ID: UP000000817) was downloaded from UniProt. Filtering and further bioinformatics and statistical analysis of the MaxQuant ProteinGroups file were performed with Perseus [48]. Reverse hits and contaminants were filtered out. Protein groups were filtered to contain minimally two peptides for protein identification of which at least one is unique and at least one is unmodified. Also, each group (eut-induced and non-induced control) required three valid values in at least one of the two experimental groups. The volcano plot was prepared based on the Student's t-test difference of eut-induced/non-induced.

### 4.2.5 Transmission Electron Microscopy

*L. monocytogenes* EGDe cultures were grown anaerobically at 30°C in eut-induced or non-induced conditions. Samples were collected at 12 h of incubation for LB (early stationary phase). About 10  $\mu$ g dry cells were fixed for 2 h in 2.5% (v/v) glutaraldehyde in 0.1 M sodium cacodylate buffer (pH 7.2). After rinsing in the same buffer, a post-fixation was done in 1% (w/v) OsO<sub>4</sub> for 1 h at room temperature. The samples were dehydrated by ethanol and were then embedded in resin (Spurr HM20) 8 h at 70°C. Thin sections (<100 nm) of polymerized resin samples were obtained with microtomes. After staining with 2% (w/v) aqueous uranyl acetate, the samples were analyzed with a Jeol 1400 plus TEM with 120 kV setting.

### 4.2.6 Ferrozine assay of ferric iron reductase activity

*L. monocytogenes* cells grown overnight in LB medium were washed with PBS twice, normalized to an OD<sub>600</sub> of 0.2, and resuspended in fresh MWB medium supplemented with 50 mM ferric ammonium citrate for anaerobic inoculation. *L. monocytogenes* Wild Type and mutant strains grew anaerobically for 24h in MWB, with 15mM EA and 20nM B12 (eut-induced), or with 15mM EA (non-induced), 15 mM glucose (positive control) and with no added substrate (blank control). Assays were initiated by adding 100  $\mu$ L of MWB cultures from 24 h anaerobic inoculation to 100  $\mu$ L demi water with 4 mM ferrozine and then spectrophotometrically

measured by OD<sub>562</sub> as described before [18]. OD<sub>562</sub> measurements were made immediately after the initial mixture of MWB cultures and Ferrozine.

#### 4.2.7 Bioinformatics Analysis

Secondary Structure of N Terminal Peptides. The N terminal secondary structures of all *eut* genes were determined by a neural network secondary structure prediction called Jpred4 [49] as described before [24]. The input to the Jpred 4 online server<sup>1</sup> was the 50 N-terminal amino acids of each protein. Jnetconf: confidence estimation for the prediction with high scores indicating high confidence. Jnetsol25: solvent accessibility, where B means buried and '-' means non-buried at 25% cut-off.

Venn analysis and STRING networks analysis of proteins. The protein IDs of significantly changed proteins from (Supplementary Table 4 and 5) were uploaded to the BioVenn online server[50] taking the default setting to generate Venn diagrams. Overlapping proteins from the Venn diagram were transferred to the STRING online server [51] for multiple proteins analysis of functional interaction using sources such as co-expression, genomic neighborhood and gene fusion.

### 4.3 Results

#### 4.3.1 EA utilization facilitates anaerobic growth

To find out whether EA utilization stimulates anaerobic growth, we added EA (15 mM) to LB medium in line with previous works in *Salmonella* species [11, 30]. The culture medium also contained 20 nM vitamin B12 for activation of the *eut* operon in *L. monocytogenes* [25]. *L. monocytogenes* EGDe cultures grown in *eut*-induced condition (LB with EA and B12) reached significantly higher OD<sub>600</sub> values after 8h of incubation compared to cultures in control conditions (LB and LB with B12) and in *eut* non-induced conditions (LB with EA) (Figure 1A). EA in *eut*-induced condition was fully utilized within the first 24h while no significant EA utilization was observed in *eut* non-induced conditions (Figure 1B). Notably, in *eut*-induced condition EA was converted into acetate and ethanol (Figure 1C and 1D), while in *eut* non-induced condition only acetate was produced conceivably originating from metabolism of other compounds in LB. From this comparative analysis on acetate production we derive a molar ratio acetate:ethanol of approximately 2:1.

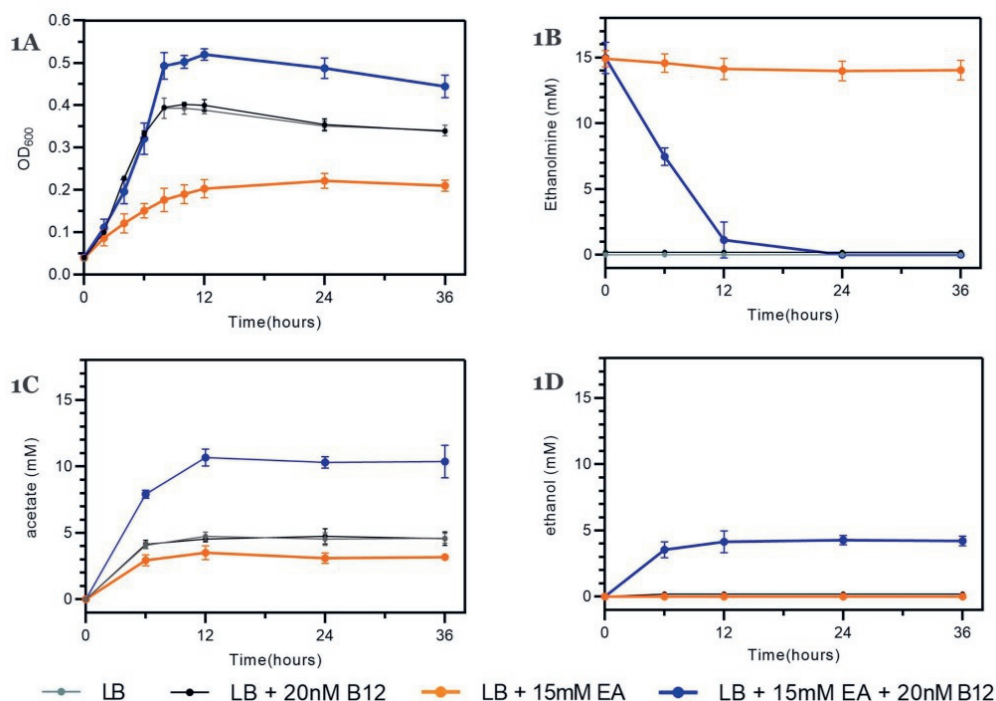


**Figure 1. Anaerobic growth and EA catabolism of *L. monocytogenes* EGDe in LB medium.**

(A) Impact of EA and/or vitamin B12 on anaerobic growth of *L. monocytogenes* EGDe; (B) EA Utilization; (C) Acetate production; (D) Ethanol production. Lines represent different growth conditions; Results from three independent experiments are expressed and visualized as means and standard errors.

Taken together, the utilization of EA with the production of acetate and ethanol contributes to the anaerobic growth of *L. monocytogenes* EGDe in *eut* induced condition.

#### 4.3.2 Ratio of ethanol and acetate production

To clarify whether *L. monocytogenes* EGDe can utilize EA as a sole carbon source, we examined EA utilization and its impact on anaerobic growth in defined medium MWB in the absence of any other carbon sources [31]. *L. monocytogenes* EGDe inoculated in *eut* induced condition (MWB with EA and B12) showed about 100-fold increase in cell counts after 24h while no significant increase in cell counts was observed in non-induced condition (MWB with EA) (Figure 2A).

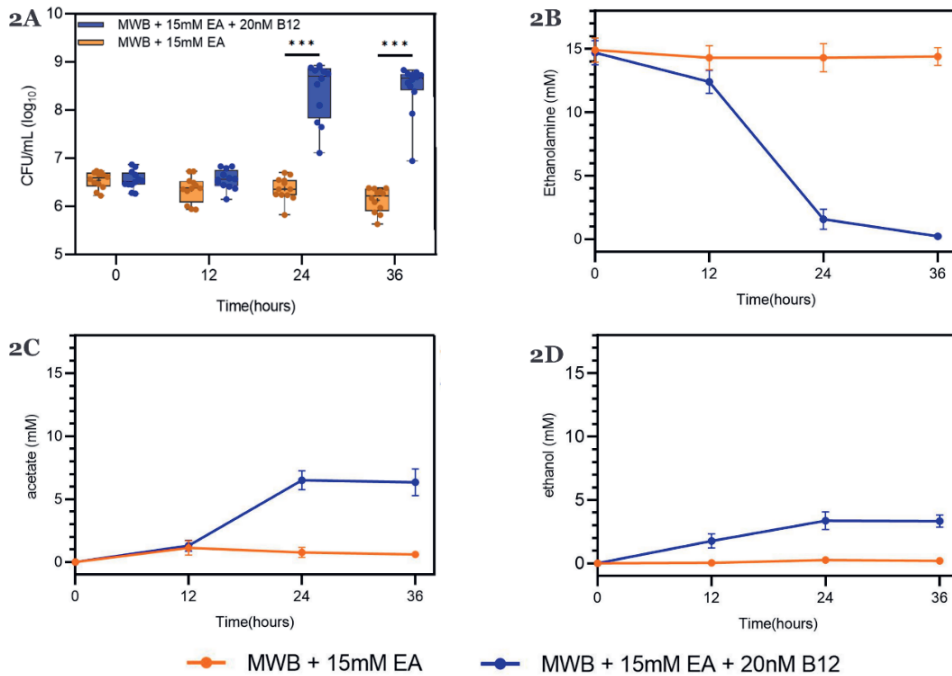


**Figure 2. Anaerobic growth and EA catabolism of *L. monocytogenes* EGDe in MWB defined medium with EA as sole carbon source.**

**(A)** Impact of EA and/or vitamin B12 on CFUs of *L. monocytogenes* EGDe; Results from three independent experiments with four technical repeats are expressed as mean and standard errors. Statistical significance is indicated (\*\*\*,  $P < 0.001$ ; Holm-Sidak T-test) **(B)** EA Utilization; **(C)** Acetate production; **(D)** Ethanol production. Cells were grown in MWB + 15 mM EA without B12 (orange symbols and lines) and with 20 nM B12 (blue symbols and lines); Error bars in (B, C, D) indicate three independent experiments expressed as mean and standard errors.

Microscopy analysis of samples showed absence of chains of cells, excluding the option that the increase in CFUs is due to disintegration of chains of cells. During the anaerobic growth of *L. monocytogenes* EGDe, 15 mM EA was converted into about 6.6 mM acetate and 3.4 mM ethanol in *eut* induced condition while no significant degradation of EA was observed in non-induced condition (Figure 2B, 2C and 2D). Calculation of the carbon mass balance, part of EA (approximately 5mM) is conceivably further catabolized in the  $\gamma$ -aminobutyrate (GABA) shunt [32], or used for lipid biosynthesis via the intermediate acetyl-CoA [6]. The utilization of EA in *eut* induced condition in defined medium MWB provides evidence that EA can act as a sole carbon source supporting anaerobic growth of *L. monocytogenes* EGDe. Notably, the observed molar ratio acetate:ethanol of 2:1 suggests an apparent redox imbalance due to higher flux via the NADH and ATP-producing

acetate branch, and reduced regeneration of NAD<sup>+</sup> in the ethanol branch resulting in a surplus of NADH.

### 4.3.3 Upregulated expression of *eut* operon including enzymes and structural shell proteins

In order to study the expression of the *eut* operon and the way it is imbedded in cell physiology, we performed proteomics to compare *L. monocytogenes* cells grown in LB and MWB medium under *eut* induced conditions and non-induced conditions. Analyses of the complete list of identified proteins, proteins' expression levels and subsequent t-test results and p-values are shown in (Supplementary Table 2) for LB and (Supplementary Table 3) for MWB grown cells. For LB, we identified 1891 total proteins where 161 are upregulated more than two-fold and 229 proteins downregulated more than two-fold in *eut* induced condition compared to non-induced condition (Figure 3A). Among these 161 upregulated proteins, the top 15 proteins are all encoded in the *eut* operon, i.e., Eut GABCLKEMTDNHQ, Imo1183 and 1185 while the other two proteins Eut VW [33] involved in *eut* operon regulation are also included. For MWB, 1736 proteins were identified of which 253 proteins are upregulated more than two times and 162 proteins downregulated more than two times in *eut* induced condition compared to non-induced condition (Figure 3B). In line with LB data, the top 15 proteins are all encoded in the *eut* operon. Analysis of the upregulated proteins in LB and MWB shows 50 proteins that overlap between the conditions pointing to a prominent role in *eut* induced conditions compared to non-induced conditions. Among these 50 proteins, 17 proteins are linked to *eut* of which 16 proteins are encoded in the *eut* operon and one gene *dra* (deoxyribose-phosphate aldolase) is predicted to have an interaction with the acetaldehyde dehydrogenase *eutE* (Imo1179) (according to STRING, Figure 3C, Supplementary Table 4). Another group of overlapping genes are potential ABC transporters, including *Imo2751-Imo2752* (ABC transporter ATP-binding protein) [34], and *ilvC* (*Imo1986*, NADP<sup>+</sup> based Ketol-acid reductoisomerase)[35]. The analysis of downregulated proteins in LB and MWB showed an overlap of 48 proteins with 18 proteins linked to vitamin B12 biosynthesis which indicates that adding vitamin B12 in the medium represses the genes involved in vitamin B12 biosynthesis (Figure 3D, Supplementary Table 5). Overlap in downregulated proteins also showed an enrichment in phospholipase (*plcA* and *plcB*), cell wall relevant (*Imo2691* and *Imo0695*), cell division relevant (*dilvB*, *rpmG1* and *Imo0111*) and zinc containing dehydrogenase (*Imo2663*, *Imo2664* and *Imo2097*). To summarize,

the significant upregulation of the *eut* operon at proteomic level including structural shell proteins strongly supports that BMC-dependent EA utilization is processed by enzymes and structural shell proteins of the *eut* operon.

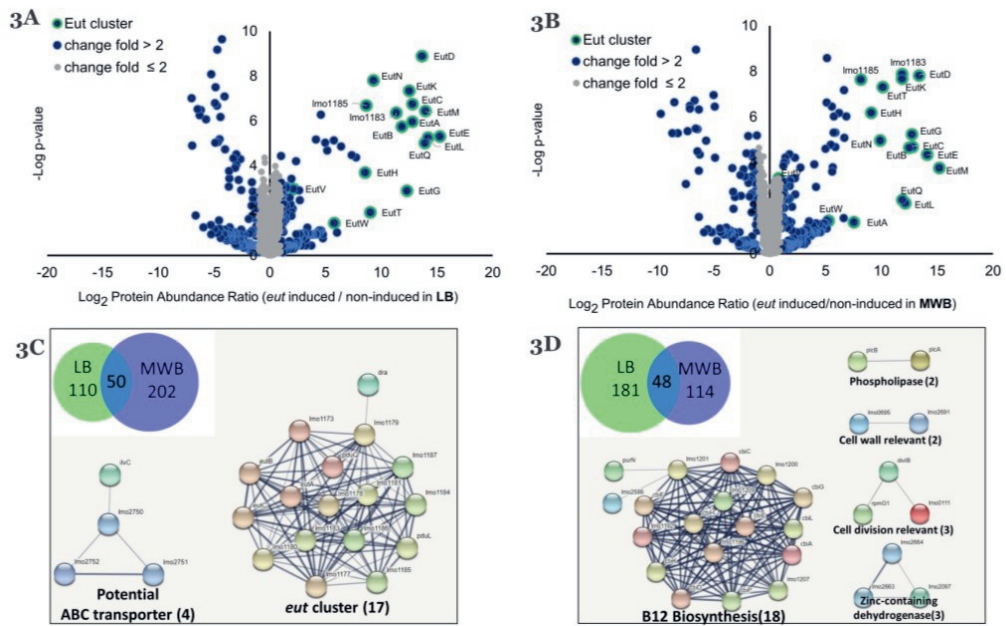


**Figure 3. Proteomics analysis of *eut* induced and non-induced *L. monocytogenes* EGDe in LB medium and MWB defined medium.**

Proteomic volcano plot of *eut* induced cells (EA + B12 added) compared to non-induced cells (EA added only) in LB medium **(A)** and MWB medium **(B)**. Venn diagram of 50 overlapping upregulated proteins **(C)**, and Venn diagram of 48 overlapping downregulated proteins **(D)**, for LB medium (green) and MWB medium (blue) and corresponding STRING protein-protein interactions. Nodes represent proteins and lines represent interactions.

#### 4.3.4 BMC structures support BMC-dependent EA catabolism

To further confirm the presence of BMCs in *eut* induced cells, we used transmission electron microscopy (TEM) and compared thin sections of both *eut*-induced and non-induced *L. monocytogenes* EGDe cells. The *eut* induced cells clearly contain BMC-like structures with an approximate diameter of 50–80 nm, which are not present in non-induced cells (Figure 4B). Notably, the identified structures strongly resemble TEM pictures of BMCs in *S. Typhimurium* and *E. coli* [36, 37], and that of recently reported BMCs found in *pdu*-induced *L. monocytogenes* [24]. Taken the metabolic, proteomic, and TEM data together, we conclude that the cytosolic BMC-like structures in *L. monocytogenes* EGDe are involved in EA utilization under anaerobic conditions.

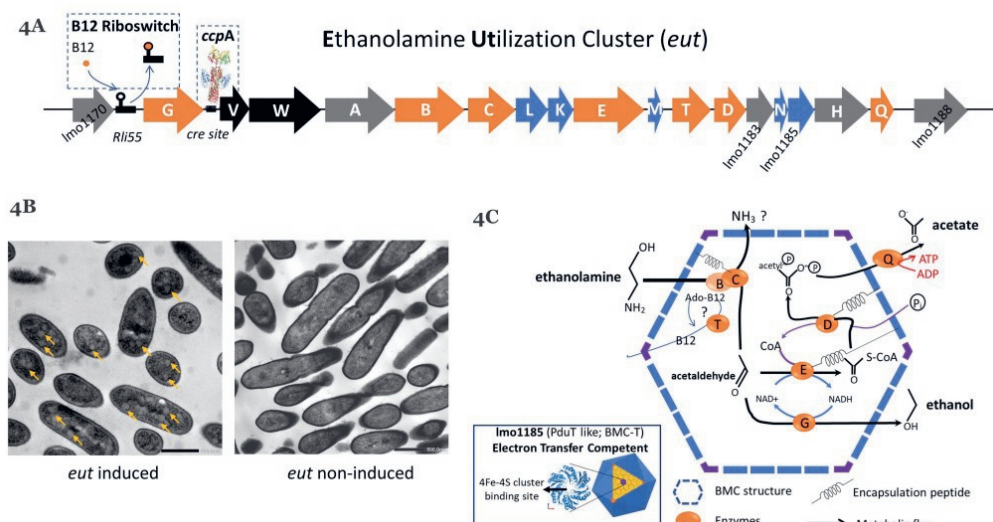


**Figure 4. Overview of BMC-dependent EA catabolism model of *L. monocytogenes***

**(A)** Analysis of the *eut* operon (Details in Supplementary Table 1). Characters in orange represent Eut enzymes, in blue represent BMC shell proteins, in black represent the two component regulation system, and in grey represent unannotated proteins; B12 riboswitch and CcpA *cre* binding site are indicated. **(B)** TEM visualization of BMCs in *eut* induced (left; yellow arrows point to BMCs) and non-induced cells (right). The scale bars in black represent 500nm in both TEM pictures. **(C)** Model of BMC-dependent EA catabolism. EutBC ethanolamine ammonia lyase, EutD phosphotransacetylase, EutE acetaldehyde dehydrogenase, EutG alcohol dehydrogenase, EutQ acetate kinase, EutT corrinoid cobalamine adenosyltransferase, with putative encapsulation peptides indicated. Zoom-in part shows the prediction of potential [4Fe-4S] cluster binding site in Eut shell protein Imo1185, that is highly similar to that previously reported for PduT shell protein by Pang et al. [39]. See text for details.

Hereby, based on the knowledge of the *eut* operon, we propose a model of the BMC-dependent EA catabolism. The *eut* operon in *L. monocytogenes* EGDe contains 17 genes and is most likely under the regulation of two-component regulators EutVW sequestered by binding of vitamin B12 to the riboswitch *rli55* [25]. In front of EutVW, we found a previously predicted *cre* site for the binding of carbon control protein CcpA pointing to catabolite repression control of the *L. monocytogenes eut* cluster [38]. Five *eut* genes, *eut LKMN* and *Imo1185*, are predicted to be structural shell proteins of the BMC (Figure 4A). EutK and EutM are the hexameric shell protein (BMC-H) consisting of one Pfam00936 domain while EutL and Imo1185 are the trimeric shell proteins (BMC-T) with two fused Pfam00936 domains (Supplementary Figure 1). Notably, the trimeric assembly of Imo1185 forms a flat approximately hexagonally shaped disc with a central pore that is suitable for a [4Fe-4S] cluster [39]. Furthermore EutN is the pentameric shell

protein (BMC-P) consisting of one Pfam03319 domain (Supplementary Figure 1). BMC is assembled by these three types of shell proteins: BMC-H, BMC-T and BMC-P [19, 20].

Based on the previous BMC-dependent EA catabolism model in *S. Typhimurium* [5], we propose a model for *L. monocytogenes* with putative encapsulation peptides supporting recruitment of selected eut enzymes to the BMC (Figure 4C). We predict a specific hydrophobic  $\alpha$ -helix in the N terminus of the encapsulated enzyme EutC, EutD and EutE (Supplementary Figure 2), similar to that of the previously described BMC encapsulated proteins in *S. Typhimurium* and for *pdu* BMCs in *L. monocytogenes* [22, 24]. EA is split into acetaldehyde and ammonia by ethanolamine ammonia lyase EutBC [6, 9, 10]. Acetaldehyde can be converted into ethanol by the alcohol dehydrogenase EutG [8], or into acetyl-CoA by the acetaldehyde dehydrogenase EutE [6, 11]. Acetyl-CoA can be converted into acetyl-phosphate and subsequently acetate and ATP production by the phosphotransacetylase EutD [12] and an alternative acetate kinase respectively EutQ [13].

#### 4.3.5 Flavin-based EET linked with BMCs maintains redox balance of EA catabolism

The observed unbalanced production of acetate and ethanol in a 2:1 molar ratio suggests a surplus of NADH, and this requires additional NAD<sup>+</sup> regeneration reactions to restore the redox balance. As discussed in previous studies, BMC is a redox-replete compartment which can generate reductants internally or facilitate the transfer of electrons from the cytosol across the shell [6, 40]. Recently it has been shown that *L. monocytogenes* uses a distinctive anaerobic flavin-based EET mechanism to deliver electrons to iron (Fe<sup>3+</sup>) or to fumarate via membrane-bound fumarate reductase [18].

In our study, MWB defined medium indeed contains ferric citrate and flavin, and proteomic analysis of *L. monocytogenes* EGDe grown in this medium identified protein Imo2637 encoding a EET-linked lipoprotein PplA and protein Imo2638 encoding a EET-linked NADH dehydrogenase Ndh2 [18] (Supplementary Table 3). Next, we tested the hypothesis that anaerobic EET could play a role in BMC-dependent EA utilization using *L. monocytogenes* 10403S wild type and mutants. Notably, *eut* induced *L. monocytogenes* 10403S showed a similar growth benefit from utilizing EA as *eut* induced *L. monocytogenes* EGDe (Figure 5A and Figure 5B).

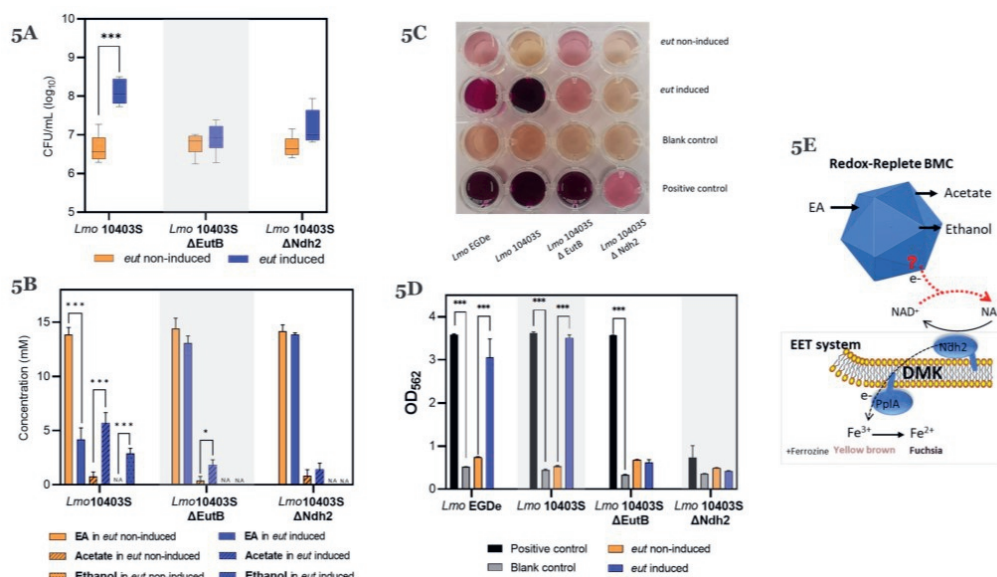


**Figure 5. BMC-dependent EA catabolism couples to flavin-based EET**

**(A)** Impact of EA and/or vitamin B12 on CFUs. **(B)** EA catabolism. Experiments in (A) and (B) were performed with *L. monocytogenes* 10403S and mutant strains grown anaerobically for 24h with initial  $6.5 \pm 0.1 \log_{10}$  CFU/mL inoculation in MWB, with 15mM EA and 20nM B12 (*eut*-induced), or with 15mM EA (*eut*-non-induced). **(C)** Colorimetric change of ferric reductase assay. **(D)** OD<sub>562</sub> measurements of ferric reductase assay. Experiments in (C) and (D) were performed with *L. monocytogenes* EGDe and 10403S and mutant strains grown anaerobically for 24h in MWB, with 15mM EA and 20nM B12 (*eut*-induced), or with 15mM EA (*eut*-non-induced), 15 mM glucose (positive control) and with no added substrate (blank control). Results in (A) (B) and (D) from three independent experiments are expressed as mean and standard errors. Statistical significance is indicated (\*\*\*,  $P < 0.001$ ; \*,  $P < 0.05$ ; Holm-Sidak T-test). **(E)** Proposed model of the electron transfer from BMC to EET. Blue geometric block represents BMC. CM represents cytoplasmic membrane; Ndh2, PplA and DMK (demethylmenaquinone) represent EET with  $\text{Fe}^{3+}$  as electron acceptor (See text for details; figure 5E adapted from [18]).

Moreover, the mutant strains *L. monocytogenes* 10403S  $\Delta\text{eutB}$ , lacking ethanolamine ammonia lyase, and  $\Delta\text{ndh2}$  lacking EET-linked NADH dehydrogenase are both impaired for EA utilization (Figure 5B), suggesting an involvement of the EET system in EA utilization and thereby a link with BMCs. Next, we used a ferrozine-based colorimetric assay to determine electron transfer between BMC and EET following *L. monocytogenes* EA utilization in MWB medium. In this assay, electrons generated from EA catabolism are transferred to  $\text{Fe}^{3+}$  generating  $\text{Fe}^{2+}$ , where binding of ferrozine to the differently charged Fe molecules results in a colorimetric change from yellow brown to fuchsia, respectively. The colorimetric changes were shown for *L. monocytogenes* EGDe and *L. monocytogenes* 10403S in *eut* induced condition following EA utilization

while *eut* mutant strain *L. monocytogenes* 10403S  $\Delta$  *eutB* and EET mutant strain *L. monocytogenes* 10403S  $\Delta$  *ndh2* showed no colorimetric changes (Figure 5C). OD<sub>562</sub> measurements indicated a significantly higher ferric iron reductase activity in *eut* induced conditions compared to non-induced conditions of *L. monocytogenes* EGDe and *L. monocytogenes* 10403S (Figure 5D). Taken together, these results provide evidence for a link between *eut* BMCs and the EET system via regeneration of NAD<sup>+</sup> by NADH oxidation in the EET using Fe<sup>3+</sup> as an electron acceptor (Figure 5E). The action of the EET as an alternative reductive pathway next to the ethanol branch, thus stimulates anaerobic growth by enhanced flux via the ATP generating acetate branch in BMC-facilitated EA catabolism.

#### 4.4 Discussion

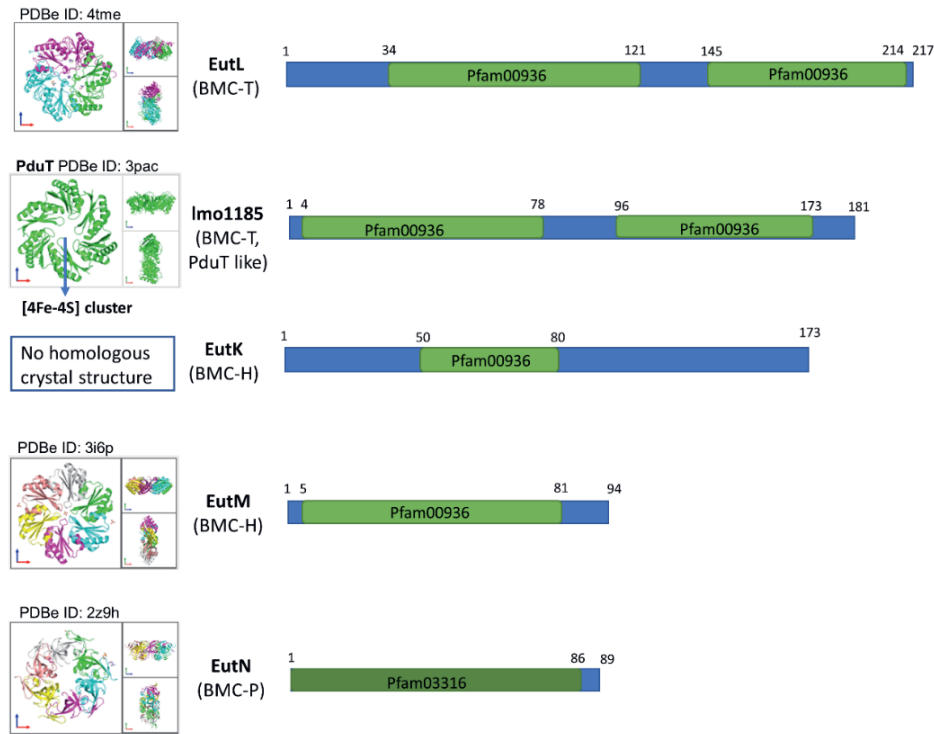
This study provides evidence for the activation of BMC-dependent ethanolamine (EA) utilization in *L. monocytogenes* in anaerobic conditions in LB and MWB medium containing EA and vitamin B12. By using metabolic analysis, proteomics and electron microscopy we demonstrated the formation of BMCs in conjunction to EA catabolism with the production of acetate and ethanol in a 2:1 molar ratio. Selected genes in the *eut* operon encode structural shell proteins that form the respective *eut* BMC [19]. Previous studies showed that BMCs for EA catabolism in *S. Typhimurium* and *E. faecalis*, are composed of five structural shell proteins, EutS, EutM, EutK, EutL, and EutN [6, 19, 21]. Notably, *L. monocytogenes* *eut* operon also encodes five putative shell proteins, EutM, EutK, EutL, EutN and lmo1185, and combined with visualization of BMC structures by TEM and our proteomic data, we conclude that *eut* BMCs are composed of these five indicated structural shell proteins. Apparently, EutS is not essential for BMC assembly in *L. monocytogenes*. EutS is hexameric BMC shell protein with a Pfam00936 domain, and it is conceivable that function of EutS is taken over by EutK and/or EutM in *L. monocytogenes*, since both are also hexameric BMC shell proteins with a Pfam00936 domain (Supplementary Figure 1).

EA is a valuable carbon source for *L. monocytogenes* to outcompete other bacteria unable to utilize EA in food environments [27, 28] or human GI tract where EA is abundant [5, 6]. Our results in defined medium reveal that *L. monocytogenes* can utilize EA as sole carbon source via a BMC-dependent *eut* pathway (Figure 2). Encasing the pathway inside BMCs is essential, since this prevents the toxic acetaldehyde intermediate to damage proteins and RNA/DNA

in the cytoplasm [19, 41]. The generated reductants are oxidized inside the BMC, while it has been hypothesized that electrons may also be shuttled to the cytosol via specific shell proteins acting as redox carriers [6, 19, 20, 40]. Our metabolite analysis showed enhanced flux via the ATP generating acetate branch in *L. monocytogenes*, and a reduced flux via the NAD<sup>+</sup> regenerating ethanol branch in a 2:1 molar ratio resulting in surplus NADH. In support of the previously mentioned putative electron shuffling from BMCs to the cytosol, using wild type, EutB and Ndh2 mutants, we identified a link between *L. monocytogenes eut* BMCs activity and the recently discovered flavin-based EET system (Figure 5E) [18]. Suggested electron acceptors, fumarate and iron, are conceivably present in the human intestine and in host cells and have been reported to contribute to *L. monocytogenes* virulence [17, 18, 42, 43]. The identified *L. monocytogenes eut* Lmo1185 shell protein belongs to the class of trimeric shell proteins (BMC-T) with two fused Pfam00936. We hypothesize that this predicted PduT-like shell protein with a [4Fe-4S] cluster [39], acts as a redox carrier in this process. Further studies are required to elucidate the role of this *eut* BMC shell protein as redox carrier.

Taken together, our results provide evidence of anaerobic EA catabolism in *L. monocytogenes* driven by BMC formation and function with a crucial role for the flavin-based EET system in redox balancing. These findings provide a new model (see Figure 5E) involving two interconnected cellular subsystems which explains how *L. monocytogenes* is able to grow and adapt in EA rich environments like in the human GI tract.

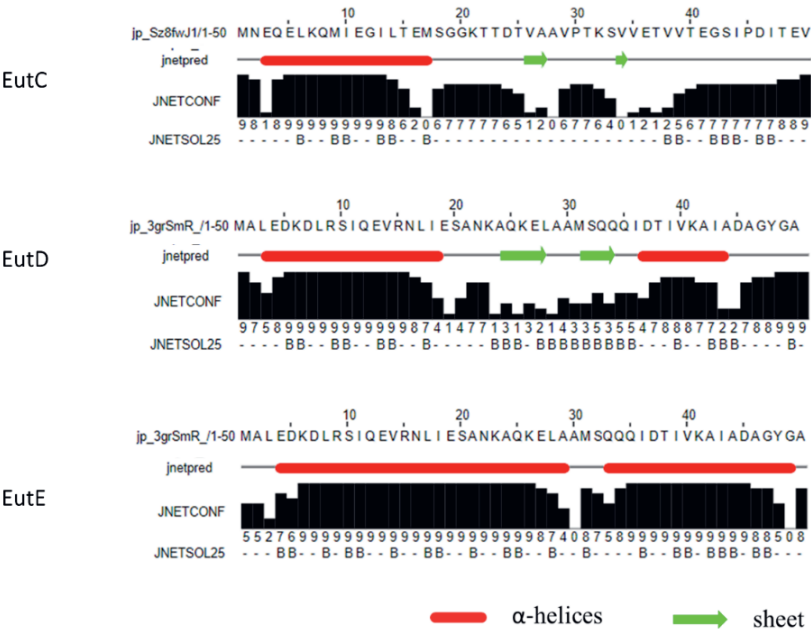
4.5 Supplementary Materials



**Supplementary figure 1. Homologous protein structures and domain architecture of shell proteins in *eut* operon**

In the left, homologous protein structures of EutL, PduT, EutM and EutN in other bacteria from Protein Data Bank in Europe (PDB). PDB ID of each proteins are listed in the top of protein structures. In the right, the domain architecture of shell proteins in *eut* operon of *L. monocytogenes* EGDe analysed by UniProtKB.





**Supplementary figure 2. Prediction of N terminal encapsulation peptides**

The predicted N-terminal encapsulation peptides of EutC, EutD, and EutE analysed by Jpred4, with alpha helices marked as red tubes and sheets as green arrows. Jnetconf: confidence estimation for the prediction with high scores indicating high confidence. Jnetsol25: solvent accessibility, where B means buried and '-' means non-buried at 25% cut-off.

**Supplementary Table 1.** The analysis of *eut* operon

Gene Name	Protein Family Membership (InterPro ID)	Prediction of shell protein by HMMER	Prediction of encapsulation peptide by Jpred4
eutG	Iron-type alcohol dehydrogenase-like (IPR039697)		
eutV	Signal transduction response regulator, antiterminator (IPR008327)		
eutW	Signal transduction histidine kinase, subgroup 2 (IPR011495)		
eutA	Ethanolamine utilisation EutA (IPR009377)		
eutB	Ethanolamine ammonia lyase large subunit (IPR010628)		
eutC	Ethanolamine ammonia-lyase light chain (IPR009246)		Yes, see supplementary figure 2
eutL	Polyhedral organelle shell protein, EutL/PduB type (IPR009193)	Yes, BMC-T containing two Pfam00936	
eutK	CcmK-like superfamily (IPR037233)	Yes, BMC-H containing Pfam00936	
eutE	Acetaldehyde dehydrogenase, acetylating (IPR013357)		Yes, see supplementary figure 2
eutM	CcmK-like superfamily (IPR037233)	Yes, BMC-H containing Pfam00936	
eutT	Adenosylcobalamin biosynthesis, ATP:cob(I)alamin adenosyltransferase, EutT-type (IPR009194)		
eutD	Phosphate propanoyltransferase (IPR008300)		Yes, see supplementary figure 2
lmo1183	Ethanolamine utilization, putative (IPR013372)		
eutN	Ethanolamine utilization protein EutN/carboxysome structural protein CcmI (IPR004992)	Yes, BMC-P containing Pfam03319	
lmo1185	Polyhedral organelle shell protein PduT (IPR011238)	Yes, BMC-T containing two Pfam00936	
eutH	Ethanolamine utilisation protein EutH (IPR007441)		
eutQ	Ethanolamine utilisation EutQ (IPR010424)		

The table lists NCBI gene ID, UniProt protein ID, Gene name, Protein Family Membership with InterPro ID, Prediction of shell protein by HMMER, Prediction of encapsulation peptide by Jpred4.

**Supplementary Table 2.** Protein profiling of the *eut* induced compared with the non-induced *L. monocytogenes* EGDe in LB medium. (Only list the top 100 rows, the full table with 1893 rows was online in following link)

UniProt Protein ID	X axis: Log2 Protein abundance ratio (eut induced/non-induced in LB)	Y axis: -Log10 p-value (eut induced/non-induced in LB)	NCBI protein Annotation (format: UniProt Protein ID_ NCBI annotation)	NCBI Gene ID
Q8Y7U1	15.27361517	5.305325517	Q8Y7U1_ Lmo1179 protein_	lmo1179
Q8Y7U3	14.21664064	5.243463578	Q8Y7U3_ Lmo1177 protein_	lmo1177
Q92CM7	13.98782913	6.436433056	Q92CM7_ Lmo1180 protein_	lmo1180
Q8Y7T4	13.93670545	5.007157111	Q8Y7T4_ Lmo1187 protein_	lmo1187
Q8Y7T9	13.6691573	8.881543936	PDUL_ Phosphate propanoyltransferase_	pduL
Q8Y7U6	12.81043116	5.958769643	Q8Y7U6_ EutA protein_	eutA
Q8Y7U4	12.80652497	6.739240335	EUTC_ Ethanolamine ammonia-lyase light chain_	eutC
Q8Y7U2	12.53242109	7.329745039	Q8Y7U2_ Lmo1178 protein_	lmo1178
Q8Y7U8	12.32117582	2.883195276	Q8Y7U8_ PduQ protein_	pduQ
Q8Y7U5	11.84114949	5.743914921	Q8Y7U5_ EutB protein_	eutB
Q8Y7T8	11.35236936	6.361100981	Q8Y7T8_ Lmo1183 protein_	lmo1183
Q8Y7T7	9.304976542	7.795515164	Q8Y7T7_ Lmo1184 protein_	lmo1184
Q8Y7U0	9.034109863	1.913433737	Q8Y7U0_ Lmo1181 protein_	lmo1181

## Chapter 4

Q8Y7T6	8.658045331	6.674236867	Q8Y7T6_Lmo1185 protein_	lmo1185
Q8Y7T5	8.573076453	3.694286009	Q8Y7T5_Lmo1186 protein_	lmo1186
Q8Y4E7	7.76853432	4.36574881	Q8Y4E7_Lmo2499 protein_	lmo2499
P63363	7.381052709	4.46357585	PSTB1_Phosphate import ATP-binding protein PstB 1_	pstB1
Q8Y4E9	6.402912681	4.843680146	PSTB2_Phosphate import ATP-binding protein PstB 2_	pstB2
Q8Y845	6.053458608	1.010819256	Q8Y845_Lmo1073 protein_	lmo1073
Q8Y7U7	5.783685431	1.435351207	Q8Y7U7_Lmo1173 protein_	lmo1173
Q8Y912	5.766408538	5.124537339	Q8Y912_Lmo0730 protein_	lmo0730
Q8Y9F1	5.169915124	4.664651928	Q8Y9F1_Putative conserved membrane protein_	lmo0578
Q8Y466	4.981831378	5.01877692	Q8Y466_Lmo2589 protein_	lmo2589
Q8Y6P7	4.786122165	0.755293974	Q8Y6P7_Lmo1637 protein_	lmo1637
Q8Y8G5	4.780078605	0.925190861	Q8Y8G5_Lmo0939 protein_	lmo0939
Q8Y9V8	4.637274563	1.107502218	Q8Y9V8_Lmo0412 protein_	lmo0412
Q8Y6H6	4.598915965	6.263692206	Q8Y6H6_Aminoglycoside N(3)-acetyltransferase_	lmo1708
Q8Y6J1	4.537288659	1.054719676	RECX_Regulatory protein RecX_	recX
Q7AP68	4.450339758	1.097045707	Q7AP68_OpuCD protein_	opuCD
Q8Y4G7	4.428439114	0.976432972	Q8Y4G7_Aldose 1-epimerase_	lmo2476
Q8Y646	4.29054817	1.023524326	Q8Y646_Lmo1854 protein_	lmo1854
Q8Y4V7	4.218548182	0.934760242	Q8Y4V7_Gp43 [Bacteriophage A118]_	lmo2323
Q8Y9G7	4.198960206	0.975066846	HIS2_Phosphoribosyl-ATP pyrophosphatase_	hisE
Q8Y3P5	4.171853421	0.933105629	Q8Y3P5_Lmo2789 protein_	lmo2789
Q8Y737	4.149682966	5.153511409	Q8Y737_Lmo1485 protein_	lmo1485
Q8Y7B1	3.89794173	0.926758397	Q8Y7B1_Lmo1375 protein_	lmo1375
Q8Y8H6	3.763318616	0.923782093	Q8Y8H6_Lmo0927 protein_	lmo0927
Q8Y608	3.75843139	0.427243412	Q8Y608_Endonuclease III_	nth
Q8Y523	3.755307177	0.920025569	Q8Y523_Lmo2254 protein_	lmo2254
Q8Y6Z0	3.646400608	0.934094339	Q8Y6Z0_Lmo1541 protein_	lmo1541
Q8Y9P7	3.535579488	0.935064311	Q8Y9P7_Putative secreted protein_	lmo0477
Q8Y7E6	3.486140679	0.953956296	Q8Y7E6_Lmo1337 protein_	lmo1337
Q8Y686	3.47781138	0.930007065	Q8Y686_ATP-dependent DNA helicase RecG_	recG
Q8Y6Z1	3.471655355	0.967447214	Q8Y6Z1_Lmo1539 protein_	lmo1539
Q8Y3K8	3.39346027	1.227955767	Q8Y3K8_Lmo2827 protein_	lmo2827
Q8Y8T4	3.251746032	0.427243412	Q8Y8T4_Lmo0810 protein_	lmo0810
Q8Y968	3.241664281	0.707352584	Q8Y968_Lmo0665 protein_	lmo0665
Q8Y552	3.214457175	0.934521539	Y2224_UPF0754 membrane protein lmo2224_	lmo2224
Q8Y6A1	3.212289181	0.880904891	Q8Y6A1_Lmo1794 protein_	lmo1794
Q8Y8F9	3.21103411	0.931992195	Q8Y8F9_Lmo0945 protein_	lmo0945
Q8Y913	3.143326284	0.998426328	Q8Y913_Lmo0729 protein_	lmo0729
Q8Y6J8	3.080310322	0.934469478	Q8Y6J8_Lmo1686 protein_	lmo1686
Q8Y9G1	3.06604993	0.934363519	HISX_Histidinol dehydrogenase_	hisD
Q8Y5I3	2.940297321	0.79132622	Q8Y5I3_Lmo2079 protein_	lmo2079
Q8Y5Q2	2.862762771	0.427243412	Q8Y5Q2_Lmo2004 protein_	lmo2004
Q8Y8J2	2.815636101	0.933402898	Q8Y8J2_Lmo0909 protein_	lmo0909
Q8Y5R1	2.722475206	2.456604705	DEOC_Deoxyribose-phosphate aldolase_	deoC
Q8Y5S0	2.70337986	0.942254257	ILVC_Ketol-acid reductoisomerase (NADP(+))_	ilvC
Q8Y8S3	2.684310386	0.928075683	Q8Y8S3_Lmo0821 protein_	lmo0821
P58414	2.668168707	2.894782483	CADA_Probable cadmium-transporting ATPase_	cadA
Q8Y8R8	2.605115785	0.64143019	Q8Y8R8_Lmo0826 protein_	lmo0826
Q8Y9T6	2.592904056	0.584147974	Q8Y9T6_Lmo0437 protein_	lmo0437
Q8Y5J9	2.556773645	0.482166992	Q8Y5J9_Lmo2061 protein_	lmo2061
Q8Y9R1	2.506961535	0.427243412	Q8Y9R1_Lmo0462 protein_	lmo0462
Q8Y5K4	2.506801021	0.578664517	Q8Y5K4_Lmo2056 protein_	lmo2056
Q8Y878	2.417702078	0.427243412	Q8Y878_Lmo1039 protein_	lmo1039
Q8Y5N5	2.396758182	0.427243412	Q8Y5N5_Lmo2022 protein_	lmo2022
Q8Y4C9	2.394089639	0.598320381	Q8Y4C9_N-acetylglucosaminyldiphosphoundecaprenol N-acetyl-beta-D-mannosaminyltransferase_	lmo2521
Q8Y585	2.390287466	0.935105222	HBP1_Hemin/hemoglobin-binding protein 1_	hbp1
Q8Y4F0	2.380918523	4.18815897	Q8Y4F0_Phosphate-specific transport system accessory protein PhoU_	lmo2494
Q8Y9V0	2.358119741	0.410853803	Q8Y9V0_Lmo0420 protein_	lmo0420
Q926Q9	2.349219667	0.427243412	Q926Q9_Lmo2850 protein_	lmo2850
Q8Y7K8	2.348916592	0.470996948	Q8Y7K8_Signal peptidase I_	lmo1269
Q8Y8K1	2.19380842	0.3531091	Q8Y8K1_Lmo0900 protein_	lmo0900
Q8Y4M1	2.18977234	0.427243412	Q8Y4M1_Lmo2416 protein_	lmo2416
P22262	2.161517669	0.292488284	PRFA_Listeriolysin regulatory protein_	prfA
Q92CN5	2.149829195	2.961038587	Q92CN5_Lmo1172 protein_	lmo1172
Q8Y735	2.106292439	0.403618061	NADD_Probable nicotinate-nucleotide adenyllyltransferase_	nadD
Q8Y6Q7	2.105357868	0.46732098	TRPA_Tryptophan synthase alpha chain_	trpA
Q8Y984	2.082232251	0.463546474	Q8Y984_Lmo0649 protein_	lmo0649

Q8Y652	2.081546899	0.421925648	MNTC_ Manganese transport system membrane protein MntC_	mntC
Q8Y8C7	2.080715817	0.427243412	Q8Y8C7_ Lmo0981 protein_	lmo0981
Q02551	2.054851431	2.080073588	FLAA_ Flagellin_	flaA
Q8Y4H7	2.053729417	0.348221468	Q8Y4H7_ Lmo2464 protein_	lmo2464
Q8Y8S8	2.030827674	0.35737583	Q8Y8S8_ Lmo0816 protein_	lmo0816
Q8Y7M1	2.012604066	0.427243412	Q8Y7M1_ Lmo1253 protein_	lmo1253
Q8Y6A5	2.006354056	0.533009215	Q8Y6A5_ Lmo1790 protein_	lmo1790
Q8Y5Z0	1.996545284	0.427243412	Q8Y5Z0_ Lmo1913 protein_	lmo1913
Q8Y3Y9	1.968824428	1.953486987	Q8Y3Y9_ Lmo2690 protein_	lmo2690
Q8Y7V2	1.960318775	3.406540764	Q8Y7V2_ GlpF protein_	glpF
Q8Y5K9	1.947694674	1.759747625	Q8Y5K9_ Lmo2050 protein_	lmo2050
Q8Y9G8	1.922384694	0.427243412	Q8Y9G8_ Glutamate dehydrogenase_	lmo0560
Q8Y5Z9	1.907993356	0.277676353	Q8Y5Z9_ Bifunctional ligase/repressor BirA_	birA
Q8Y635	1.875962913	2.268263624	Q8Y635_ Lmo1865 protein_	lmo1865
Q8Y9V7	1.872887276	0.427243412	Q8Y9V7_ Lmo0413 protein_	lmo0413
P60073	1.863125497	0.427243412	Y496_ UPF0291 protein lmo0496_	lmo0496
Q8Y5H4	1.857927803	0.427243412	Q8Y5H4_ Lmo2088 protein_	lmo2088
Q8Y7V0	1.85272219	0.510261968	Q8Y7V0_ CobD protein_	cobD

The table lists UniProt protein ID, X value representing Log<sub>2</sub> Protein abundance ratio (eut induced/non-induced in LB), Y value representing -Log<sub>10</sub> p-value (eut induced/non-induced in LB), NCBI protein Annotation and NCBI Gene ID.

**Supplementary Table 3.** Protein profiling of the *eut* induced compared with the non-induced *L. monocytogenes* EGDe in MWB medium (Only list the top 100 rows, the full table with 1893 rows was online in bellowing link)

UniProt Protein ID	X axis Log <sub>2</sub> Protein abundance ratio (eut induced/non-induced in MWB)	Y axis -Log <sub>10</sub> p-value (eut induced/non-induced in MWB)	NCBI protein Annotation (format: UniProt Protein ID_ NCBI annotation)	NCBI Gene ID
Q92CM7	15.20484394	3.758553264	Q92CM7_ Lmo1180 protein_	lmo1180
Q8Y7U1	14.11500841	4.335891133	Q8Y7U1_ Lmo1179 protein_	lmo1179
Q8Y7T9	13.39069841	7.817580222	PDUL_ Phosphate propanoyltransferase_	pduL
Q8Y7U4	12.79543156	4.683137942	EUTC_ Ethanolamine ammonia-lyase light chain_	eutC
Q8Y7U8	12.75574239	5.226873253	Q8Y7U8_ PduQ protein_	pduQ
Q8Y7U5	12.51614952	4.642733981	Q8Y7U5_ EutB protein_	eutB
Q8Y7U3	12.1567251	2.21531821	Q8Y7U3_ Lmo1177 protein_	lmo1177
Q8Y7T4	11.88311015	2.348235502	Q8Y7T4_ Lmo1187 protein_	lmo1187
Q8Y7T8	11.87372062	7.871267843	Q8Y7T8_ Lmo1183 protein_	lmo1183
Q8Y7U2	11.86737504	7.672578522	Q8Y7U2_ Lmo1178 protein_	lmo1178
Q8Y7U0	10.14830496	7.305796761	Q8Y7U0_ Lmo1181 protein_	lmo1181
Q8Y7T7	9.903454731	4.966591904	Q8Y7T7_ Lmo1184 protein_	lmo1184
Q8Y7T5	9.098751028	6.178132441	Q8Y7T5_ Lmo1186 protein_	lmo1186
Q8Y7T6	8.168099883	7.631268459	Q8Y7T6_ Lmo1185 protein_	lmo1185
Q8Y7U6	7.565372299	1.378647233	Q8Y7U6_ EutA protein_	eutA
Q8YA97	6.876574417	6.010031408	Q8YA97_ Lmo0257 protein_	lmo0257
Q8Y7I1	6.699525473	5.071416222	Q8Y7I1_ Lmo1297 protein_	lmo1297
Q8Y4T9	6.672670019	7.171055674	Q8Y4T9_ Lmo2343 protein_	lmo2343
Q8Y5S1	6.658679437	1.551483894	Q8Y5S1_ Acetolactate synthase_	ilvB
Q8Y5R6	6.243682892	6.168669423	LEUD_ 3-isopropylmalate dehydratase small subunit_	leuD
Q8Y5V5	5.897633932	5.309836207	SCPB_ Segregation and condensation protein B_	scpB
Q8YAI9	5.886276517	4.669437026	Q8YAI9_ Lmo0137 protein_	lmo0137
Q8Y8I0	5.765573232	6.018282084	COAA_ Pantothenate kinase_	coaA
Q8Y552	5.746295724	5.301196906	Y2224_ UPF0754 membrane protein lmo2224_	lmo2224
Q8Y7W9	5.661334766	3.785605215	Q8Y7W9_ Regulatory protein similar to Salmonella typhimurium Pocr protein_	lmo1150
Q8Y5R1	5.617219844	3.595777888	DEOC_ Deoxyribose-phosphate aldolase_	deoC
Q8YAL2	5.601011636	6.439761045	Q8YAL2_ Lmo0106 protein_	lmo0106
Q8Y7X0	5.475707305	4.767623918	Q8Y7X0_ Lmo1149 protein_	lmo1149
Q8Y7U7	5.271637113	1.44103376	Q8Y7U7_ Lmo1173 protein_	lmo1173

## Chapter 4

Q8Y921	5.138539409	8.568685769	Q8Y921_Putative fibronectin-binding protein_	lmo0721
Q8Y5R5	5.135346555	1.449353298	Q8Y5R5_L-threonine dehydratase_	ilvA
Q8Y4Q2	5.12037969	6.62318026	Q8Y4Q2_Lmo2382 protein_	lmo2382
Q8Y5R7	5.116465052	1.100841225	LEUC_3-isopropylmalate dehydratase large subunit_	leuC
Q8Y959	5.026281584	4.598831894	Q8Y959_Lmo0675 protein_	lmo0675
Q92A30	5.00317339	1.343866553	Q92A30_IllN protein_	ilvN
Q8YA73	4.856234531	1.322444182	Q8YA73_Lmo0286 protein_	lmo0286
Q93RD9	4.733852714	1.178220443	DTD_D-aminoacyl-tRNA deacylase_	dtd
Q8Y6J7	4.702962236	1.096563642	Y1687_UPF0374 protein lmo1687_	lmo1687
Q8Y5K0	4.613823165	1.013137503	Q8Y5K0_Lmo2060 protein_	lmo2060
Q8Y8V2	4.586203158	0.9350009	Q8Y8V2_Cys-tRNA(Pro)/Cys-tRNA(Cys) deacylase_	lmo0790
Q8Y9J5	4.508238811	0.934583887	Q8Y9J5_Lmo0532 protein_	lmo0532
Q8Y4Q1	4.424631133	1.28610944	Q8Y4Q1_Lmo2384 protein_	lmo2384
Q8Y8J7	4.233516103	0.94953969	Q8Y8J7_Lmo0904 protein_	lmo0904
Q8Y727	4.210910043	1.024973649	URK_Uridine kinase_	udk
Q8Y735	4.188457105	0.921388959	NADD_Probable nicotinate-nucleotide adenyllyltransferase_	nadD
Q8Y5R9	4.166950355	2.921620941	LEU1_2-isopropylmalate synthase_	leuA
Q8Y937	4.154920788	1.329405172	Q8Y937_Lmo0704 protein_	lmo0704
Q8Y6M5	4.096829013	0.93209628	Q8Y6M5_Lmo1659 protein_	lmo1659
Q8YAB0	4.086093062	0.908255717	MRNC_Mini-ribonuclease 3_	mrnC
Q8Y6N3	4.022201665	3.912152697	Q8Y6N3_Lmo1651 protein_	lmo1651
Q8Y5I2	4.007000365	0.950638527	Q8Y5I2_Lmo2080 protein_	lmo2080
Q8YAG1	4.00405937	1.161840891	Q8YAG1_Lmo0165 protein_	lmo0165
Q8Y792	3.97837081	0.934626287	Q8Y792_Lmo1400 protein_	lmo1400
Q8Y7C3	3.909040949	0.89372086	EX75_Exodeoxyribonuclease 7 small subunit_	xseB
Q8Y6N6	3.87348184	1.2470383	Q8Y6N6_Lmo1648 protein_	lmo1648
Q8Y8J9	3.848365111	0.983936919	Q8Y8J9_Lmo0902 protein_	lmo0902
Q8Y941	3.722668999	0.783712594	Q8Y941_Lmo0700 protein_	lmo0700
Q8YAE8	3.707128191	0.923268899	Q8YAE8_Lmo0182 protein_	lmo0182
Q8Y646	3.697783008	0.901060371	Q8Y646_Lmo1854 protein_	lmo1854
Q8Y4F1	3.69739334	0.93064246	Q8Y4F1_Lmo2493 protein_	lmo2493
Q8YAD2	3.679574185	0.935098703	Q8YAD2_Lmo0212 protein_	lmo0212
Q8Y452	3.610038402	0.924620364	Q8Y452_Transmembrane protein_	lmo2360
Q8Y686	3.604270989	0.935105112	Q8Y686_ATP-dependent DNA helicase RecG_	recG
Q8Y802	3.577403919	0.80805801	Q8Y802_Lmo1117 protein_	lmo1117
Q8Y5M9	3.5527983	0.972726372	Q8Y5M9_Lmo2028 protein_	lmo2028
Q8Y4U5	3.550096492	1.420029667	Q8Y4U5_Tagatose-6-phosphate kinase_	fruB
Q8Y951	3.509451627	0.917736162	Q8Y951_Lmo0684 protein_	lmo0684
Q8Y8F3	3.434802631	0.969630102	Q8Y8F3_Lmo0951 protein_	lmo0951
Q92DC5	3.341127986	0.52824511	Q92DC5_RsbS protein_	rsbS
Q8Y8J2	3.339227692	1.119514895	Q8Y8J2_Lmo0909 protein_	lmo0909
Q8YA19	3.338372322	0.934054229	Q8YA19_Lmo0347 protein_	lmo0347
Q8Y6R7	3.318985516	1.062633229	Q8Y6R7_Lmo1616 protein_	lmo1616
Q8Y9J1	3.125465945	0.41538696	Q8Y9J1_Lmo0537 protein_	lmo0537
Q8Y408	3.079063172	0.934688469	Q8Y408_Lmo2670 protein_	lmo2670
Q8Y913	3.043093274	0.934898766	Q8Y913_Lmo0729 protein_	lmo0729
Q8Y694	3.037453111	0.935047824	Y1802_UPF0122 protein lmo1802_	lmo1802
Q8Y997	3.023973112	0.934904684	Q8Y997_Lmo0635 protein_	lmo0635
Q8YA24	2.979899902	0.934638695	Q8YA24_Lmo0341 protein_	lmo0341
Q8Y4N2	2.975896558	0.730537975	Q8Y4N2_Probable membrane transporter protein_	lmo2404
Q8Y9F3	2.963788319	0.707463897	Q8Y9F3_Lmo0575 protein_	lmo0575
Q8Y5D3	2.955165449	0.967044224	Q8Y5D3_Lmo2132 protein_	lmo2132
Q8Y747	2.936923361	0.431873153	YBEY_Endoribonuclease YbeY_	ybeY
Q8Y3S0	2.913559084	0.427243412	Q8Y3S0_Lmo2762 protein_	lmo2762
Q8Y9V7	2.874222619	0.601476713	Q8Y9V7_Lmo0413 protein_	lmo0413
Q8Y532	2.862393167	0.539564141	Q8Y532_Pseudouridine synthase_	lmo2244
Q8Y419	2.86094643	0.934382509	Q8Y419_Lmo2658 protein_	lmo2658
P66957	2.835893589	0.637183624	TAL2_Probable transaldolase 2_	tal2
Q8Y4E4	2.80367676	0.631726816	Q8Y4E4_Lmo2502 protein_	lmo2502
Q8YAJ0	2.775973856	3.774730988	Q8YAJ0_Lmo0135 protein_	lmo0135
Q8YAA2	2.623083838	0.608091172	Q8YAA2_Lmo0252 protein_	lmo0252
Q8Y9W7	2.583959102	0.522170939	Q8Y9W7_Lmo0402 protein_	lmo0402
Q8Y687	2.577456705	0.489440668	FAPR_Transcription factor FapR_	fapR
Q8Y8F2	2.543434095	0.42783477	Q8Y8F2_Lmo0952 protein_	lmo0952
Q8YA59	2.522209299	0.528101339	Q8YA59_Lmo0302 protein_	lmo0302
Q8Y726	2.51668741	0.724386849	Q8Y726_Lmo1498 protein_	lmo1498
Q8Y9N9	2.514860508	0.512241747	RL321_50S ribosomal protein L32-1_	rpmF1
Q928S1	2.496507011	0.624383528	Q928S1_Lmo2361 protein_	lmo2361
Q8Y5S6	2.490081703	0.635768941	Q8Y5S6_Lmo1979 protein_	lmo1979

The table lists UniProt protein ID, X value representing Log<sub>2</sub> Protein abundance ratio (eut induced/non-induced in MWB), Y value representing -Log<sub>10</sub> p-value (eut induced/non-induced in MWB), NCBI protein Annotation and NCBI Gene ID.

**Supplementary Table 4.** Overlap proteins of LB upregulated proteins and MWB upregulated proteins (>2 fold)

UniProt Protein ID	KEGG gene ID	NCBI Annotation	STRING interactions
Q8Y7U1	lmo:lmo1179	eutE; alcohol dehydrogenase	eut cluster
Q8Y7U3	lmo:lmo1177	carboxysome structural protein EutL	eut cluster
Q92CM7	lmo:lmo1180	carboxysome structural protein	eut cluster
Q8Y7T4	lmo:lmo1187	ethanolamine utilization protein EutQ	eut cluster
Q8Y7T9	lmo:lmo1182	eutD; ethanolamine utilization protein EutD	eut cluster
Q8Y7U6	lmo:lmo1174	eutA; ethanolamine utilization protein EutA	eut cluster
Q8Y7U4	lmo:lmo1176	eutC; ethanolamine ammonia-lyase small subunit	eut cluster
Q8Y7U2	lmo:lmo1178	carboxysome structural protein	eut cluster
Q8Y7U8	lmo:lmo1171	eutG ; NADPH-dependent butanol dehydrogenase	eut cluster
Q8Y7U5	lmo:lmo1175	eutB; ethanolamine ammonia-lyase large subunit	eut cluster
Q8Y7T8	lmo:lmo1183	hypothetical protein	eut cluster
Q8Y7T7	lmo:lmo1184	carbon dioxide concentrating mechanism protein	eut cluster
Q8Y7U0	lmo:lmo1181	cobalamin adenosyl transferase	eut cluster
Q8Y7T6	lmo:lmo1185	PduT like protein	eut cluster
Q8Y7T5	lmo:lmo1186	ethanolamine utilization protein EutH	eut cluster
P63363	lmo:lmo2495	phosphate ABC transporter ATP-binding protein	
Q8Y7U7	lmo:lmo1173	two-component sensor histidine kinase	eut cluster
Q8Y9F1	lmo:lmo0578	hypothetical protein	
Q8Y646	lmo:lmo1854	hypothetical protein	
Q8Y7B1	lmo:lmo1375	aminotripeptidase	
Q8Y686	lmo:lmo1811	ATP-dependent DNA helicase RecG	
Q8Y3K8	lmo:lmo2827	MarR family transcriptional regulator	
Q8Y552	lmo:lmo2224	hypothetical protein	
Q8Y6A1	lmo:lmo1794	hypothetical protein	
Q8Y913	lmo:lmo0729	hypothetical protein	
Q8Y8J2	lmo:lmo0909	GntR family transcriptional regulator	
Q8Y5R1	lmo:lmo1995	dra; deoxyribose-phosphate aldolase	eut cluster-relevant
Q8Y5S0	lmo:lmo1986	ilvC; ketol-acid reductoisomerase	Potential ABC transporter
Q8Y9T6	lmo:lmo0437	hypothetical protein	
Q8Y5K4	lmo:lmo2056	hypothetical protein	
Q8Y4M1	lmo:lmo2416	hypothetical protein	
Q8Y735	lmo:lmo1488	nadD; nicotinic acid mononucleotide adenylyltransferase	
Q8Y4H7	lmo:lmo2464	transcriptional regulator	
Q8Y8S8	lmo:lmo0816	regulatory protein PaiA	
Q8Y6A5	lmo:lmo1790	hypothetical protein	
Q8Y9V7	lmo:lmo0413	hypothetical protein	
Q8Y5H4	lmo:lmo2088	transcriptional regulator	
Q8Y3T1	lmo:lmo2750	para-aminobenzoate synthase subunit I	Potential ABC transporter
Q8Y6N3	lmo:lmo1651	ABC transporter ATP-binding protein	
Q8Y8A6	lmo:lmo1004	hypothetical protein	
Q8YA73	lmo:lmo0286	Pyridoxal phosphate-dependent aminotransferase	
Q8Y622	lmo:lmo1880	RNase HI	
Q8YA27	lmo:lmo0338	hypothetical protein	
Q8Y3T0	lmo:lmo2751	ABC transporter ATP-binding protein	Potential ABC transporter
Q8Y3S9	lmo:lmo2752	ABC transporter ATP-binding protein	Potential ABC transporter
Q8Y4Q2	lmo:lmo2382	monovalent cation/H <sup>+</sup> antiporter subunit E	
P66957	lmo:lmo0343	transaldolase	
Q8Y4K5	lmo:lmo2433	acetyltransferase	
Q92E21	lmo:lmo0636	hypothetical protein	
Q8Y9K5	lmo:lmo0522	transcriptional regulator	

The table lists UniProt protein ID, KEGG gene ID, NCBI protein Annotation and STRING interactions.



**Supplementary Table 5.** Overlap proteins of LB downregulated proteins and MWB downregulated proteins (>2 fold)

UniProt Protein ID	KEGG gene ID	Annotation	STRING interactions
Q8Y5Y6 P66219	lmo:lmo1917 lmo:lmo1335	pflA; pyruvate formate-lyase rpmG; 50S ribosomal protein L33; putative interaction with divlB	cell division relevant
Q8Y469 Q8Y768 Q8Y6C4	lmo:lmo2586 lmo:lmo1433 lmo:lmo1766	formate dehydrogenase subunit alpha glutathione reductase purN; phosphoribosylglycinamide formyltransferase	B12 biosynthesis-relevant B12 biosynthesis-relevant
Q8Y413 Q8Y537 Q8Y4Z4 Q8Y3Y8 Q8Y542 Q8YAJ8 Q8Y5G6 Q8Y7R2 Q8Y414 P34024 Q8Y5X2 Q8Y9F6 Q8Y8P7 Q8Y4X5 Q8Y7T0 Q8Y3P0 Q8Y6W8 Q8Y7R8 P33378 Q8Y7S2	lmo:lmo2664 lmo:lmo2239 lmo:lmo2285 lmo:lmo2691 lmo:lmo2234 lmo:lmo0126 lmo:lmo2097 lmo:lmo1209 lmo:lmo2663 lmo:lmo0201 lmo:lmo1932 lmo:lmo0572 lmo:lmo0849 lmo:lmo2304 lmo:lmo1191 lmo:lmo2795 lmo:lmo1563 lmo:lmo1203 lmo:lmo0205 lmo:lmo1199	sorbitol dehydrogenase hypothetical protein protein gp18 peptidoglycan hydrolase, autolysin hypothetical protein hypothetical protein PTS galacticol transporter subunit IIB hypothetical protein polyol dehydrogenase plcA; phosphatidylinositol-specific phospholipase c heptaprenyl diphosphate synthase subunit I hypothetical protein hypothetical protein cbiA; cobyrinic acid a,c-diamide synthase RpiR family transcription regulator coaE; dephospho-CoA kinase cbiL; cobalt-precorrin-2 C(20)-methyltransferase plcB; Phospholipase C cbiH; Catalyzes the formation of precorrin-4 from precorrin-3B and S-adenosyl-L-methionine	Zinc-containing dehydrogenase   cell wall relevant   Zinc-containing dehydrogenase B12 biosynthesis Zinc-containing dehydrogenase phospholipase    B12 biosynthesis    B12 biosynthesis phospholipase B12 biosynthesis
Q8Y7S4 Q8Y7R3	lmo:lmo1197 lmo:lmo1208	cbiF; precorrin-3 methylase cbiP; Cobyrinic acid synthase; Catalyzes amidations at positions B, D, E, and G on adenosylcobyrinic A,C-diamide.	B12 biosynthesis B12 biosynthesis
Q8Y4J9 Q8Y7S6 Q8YAK7 Q8Y891 Q8Y8A5 Q8Y7S8	lmo:lmo2439 lmo:lmo1198 lmo:lmo0111 lmo:lmo1024 lmo:lmo0274 lmo:lmo1193	hypothetical protein cbiG; cobalamin biosynthesis protein CbiG hypothetical protein, putative interaction with divlB hypothetical protein hypothetical protein cbiC; Catalyzes the interconversion of cobalt-precorrin-8X and cobyrinic acid in the anaerobic biosynthesis of cobalamin	B12 biosynthesis cell division relevant   B12 biosynthesis
Q8Y7S5 Q8Y945	lmo:lmo1197 lmo:lmo0695	cbiF; precorrin-3 methylase hypothetical protein, flagellar hook-length control protein Flk	B12 biosynthesis cell wall relevant
Q8Y7S0 Q8Y5R2 Q8Y4M5 Q8Y7S7 Q8Y7S9	lmo:lmo1201 lmo:lmo1994 lmo:lmo2412 lmo:lmo1194 lmo:lmo1192	cysG; Uroporphyrinogen-III C-methyltransferase LacI family transcriptional regulator hypothetical protein cbiD; Cobalt-precorrin-5B C(1)-methyltransferase CobD; Converts cobyrinic acid to cobinamide by the addition of aminopropanol on the F carboxylic group	B12 biosynthesis   B12 biosynthesis B12 biosynthesis
Q8Y5M3 Q8Y5K5 Q8Y7S1 PODJM0	lmo:lmo2034 lmo:lmo2055 lmo:lmo1200 lmo:lmo0433	divlB; cell division protein FtsQ hypothetical protein CbiJ; precorrin-6A reductase inlA; Internalin-A; Mediates the entry of L.monocytogenes into cells	cell division relevant  B12 biosynthesis
Q8Y7R9 Q8Y3T5 Q8Y7R4	lmo:lmo1202 lmo:lmo2746 lmo:lmo1207	cbiK; annotation not available hypothetical protein Putative ABC transporter ATP-binding protein lmo1207	B12 biosynthesis  B12 biosynthesis
Q8Y7S3	lmo:lmo1198	cbiG; Catalyzes the formation of cobalt-precorrin 4 from cobalt-precorrin 3	B12 biosynthesis

The table lists UniProt protein ID, KEGG gene ID, NCBI protein Annotation and STRING interactions.

**Supplementary Table 6.** Strains used in this study

Strain	Source
<i>Listeria monocytogenes</i> EGDe	ATCC® BAA-679™
<i>Listeria monocytogenes</i> 10403S	Light SH, et al. 2018.
<i>Listeria monocytogenes</i> 10403S ΔeutB	This study
<i>Listeria monocytogenes</i> 10403S Δndh2	Light SH, et al. 2018.

The table lists name of the stains and their source.

**Supplementary Table 7.** Primers used for Construction of strain *L. monocytogenes* 10403S ΔeutB

Primer	Sequence (5' to 3')
EutB Fragment A (forward)	ATGGGGTCCAGCGCGCTGGATCCTTGCAGACTGTATTTCAACTGGTG
EutB Fragment A (reverse)	AGGATTTATCGAATGATTTTAAAAACGAATTCTATTTTCCTAAAATAA
EutB Fragment B (forward)	ATGATTTTAAAAACGAATTCTATTTTCCTAAAATAAGGAAGGGAGG
EutB Fragment B (reverse)	TACAAATCGTTGTTGGTGATGGACGCTGCAGGAGGCAGTGAGCGAGC
ΔEutB validation (forward)	GCTTGCTTAGATATTGGTGGTCG
ΔEutB validation (reverse)	GAGGAAC TAAGCGATGAACGAACA

The table lists name of the primers and their sequences

**The Supplementary Materials for this article can also be found online at:**

<https://doi.org/10.1128/mSystems.01349-20>



## 4.6 References

1. Ley, R.E., D.A. Peterson, and J.I. Gordon, *Ecological and evolutionary forces shaping microbial diversity in the human intestine*. Cell, 2006. **124**(4): p. 837-848.
2. Bäumler, A.J. and V. Sperandio, *Interactions between the microbiota and pathogenic bacteria in the gut*. Nature, 2016. **535**(7610): p. 85-93.
3. Luzader, D.H. and M.M. Kendall, *Commensal 'trail of bread crumbs' provide pathogens with a map to the intestinal landscape*. Current opinion in microbiology, 2016. **29**: p. 68-73.
4. Sperandio, V., *Pathogens' adaptation to the human host*. Proceedings of the National Academy of Sciences, 2018. **115**(38): p. 9342-9343.
5. Garsin, D.A., *Ethanolamine utilization in bacterial pathogens: roles and regulation*. Nature Reviews Microbiology, 2010. **8**(4): p. 290-295.
6. Kaval, K.G. and D.A. Garsin, *Ethanolamine utilization in bacteria*. mBio, 2018. **9**(1): p. e00066-18.
7. Tsoy, O., D. Ravcheev, and A. Mushegian, *Comparative genomics of ethanolamine utilization*. Journal of bacteriology, 2009. **191**(23): p. 7157-7164.
8. Stojiljkovic, I., A.J. Bäumler, and F. Heffron, *Ethanolamine utilization in Salmonella typhimurium: nucleotide sequence, protein expression, and mutational analysis of the cchA cchB eutE eutJ eutG eutH gene cluster*. Journal of bacteriology, 1995. **177**(5): p. 1357-1366.
9. Chang, G.W. and J.T. Chang, *Evidence for the B12-dependent enzyme ethanolamine deaminase in Salmonella*. Nature, 1975. **254**(5496): p. 150-151.
10. Blackwell, C.M. and J.M. Turner, *Microbial metabolism of amino alcohols. Formation of coenzyme B12-dependent ethanolamine ammonia-lyase and its concerted induction in Escherichia coli*. Biochemical Journal, 1978. **176**(3): p. 751-757.
11. Roof, D.M. and J.R. Roth, *Ethanolamine utilization in Salmonella typhimurium*. Journal of bacteriology, 1988. **170**(9): p. 3855-3863.
12. Brinsmade, S.R. and J.C. Escalante-Semerena, *The eutD gene of Salmonella enterica encodes a protein with phosphotransacetylase enzyme activity*. Journal of bacteriology, 2004. **186**(6): p. 1890-1892.
13. Moore, T.C. and J.C. Escalante-Semerena, *The EutQ and EutP proteins are novel acetate kinases involved in ethanolamine catabolism: physiological implications for the function of the ethanolamine metabolosome in S almonella enterica*. Molecular microbiology, 2016. **99**(3): p. 497-511.
14. Price-Carter, M., et al., *The Alternative Electron Acceptor Tetrathionate Supports B12-Dependent Anaerobic Growth of Salmonella enterica Serovar Typhimurium on Ethanolamine or 1, 2-Propanediol*. Journal of bacteriology, 2001. **183**(8): p. 2463-2475.
15. Thiennimitr, P., et al., *Intestinal inflammation allows Salmonella to use ethanolamine to compete with the microbiota*. Proceedings of the National Academy of Sciences, 2011. **108**(42): p. 17480-17485.

16. Stewart, K.L., A.M. Stewart, and T.A. Bobik, *Prokaryotic Organelles: Bacterial Microcompartments in E. coli and Salmonella*. Ecosal Plus, 2020. **9**(1).
17. Light, S.H., et al., *Extracellular electron transfer powers flavinylated extracellular reductases in Gram-positive bacteria*. Proceedings of the National Academy of Sciences, 2019. **116**(52): p. 26892-26899.
18. Light, S.H., et al., *A flavin-based extracellular electron transfer mechanism in diverse Gram-positive bacteria*. Nature, 2018. **562**(7725): p. 140.
19. Kerfeld, C.A., et al., *Bacterial microcompartments*. Nature Reviews Microbiology, 2018. **6**(5): p. 227.
20. Greening, C. and T. Lithgow, *Formation and function of bacterial organelles*. Nature Reviews Microbiology, 2020: p. 1-13.
21. Huseby, D.L. and J.R. Roth, *Evidence that a metabolic microcompartment contains and recycles private cofactor pools*. Journal of bacteriology, 2013. **195**(12): p. 2864-2879.
22. Fan, C., et al., *Interactions between the termini of lumen enzymes and shell proteins mediate enzyme encapsulation into bacterial microcompartments*. Proceedings of the National Academy of Sciences, 2012. **109**(37): p. 14995-15000.
23. Kalnins, G., et al., *Encapsulation mechanisms and structural studies of GRM2 bacterial microcompartment particles*. Nature communications, 2020. **11**(1): p. 1-13.
24. Zeng, Z., et al., *Bacterial microcompartment-dependent 1, 2-propanediol utilization stimulates anaerobic growth of Listeria monocytogenes EGDe*. Frontiers in Microbiology, 2019. **10**: p. 2660.
25. Mellin, J., et al., *Sequestration of a two-component response regulator by a riboswitch-regulated noncoding RNA*. Science, 2014. **345**(6199): p. 940-943.
26. Kendall, M.M. and V. Sperandio, *What a dinner party! Mechanisms and functions of interkingdom signaling in host-pathogen associations*. mBio, 2016. **7**(2).
27. Tang, S., et al., *Transcriptomic analysis of the adaptation of Listeria monocytogenes to growth on vacuum-packed cold smoked salmon*. Appl. Environ. Microbiol., 2015. **81**(19): p. 6812-6824.
28. Anast, J.M. and S. Schmitz-Esser, *The transcriptome of Listeria monocytogenes during co-cultivation with cheese rind bacteria suggests adaptation by induction of ethanolamine and 1, 2-propanediol catabolism pathway genes*. PLoS ONE, 2020. **15**(7): p. e0233945.
29. Joseph, B., et al., *Identification of Listeria monocytogenes genes contributing to intracellular replication by expression profiling and mutant screening*. Journal of bacteriology, 2006. **188**(2): p. 556-568.
30. Anderson, C.J., et al., *Ethanolamine signaling promotes Salmonella niche recognition and adaptation during infection*. PLoS pathogens, 2015. **11**(11): p. e1005278.

31. Tsai, H.-N. and D.A. Hodgson, *Development of a synthetic minimal medium for Listeria monocytogenes*. Appl. Environ. Microbiol., 2003. **69**(11): p. 6943-6945.
32. Feehily, C., C.P. O'Byrne, and K.A.G. Karatzas, *Functional  $\gamma$ -aminobutyrate shunt in Listeria monocytogenes: role in acid tolerance and succinate biosynthesis*. Applied and environmental microbiology, 2013. **79**(1): p. 74-80.
33. Lebreton, A. and P. Cossart, *RNA-and protein-mediated control of Listeria monocytogenes virulence gene expression*. RNA biology, 2017. **14**(5): p. 460-470.
34. Li, Z., et al., *Whole genome sequencing analyses of Listeria monocytogenes that persisted in a milkshake machine for a year and caused illnesses in Washington State*. BMC microbiology, 2017. **17**(1): p. 134.
35. Lobel, L., et al., *Integrative genomic analysis identifies isoleucine and CodY as regulators of Listeria monocytogenes virulence*. PLoS Genet, 2012. **8**(9): p. e1002887.
36. Cheng, S., et al., *Genetic analysis of the protein shell of the microcompartments involved in coenzyme B12-dependent 1, 2-propanediol degradation by Salmonella*. Journal of bacteriology, 2011. **193**(6): p. 1385-1392.
37. Dadswell, K., et al., *Bacterial microcompartment-mediated ethanolamine metabolism in E. coli urinary tract infection*. Infection and immunity, 2019: p. IAI. 00211-19.
38. Kaval, K.G., et al., *Ethanolamine Utilization and Bacterial Microcompartment Formation Are Subject to Carbon Catabolite Repression*. Journal of bacteriology, 2019. **201**(10): p. e00703-18.
39. Pang, A., M.J. Warren, and R.W. Pickersgill, *Structure of PduT, a trimeric bacterial microcompartment protein with a 4Fe-4S cluster-binding site*. Acta Crystallographica Section D: Biological Crystallography, 2011. **67**(2): p. 91-96.
40. Ferlez, B., M. Sutter, and C.A. Kerfeld, *Glycyl radical enzyme-associated microcompartments: redox-replete bacterial organelles*. mBio, 2019. **10**(1): p. e02327-18.
41. Singh, S., et al., *Aldehyde dehydrogenases in cellular responses to oxidative/electrophilic stress*. Free radical biology and medicine, 2013. **56**: p. 89-101.
42. McLaughlin, H.P., C. Hill, and C.G. Gahan, *The impact of iron on Listeria monocytogenes; inside and outside the host*. Current opinion in biotechnology, 2011. **22**(2): p. 194-199.
43. Portman, J.L., et al., *Activation of the Listeria monocytogenes virulence program by a reducing environment*. mBio, 2017. **8**(5): p. e01595-17.
44. Smith, K. and P. Youngman, *Use of a new integrational vector to investigate compartment-specific expression of the Bacillus subtilis spoIIIM gene*. Biochimie, 1992. **74**(7-8): p. 705-711.

45. Reynolds, A.J., et al., *Quantification of aqueous monoethanolamine concentration by gas chromatography for postcombustion capture of CO<sub>2</sub>*. Industrial & Engineering Chemistry Research, 2014. **53**(12): p. 4805-4811.
46. Wiśniewski, J.R., et al., *Universal sample preparation method for proteome analysis*. Nature methods, 2009. **6**(5): p. 359.
47. Smaczniak, C., et al., *Characterization of MADS-domain transcription factor complexes in Arabidopsis flower development*. Proceedings of the National Academy of Sciences, 2012. **109**(5): p. 1560-1565.
48. Tyanova, S., et al., *The Perseus computational platform for comprehensive analysis of (prote) omics data*. Nature methods, 2016. **13**(9): p. 731-740.
49. Drozdetskiy, A., et al., *JPred4: a protein secondary structure prediction server*. Nucleic acids research, 2015. **43**(W1): p. W389-W394.
50. Hulsen, T., J. de Vlieg, and W. Alkema, *BioVenn-a web application for the comparison and visualization of biological lists using area-proportional Venn diagrams*. BMC genomics, 2008. **9**(1): p. 1-6.
51. Szklarczyk, D., et al., *STRING v11: protein-protein association networks with increased coverage, supporting functional discovery in genome-wide experimental datasets*. Nucleic acids research, 2019. **47**(D1): p. D607-D613.



# 5

---

## **Impact of vitamin B12 on rhamnose metabolism, stress defense and *in vitro* virulence of *Listeria monocytogenes***

Submitted for publication:

**Zeng, Z.**, Wijnands, L. M, Boeren, S, Smid, E. J., Notebaart, R. A., & Abee, T.  
Impact of vitamin B12 on rhamnose metabolism, stress defense and in-vitro  
virulence of *Listeria monocytogenes*

Preprint in bioRxiv: doi: <https://doi.org/10.1101/2021.08.26.457850>

## Abstract

*Listeria monocytogenes* is a facultative anaerobe which can cause a severe food-borne infection known as listeriosis. Rhamnose is a deoxyhexose sugar abundant in a range of environments, including the human intestine, and can be degraded by *L. monocytogenes* in aerobic and anaerobic conditions into lactate, acetate and 1,2-propanediol. Our previous study showed that addition of vitamin B12 stimulates anaerobic growth of *L. monocytogenes* on rhamnose due to the activation of bacterial microcompartment (BMC)-dependent 1,2-propanediol utilization with concomitant production of propionate and propanol. Notably, anaerobic propanediol metabolism has been linked to virulence of enteric pathogens including *Salmonella* spp. and *L. monocytogenes*. In this study we investigate the impact of B12 on aerobic and anaerobic growth of *L. monocytogenes* on rhamnose, and observed growth stimulation and *pdu* BMC activation only in anaerobically grown cells with B12 added to the medium. Comparative Caco-2 virulence assays, showed that these *pdu* BMC induced cells have significantly higher translocation efficiency compared to aerobically grown cells (without and with added B12) and non-induced anaerobically grown cells, while adhesion and invasion capacity is similar for all cells. Comparative proteomics analysis showed specific and overlapping responses linked to metabolic shifts, activation of stress defense proteins and virulence factors, with RNA polymerase sigma factor SigL; teichoic acids export ATP-binding protein, TagH; DNA repair and protection proteins RadA and DPS; and glutathione synthase GshAB previously linked to activation of virulence response in *L. monocytogenes*, uniquely upregulated in anaerobically rhamnose grown *pdu* BMC induced cells. Our results shed new light into B12 impact on *L. monocytogenes* competitive fitness and virulence.

## 5.1 Introduction

*Listeria monocytogenes* is the causative agent of the foodborne illness listeriosis, a rare but severe disease with a high mortality rate in the immunocompromised, very young, and elderly populations. Furthermore, listeriosis also causes abortions in pregnant women [1,2]. Acquisition of this infection is mainly caused by consumption of contaminated food (predominantly ready-to-eat food) [1, 2]. *L. monocytogenes* is found ubiquitously in natural environments such as soil, silage, groundwater, sewage and vegetation [2, 3]. The food-borne pathogen can grow at low temperatures and can survive a range of environmental stresses, such as low pH and high salt concentrations [3, 4]. Upon ingestion of contaminated food by the host, and following gastric passage, *L. monocytogenes* can bind to epithelial cells in the intestine [3, 5]. Following entry into epithelial cells mediated by Internalin A (InlA) and Internalin B (InlB), *L. monocytogenes* is internalized into the vacuole [3, 6]. After the internalization, *L. monocytogenes* applies listeriolysin O (LLO) encoded by *hly* [5] and two phospholipases, phospholipase A (PlcA) and phospholipase B (PlcB), for vacuolar rupture and escape, which are crucial steps in *L. monocytogenes* pathogenesis [2, 3, 7]. Notably, alternative invasion and translocation routes involving LLO and Listeria adhesion protein (LAP) have been described [8, 9]. All of these features make the transmission and contamination of *L. monocytogenes* a severe concern for the food industry [4, 10, 11].

Recent studies on anaerobic growth of *L. monocytogenes* provided evidence that it has the capacity to form proteinaceous organelles so-called bacterial microcompartments (BMCs) which enable extension of its metabolic repertoire by supporting the utilization of rhamnose-derived 1,2-propanediol and ethanolamine derived from degradation of phospholipids [12-14]. BMCs are self-assembling organelles that consist of an enzymatic core that is encapsulated by a semi-permeable protein shell [14-16]. The separation of the encapsulated enzymes from the cytosol is thought to protect the cell from toxic metabolic intermediates such as aldehydes, and prevent unwanted side reactions [14-16]. These compartmentalized metabolic pathways may confer a competitive advantage to *L. monocytogenes* over commensal gut microbiota, which typically lack BMC operons and thus are unable to utilize the corresponding substrates in anaerobic conditions [13, 17]. Rhamnose is a deoxyhexose sugar abundant in a range of environments including the human intestine, and can be degraded in anaerobic conditions into 1,2-propanediol which can be further metabolized by a range of bacteria including *L. monocytogenes* that contain so-called propanediol

utilization (*pdu*) BMCs [13, 18]. The *L. monocytogenes pdu* cluster is organized together with the ethanolamine utilization (*eut*) cluster and cobalamin synthesis (*cob/cbi*) operons, as a single large locus, referred to as the cobalamin-dependent gene cluster (CDGC) [19, 20]. Previous work suggests that the *pdu* pathway contributes to *L. monocytogenes* establishment in the gastrointestinal tract, while the *eut* pathway may be more important during intracellular replication [19, 21]. We recently provided evidence that anaerobically ethanolamine and propanediol grown *eut* and *pdu* BMC induced *L. monocytogenes* cells showed significantly higher Caco-2 translocation efficacy in trans-well assays compared to non-induced cells, while adhesion and invasion capacity was similar.

We previously reported that addition of vitamin B12 enhances anaerobic utilization of rhamnose via *pdu* BMC in *L. monocytogenes* [13], but the impact of B12 on aerobic and anaerobic growth, metabolism and *in vitro* virulence of *L. monocytogenes* cells grown with rhamnose remains to be determined. We therefore assessed the impact of B12 on rhamnose metabolism in aerobically and anaerobically grown *L. monocytogenes*, aligned with metabolic analysis, proteomics and Caco-2 adhesion, invasion and translocation studies. Possible correlations between these parameters are discussed.

## 5.2. Materials and Methods

### 5.2.1 Strain and Culture Conditions

All experiments in this study were carried out with *L. monocytogenes* EGDe aerobically or anaerobically grown at 30°C in defined medium MWB (Modified Welshimer's broth) [22]. Overnight grown cells in Luria Broth (LB) were washed three times in PBS before inoculation into MWB. MWB was supplemented with 20mM L-rhamnose as sole carbon source with addition of 20nM B12 (defined as *pdu* BMC induced) or without addition of 20nM B12 (defined as *pdu* BMC non-induced). Anaerobic conditions were achieved by Anoxomat Anaerobic Culture System with a gas mixture composed of 10% CO<sub>2</sub>, 5% H<sub>2</sub>, 85% N<sub>2</sub>. OD<sub>600</sub> measurements in MWB were performed every 12 h for 3 days. Plate counting in MWB to quantify Colony Forming Units (CFUs) was performed every 24 h for 3 days. All the growth measurements were performed with three independent experiments with three technical repeats.

### 5.2.2 Analysis of metabolites for Rhamnose metabolism using High Pressure Liquid Chromatography (HPLC)

Samples were taken from the cultures at 0, 24, 48, and 72 h. After centrifugation, the supernatant was collected for the HPLC measurements of rhamnose while the measurement of acetate, lactate, 1,2-propanediol, 1-propanol and propionate was only performed in 72h. The experiment was performed with three biological replicates. Additionally, the standard curves of all the metabolites were measured in the concentrations 0.1, 1, 5, 10, and 50 mM. HPLC was performed using an Ultimate 3000 HPLC (Dionex) equipped with an RI-101 refractive index detector (Shodex, Kawasaki, Japan), an autosampler and an ion-exclusion Aminex HPX-87H column (7.8 mm × 300 mm) with a guard column (Bio-Rad, Hercules, CA). As the mobile phase 5 mM H<sub>2</sub>SO<sub>4</sub> was used at a flow rate of 0.6 ml/min, the column was kept at 40°C. The total run time was 30 min and the injection volume was 10 µl. All the HPLC measurements were performed with three independent experiments with three technical repeats as described before [13].

### 5.2.3 Proteomics

*L. monocytogenes* EGDe cultures were aerobically or anaerobically grown at 30°C in MWB with 20 mM rhamnose adding 20nM B12 or not. Samples were collected at 48 h of the inoculation and processed as described before [13]. The mass spectrometry proteomics data have been deposited to the ProteomeXchange Consortium via the PRIDE [23] partner repository with the dataset identifier PXD025734 for *pdu* BMC induced and *pdu* BMC non-induced conditions.

### 5.2.4 Caco-2 adhesion, invasion and translocation

Cultures of Caco-2 cells (human intestinal epithelial cells, ATCC HTB-37), production of differentiated cells in 12-well plates were carried out as described before [24, 25]. *L. monocytogenes* overnight grown cells used for adhesion, invasion and translocation were normalized to get the concentration of  $8.4 \pm 0.1$  log CFU/ml.

For adhesion and invasion experiments, Caco-2 with the inoculum  $1.6 \times 10^5$  cells/well were seeded into the 12-well tissue culture plates (Corning Inc. ID 3513). Inoculated 12-well plates and were incubated for 12-14 days with the medium refreshing every 2 days at 37 °C to establish a confluent monolayer of cells. Adhesion and invasion experiments were started by inoculation with 40 µl of late exponential phase cells of Rhamnose *pdu* BMC induced and non-induced *L. monocytogenes* EGDe resulting in an final inoculum of approximate 7.41 log

CFU/well. Then the 12 well plates were centrifuged for 1 min at 175 ×g to create a proximity between the Caco-2 and *L. monocytogenes* cells.

For adhesion and invasion enumeration, after 1h anaerobic incubation without gentamicin, *L. monocytogenes* cells that have not adhered to Caco-2 cells were removed by washing three times with PBS buffer. Half of the wells containing Caco-2 cells were lysed with 1 ml of 1% v/v Triton X-100 in PBS and serially diluted in PBS for quantification of the number of adhered and invaded *L. monocytogenes* cells. The other half of the wells of the Caco-2 cells was subsequently incubated anaerobically for 3 h with 0.3% gentamicin (50 µg/ml, Gibco) to eliminate all extracellular *L. monocytogenes* cells. Thereafter, gentamycin containing medium was removed by washing three times with PBS buffer. The Caco-2 cells were lysed with 1 ml of 1% v/v Triton X-100 in PBS and serially diluted in PBS for quantification of the number of invaded *L. monocytogenes* EGDe cells.

For translocation experiments,  $0.8 \times 10^5$  Caco-2 cells per mL were seeded ThinCert PET inserts Griener Bio-One 665640) for 12-14 day differentiation. Prior to the translocation assay wells and inserts were washed three times with PBS, and placed in TCM without gentamycin and fetal bovine serum. Translocation was started by adding 20 µl of late exponential cells of Rhamnose *pdu* BMC induced and non-induced *L. monocytogenes* EGDe into the inserts, resulting in an inoculum of approximately 7.17 log CFU/well. After centrifuging the Transwell plates for 1 min at 175x g, the plates were incubated 2 hrs anaerobically. After incubation, the inserts were removed with a sterile forceps and discarded. The contents in the wells was collected for quantification of the translocated number of *L. monocytogenes* EGDe cells.

### 5.2.5 Venn diagram analysis and STRING networks analysis

The protein IDs of significantly changed proteins from Supplementary Table 1, 2 and 3 were uploaded to the BioVenn online server [26] taking the default setting to generate Venn diagrams. The analysis of Venn diagram and details of overlap upregulated proteins are shown in Supplementary Table 4. Overlapping proteins from the Venn diagram were transferred to the STRING online server[27] for multiple proteins analysis of functional interaction using sources such as co-expression, genomic neighbourhood and gene fusion.

Statistical analyses were performed in Prism 8.0.1 for Windows (GraphPad Software). As indicated in the figure legend, Statistical significances are shown in \*\*\*,  $P < 0.001$ ; \*,  $P < 0.05$ ; ns,  $P > 0.05$  with Holm-Sidak T-test.

## 5.3. Results

### 5.3.1 Impact of vitamin B12 on *L. monocytogenes* grown on rhamnose

We first examined the impact of B12 on aerobic or anaerobic growth of *L. monocytogenes* EGDe in MWB defined medium without and with added vitamin B12 (Figure 1).

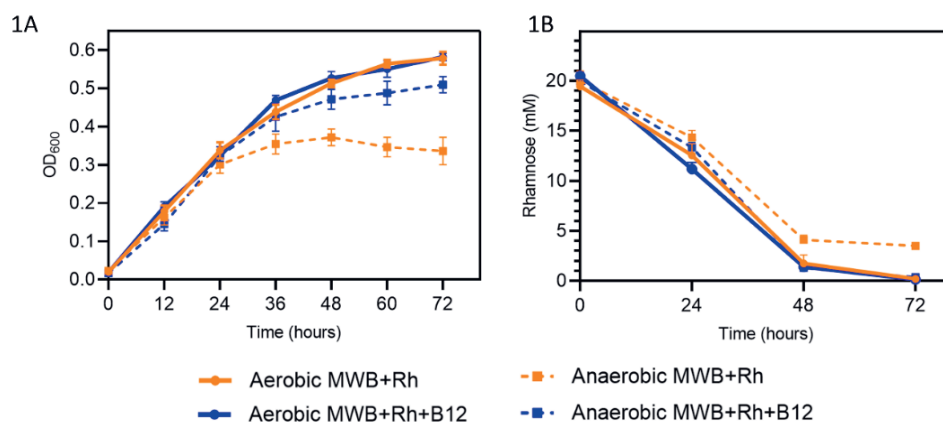


**Figure 1. Growth and Rhamnose catabolism of *L. monocytogenes* EGDe in MWB medium with 20mM Rhamnose.**

**(A)** Impact of vitamin B12 on aerobic or anaerobic growth of *L. monocytogenes* EGDe in MWB medium with 20mM Rhamnose; **(1B)** Rhamnose utilization. Orange lines with closed circles represent *L. monocytogenes* grown in MWB medium with 20 mM Rhamnose, while blue lines with closed circles represent *L. monocytogenes* grown in MWB medium with 20 mM Rhamnose and 20nM B12. Solid lines represent aerobic condition, and striped lines represent anaerobic condition; data published in [13]. Results from three independent experiments are expressed and visualized as means and standard errors.

In Figure 1A, *L. monocytogenes* showed a similar aerobic growth in MWB defined medium plus 20mM rhamnose with or without 20mM B12 where OD<sub>600</sub> reaches a maximum of approximate 0.56 after 72 h. But for anaerobic conditions, in MWB defined medium supplied with 20mM rhamnose OD<sub>600</sub> reaches a maximum of about 0.37 after 48 h, while in MWB supplied with 20mM rhamnose and 20nM B12 OD<sub>600</sub> continues to increase after 48 h, reaching a significant higher OD<sub>600</sub> of 0.51 at 72 h as described before [13]. The growth phenotypes indicate that

addition of 20nM of B12 into MWB defined medium plus 20mM rhamnose stimulates anaerobic growth of *L. monocytogenes*, but has no significant effect on aerobic growth which is already enhanced compared to that in anaerobic conditions. Next, utilization of rhamnose in aerobic and anaerobic conditions with or without B12 was quantified. The aerobic growth of *L. monocytogenes* with or without B12 appears similar including the rhamnose degradation capacity, that showed complete consumption of 20mM rhamnose within 72 h (Figure 1B). Complete consumption of rhamnose was also observed in anaerobically grown cells in MWB plus 20mM rhamnose and B12, whereas 3.5 mM of rhamnose was still present at 72 h in MWB plus 20mM rhamnose without added B12. These results indicate that addition of B12 stimulates anaerobic growth and rhamnose metabolism of *L. monocytogenes* EGDe, while no significant impact of B12 was detected with aerobically grown cells.

### 5.3.2 Impact of B12 on aerobic or anaerobic metabolism of rhamnose

Metabolite production in the different growth conditions was analysed by HPLC. As shown in Figure 2, at 72 h, rhamnose was degraded by *L. monocytogenes* EGDe into acetate, lactate and 1,2-propanediol in anaerobic and aerobic conditions with or without B12, albeit to different levels.

2

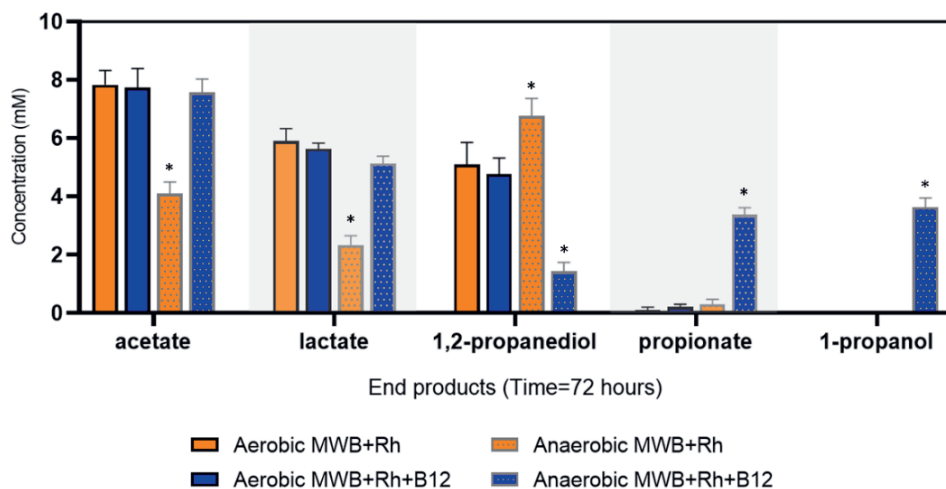


**Figure 2. Metabolites from rhamnose metabolism of *L. monocytogenes* EGDe aerobically or anaerobically grown in MWB with 20mM Rhamnose with/without 20nM vitamin B12**

Orange bars represent *L. monocytogenes* grown in MWB medium with 20 mM Rhamnose, while blue bars represent *L. monocytogenes* grown in MWB medium with 20 mM Rhamnose and 20nM B12.

Metabolites are grouped as indicated in X-axis, successively, acetate, lactate, 1,2-propanediol, propionate and 1-propanol. Bars with black outline represent aerobic condition, and Bars with grey outline and filled pattern represent anaerobic condition; data published in [13]. Results from three independent experiments are expressed and visualized as means and standard errors.

Metabolites following growth in MWB medium plus 20mM rhamnose with and without B12 in aerobic conditions, showed no significant differences in acetate, lactate and 1,2-propanediol production, in line with the corresponding similar growth phenotypes and rhamnose utilization in Figure 1. Notably, the type and amount of end products formed during rhamnose utilization in anaerobic conditions with B12 added, are significantly different from all other tested conditions, and include 4.1 mM acetate, 2.3 mM lactate, 1.4 mM 1,2-propanediol, and 3.2 mM propionate and 3.6 mM 1-propanol, indicative of activated *pdu* BMC. These data provide evidence for specific activation of *pdu* BMC in *L. monocytogenes* during growth on rhamnose in anaerobic conditions with B12 added to the medium.

### **5.3.3 Proteomic analysis on the impact of B12 on aerobic or anaerobic growth of *L.monocytogenes* on rhamnose**

Comparative proteomics analysis identified differentially expressed proteins in cells grown in MWB medium plus 20mM rhamnose with or without B12 in aerobic and anaerobic conditions (Figure 3). Figure 3A shows data for MWB plus 20mM rhamnose in anaerobic condition compared to MWB plus 20 mM rhamnose in aerobic condition. Obviously, 21 proteins out of 23 Pdu proteins (yellow dots encircled in black lines in Figure 3A) in the BMC-dependent 1,2-propanediol utilization cluster, are upregulated in anaerobically grown cells on rhamnose compared to aerobically grown cells (Details in Supplementary Table 1). Notably, despite expression of Pdu proteins, no production of *pdu* BMC signature metabolites propionate and 1-propanol was detected as shown above (figure 2), in line with our previously reported data [13], that showed only presence of BMCs and activation of *pdu* BMC in anaerobically rhamnose grown cells with added B12. Our data extend previous RNAseq studies that showed slight increase in *pdu* expression in the presence of propanediol, and highest expression when B12 was also present [28, 29]. The lack of *pdu* BMC activation in anaerobic MWB plus rhamnose conditions, suggests that the observed activation of B12 synthesis enzymes does not result in the production of sufficiently high levels of (de novo) B12 to trigger full induction (Figure 3A and Supplementary Table 5). Comparative analysis of anaerobically versus aerobically grown cells, points to repression of

propanediol-induced *pdu* expression in the latter condition. Notably, highlighted virulence factors in the volcano plot (Figure 3 A), show that actin assembly-inducing protein ActA, Listeriolysin O (LLO) encoded by *hly*, Listeriolysin regulatory protein PrfA, and phospholipase C encoded by *clpB*, are slightly upregulated in anaerobic growth compared to aerobic growth of *L. monocytogenes* on rhamnose, while PlcA, phospholipase A, shows no significant difference, and internalin C was repressed. Rha proteins for rhamnose utilization including *rhaA*, *rhaB*, *rhaD*, *rhaM* and Imo2850 contained in the *rha* cluster, are all slightly upregulated in anaerobic growth compared to aerobic growth of *L. monocytogenes* on rhamnose.

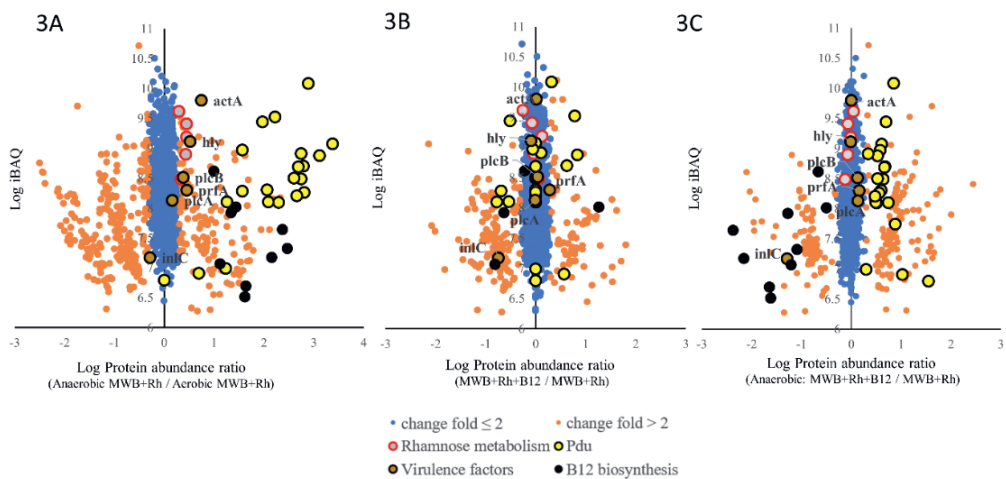


**Figure 3. Proteomic analysis of *L. monocytogenes* EGDc aerobically or anaerobically grown in MWB with 20mM Rhamnose with/without 20nM vitamin B12**

**(A)** Proteomic ratio plot of *L. monocytogenes* anaerobically grown in MWB plus 20 mM rhamnose compared to *L. monocytogenes* aerobically grown in MWB plus 20 mM rhamnose, (full list in Supplementary Table 1). **(B)** Proteomic ratio plot of *L. monocytogenes* aerobically grown in MWB plus 20 mM rhamnose and 20nM B12 compared to *L. monocytogenes* aerobically grown in MWB plus 20 mM rhamnose, (full list in Supplementary Table 2). **(C)** Proteomic ratio plot of *L. monocytogenes* anaerobically grown in MWB plus 20 mM rhamnose and 20nM B12 compared to *L. monocytogenes* anaerobically grown in MWB plus 20 mM rhamnose, (full list in Supplementary Table 3). Fold change  $\leq 2$  in blue, fold change  $> 2$  in light orange, proteins in the *pdu* cluster are in yellow, and proteins in the rhamnose cluster are in gray. Virulence factors in Supplementary Table 4 are dark orange. Genes of *cob/cbi* operon for B12 biosynthesis are in black.

Anaerobic growth of *L. monocytogenes* on rhamnose with added B12 results in increased expression of Pdu proteins (Figure 3C) and presence of BMCs was evidenced by TEM (Shown in our recent study [13]). Rha proteins do not show

significant differences, while PrfA, PlcB and ActA are induced, but PlcA, hly and InlC are repressed in MWB plus 20mM rhamnose with B12 compared cells grown without B12 (Details in Supplementary Table 3). Notably, addition of B12 and induction of *pdu* BMC in anaerobic conditions, results in a significant repression of B12 biosynthesis proteins (8 identified B12 proteins, Figure 3C). Reduced expression is also seen in aerobically grown cells, where only 4 B12 biosynthesis proteins are identified (Figure 3B). Combining these results suggests that addition of B12 has a repressive effect on B12 biosynthesis proteins in anaerobically rhamnose grown *L. monocytogenes* EGDc cells, with the B12 biosynthesis proteins largely repressed in aerobically grown cells (Details in Supplementary Table 5).

### **5.3.4 Stress and virulence proteins triggered by B12-activated *pdu* BMC**

The Venn diagram provides an overview of differentially expressed proteins in conditions without and with added B12 in aerobically and anaerobically rhamnose grown *L. monocytogenes* (Figure 4). As shown in Figure 4A, 145 proteins (Group X, red pie chart) are upregulated more than two fold in anaerobic MWB plus rhamnose with B12 compared to anaerobic condition without B12, and 81 proteins (Group Y, yellow pie chart) are upregulated more than two fold in aerobic condition with B12 compared to aerobic condition without B12, while 162 proteins (Group Z, blue pie chart) are upregulated more than two fold in anaerobic condition without B12 compared to aerobic condition without B12 (details in Supplementary Table 4). The overlap of group X and group Y contains 25 proteins that are upregulated in anaerobic and aerobic rhamnose conditions with added B12, with eight of the proteins present also in group Z. The proportion in red group X without overlap with other groups represents 103 proteins upregulated in *pdu* BMC induced cells grown in rhamnose with added B12 (Figure 4B, details in Supplementary Table 4). STRING protein-protein interaction analysis of these 103 proteins uniquely upregulated in anaerobically rhamnose grown *pdu* BMC induced *L. monocytogenes* cells, points to differential expression of a range of ribosomal and ribosome-associated proteins, including RplB, 50S ribosomal protein L28, RpsO, 30S ribosomal protein S15, Rnc, ribonuclease 3, involved in the processing of primary rRNA, and YbeY, an endoribonuclease involved in late-stage 70S ribosome maturation, while other proteins point to metabolic shifts, activation of stress defense, and links to virulence, such as RNA polymerase sigma factor SigL, Teichoic acids export ATP-binding protein, TagH, DNA repair and protection proteins RadA and DPS, and glutathione synthase

GshAB, previously linked to activation of virulence response in *L. monocytogenes* [30-32]. In addition, *pdu* BMC induced cells share a range of other virulence factors also expressed in anaerobic non-induced cells (Supplementary Table 3), including endopeptidase p60 (lap), (higher expressed in *pdu* BMC cells), Listeriolysin regulatory protein (PrfA), 1-phosphatidylinositol phosphodiesterase (PlcA), Phospholipase C (PlcB), Actin assembly-inducing protein (ActA), Internalin C (InlC) and Internalin B (InlB) (both higher expressed in in non-induced cells), and bi-functional Listeria associated protein (LAP, lmo1634) [2, 3, 8, 33, 34]. Next, *in vitro* virulence assays were performed to compare performance of anaerobic *pdu* BMC induced cells to non-induced anaerobic and aerobic cells.

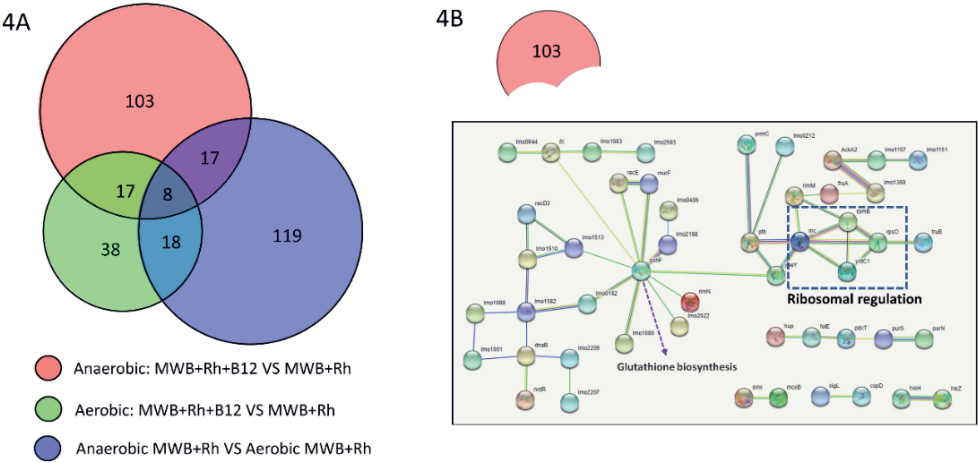


**Figure 4. Proteomics analysis of vitamin B12 impact on *L. monocytogenes* EGDe general stress response and virulence factors.**

**(A)** Venn diagram of overlapping upregulated proteins among three groups. Group X in red: anaerobic growth of *L. monocytogenes* on MWB with 20mM rhamnose and 20nM B12, compared to MWB with 20mM rhamnose without B12; Group Y in yellow: aerobic growth of *L. monocytogenes* on MWB with 20mM rhamnose and 20nM B12 compared MWB with 20mM rhamnose without B12; Group Z in blue: anaerobic growth of *L. monocytogenes* on MWB with 20mM rhamnose without B12 compared aerobic MWB with 20mM rhamnose without B12; **(B)** STRING analysis of proteins specifically upregulated by the addition of B12 in anaerobically grown *L. monocytogenes* in MWB with 20mM rhamnose; Nodes represent proteins, and lines represent interactions, disconnected proteins are not shown in the network (Details in Supplementary Table 4).

### 5.3.5 Impact of B12 on Caco-2 cell adhesion, invasion and translocation of *L. monocytogenes* grown aerobically or anaerobically on rhamnose

To address the impact of B12 on *L. monocytogenes* *in vitro* virulence, we conducted adhesion, invasion and translocation assays with Caco-2 cells using rhamnose *pdu* BMC induced and non-induced cells grown anaerobically and aerobically. As shown in Figure 5, *L. monocytogenes* cells grown anaerobically or aerobically in MWB plus 20mM rhamnose with or without B12 show similar adhesion and invasion efficacy of  $\sim 5.2$  log and  $\sim 4.1$  log CFU/well, respectively. Strikingly, the ability to translocate Caco-2 cells monolayers in a trans-well system, is significantly higher for *L. monocytogenes* cells grown anaerobically in MWB plus rhamnose with B12 compared to the other cells ( $\sim 1$  log CFU/well improvement), grown anaerobically without B12 and aerobically without and with B12 (Figure 5). These results indicate similar adhesion and invasion capacity of all four tested cell types, while anaerobically rhamnose grown *pdu* BMC induced *L. monocytogenes* cells show significantly higher translocation efficacy compared to the three non-induced cell types.

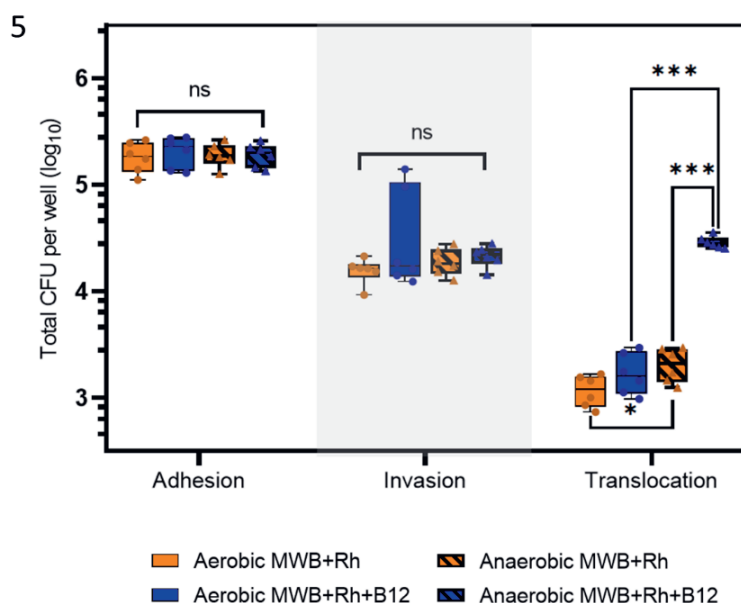


**Figure 5. Caco-2 cell assays with *L. monocytogenes* EGDe aerobically or anaerobically grown in MWB with 20mM Rhamnose with/without 20nM vitamin B12.**

Orange bars represent *L. monocytogenes* grown in MWB medium with 20 mM Rhamnose, while blue bars represent *L. monocytogenes* grown in MWB medium with 20 mM Rhamnose and 20nM B12. Bars

without filled pattern represent aerobic conditions, and Bars with filled pattern represent anaerobic conditions. X axis shows three groups of columns with results from adhesion, invasion and translocation assays. Y axis is the total CFU per well in log10 after the assays while initial inputs for adhesion and invasion are  $7.41 \pm 0.02$  in log10 CFU per well and the initial inputs for translocation are  $7.17 \pm 0.03$  in log10 CFU per well. Statistical significance is indicated (\*\*\*) means  $P \leq 0.001$ ; \* means  $P \leq 0.05$ ; ns means  $P > 0.05$  by Holm-Sidak T-test)

### 5.4 Discussion

The results in this study show a unique stimulating effect of B12 supplementation on anaerobic growth of *L. monocytogenes* with rhamnose, linked to *pdu* BMC activation and production of signature metabolites propionate and propanol, while no effect is observed in aerobic conditions. Growth in the latter condition with and without added B12 results in higher biomass production compared to anaerobically grown cells with and without added B12, conceivably due to increased energy generation via respiration [33]. Observed growth stimulation in rhamnose *pdu* BMC induced cells compared to non-induced cells is in line with previously described results [13]. *L. monocytogenes* has to cope with anaerobic conditions encountered during transmission along the food chain, for example in modified atmosphere and vacuum-packed foods, and in the GI tract. Notably, a significant upregulation of Pdu proteins involved in 1,2-propanediol utilization is observed in anaerobic MWB plus 20mM rhamnose grown cells compared to aerobic MWB plus 20mM rhamnose grown cells. This could point to activation of 1,2-propanediol utilization, in line with concomitant increase in expression of B12 synthesis enzymes in these anaerobically rhamnose grown *L. monocytogenes* cells, but HPLC analysis indicates that *pdu* BMC signature metabolites, propionate and 1-propanol are not produced, in line with absence of BMCs in TEM analysis [13]. Addition of B12 to anaerobically rhamnose grown cells results in further, significantly increased, expression of Pdu proteins, and activation of *pdu* BMC as evidenced by the production of propionate and 1-propanol (Figure 2), and presence of BMCs detected by TEM [11,19]. It is conceivable, that B12 dependent activation of *pdu* BMC in anaerobic conditions is not only crucial due to the role of B12 as a cofactor for the signature enzyme PduCDE, a B12-dependent diol dehydratase [20], but also because the PduCDE-B12 complex plays a role in triggering the construction of BMC with the shell proteins thereby encasing *pdu* enzymes, with the respective signature peptide sequences directing enzyme complexes to the correct locations inside the microcompartment [14, 35-37]. Our results with aerobically and anaerobically rhamnose grown cells, indicate that RNAseq data of *pdu* operon, including identification of factors involved in control

of gene expression, such as regulator PocR, B12-dependent riboswitch(es) and sRNAs [28, 38], require confirmation by proteomics, TEM and metabolic profiling to enable conclusions about activation of functional *pdu* BMC in *L. monocytogenes*.

B12-dependent activation of *pdu* BMC in *L. monocytogenes* also results in additional cellular responses. Comparative proteome analysis identified 103 proteins uniquely upregulated in *pdu* BMC induced cells with functions in protein synthesis, ribosomal proteins and ribosome-associated proteins, and in metabolism and stress defense, including RNA polymerase sigma factor SigL, Teichoic acids export ATP-binding protein, TagH, DNA repair and protection proteins RadA and DPS, and glutathione (GSH) synthase GshF, a multidomain protein encoded by *gshAB* (Fig 3 and 4, Supplementary Table 2 and 3). GshF mediated production of glutathione was recently linked to activation of virulence response in *L. monocytogenes*, with glutathione acting as an allosteric activator of Listeriolysin regulatory protein PrfA [30]. Notably, a range of virulence factors is expressed both in anaerobic *pdu* BMC induced and non-induced cells (Table 3), including regulatory protein PrfA, phosphatidylinositol phosphodiesterase (PlcA), Phospholipase C (PlcB), listeriolysin O (LLO), Actin assembly-inducing protein (ActA), Internalin C (InlC) and Internalin B (InlB), and bi-functional Listeria associated protein (LAP, Imo1634) [8, 9]. Extracellular cell wall associated LAP, has been suggested to play a role in *L. monocytogenes* interaction with the host by affecting cellular redistribution of epithelial junction proteins enhancing bacterial translocation [8, 9]. Analysis of proteomes from aerobically rhamnose grown cells without and with added B12) (Supplementary Table 1 and 3) also indicate (low level) presence of the virulence factors described above.

Our comparative *in vitro* virulence assays indicate similar Caco-2 adhesion and invasion capacity of aerobically and anaerobically rhamnose grown cells without and with added B12, while only anaerobically rhamnose grown *pdu* BMC induced *L. monocytogenes* cells show significantly higher Caco-2 translocation efficacy compared to the three other non-induced cell types. These results suggest that anaerobically rhamnose grown *pdu* BMC primed *L. monocytogenes* cells show enhanced transcellular and/or paracellular translocation in the Caco-2 cells transwell assay. Transcellular translocation involves *L. monocytogenes* binding and internalization into epithelial cells, and proceeds by intracellular replication and/or movement into neighboring epithelial cells by hijacking host cellular machinery via PrfA-activated virulence factors [34, 39, 40]. Based on similar

performance in our *L. monocytogenes* EGDe adhesion and invasion studies, with 1 h and 3 h incubation periods, respectively, it is unlikely that enhanced translocation capacity, with a 2 h incubation period, is linked to enhanced transcellular performance of rhamnose *pdu* BMC primed cells. An alternative explanation could be offered by enhanced paracellular translocation of *L. monocytogenes* cells, i.e., passing through an intercellular space between the Caco-2 cells, such as tight junctions [41, 42]. Tight junctions play a major role in maintaining the integrity and impermeability of epithelial cells, including the intestinal barrier [41-43]. Different strategies are used by pathogens aimed at destabilizing tight junctions, and roles for internalin A, LAP and listeriolysin O (LLO) in paracellular translocation of *L. monocytogenes* have been reported [8, 42, 43]. Combined with adapted physiology and metabolic shifts in *pdu* BMC induced cells including activated stress defense and GSH production, action of LAP and/or LLO, may have supported enhanced translocation in the trans-well assay. Notably, our previous results with anaerobically grown *L. monocytogenes* EGDe in LB medium with propanediol or ethanolamine, with and without added B12, showed similar adhesion and invasion capacity, but significantly higher translocation efficacy of respective *pdu* BMC and *eut* BMC induced cells.

We previously provided evidence for *L. monocytogenes* growth stimulation via B12 dependent activation of *pdu* BMC in anaerobically propanediol and rhamnose grown cells [13, 20]. The *pdu* BMC may thus enhance competitive fitness in the intestine, in line with observations that showed reduced *L. monocytogenes* persistence in stool and ileal colonization of female BALB/c mice of a *pduD* (subunit of propanediol dehydratase) deletion mutant compared to the wild type [44]. Our results obtained in Caco-2 virulence assays may point to an additional impact of (rhamnose) *pdu* BMC activation on *L. monocytogenes* interaction with host intestinal epithelial barrier, more specifically, interaction with tight junctions. Additional experiments are required to confirm our hypothesis and to elucidate underlying mechanisms.

5.5 Supplementary Materials

**Supplementary Table 1.** Protein profiling of *L. monocytogenes* EGDe anaerobically grown on MWB with 20mM rhamnose compared to *L. monocytogenes* EGDe aerobically grown on MWB with 20mM rhamnose. (Only list the top 100 rows, the full table with 1294 rows was online in bellowing link)

log <sub>2</sub> (Anaerobic control vs Aerobic control)	log <sub>2</sub> (iBAQ)	change fold > 2	change fold ≤ 2	Virulence factors	B12 biosynthesis	Protein IDs	Gene Name
X Axis	Y Axis						
3.375752926	9.073718	9.07371835				Q8Y7V3	lmo1166

# B12 impact on rhamnose BMC in *Listeria monocytogenes*

3.11286974	8.878378	8.878378156		Q8Y7W5	lmo1154
2.889710426	10.08554	10.08554031		Q8Y7W0	lmo1159
2.805953026	8.261739	8.261738547		Q8Y7W3	lmo1156
2.791836739	8.700358	8.700357528		Q8Y7X6	lmo1143
2.744400024	8.490422	8.490422042		Q8Y7V5	lmo1164
2.74358511	8.912536	8.912535571		Q8Y7W6	lmo1153
2.690611362	8.687493	8.687493289		Q8Y7W1	lmo1158
2.659667969	8.205664	8.205664407		Q8Y7V4	lmo1165
2.599720955	8.500442	8.500442318		Q8Y7V8	lmo1161
2.46775198	7.322343	7.322343361	7.322343361	Q8Y7S0	lmo1201
2.371239185	7.63777	7.637769829	7.637769829	Q8Y7S2	cbiH
2.332382679	8.169968	8.169968174		Q8Y773	mntH
2.291455269	8.096319	8.096318971		Q8Y7W7	lmo1152
2.222490549	9.523941	9.523941465		Q8Y7W8	lmo1151
2.19250083	8.148078	8.148077977		Q8YAJ6	lmo0129
2.154970884	7.1712	7.171199717	7.171199717	Q8Y770	cbiA
2.116625309	7.635534	7.635534009		Q8Y529	birA
2.090326071	8.103667	8.103666914		Q8Y7X7	lmo1142
2.063484907	8.304103	8.304102592		Q8Y7V6	lmo1163
1.969180822	9.444326	9.444325903		Q8Y7W4	lmo1155
1.946399927	7.632771	7.632771005		Q8Y429	lmo2280
1.787874222	7.288585	7.288584545		Q8Y554	lmo2222
1.717632055	7.117371	7.117370741		Q8Y6F4	lmo1733
1.700398207	7.369309	7.369308645		Q7AP93	lmaA
1.689100266	8.469925	8.469925057		Q8Y3T5	lmo2746
1.676471472	7.109444	7.109443547		Q8Y8H0	queG
1.670406103	8.034829	8.034828916		Q8YAJ7	lmo0127
1.660499334	7.342205	7.342205479		Q8Y609	lmo1893
1.64124608	6.694035	6.694034538	6.694034538	Q8Y7R4	lmo1207
1.625446081	8.872704	8.872703896		Q8Y4W1	lmo2318
1.620543957	6.728638	6.728637807		Q8Y3S1	lmo2761
1.617798567	6.512044	6.512043686	6.512043686	Q8Y7S3	cbiG
1.612308979	7.49167	7.491669794		Q8Y945	lmo0695
1.60121417	7.648399	7.648399047		Q8Y5R4	lmo1992
1.585050344	6.952158	6.952157726		Q8Y7H2	lmo1308
1.566908598	8.283007	8.283007076		Q8Y7V1	ackA2
1.565846205	8.97173	8.971730321		Q8Y7X5	lmo1144
1.536111792	7.097084	7.097083696		Q8Y4W2	lmo2317
1.510450363	6.877579	6.877578652		Q8Y4U8	int
1.50801897	6.746175	6.746174756		Q8Y5R9	leuA
1.462916136	6.97574	6.975739612		Q8Y469	lmo2586
1.440248013	8.013511	8.013511333	8.013511333	Q8Y7S8	lmo1193
1.424135208	8.8033	8.803300031		Q8YAJ1	lmo0355
1.415513992	8.908303	8.908302684		Q8Y6Q0	lmo1634
1.401859522	7.225439	7.225438517		Q8Y526	lmo2251
1.401520252	6.88887	6.888869995		Q8YAT2	lmo0031
1.361497402	7.41519	7.415190441		Q8Y425	lmo2284
1.344648361	6.715937	6.715936524		Q8Y4A0	lmo2554
1.343981504	7.92089	7.920889972	7.920889972	Q8Y7S4	cbiF
1.292231798	8.133571	8.133570841		Q7AP51	lysA
1.264305353	7.853668	7.853667798		Q8Y644	deoD
1.263563871	6.744715	6.744715334		Q8Y474	lmo2581
1.257394075	7.688108	7.688108229		Q8Y929	lmo0713
1.256662369	8.102331	8.10233078		Q8Y7V9	lmo1160
1.233086586	6.992005	6.992005334		Q8Y7X4	lmo1145
1.150750399	6.952163	6.952162574		Q8Y8R6	nifJ
1.148393154	9.093667	9.093666782		Q8Y992	lmo0641
1.142185211	7.957574	7.957573768		P0A442	pflA
1.126757383	8.341098	8.341098039		Q8Y4Y2	lmo2297
1.121907473	7.065542	7.065542371	7.065542371	Q8Y7R3	cobQ
1.113847017	6.55184	6.5518402		Q7AP82	lmo0685
1.045382023	8.843407	8.843407209		Q92CE7	lmo1257
1.035565138	7.750717	7.750716621		Q8Y4U1	lmo2341
1.026252508	8.026002	8.026001817		Q927F6	lmo2685
1.025926828	7.442558	7.442558154		P25147	inlB
1.023258448	7.287354	7.287353773		Q8Y8E4	lmo0960
1.000617981	8.613504	8.613503553	8.613503553	Q8Y7R2	lmo1209
0.99486804	6.54658	6.546579676		Q8Y8V4	lmo0788
0.993393183	7.196038	7.196037941		Q8Y8T0	lmo0814
0.993283987	6.977051	6.977051071		Q8Y9S2	lmo0451
0.984838247	7.572256	7.572255722		Q8Y9N5	aroE
0.959782839	6.889447	6.889447377		Q8Y870	moaA
0.956775188	9.11581	9.115810141		Q8Y3T4	serS
0.946940422	7.953914	7.953914252		Q8Y849	lmo1069
0.946549177	7.805004	7.805004432		Q8Y4V4	lmo2326
0.933475971	8.688073	8.688072604		Q8Y4Y8	lmo2291
0.927187443	6.295501	6.295501126		Q8YAE6	lmo0184

0.917775393	6.95673	6.956730152	Q8Y928	lmo0714
0.906856298	6.692406	6.692406235	Q8Y4Z2	lmo2287
0.897176027	7.1321	7.132099522	Q8Y6D6	lmo1751
0.877289772	7.714874	7.714874382	Q8Y4Y3	lmo2296
0.86866641	7.489649	7.489649163	Q8Y5Q0	alsS
0.868249416	7.419229	7.419228564	Q8Y5C4	lmo2141
0.853745461	7.339372	7.339371929	Q8YAL2	lmo0106
0.842061281	7.486133	7.486132818	Q8Y4V0	lmo2330
0.841254473	7.273256	7.273255983	Q8Y6U0	thil
0.830568552	7.752072	7.752071507	Q8Y4W0	lmo2319
0.826544046	7.786063	7.786062534	Q8Y7K8	lmo1269
0.812473059	7.844632	7.844632475	Q8Y405	lmo2673
0.80316186	7.234796	7.234795588	Q8Y4I7	lmo2452
0.801748514	7.374051	7.37405145	Q8Y7F2	ribC
0.801725864	7.312029	7.31202918	Q8Y6D7	lmo1750
0.794469118	7.513231	7.513230922	Q8Y5K4	lmo2056
0.791771412	7.727801	7.72780143	Q8Y894	lmo1020
0.768510342	6.908051	6.908050507	Q8YA57	lmo0304
0.752810001	7.339352	7.339352049	Q8YAB0	mrnC
0.751938343	7.291813	7.291812687	Q8Y555	lmo2221

**Supplementary Table 2.** Protein profiling of *L. monocytogenes* EGDe aerobically grown on MWB with 20mM rhamnose and 20nM B12 compared to MWB with 20mM rhamnose without B12. (Only list the top 100 rows, the full table with 1294 rows was online in bellowing link)

log <sub>2</sub> (Aerobic Pdu induced vs Pdu control)	log <sub>2</sub> (iBAQ)	change fold > 2	change fold ≤ 2	Virulence factors	B12 biosynthesis	Protein IDs	Gene Name
<b>X Axis</b>	<b>Y Axis</b>						
1.805222511	7.387710089	7.387710089				Q8Y8H1	lmo0933
1.712907791	7.117370741	7.117370741				Q8Y6F4	lmo1733
1.620878696	7.953914252	7.953914252				Q8Y849	lmo1069
1.540885448	6.773230426	6.773230426				Q8Y7C1	dxs
1.536102772	7.018201022	7.018201022				Q8Y9D3	lmo0597
1.529257298	8.138334282	8.138334282				Q92AP5	lmo1763
1.366000652	6.877578652	6.877578652				Q8Y4U8	int
1.292232399	7.3733902	7.3733902				Q8Y4P2	lmo2393
1.265316963	8.013511333	8.013511333			8.013511	Q8Y7S8	lmo1193
1.219377518	7.860565577	7.860565577				Q8YAG2	lmo0164
1.207216501	8.617912031	8.617912031				Q92IM1	lmo0216
1.201541424	7.814021064	7.814021064				Q8Y7M6	lmo1248
1.131763697	6.715936524	6.715936524				Q8Y4A0	lmo2554
1.0938375	7.853667798	7.853667798				Q8Y644	deoD
1.039900303	7.795817474	7.795817474				Q8Y4Q1	lmo2384
1.035443544	7.935446803	7.935446803				Q8Y4M5	lmo2412
1.034816265	6.443638431	6.443638431				Q8Y745	hemN
1.029500008	7.750716621	7.750716621				Q8Y4U1	lmo2341
0.993444492	7.743854555	7.743854555				Q92CN5	lmo1172
0.99298811	7.786062534	7.786062534				Q8Y7K8	lmo1269
0.976891518	7.958544772	7.958544772				Q8Y409	lmo2669
0.96556282	7.025059969	7.025059969				Q8YAE4	lmo0186
0.958362818	8.892717758	8.892717758				Q8Y7C8	lmo1356
0.940654755	7.72780143	7.72780143				Q8Y894	lmo1020
0.938318491	7.313276516	7.313276516				Q8YAU3	lmo0020
0.935515165	7.37405145	7.37405145				Q8Y7F2	ribC
0.830783129	8.878378156	8.878378156				Q8Y7W5	lmo1154
0.825019836	8.180613251	8.180613251				Q8Y6S1	lmo1612
0.821718931	7.766858811	7.766858811				Q8Y8U5	lmo0797
0.815946341	7.500935943	7.500935943				Q8Y8A2	lmo1010
0.814572573	7.336879816	7.336879816				Q8Y4H9	lmo2462
0.809592962	7.31202918	7.31202918				Q8Y6D7	lmo1750
0.799630404	7.121362841	7.121362841				Q8Y8Z0	lmo0752
0.781103849	7.234795588	7.234795588				Q8Y4I7	lmo2452
0.780045033	9.523941465	9.523941465				Q8Y7W8	lmo1151
0.77283144	8.148077977	8.148077977				Q8YAJ6	lmo0129
0.742275715	7.572674151	7.572674151				Q8Y7A7	acyP
0.737600088	7.349277527	7.349277527				Q927T1	lmo2562
0.73535037	7.117470164	7.117470164				Q8Y6N8	sbcd
0.728060722	7.503204876	7.503204876				Q8Y7M3	lmo1251
0.724033833	6.8469059	6.8469059				Q8Y4Z6	lmo2283
0.719837189	7.310204589	7.310204589				Q8Y871	moaC
0.707377911	7.535572587	7.535572587				Q8Y4J9	lmo2439

## B12 impact on rhamnose BMC in *Listeria monocytogenes*

0.684610844	7.118958778	7.118958778		Q8Y3V1	lmo2730
0.673069239	7.07371835	7.07371835		Q8Y8N8	lmo0858
0.671754599	7.225438517	7.225438517		Q8Y526	lmo2251
0.654554844	7.408104227	7.408104227		Q8Y457	truA
0.631908417	7.752071507	7.752071507		Q8Y4W0	lmo2319
0.619845152	8.700357528	8.700357528		Q8Y7X6	lmo1143
0.605652571	7.224066664	7.224066664		Q8Y978	lmo0655
0.601598263	NaN	NaN		Q929L4	lmo2158
0.575286388	7.288584545	7.288584545		Q8Y554	lmo2222
0.565071821	7.419228564	7.419228564		Q8Y5C4	lmo2141
0.563715458	6.907368359	6.907368359		Q8Y7W9	lmo1150
0.560279846	7.050843581	7.050843581		Q8Y5F6	lmo2108
0.544549942	9.790102116	9.790102116		Q927L6	rpsQ
0.534108162	6.660780128	6.660780128		Q8Y903	lmo0739
0.487774134	7.395046677	7.395046677		Q8YAT6	lmo0027
0.459897995	7.468125695	7.468125695		Q8Y5N2	nadA
0.446807146	7.402811427	7.402811427		Q8Y7L7	lmo1258
0.435107708	6.956730152	6.956730152		Q8Y928	lmo0714
0.432347775	8.309310716	8.309310716		Q8Y9X6	lmo0391
0.432201385	10.10994958	10.10994958		Q8Y704	lmo1526
0.429923534	8.329072291	8.329072291		Q8Y640	msrA
0.428799152	8.527101209	8.527101209		Q8Y9X5	lmo0393
0.421207666	8.287980784	8.287980784		Q8Y5V2	pnp
0.387801647	8.826042391	8.826042391		Q8Y6A4	lmo1791
0.386339188	9.319314304	9.319314304		Q8Y458	rplM
0.379296303	6.759871726	6.759871726		Q8Y8V2	lmo0790
0.363970757	8.743995526	8.743995526		P66401	rpsZ
0.357334614	8.261928673	8.261928673		Q8Y728	lmo1495
0.354423285	8.220709405	8.220709405		Q7AP66	opuCB
0.349323273	9.785230149	9.785230149		P66503	rpsT
0.344707251	7.637079257	7.637079257		Q8Y607	dnaD
0.344486475	8.604927703	8.604927703		Q8Y415	lmo2454
0.340812445	8.202678994	8.202678994		Q927H3	lmo2666
0.321591616	7.929633465	7.929633465		Q8Y4U7	lmo2334
0.316426039	10.08554031	10.08554031		Q8Y7W0	lmo1159
0.312723637	9.404850814	9.404850814		Q927M5	rpmD
0.311442375	8.243434937	8.243434937		Q8Y5X4	ndk
0.302579165	6.8521688	6.8521688		Q8Y9P2	rlmN
0.299002647	9.138839312	9.138839		P0A491	rplM
0.290863276	8.213119139	8.213119		Q8Y4N7	ltrC
0.290675402	7.941039117	7.941039		Q8YAE5	lmo0185
0.287810087	7.777172987	7.777173		Q8Y627	lmo1873
0.282749176	7.930199953	7.9302		Q8YAG3	lmo0163
0.278865337	7.408121197	7.408121		Q8YAK8	lmo0110
0.278789759	6.89356759	6.893568		Q7AP50	sigL
0.277992487	7.377688641	7.377689		Q92EC0	lmo0536
0.277251482	8.299790489	8.29979	8.29979	P22262	prfA
0.273253202	7.864083696	7.864084		Q926W7	parA
0.27296114	8.976702958	8.976703		Q92C55	glnR
0.27288866	8.693937891	8.693938		Q8YAC8	lmo0218
0.260741234	7.6776252	7.677625		Q8Y899	lmo1013
0.259607315	8.931244231	8.931244		Q8YAJ1	lmo0134
0.258891106	7.196037941	7.196038		Q8Y8T0	lmo0814
0.251602173	9.021396057	9.021396		Q8Y440	rplC
0.251134872	7.98156493	7.981565		Q8Y6S2	lmo1611



5

**Supplementary Table 3.** Protein profiling of *L. monocytogenes* EGDe anaerobically grown on MWB with 20mM rhamnose and 20nM B12 compared to MWB plus 20mM rhamnose without B12. (Only list the top 100 rows, the full table with 1294 rows was online in bellowing link)

log(Anaerobic Pdu induced vs Pdu non-induced)	Log(iBAQ)	change fold > 2	change fold ≤ 2	Virulence factors	B12 biosynthesis	Protein IDs	Gene Name
<b>X Axis</b>	<b>Y Axis</b>						
2.444868565	8.40715287	8.40715287				Q8Y523	lmo2254
2.001654863	7.898719698	7.898719698				Q8Y7A9	yidC1
1.78644681	8.319189369	8.319189369				Q8Y8G0	lmo0944
1.756666899	7.671006131	7.671006131				Q8Y985	lmo0648
1.708023787	8.235679919	8.235679919				Q8Y569	lmo2207
1.657866478	7.27186483	7.27186483				Q8Y9F9	hisZ
1.631134987	7.176756667	7.176756667				Q8Y6X0	dnaB
1.619628191	9.703540703	9.703540703				Q92AD0	cspD

## Chapter 5

1.598968029	7.372672707	7.372672707	Q8Y403	lmo2675
1.578961134	7.539527731	7.539527731	Q8Y5N5	lmo2022
1.556344271	7.28302971	7.28302971	Q8Y455	ecfA2
1.546034813	6.794348604	6.794348604	Q8Y7W2	PduH
1.532580137	8.07081336	8.07081336	Q8Y9C3	lmo0609
1.482708454	7.121362841	7.121362841	Q8Y8Z0	lmo0752
1.441064358	7.834585997	7.834585997	Q8Y6C4	purN
1.358945608	7.974728095	7.974728095	Q8Y717	recD2
1.340945005	7.471247692	7.471247692	Q8Y9Q0	lmo0474
1.32920599	7.308030554	7.308030554	Q8Y7B7	lmo1369
1.315590143	8.934574194	8.934574194	P0A4Q8	lmo0208
1.288183928	7.050843581	7.050843581	Q8Y5F6	lmo2108
1.281007528	8.768882185	8.768882185	Q92C24	rpsO
1.246596575	7.978782905	7.978782905	Q8Y3R3	gshAB
1.228598833	8.536634185	8.536634185	Q8Y6F1	lmo1736
1.219435215	7.448489892	7.448489892	Q8YAN3	lmo0084
1.216575861	7.752071507	7.752071507	Q8Y4W0	lmo2319
1.179326057	8.457306492	8.457306492	Q8Y9W3	lmo0406
1.171905041	9.523941465	9.523941465	Q8Y7W8	PduA
1.152827501	6.912928473	6.912928473	Q8Y3U4	lmo2737
1.115174055	7.953914252	7.953914252	Q8Y849	lmo1069
1.105092049	6.307816827	6.307816827	Q8Y6P0	lmo1644
1.091968298	6.8521688	6.8521688	Q8Y9P2	rlmN
1.089939833	8.363066419	8.363066419	Q8Y6K1	lmo1683
1.068555117	6.817413307	6.817413307	Q8Y4N3	lmo2403
1.058516741	8.603772075	8.603772075	Q8YAU8	qoxC
1.05541873	8.257102333	8.257102333	Q8Y747	ybeY
1.051350832	8.617912031	8.617912031	Q9ZIM1	lmo0216
1.04192996	8.22960506	8.22960506	Q8Y6P1	lmo1643
1.035909176	8.268086304	8.268086304	Q8Y3V7	lmo2724
1.031580925	7.932625944	7.932625944	Q8Y4A7	tdk
1.022472382	6.907368359	6.907368359	Q8Y7W9	PcoR
1.010482788	7.834401627	7.834401627	Q8Y8Q2	lmo0844
0.99387002	8.6164335	8.6164335	Q92AN7	purS
0.980150938	7.937141608	7.937141608	Q8Y713	lmo1513
0.975621223	8.195124423	8.195124423	Q8Y6A2	rimM
0.967209101	7.859228391	7.859228391	Q8Y9E9	lmo0580
0.960325956	8.146778989	8.146778989	Q8Y5Y4	lmo1919
0.959985971	7.179896333	7.179896333	Q8Y638	lmo1862
0.958674908	7.766858811	7.766858811	Q8Y8U5	lmo0797
0.945564508	7.958544772	7.958544772	Q8Y409	lmo2669
0.936180592	8.409645752	8.409645752	Q8Y8A7	lmo1001
0.933904648	7.745152895	7.745152895	Q8Y691	rrc
0.925149918	7.442354323	7.442354323	Q8Y7F3	truB
0.919288158	8.3232521	8.3232521	Q8Y6W9	nrdR
0.916373968	7.32130839	7.32130839	Q8Y552	ilvD
0.902123213	7.971572701	7.971572701	Q8YA78	lmo0281
0.901861429	7.526326352	7.526326352	Q8Y433	lmo2641
0.901158571	8.33655979	8.33655979	Q8Y9Y0	lmo0387
0.899579525	8.070555016	8.070555016	Q8YA86	lmo0273
0.89653945	7.759138816	7.759138816	Q8Y5X1	folE
0.894593716	8.283007076	8.283007076	Q8Y7V1	ackA2
0.892370224	7.801527189	7.801527189	Q8Y8H6	lmo0927
0.892153263	8.192009593	8.192009593	Q8Y3X2	lmo2707
0.883132219	7.637079257	7.637079257	Q8Y607	dnaD
0.882959127	7.743854555	7.743854555	Q92CN5	EutV
0.88265419	8.25161389	8.25161389	Q8Y963	lmo0670
0.873026371	8.573173413	8.573173413	Q8Y6D8	aroK
0.872084141	7.768171743	7.768171743	Q8Y8A5	lmo1005
0.864576817	8.089304452	8.089304452	Q8Y5A1	lmo2168
0.859047174	7.401262648	7.401262648	Q8Y4U6	fruA
0.857785702	8.104760167	8.104760167	Q8Y8L1	lmo0887
0.84902668	10.08554031	10.08554031	Q8Y7W0	PduJ
0.843302965	7.603707183	7.603707183	Q8Y8F4	lmo0950
0.82746768	8.17773845	8.17773845	Q8Y560	lmo2216
0.826002836	7.336879816	7.336879816	Q8Y4H9	lmo2462
0.818063736	7.325515663	7.325515663	Q8YAG4	lmo0162
0.814146519	7.507950273	7.507950273	Q8Y6E6	lmo1741
0.804112196	6.907599443	6.907599443	Q8YAC0	lmo0067
0.799869061	7.805004432	7.805004432	Q8Y4V4	lmo2326
0.797634602	8.023005397	8.023005397	Q8Y9L5	lmo0512
0.796156883	9.056180423	9.056180423	P66144	rpmB
0.789059401	7.549579485	7.549579485	Q8Y6U9	lmo1582
0.787975311	6.8469059	6.8469059	Q8Y4Z6	lmo2283
0.785645723	7.535572587	7.535572587	Q8Y4J9	lmo2439
0.779451132	7.056752441	7.056752441	Q48759	mcsB
0.779250622	7.408104227	7.408104227	Q8Y457	truA

0.769850254	7.460597189	7.460597189	Q8Y6X3	engB
0.766243935	7.87653536	7.87653536	Q8Y9G3	hisH
0.764287472	7.400123355	7.400123355	Q8YAD1	pth
0.763047457	7.635735002	7.635735002	Q8Y6V4	lmo1577
0.749732971	7.424342516	7.424342516	Q8Y8R9	lmo0825
0.744203329	8.10233078	8.10233078	Q8Y7V9	PduL
0.739841223	7.28302971	7.28302971	Q8Y7N7	murl
0.739699364	7.427567248	7.427567248	Q8Y6K4	lmo1680
0.739346743	7.503204876	7.503204876	Q8Y7M3	lmo1251
0.720335007	6.908050507	6.908050507	Q8YA57	lmo0304
0.718988895	7.432600545	7.432600545	Q8Y9T7	lmo0436
0.706874132	7.117470164	7.117470164	Q8Y6N8	sbcD
0.70556736	6.660780128	6.660780128	Q8Y903	lmo0739

**Supplementary Table 4.** Details of overlap in upregulated proteins among Group X, Y and Z

X-Y only (17)		X-Z only (17)		Y-Z only (18)		X-Y-Z overlap (8)	
Protein IDs	Gene Name	Protein IDs	Gene Name	Protein IDs	Gene Name	Protein IDs	Gene Name
Q8Y8Z0	lmo0752	Q8Y7V1	ackA2	Q8Y6F4	lmo1733	Q8Y4W0	lmo2319
Q8Y5F6	lmo2108	Q8Y4V4	lmo2326	int		Q8Y6P1	lmo1643
Q9ZIM1	lmo0216	Q8Y7V9	PduL	Q8Y4U8	lmo1193	Q8Y3V7	lmo2724
Q8Y8U5	lmo0797	Q8YA57	lmo0304	Q8Y7S8	lmo2554	Q8Y8H6	lmo0927
Q8Y409	lmo2669	Q8Y705	lmo1525	Q8Y4A0	deoD	Q8Y7W0	PduJ
Q8Y607	dnaD		PduE	Q8Y644	lmo2341	Q8Y7M3	lmo1251
	EutV	Q8Y7W4	PduK	Q8Y4U1	lmo1269	Q8Y7X6	PduT
Q92CN5		Q8Y7W1		Q8Y7K8	lmo1020	Q8Y7W5	PduD
Q8Y4H9	lmo2462	Q8Y7V5	PduO	Q8Y894	ribC		
Q8Y4Z6	lmo2283	Q8Y7V3	PduQ	Q8Y7F2	lmo1750		
Q8Y4J9	lmo2439	Q8Y7V6	PduN	Q8Y6D7			
Q8Y457	truA	Q8Y7X5	PduU	Q8Y4I7	lmo2452		
Q8Y6N8	sbcD		PduG	lmo0129			
		Q8Y7W3		Q8YAJ6	lmo2251		
Q8Y903	lmo0739	Q8Y7V8	EutJ	Q8Y526	lmo2222		
Q8Y7L7	lmo1258		PduB	Q8Y554	lmo2141		
Q929L4	lmo2158	Q8Y7W7	PduS	Q8Y5C4	lmo0027		
Q8Y5V2	pnp	Q8Y7V4	PduP	Q8YAT6	lmo0714		
Q8Y9P2	rImN		PduC	Q8Y928			
		Q8Y7W6		P66401	rpsZ		

Group X (145) Anaerobic: MWB+Rh+B12 VS MWB+Rh; Group Y (81) Aerobic: MWB+Rh+B12 VS MWB+Rh; Group Z (162) Anaerobic MWB+Rh VS Aerobic MWB+Rh;

**Supplementary Table 5.** Overview of B12 biosynthesis protein expression among Group X, Y and Z

Protein IDs	Gene Name	log <sub>2</sub> (Anaerobic control vs Aerobic control) Group Z	log <sub>2</sub> (Aerobic Pdu induced vs Pdu control) Group Y	log <sub>2</sub> (Anaerobic Pdu induced vs Pdu non-induced) Group X
Q8Y7S0	lmo1201	2.46775198		-1.088737249
Q8Y7S2	cbiH	2.371239185		-2.371239185
Q8Y7T0	cbiA	2.154970884		-2.154970884
Q8Y7R4	lmo1207	1.64124608		-1.64124608

Q8Y7S3	cbiG	1.617798567		-1.617798567
Q8Y7S8	lmo1193	1.440248013	1.265316963	-0.497404814
Q8Y7S4	cbiF	1.343981504	-0.630130291	-1.27417469
Q8Y7R3	cobQ	1.121907473	-0.810967684	-1.207518578
Q8Y7R2	lmo1209	1.000617981	-0.213595629	-0.658695221

The table lists UniProt protein ID, X value representing Log2 Protein abundance ratio (Rhamnose *pdu* BMC induced/non-induced in MWB), Y value representing -Log10 p-value (Rhamnose *pdu* BMC induced/non-induced in MWB), NCBI protein Annotation and NCBI Gene ID.

**The Supplementary Materials for this chapter can also be found online at:**

<https://www.biorxiv.org/content/10.1101/2021.08.26.457850v1.supplementary-material>

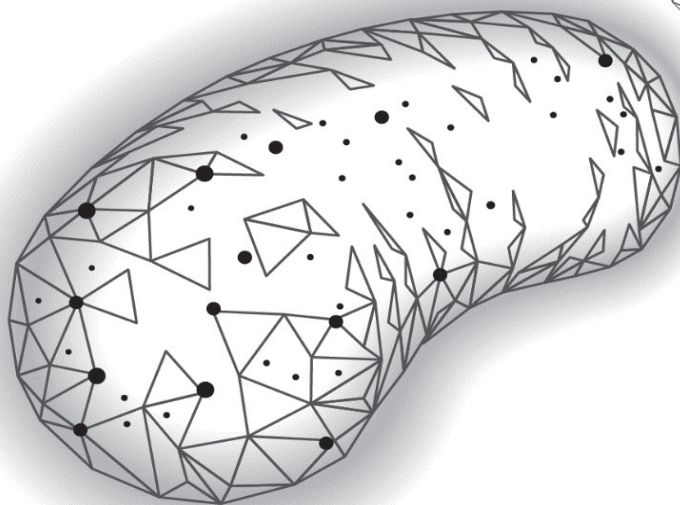
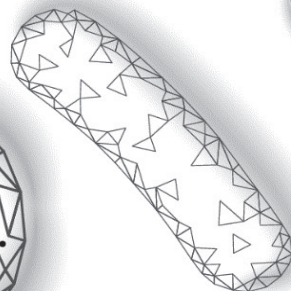
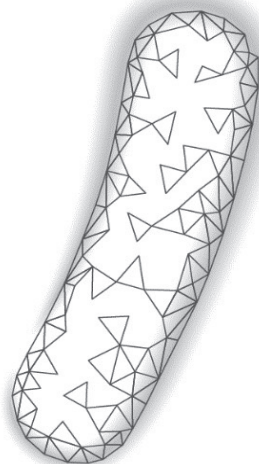
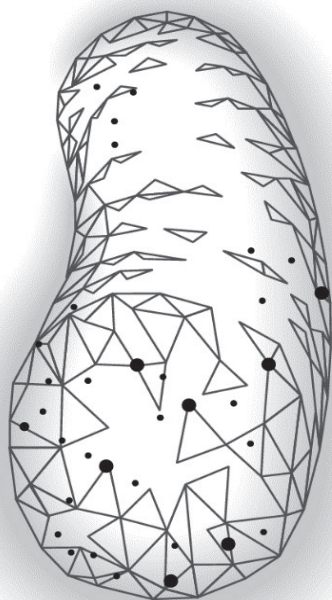
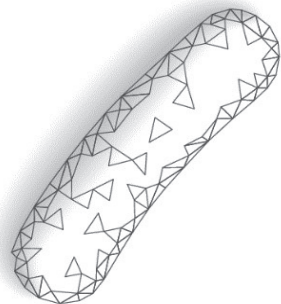
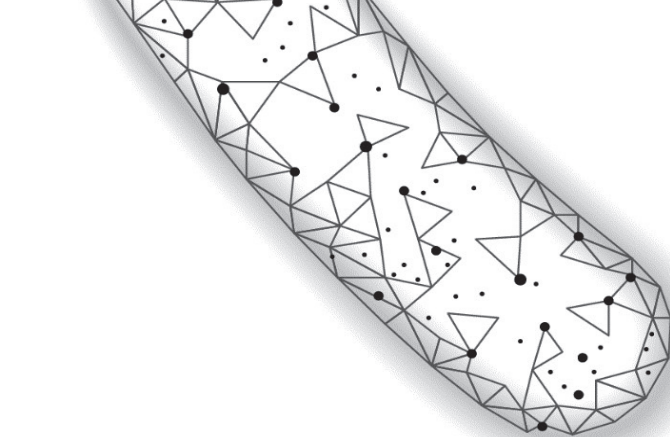
## 5.6 References

1. Prevention, C.f.D.C.a., *Quantitative assessment of the relative risk to public health from foodborne Listeria monocytogenes among selected categories of ready-to-eat foods*. 2003, US Department of Agriculture–Food Safety and Inspection Service Washington, DC.
2. Freitag, N.E., G.C. Port, and M.D. Miner, *Listeria monocytogenes—from saprophyte to intracellular pathogen*. Nature Reviews Microbiology, 2009. **7**(9): p. 623-628.
3. Radoshevich, L. and P. Cossart, *Listeria monocytogenes: towards a complete picture of its physiology and pathogenesis*. Nature Reviews Microbiology, 2018. **16**(1): p. 32.
4. Gandhi, M. and M.L. Chikindas, *Listeria: a foodborne pathogen that knows how to survive*. International journal of food microbiology, 2007. **113**(1): p. 1-15.
5. Portnoy, D.A., V. Auerbuch, and I.J. Glomski, *The cell biology of Listeria monocytogenes infection: the intersection of bacterial pathogenesis and cell-mediated immunity*. The Journal of cell biology, 2002. **158**(3): p. 409-414.
6. Mengaud, J., et al., *E-cadherin is the receptor for internalin, a surface protein required for entry of L. monocytogenes into epithelial cells*. Cell, 1996. **84**(6): p. 923-932.
7. Tattoli, I., et al., *Listeria phospholipases subvert host autophagic defenses by stalling pre-autophagosomal structures*. The EMBO journal, 2013. **32**(23): p. 3066-3078.
8. Kim, H. and A.K. Bhunia, *Secreted Listeria adhesion protein (Lap) influences Lap-mediated Listeria monocytogenes paracellular*

- translocation through epithelial barrier. Gut pathogens, 2013. **5**(1): p. 1-11.
9. Burkholder, K.M. and A.K. Bhunia, *Listeria monocytogenes uses Listeria adhesion protein (LAP) to promote bacterial transepithelial translocation and induces expression of LAP receptor Hsp60*. Infection and immunity, 2010. **78**(12): p. 5062-5073.
  10. Desai, A.N., et al., *Changing epidemiology of Listeria monocytogenes outbreaks, sporadic cases, and recalls globally: A review of ProMED reports from 1996 to 2018*. International Journal of Infectious Diseases, 2019. **84**: p. 48-53.
  11. Tasara, T. and R. Stephan, *Cold stress tolerance of Listeria monocytogenes: a review of molecular adaptive mechanisms and food safety implications*. Journal of food protection, 2006. **69**(6): p. 1473-1484.
  12. Zeng, Z., et al., *Bacterial Microcompartments Coupled with Extracellular Electron Transfer Drive the Anaerobic Utilization of Ethanolamine in Listeria monocytogenes*. mSystems, 2021. **6**(2).
  13. Zeng, Z., et al., *Anaerobic Growth of Listeria monocytogenes on Rhamnose Is Stimulated by Vitamin B(12) and Bacterial Microcompartment-Dependent 1,2-Propanediol Utilization*. mSphere, 2021: p. e0043421.
  14. Kerfeld, C.A., et al., *Bacterial microcompartments*. Nature Reviews Microbiology, 2018.
  15. Yeates, T.O., C.S. Crowley, and S. Tanaka, *Bacterial microcompartment organelles: protein shell structure and evolution*. Annual review of biophysics, 2010. **39**: p. 185-205.
  16. Liu, L.N., *Bacterial metabolosomes: new insights into their structure and bioengineering*. Microbial Biotechnology, 2021. **14**(1): p. 88-93.
  17. Jakobson, C.M. and D. Tullman-Ercek, *Dumpster diving in the gut: bacterial microcompartments as part of a host-associated lifestyle*. PLoS pathogens, 2016. **12**(5): p. e1005558.
  18. Petit, E., et al., *Involvement of a bacterial microcompartment in the metabolism of fucose and rhamnose by Clostridium phytofermentans*. PLoS One, 2013. **8**(1): p. e54337.
  19. Anast, J.M., T.A. Bobik, and S. Schmitz-Esser, *The Cobalamin-dependent gene cluster of Listeria monocytogenes: implications for virulence, stress response, and food safety*. Frontiers in microbiology, 2020. **11**.

20. Zeng, Z., et al., *Bacterial microcompartment-dependent 1, 2-propanediol utilization stimulates anaerobic growth of Listeria monocytogenes EGDe*. *Frontiers in Microbiology*, 2019. **10**: p. 2660.
21. Prentice, M.B., *Bacterial microcompartments and their role in pathogenicity*. *Current Opinion in Microbiology*, 2021. **63**: p. 19-28.
22. Schneebeli, R. and T. Egli, *A defined, glucose-limited mineral medium for the cultivation of Listeria*. *Applied and environmental microbiology*, 2013: p. AEM. 03538-12.
23. Vizcaino, J.A., et al., *2016 update of the PRIDE database and its related tools (vol 44, pg D447, 2016)*. *Nucleic Acids Research*, 2016. **44**(22): p. 11033-11033.
24. Oliveira, M., et al., *Pathogenic potential of Salmonella Typhimurium DT104 following sequential passage through soil, packaged fresh-cut lettuce and a model gastrointestinal tract*. *International journal of food microbiology*, 2011. **148**(3): p. 149-155.
25. Koomen, J., et al., *Gene profiling-based phenotyping for identification of cellular parameters that contribute to fitness, stress-tolerance and virulence of Listeria monocytogenes variants*. *International journal of food microbiology*, 2018. **283**: p. 14-21.
26. Hulsen, T., J. de Vlieg, and W. Alkema, *BioVenn-a web application for the comparison and visualization of biological lists using area-proportional Venn diagrams*. *BMC genomics*, 2008. **9**(1): p. 1-6.
27. Szklarczyk, D., et al., *STRING v11: protein-protein association networks with increased coverage, supporting functional discovery in genome-wide experimental datasets*. *Nucleic acids research*, 2019. **47**(D1): p. D607-D613.
28. Mellin, J., et al., *A riboswitch-regulated antisense RNA in Listeria monocytogenes*. *Proceedings of the National Academy of Sciences*, 2013. **110**(32): p. 13132-13137.
29. Salazar, J.K., et al., *PrfA-like transcription factor gene Imo0753 contributes to L-rhamnose utilization in Listeria monocytogenes strains associated with human food-borne infections*. *Applied and environmental microbiology*, 2013. **79**(18): p. 5584-5592.
30. Reniere, M.L., A.T. Whiteley, and D.A. Portnoy, *An in vivo selection identifies Listeria monocytogenes genes required to sense the intracellular environment and activate virulence factor expression*. *PLoS pathogens*, 2016. **12**(7): p. e1005741.

31. Raimann, E., et al., *The alternative sigma factor  $\sigma_L$  of *L. monocytogenes* promotes growth under diverse environmental stresses*. Foodborne pathogens and disease, 2009. **6**(5): p. 583-591.
32. Liu, Y., et al., *Home alone: elimination of all but one alternative sigma factor in *Listeria monocytogenes* allows prediction of new roles for  $\sigma_B$* . Frontiers in microbiology, 2017. **8**: p. 1910.
33. Lungu, B., S. Ricke, and M. Johnson, *Growth, survival, proliferation and pathogenesis of *Listeria monocytogenes* under low oxygen or anaerobic conditions: a review*. Anaerobe, 2009. **15**(1-2): p. 7-17.
34. Scotti, M., et al., *The PrfA virulence regulon*. Microbes and Infection, 2007. **9**(10): p. 1196-1207.
35. Stewart, A.M., et al., *Advances in the World of Bacterial Microcompartments*. Trends in Biochemical Sciences, 2021.
36. Kennedy, N.W., et al., *Bacterial microcompartments: tiny organelles with big potential*. Current Opinion in Microbiology, 2021. **63**: p. 36-42.
37. Liu, L.-N., et al., *Protein stoichiometry, structural plasticity and regulation of bacterial microcompartments*. Current Opinion in Microbiology, 2021. **63**: p. 133-141.
38. Lebreton, A. and P. Cossart, *RNA-and protein-mediated control of *Listeria monocytogenes* virulence gene expression*. RNA biology, 2017. **14**(5): p. 460-470.
39. de las Heras, A., et al., *Regulation of *Listeria* virulence: PrfA master and commander*. Current opinion in microbiology, 2011. **14**(2): p. 118-127.
40. Nadon, C.A., et al., *Sigma B contributes to PrfA-mediated virulence in *Listeria monocytogenes**. Infection and immunity, 2002. **70**(7): p. 3948-3952.
41. Pentecost, M., et al., **Listeria monocytogenes* invades the epithelial junctions at sites of cell extrusion*. PLoS pathogens, 2006. **2**(1): p. e3.
42. Drolia, R., et al., **Listeria* adhesion protein induces intestinal epithelial barrier dysfunction for bacterial translocation*. Cell host & microbe, 2018. **23**(4): p. 470-484. e7.
43. Chelakkot, C., J. Ghim, and S.H. Ryu, *Mechanisms regulating intestinal barrier integrity and its pathological implications*. Experimental & molecular medicine, 2018. **50**(8): p. 1-9.
44. Schardt, J., et al., *Comparison between *Listeria sensu stricto* and *Listeria sensu lato* strains identifies novel determinants involved in infection*. Scientific reports, 2017. **7**(1): p. 17821.



# 6

---

## **Impact of bacterial microcompartment-dependent ethanolamine and propanediol metabolism on *Listeria monocytogenes* interactions with Caco-2 cells**

Submitted for publication:

**Zeng, Z.**, Wijnands, L. M, Boeren, S, Smid, E. J., Notebaart, R. A., & Abee, T.  
Impact of bacterial microcompartment-dependent ethanolamine and  
propanediol metabolism on *Listeria monocytogenes* interactions with Caco-2  
cells

Preprint in bioRxiv: doi: <https://doi.org/10.1101/2021.08.26.457845>

## Abstract

Bacterial microcompartment (BMC) dependent ethanolamine (*eut*) and propanediol utilization (*pdu*) has recently been shown to stimulate anaerobic growth of *Listeria monocytogenes*. This metabolic repertoire conceivably contributes to the competitive fitness of *L. monocytogenes* in the human gastrointestinal (GI) tract, where these compounds become available following phospholipid degradation and mucus-derived rhamnose metabolism by commensal microbiota. Previous transcriptomics and mutant studies of *eut* and *pdu* *L. monocytogenes* suggested a possible role of *eut* and *pdu* BMC metabolism in transmission in foods and pathogenicity, but data on a potential role of *L. monocytogenes* interaction with human cells is currently absent. First, we ask which cellular systems are expressed in the activation of *eut* and *pdu* BMC metabolism and the extent to which these systems are conserved between the states. We find common and unique systems related to metabolic shifts, stress and virulence factors. Next, we hypothesize that these common and unique activated cellular systems contribute to a role in the interaction of *L. monocytogenes* interaction with human cells. We present evidence that metabolically primed *L. monocytogenes* with active *eut* and *pdu* BMCs, as confirmed by metabolic analysis, transmission electron microscopy and proteomics, show significantly enhanced translocation efficacy compared to non-induced cells in a trans-well assay using Caco-2 cells, while adhesion and invasion capacity was similar. Taken together, our results provide insights into the possible key cellular players that drive translocation efficacy upon *eut* and *pdu* BMC activation.

## 6.1 Introduction

*Listeria monocytogenes* is a food-borne pathogen responsible for a severe infection called listeriosis, which case-fatality can reach up to 30% in specific high-risk population groups such as the elderly, immunocompromised individuals, fetuses and newborns [1]. Acquisition of this infection is mainly caused by consumption of contaminated food (predominantly ready-to-eat food) [2]. *L. monocytogenes* is found ubiquitously in nature environments such as soil, silage, groundwater, sewage and vegetation [1, 3]. The food-borne pathogen can grow at low temperatures and is very robust to survive in environmental stresses, such as low pH and high salt concentrations [1, 2]. All of these features make the transmission and contamination of *L. monocytogenes* a severe concern for the food industry [2, 4, 5].

Upon ingestion of contaminated food by the host, *L. monocytogenes* needs to overcome acidic conditions in the stomach before reaching the GI tract and subsequent interaction with the mucus-coated epithelial barrier [1, 6]. *L. monocytogenes* has evolved a number of mechanisms to cross various host barriers and survive with its unique intracellular lifestyle [1, 6, 7]. Following the entry into epithelial cells mediated by Internalin A (InlA) and Internalin B (InlB), *L. monocytogenes* is internalized into the vacuole [1, 8]. Subsequently, *L. monocytogenes* produces listeriolysin O (LLO) [6] and two phospholipases, phospholipase A (PlcA) and phospholipase B (PlcB), for vacuolar rupture and escape, which together with Actin (ActA), involved in intracellular motility and cell to cell spread, mediate crucial steps in *L. monocytogenes* pathogenesis [1, 3, 9]. *L. monocytogenes* can survive and duplicate within the cytosol of the host cell and even induce changes in the morphology of host cell organelles, thereby altering their function to promote infection [1, 3]. Notably, alternative routes of entry and translocation have been described including possible roles for so-called Listeria Adhesion Protein (LAP, Imo1634) [10, 11], and listeriolysin/LLO [12]. The bacterium, first used as a model to study cell-mediated immunity, has emerged over the past 20 years as a paradigm in the study of bacterial regulation and host-pathogen interactions and, more recently, interactions with the gut microbiome. (Reviewed in [1, 3]).

Upon arriving in the host gut, *L. monocytogenes* needs to adapt to an environment already rich in commensal microbes and poor in available nutrients. Recent evidences suggest that *Salmonella* and other enteric bacteria conduct cellular organelles called bacterial microcompartments (BMCs) to facilitate their

pathogenesis in host gut [13-15]. BMCs are proteinaceous organelles that optimize the utilization of some specific substrates, such as 1,2-propanediol, ethanolamine, rhamnose and choline, with the encased enzymes producing toxic intermediate aldehydes, thereby preventing damage to cells' DNA and proteins [14, 16]. Substrates for BMC-dependent metabolism like ethanolamine and 1,2-propanediol can be produced in the GI tract by bacterial metabolism of (host) phospholipids and following mucus degradation and rhamnose metabolism, respectively [13, 17, 18]. Enteric pathogens gain a competitive advantage in the intestine by utilizing these substrates, an advantage enhanced by the host inflammatory response (Reviewed in [17]). Previous studies using cell lines and animal models and assessing performance of pathogen wild type and selected mutants in BMC dependent *eut* and *pdu*, pointed to a role in virulence of foodborne pathogens including *Salmonella enterica* Serovar Typhimurium, *Escherichia coli*, and *L. monocytogenes* [17, 19, 20].

The transcriptomics and mutant studies of *pdu* and *eut* *L. monocytogenes* suggested a possible role in transmission in foods and pathogenicity. Transcriptomics in *L. monocytogenes* showed the upregulated expression of *pdu* and *eut* for growth on vacuum-packed cold smoked salmon[21] and mouse infection model [22]. A deleted *pduD* mutant of the *L. monocytogenes* showed attenuated virulence and faster clearing of *L. monocytogenes* in the GI tract which indicate the importance of *pdu* for the fitness of *L. monocytogenes* during infection in the GI tract [22]. The importance of *eut* and *pdu* activation in stress survival and virulence of *L. monocytogenes* was highlighted in recent reviews [19]. Notably, we recently provided experimental evidence including metabolic and proteomic analysis, combined with transmission electron microscopy, for activation of *L. monocytogenes pdu* and *eut* BMCs and corresponding growth stimulation in anaerobic conditions [23, 24]. Combining our data with previous studies, we hypothesize that priming of *L. monocytogenes pdu* and *eut* BMCs in foods and/or the intestine, may affect interaction with the host epithelial barrier. In this study we quantified adhesion, invasion and translocation efficacy of *pdu-induced* and *eut-induced* *L. monocytogenes* compared to non-induced cells in Caco-2 cell assays. Correlations of virulence results with *L. monocytogenes* metabolic, stress and virulence factors, that show significant differential expression in *pdu-induced* and *eut-induced* cells versus non-induced cells, are discussed.

## 6.2 Materials and Methods

### 6.2.1 Strain and Culture Conditions

*L. monocytogenes* EGDe was used in this study. *L. monocytogenes* EGDe was anaerobically grown at 30°C in Luria Broth (LB) medium supplemented with 50mM 1,2-propanediol or 15mM ethanolamine (EA) as extra carbon source as described before [23, 24]. 20nM Cobalamine B12 was added to induce *pdu* and *eut* cluster as B12 controls riboswitch-based regulator of *pdu* and *eut* cluster [25, 26]. Anaerobic conditions were achieved by Anoxomat Anaerobic Culture System with the environment 10% CO<sub>2</sub>, 5% H<sub>2</sub>, 85% N<sub>2</sub>. LB with 50 mM 1,2-propanediol or 15 mM ethanolamine plus 20 nM vitamin B12 was defined as *pdu*-induced and *eut*-induced condition, respectively, while LB with 50 mM 1,2-propanediol or 15 mM ethanolamine conditions without B12 were defined as *pdu* and *eut* non-induced conditions. *L. monocytogenes* cells were harvested until the late-exponential growth phase (OD<sub>600</sub> = 0.4–0.5) for proteomics analysis and Caco-2 infection test.

### 6.2.2 Proteomics

*L. monocytogenes* EGDe cultures were anaerobically grown at 30°C in *pdu/eut* induced and in non-induced conditions. Samples were collected at 12 h of the inoculation and processed as described before [23, 24]. The mass spectrometry proteomics data have been deposited to the ProteomeXchange Consortium via the PRIDE [27] partner repository with the dataset identifier PXD027979 for *eut* induced and in non-induced conditions (retrieved from Zeng Z, et al, 2021 [24]) and identifier PXD028010 for *pdu* induced and in non-induced conditions.

### 6.2.3 Caco-2 adhesion, invasion and translocation

Cultures of Caco-2 cells (human intestinal epithelial cells, ATCC HTB-37), production of differentiated cells in 12-well plates were carried out as described before [25]. *L. monocytogenes* overnight grown cells used for adhesion, invasion and translocation were normalized to obtain cell concentrations of  $8.0 \pm 0.2$  log CFU/ml.

The adhesion, invasion and translocation experiments were performed as described in Chapter 5. Adhesion and invasion experiments were started by inoculation with 40 µl of late exponential phase cells of *pdu/eut* induced and non-induced *L. monocytogenes* EGDe resulting in an final inoculum of approximate 6.8 log CFU/well. Translocation was started by adding 20 µl of late exponential

cells of *pdu/eut* induced and non-induced *L. monocytogenes* EGDe into the inserts, resulting in an inoculum of approximately 6.5 log CFU/well.

### 6.2.4 BMC gene loci analysis

The Hidden Markov Models (HMMs) of two BMC shell protein domains listed as Pf00936 and Pf03319 were retrieved from the Pfam database to predict BMC shell proteins in *L. monocytogenes* EGDe as described before [23, 24]. Shell proteins were predicted by a HMM search using the HMMER package and a local protein database of *L. monocytogenes* EGDe genome [28]. All hits with an e-value less than or equal to 1e-05 that correspond to a genomic record from Genbank, RefSeq, EMBL, or DDBJ databases were accepted as BMC shell protein homologs. The annotation from InterPro are taken to fulfill the annotation of some unannotated proteins in BMC loci. Details in Supplementary Table1.

### 6.2.5 Venn analysis and STRING networks analysis

The protein IDs of significantly changed proteins from Supplementary Table 2 and 3 were uploaded to the BioVenn online server [29] taking the default setting to generate Venn diagrams. Overlapping proteins from the Venn diagram were transferred to the STRING online server[30] for multiple proteins analysis of functional interaction using sources such as co-expression, genomic neighbourhood and gene fusion.

### 6.2.6 Pathway visualization of protein expression via Pathview

The UniProt protein IDs from Supplementary Table 2 and Supplementary Table 3 were collected and retrieved to Entrez IDs. A list of Entrez IDs, protein expression indicated by LFQ intensity (Supplementary Table 4 and Supplementary Table 5) was mapped to the *L. monocytogenes* EGDe KEGG pathway database using the tool Pathview (R version 3.2.1) [31]. The box represent genes and the different color indicates level of expression with default setting.

Statistical analyses were performed in Prism 8.0.1 for Windows (GraphPad Software). As indicated in the figure legend, Statistical significances are shown in \*\*\*,  $P < 0.001$ ; \*,  $P < 0.05$ ; ns,  $P > 0.05$  with Holm-Sidak T-test.

## 6.3 Results

### 6.3.1 *pdu* and *eut* BMC gene loci organization and core metabolic reactions

The genes encoding conserved BMC shell proteins and core enzymes are located in respective *pdu* and *eut* clusters, and corresponding metabolic reactions in *L. monocytogenes* EGDe are shown in Figure 1. Briefly, the *pdu* cluster contains

seven BMC shell proteins PduTUABKJN and the *eut* cluster contains five BMC shell proteins EutLKMN and Lmo1185 (Figure 1A and Supplementary Table 1) as previously described [23, 24]. BMC substrates 1,2-propanediol and ethanolamine, enter respective BMCs and are degraded via their signature enzymes, propanediol dehydratase PduCDE and ethanolamine ammonia lyase EutBC, into corresponding aldehydes, followed by action of aldehyde dehydrogenase and phosphotransacylase to generate an acyl-phosphate leading to ATP generation in the oxidative branch, while in the reductive branch, an alcohol dehydrogenase is used for cofactor regeneration (Figure 1A and Supplementary Table 1).

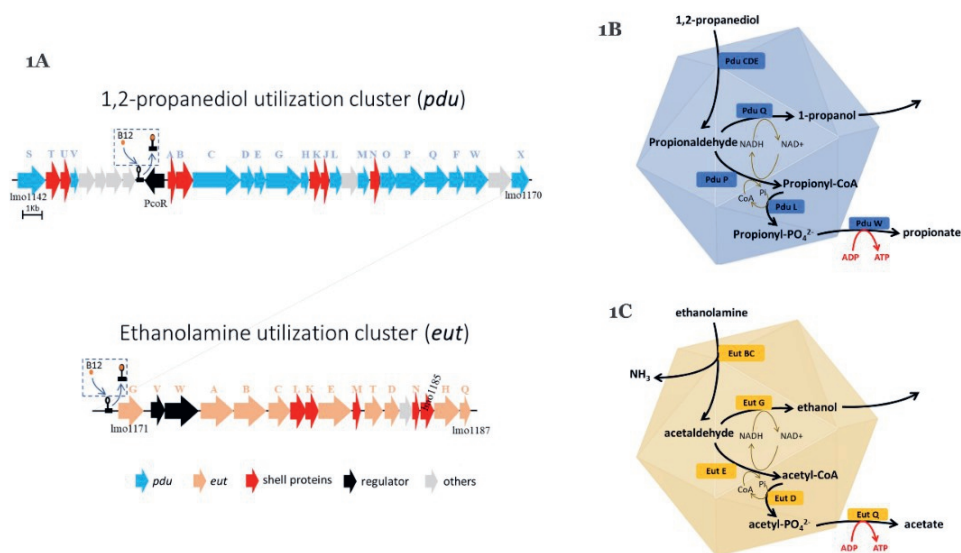


**Figure 1. Gene loci organization and core metabolic reactions of bacterial microcompartments (BMCs) in *Listeria monocytogenes* EGDe.**

**(A)** Gene loci organization of 1,2-propanediol utilization cluster (*pdu*) and ethanolamine utilization cluster (*eut*). Letters above the gene characters indicate the gene name for *pdu* and *eut* separately, see text for details. Vitamin B12-dependent riboswitches to activate *pdu* and *eut* are shown in box. Genes name and proteins ID are in Supplementary Table1. **(B)** *pdu* BMC for 1,2-propanediol utilization. PduCDE, diol dehydratase; PduQ, propanol dehydrogenase. PduP, CoA-dependent propionaldehyde dehydrogenase; PduL, Phosphotransacylase; PduW, propionate kinase. **(C)** *eut* BMC for ethanolamine utilization. EutBC, ethanolamine ammonia lyase; EutG, alcohol dehydrogenase; EutE, acetaldehyde dehydrogenase; EutD, phosphotransacylase; EutQ, acetate kinase.

### 6.3.2 Activation of *L. monocytogenes* BMC-dependent *pdu* and *eut*

Growth performance, metabolism, transmission electron microscopy and proteomics confirmed B12-dependent BMC activation in *L. monocytogenes pdu* and *eut*-induced cells (data not shown), in line with previous observations [23, 24].

Comparative proteomic profiling of *pdu* and *eut* BMC induced and respective non-induced cells enabled identification of differentially expressed proteins linked to metabolism, stress response and virulence.

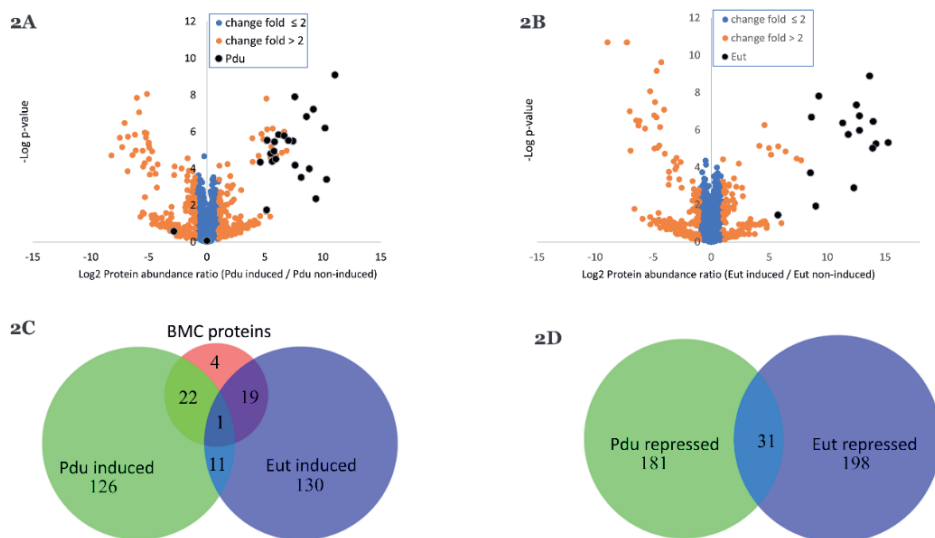


**Figure 2. Proteomics analysis of BMC induced and BMC non-induced *Listeria monocytogenes* EGDc.**

**(A)** Proteomic volcano plot of *pdu* induced cells (Pd + B12 added) compared to *pdu* noninduced cells (Pd added only), full list of proteins is in Supplementary Table 2. **(B)** Proteomic volcano plot of *eut* induced cells (EA + B12 added) compared to *eut* noninduced cells (EA added only), full list of proteins is in Supplementary Table 3, this dataset has been retrieved from Zeng Z, et al, 2021 [24]. In (A) and (B) proteins with the fold change  $\leq 2$  are in blue, proteins with the fold change  $> 2$  are in orange; Pdu or Eut proteins are indicated in dark blue. **(C)** Venn diagram of the overlapping *pdu* and *eut* induced proteins and **(D)** Venn diagram of the overlapping *pdu* and *eut* repressed proteins. Details of the proteins in (C) and (D) are in Supplementary Table 4 and Supplementary Table 5.

Analysis of the complete list of identified proteins and subsequent Student's t-test difference scores of *pdu* induced compared to *pdu* non-induced control cells (Supplementary Table 2), resulted in a selection of 1444 proteins shown in a volcano plot (Figure 2A), with 160 proteins upregulated more than two fold in *pdu* induced cells including 20 proteins encoded in the Pdu cluster, Pdu STUVABCDEGHKJMNOPQFX (Figure 2A blue dots, details in Supplementary Table 2). Comparing *eut* induced cells with *eut* non-induced cells, 161 proteins were upregulated more than 2 fold in *eut* induced cells with in total 1891 identified proteins (Figure 2B blue dots, details in Supplementary Table 3). All of 13 Eut proteins in the *eut* cluster were significant upregulated in *eut* induced cells

compared to *eut* non-induced cells. The increased expression of the *pdu* and *eut*-encoded proteins in the tested conditions is in line with previously published results [23, 24]. Analysis of the differentially expressed proteins in *pdu* induced and *eut* induced cells shows shared and specific responses that will be discussed in the next section.

### 6.3.3 Comparative proteome analysis of *pdu* and *eut* BMC induced cells shows overlap in induced and repressed proteins

Shared and specific responses of *pdu* and *eut* BMC induced cells and non-induced cells are shown in Figure 2C and 2D. Shared induced proteins are shown in Figure 2C, with 160 proteins upregulated more than two fold in *pdu* induced cells and 161 proteins upregulated more than two fold in *eut* induced cells, showing 12 common induced proteins. These 12 proteins include several metabolic enzymes, Acetate kinase 2 (Uniprot ID: Q8Y7V1, Gene ID: *Imo1168*), pyruvate - phosphate di-kinase (Q8Y633, *Imo1867*), putative pyruvate- phosphate di-kinase regulatory protein 2 (Q8Y634, *Imo1866*), putative transaldolase 2 (P66957, *Imo0343*), proteins Q8YA21 (*Imo0345*), Q8YA22 (*Imo0344*) and Q8YA23 (*Imo0343*), together function as transketolase (Supplementary Table 4 and Supplementary Figure 2). Additional shared induced proteins include *Imo2158* encoded protein CsbD (Q929L4), a SigB regulon member involved in osmotic and heat stress defense [32], *Imo0818* encoded protein Q8Y8S6, a putative Ca<sup>2+</sup> ATPase contributing to metal homeostasis [33, 34], and protein *Imo2323* encoded Gp43 (Q8Y4V7), a protein encoded in the bacteriophage A118 gene cluster [35]. In Figure 2D, 212 proteins downregulated more than two fold in *pdu* induced cells and 229 proteins downregulated more than two fold in *eut* induced cells, show 31 common repressed proteins including protein P0DJM0 Internalin A (*Imo0433*) and protein P34024 phospholipase A (*Imo0201*). The remaining set of proteins includes protein Q8Y7U1, zinc uptake regulator (ZurR), that is predicted to coordinate uptake of zinc from the external environment, and a variety of proteins with diverse putative functions and hypotheticals [36] (Supplementary Table 5 and Supplementary Figure 3). Shared and specific *pdu* and *eut* BMC induced and repressed proteins point to metabolic shifts, stress response and virulence, with selected aspects discussed in more detail in sections below.

### 6.3.4 Activation of *pdu* and *eut* BMC metabolism represses glycolysis in *L. monocytogenes*

To visualize the impact of BMC-associated shifts in metabolism, the identified proteins and expression levels (Figure 3A) are mapped to the glycolysis pathway in *L. monocytogenes* EGDe (Supplementary Table 2). Obviously, enzymes involved in the conversion of glyceraldehyde 3-phosphate to pyruvate (Figure 3A, pointed with red arrow) were mostly repressed in *pdu* induced cells compared with *pdu* non-induced cells. Activation of propanoate metabolism (Supplementary Figure 1) is in accordance with increased expression of *pdu* cluster and degradation of 1,2-propanediol to 1-propanol and propionate. Similar to *pdu* induced cells, *eut* induced cells also show a clear restraint of glycolysis (Figure 3B). The enzymes mediating conversion of glyceraldehyde 3-phosphate to pyruvate (Figure 3B, pointed with red arrow) are downregulated in *eut* induced cells compared with *eut* non-induced cells (Figure 3B). Activation of ethanolamine ammonia lyase EutBC in *eut* induced cells degrades ethanolamine into acetaldehyde inside BMCs, that is metabolized into end products acetate and ethanol.

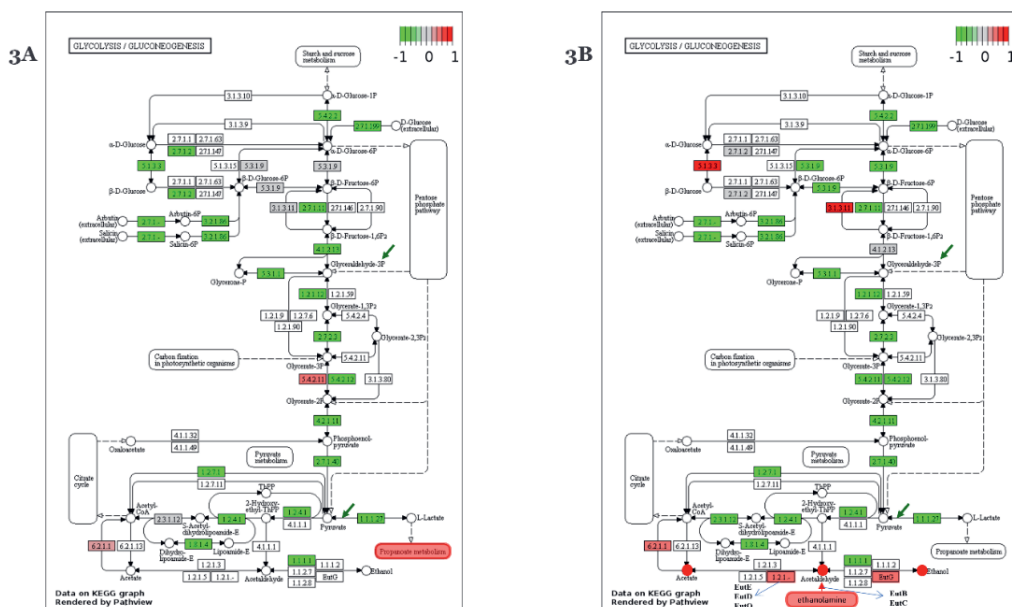


**Figure 3. Glycolysis metabolism visualized with proteomic profiling in BMC induced compared BMC non-induced *Listeria monocytogenes* EGDe.**

**(A)** Glycolysis metabolism visualized with proteomic profiling in *pdu* BMC induced compared with *pdu* BMC non-induced *Listeria monocytogenes* EGDe via Pathview. Details of upregulated propanoate metabolism are shown in Supplementary Figure 1. **(B)** Glycolysis metabolism visualized with proteomic profiling in *eut* BMC induced compared with *eut* BMC non-induced *Listeria monocytogenes* EGDe via Pathview. Upregulated ethanolamine metabolism is customized to be included. In (A) and (B), Colors

represent the change intensity of protein expression in BMC induced compared to BMC non-induced *Listeria monocytogenes* EGDe. Lines with arrow represent the metabolic reactions, circles represent metabolites while rectangles represent enzymes with EC number or gene name.

### 6.3.5 *pdu* and *eut* BMC induced stress and virulence associated proteins

Next to shared induced and repressed responses, *pdu* and *eut* specific responses were observed (Supplementary Table 4 for shared induced proteins of *pdu* and *eut* BMC cells, Supplementary Table 5 for shared repressed proteins of *pdu* and *eut* BMC cells). The *pdu* induced cells contained significant higher levels of CtsR, transcript regulator of heat shock stress proteins [37]; Stressosome component Blue-light photoreceptor Imo0799, involved in light and redox control of SigB expression [38]; Sigma B anti-anti-sigma factor, Serine-protein kinase RsbW, GbuB; Sigma B-dependent osmoprotectant betaine transporter [39]; Heat-inducible transcription repressor HrcA [40]; Imo1021, encoding histidine kinase of the LiaSR two-component system (Imo1021 and Imo1022) that plays a role in resistance to antimicrobials [41]; Protease HtpX homolog, involved in membrane/cell envelope stress response [42]; LexA repressor, involved in DNA damage repair, and DPS, DNA protection during starvation protein [42]. In addition, a number of bacteriophage A118 encoded proteins are higher expressed in *pdu* induced cells, conceivably due to activation of gene expression following DNA damage [35]. No significant higher expression of PrfA or sigmaB controlled virulence factors is observed in *pdu* induced cells.

However, both *pdu* induced and non-induced control cells contain internalin B, Q8Y7G3 encoded putative membrane bound zinc metalloprotease (Lmo1318) involved in release of Q8Y436 peptide pheromone encoding lipoprotein A, PplA (Lmo2637), that conceivably supports activation of PrfA [43, 44], and Listeria Adhesion Protein (LAP, Imo1634), involved in host cell invasion [45], with the latter protein significantly higher expressed in *pdu* non-induced cells.

The *eut* induced cells express higher levels of Phosphate import ATP-binding proteins PstB 1 and PstB 2 [3]; Phosphate-specific transport system accessory protein PhoU (Imo2494) [3]; Manganese transport system membrane protein MntC [3]; OpuCD protein, involved in sigB dependent uptake of osmoprotectant carnitine [46]; Fosfomycin resistance protein FosX, involved in resistance to antimicrobials [47]; ATP-dependent protease ClpE, involved in protein quality control [48]; and RecS protein, ATP-dependent DNA helicase [3]; RecG, and Endonuclease III, all three involved in DNA damage repair [3]. In addition, a number of bacteriophage A118 encoded proteins are higher expressed in *eut*

induced cells, conceivably due to activation of gene expression following DNA damage. Concerning activation of virulence factors, the *eut* induced cells showed significantly higher levels of Listeriolysin regulatory protein PrfA and P13128 encoded Listeriolysin O (*hly*). The *eut* induced and control cells also express Q8Y7G3 encoded zinc metalloprotease (*lmo1318*) and Q8Y436 encoded PplA (*lmo2637*), and LAP (*lmo1634*) as described above, and in addition produce P33379 encoded Actin assembly-inducing protein ActA, P34024 encoded 1-phosphatidylinositol phosphodiesterase PlcA; and P33378 encoded Phospholipase B, PlcB, although the latter is significantly higher expressed in *eut* non-induced cells.

These results point to shared stress defense responses in *pdu* and *eut* induced cells including uptake of osmoprotectants (Gbu and OpuC transport proteins), activation of chaperons for quality control (ClpP and ClpE), and enzymes involved in DNA damage repair (LexA and RecS, RecG, recombinase), with a more extensive response in *eut* cells at the level of regulators and proteins involved in transport of phosphate and transition metals such as manganese (Mn), calcium (Ca), Iron/heme, and cadmium (Cd). Notably, only *eut* induced cells showed significant higher expression of virulence factors PrfA and listeriolysin O (LLO, Hly). Subsequent *in vitro* virulence assays with *pdu* and *eut* BMC primed cells are discussed in the next section.

### **6.3.6 Impact of *pdu* and *eut* BMC activation on Caco-2 cell adhesion, invasion and translocation**

*In vitro* adhesion, invasion and translocation assays with Caco-2 cells were performed using primed *pdu* and *eut* BMC cells and non-induced control cells (Figure 4). As shown in Figure 4A, the ability to translocate Caco-2 cells monolayers in a trans-well system, is significantly higher for *pdu* induced *L. monocytogenes* cells compared to *pdu* non-induced cells (0.5 log of CFU/well improvement), while no significant differences were observed for adhesion and invasion efficacy (Figure 4A). Similar to *pdu* induced cells, *eut* induced cells show significantly higher translocation efficacy (0.6 log of CFU/well increase), while no significant improvement of adhesion and invasion capacity is observed (Figure 4B). Our results provide evidence for enhanced Caco-2 cell monolayer translocation efficacy of *pdu* and *eut* BMC primed cells compared to non-induced control cells.

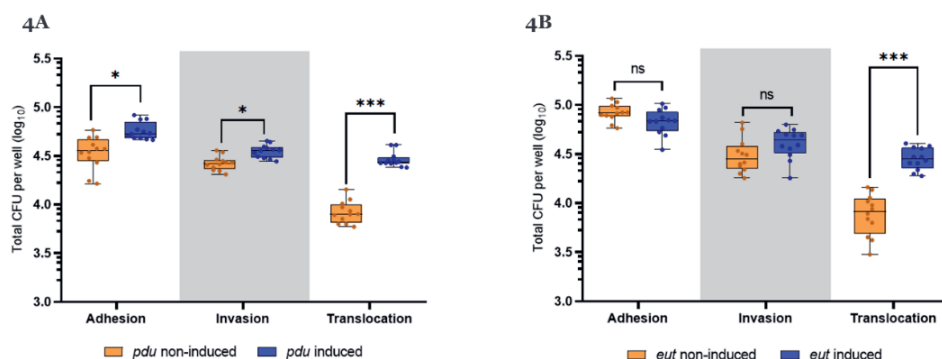


**Figure 4. Caco-2 cell assays with BMC induced and BMC non-induced *Listeria monocytogenes* EGDe.**

**(A)** is for *pdu* BMC induced and *pdu* BMC non-induced cells. **(B)** is for *eut* BMC induced and *eut* BMC non-induced cells. X axis show three groups of columns which are adhesion assay, invasion assay and translocation assay. Y axis is the total CFU per well in log<sub>10</sub> after the assays while initial inputs for adhesion and invasion are approximate 6.8 log<sub>10</sub> CFU/well and the initial inputs for translocation are approximate 6.5 log<sub>10</sub> CFU/well. Statistical significance are indicated (\*\*\* means  $P \leq 0.001$ ; \* means  $P \leq 0.05$ ; ns means  $P > 0.05$  by Holm-Sidak T-test)

## 6.4 Discussion

Bacterial microcompartments (BMCs) are proteinaceous organelles that optimize specific metabolic pathways referred to as metabolosomes involving transient production of toxic volatile metabolites such as aldehydes [17, 49]. We recently provided evidence for a role of BMC-dependent utilization of propanediol (*pdu*) and ethanolamine (*eut*) in *L. monocytogenes* resulting in growth stimulation under anaerobic conditions [23, 24]. In this study we performed a comparative proteomics analysis of *pdu* and *eut* BMC primed *L. monocytogenes* cells and non-induced control cells, to identify specific and shared responses focusing on metabolic, stress response and virulence parameters, and to correlate these to adhesion, invasion and translocation efficacy in caco-2 assays. Expression analysis of the complete lists of identified proteins showed 160 of 1444 proteins upregulated more than two fold in *pdu* induced cells including 20 proteins encoded in the *pdu* cluster, and 161 of 1891 identified proteins in *eut* induced cells, including all 13 proteins encoded in the *eut* cluster. Creation of BMCs with key metabolic turnover steps of *pdu* and *eut* enzymes encapsulated, occurs in a stepwise manner [13, 14], thereby creating a protection against the respective toxic intermediates propionaldehyde and acetaldehyde. Proteomics analysis of shared and specific *pdu* BMC and *eut* BMC responses indicates metabolic shifts

and activation of stress defense proteins, conceivably as a response to aldehyde-induced redox stress before BMC production is completed. Shared main themes in *pdu* and *eut* BMC primed cells include expression of transcriptional regulators and/or respective regulon members of ZurR, a transcriptional repressor of zinc (Zn) transporters [50]; SigB, CtsR, and HrcA, transcriptional activators/repressors involved in coordinating cellular stress defense including uptake systems for osmoprotectants and synthesis of a range of chaperons contributing to maintenance of protein quality and functionality [51], and RecA/LexA, regulators of *L. monocytogenes* SOS response including enzymes involved in DNA damage repair [52, 53]. The latter stress phenomenon is conceivable linked to expression activation of *L. monocytogenes* EGDe prophage A118 [35], with highest relative abundance of A118 GP43 protein (Lmo2323) in both *pdu* and *eut* primed cells. Expression of additional phage proteins was noted, but holin and lysin proteins were not detected (Supplementary Table 1), in line with the observation that *pdu* and *eut* induced cells reach high cell counts during anaerobic growth indicating no or very limited lysis of cells (data not show, [23, 24]). Notably, previous studies showed that the A118 gene cluster is inserted in the *L. monocytogenes* EGDe *comK* gene, which renders it inactive in cells grown at 30°C, while excision of the cluster leading to expression of the *L. monocytogenes* *comK* gene and corresponding competence genes at 37°C, contributes to intracellular growth following bacterial escape from macrophage phagosomes [54, 55]. Notably, activation of SOS response is another facet of *pdu* and *eut* BMC priming that can affect efficacy and timing of the BMC encased pathways with concomitant aldehyde production, an aspect that has been largely ignored up to now including possible activation of lytic or lysogenic phages, that may affect competitive fitness of producer cells.

Analysis of specific responses shows a higher expression in *eut* induced cells of proteins involved in transport of phosphate and transition metals such as manganese (Mn), calcium (Ca), Iron/heme, and cadmium (Cd). This might point to increased acetaldehyde-induced oxidative stress affecting transition metal homeostasis leading to activation of DNA-binding metal-responsive transcription factors, metal-acquisition or secretion, metal-detoxification and metal-storage systems, some of which represent key *L. monocytogenes* virulence determinants [56]. In addition, BMC-dependent metabolism may be affected by availability of compounds including  $\text{Fe}^{3+}$  that can act as extracellular electron acceptors allowing a shift towards the ATP generating oxidative branch resulting in higher

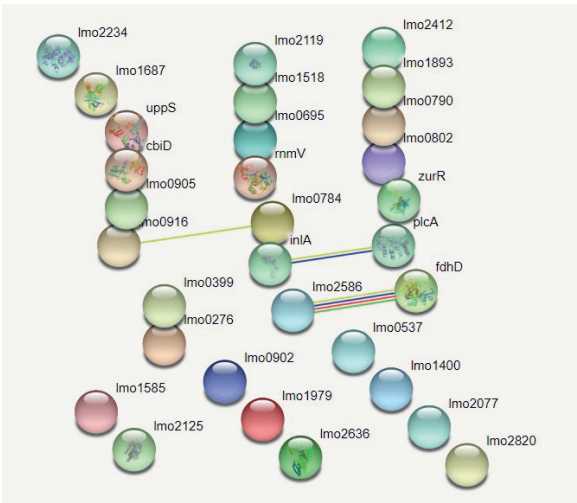
cell numbers, as we previously showed for *eut* BMC primed *L. monocytogenes* cells anaerobically grown in defined medium without and with added  $\text{Fe}^{3+}$  [24]. A physiological link between the large number of differentially expressed metal transport systems and significant higher expression of PrfA and listeriolysin (LLO) in BMC *eut* induced cells, may be explained by recent findings reported by Gaballa et al. (2021) [57], about the role of divalent metal ion scavengers Chelex and activated charcoal in the induction of PrfA regulon expression in complex medium. This study showed that the expression of the PrfA-regulated gene *hly*, which encodes listeriolysin O (LLO), is induced 5- and 8-fold in *L. monocytogenes* cells grown in Chelex-treated BHI (Ch-BHI) and in the presence of activated charcoal (AC-BHI), respectively, relative to cells grown in BHI medium. Additional experiments provide evidence that intracellular metal depletion contributes to activation of PrfA and that genes in its regulon are differentially expressed with LLO showing highest modulation. The authors suggest that metal ion abundance plays a role in modulating expression of PrfA-regulated virulence genes in *L. monocytogenes* [49]. Additional experiments are required to confirm the hypothesis that increased expression of metal transporters in *eut* BMC induced cells signifies a homeostatic response to metal depletion, concomitant with increased expression of PrfA and LLO in *eut* BMC induced cells.

Comparative analysis of Caco-2 cell monolayer adhesion, invasion and translocation, showed similar adhesion and invasion efficacy of *pdu* and *eut* non-induced compared to *pdu* and *eut* BMC primed cells, with the latter BMC activated cells showing significantly higher translocation efficacy. Comparative analysis of virulence factor expression, shows specific activation of PrfA and listeriolysin LLO in *eut* induced cells but not in *pdu* induced cells, while no increased expression of *L. monocytogenes* virulence factors Internalin A (InlA), Internalin B (InlB), Phospholipase A and B (PlcA, PlcB), and Actin (ActA), is observed. Analysis of the complete list of proteins in *eut* non-induced and *eut* induced cells (Supplementary Table 3), showed the presence of Actin assembly-inducing protein ActA, 1-phosphatidylinositol phosphodiesterase PlcA, and Phospholipase B, PlcB, in both types of cells. It is therefore possible that enhanced translocation of *eut* induced cells is not solely linked to activation of PrfA and more importantly to LLO activity, but is supported by activity of PlcA, PlcB and ActA. To confirm roles of LLO, that has been shown to mediate alternative routes of invasion and translocation and possible contributions by other virulence factors in enhanced translocation efficacy of *eut* induced cells [12, 43, 44, 58], further

studies are required. Obviously, the same holds for identification of factors that contribute to enhanced Caco-2 cell monolayer translocation of pdu induced cells. Notably, analysis of the complete list of proteins present in pdu non-induced and induced cells (Supplementary Table 2), shows the presence of internalin B, next to putative membrane bound zinc metalloprotease (*Imo1318*) involved in release of peptide pheromone encoding lipoprotein A, PplA (*Imo2637*), that conceivably supports activation of PrfA [43, 57], and Aldehyde-alcohol dehydrogenase/Listeria Adhesion Protein (LAP, *Imo1634*) . Notably, with the exception of InlB, these proteins are also present in eut non induced and induced cells, with LAP, previously shown to provide an alternative route of entry and translocation [10, 11]. Whether these virulence factors in combination with other cellular and physiological features of pdu BMC primed cells contribute to enhanced translocation efficacy remains to be confirmed.

In conclusion, we have provided evidence for shared and specific metabolic, stress resistance and virulence associated responses at proteome level in pdu and eut BMC primed *L. monocytogenes* cells. Shared stress responses include activation of stress defense proteins and SOS DNA damage repair enzymes [52, 53], conceivably linked to activation and selected expression of previously described lysogenic prophage A118 gene cluster. Most *L. monocytogenes* strains carry prophages in their genome, including A118 and A118-like prophages such as in *L. monocytogenes* 10403S [35, 54, 55]. Using *L. monocytogenes* 10403S as a model, Pasechnik et al. [55] recently provided evidence for temperature-dependent activation of lysogeny as a bacteria-phage adaptive response in the mammalian environment, with temperature as a crucial factor controlling excision of the phage gene cluster and expression of selected phage proteins that excluded the holin and lysin proteins, associated with bacterial host cell lysis. Since in our studies we used *L. monocytogenes* EGDe grown at 30°C, mimicking priming of pdu and eut BMCs before entering the human host for example during transmission in foods, future experiments should also include cells primed at 37°C to mimic activation of BMCs inside the mammalian host. Inclusion of multiple *L. monocytogenes* strains, without and with lysogenic prophages, will further add to our understanding of mechanisms underlying production and functionality of pdu and eut BMCs in *L. monocytogenes* competitive fitness and survival during transmission in the food chain and inside the mammalian host.





**Supplementary figure 3. STRING protein-protein interactions of common repressed 31 proteins in pdu-induced cells and eut-induced cells.**

**Supplementary Table 1.** Gene annotation, proteins IDs and protein domain annotation of pdu and eut cluster (Part of this table is also shown in chapter 2 and chapter 4)

UniProt Protein ID	Gene tag	Gene Name	Pfam Domain
Q8Y7X7	Imo1142	pduS	NADH-ubiquinone oxidoreductase 51kDa subunit, FMN-binding domain (IPR011538)
Q8Y7X6	Imo1143	pduT	Microcompartment protein, bacteria (IPR000249)
Q8Y7X5	Imo1144	pduU	Microcompartment protein, bacteria (IPR000249)
Q8Y7X4	Imo1145	pduV	P-loop containing nucleoside triphosphate hydrolase (IPR027417)
Q8Y7X3	Imo1146		
Q8Y7X2	Imo1147	copB	Cobinamide kinase/cobinamide phosphate guanylttransferase (IPR003203)
Q8Y7X1	Imo1148	copD	Adenosylcobinamide-GDP ribazoletransferase (IPR003805)
Q8Y7X0	Imo1149	copE	Histidine phosphatase superfamily, clade-1 (IPR013078)
	rli39		Riboswitch
Q8Y7W9	Imo1150	pocR	Transcription regulator HTH, AraC- type (IPR020449)
Q8Y7W8	Imo1151	pduA	Domain Microcompartment protein, bacteria (IPR000249)
Q8Y7W7	Imo1152	pduB	Polyhedral organelle shell protein, EutL/PduB type (IPR009193)
Q8Y7W6	Imo1153	pduC	Homologous superfamily: Diol/glycerol dehydratase, large subunit superfamily (IPR036999)
Q8Y7W5	Imo1154	pduD	Propanediol/glycerol dehydratase, medium subunit (IPR025541)
Q8Y7W4	Imo1155	pduE	Propanediol/glycerol dehydratase, small subunit (IPR003207)

Q8Y7W3	lmo1156	pduG	Diol dehydratase-reactivating factor alpha subunit (IPR009191)
Q8Y7W2	lmo1157	pduH	Diol/glycerol dehydratase/dehydratase reactivating factor (IPR003208)
Q8Y7W1	lmo1158	pduK	Homologous superfamily CcmK-like superfamily (IPR037233)
Q8Y7W0	lmo1159	pduJ	Domain Microcompartment protein, bacteria (IPR000249)
Q8Y7V9	lmo1160	pduL	Phosphate propanoyltransferase (IPR008300)
Q8Y7V8	lmo1161	eutJ	Ethanolamine utilisation EutJ (IPR013366)
Q8Y7V7	lmo1162	pduM	Microcompartment protein PduM (IPR030992)
Q8Y7V6	lmo1163	pduN	Ethanolamine utilization protein EutN/carboxysome structural protein Ccml (IPR004992)
Q8Y7V5	lmo1164	pduO	Adenosylcobalamin biosynthesis, ATP:cob(I)alamin adenosyltransferase, bifunctional PduO (IPR009221)
Q8Y7V4	lmo1165	pduP	Acetaldehyde/propionaldehyde dehydrogenase, EutE/PduP-related (IPR012408)
Q8Y7V3	lmo1166	pduQ	Iron-type alcohol dehydrogenase-like (IPR039697)
Q8Y7V2	lmo1167	pduF	Major intrinsic protein (IPR000425)
Q8Y7V1	lmo1168	pduW	Acetate/propionate kinase (IPR004372)
Q8Y7V0	lmo1169	cobD	L-threonine-O-3-phosphate decarboxylase (IPR005860)
Q8Y7U9	lmo1170	pduX	Propanediol utilisation/coumermycin biosynthesis, PduX-related (IPR012363)
Q8Y7U8	lmo1171	eutG	Iron-type alcohol dehydrogenase-like (IPR039697)
	rli55		Riboswitch
Q92CN5	lmo1172	eutV	Signal transduction response regulator, antiterminator (IPR008327)
Q8Y7U7	lmo1173	eutW	Signal transduction histidine kinase, subgroup 2 (IPR011495)
Q8Y7U6	lmo1174	eutA	Ethanolamine utilisation EutA (IPR009377)
Q8Y7U5	lmo1175	eutB	Ethanolamine ammonia lyase large subunit (IPR010628)
Q8Y7U4	lmo1176	eutC	Ethanolamine ammonia-lyase light chain (IPR009246)
Q8Y7U3	lmo1177	eutL	Polyhedral organelle shell protein, EutL/PduB type (IPR009193)
Q8Y7U2	lmo1178	eutK	CcmK-like superfamily (IPR037233)
Q8Y7U1	lmo1179	eutE	Acetaldehyde dehydrogenase, acetylating (IPR013357)
Q92CM7	lmo1180	eutM	CcmK-like superfamily (IPR037233)
Q8Y7U0	lmo1181	eutT	Adenosylcobalamin biosynthesis, ATP:cob(I)alamin adenosyltransferase, EutT-type (IPR009194)
Q8Y7T9	lmo1182	eutD	Phosphate propanoyltransferase (IPR008300)
Q8Y7T8	lmo1183	lmo1183	Ethanolamine utilization, putative (IPR013372)
Q8Y7T7	lmo1184	eutN	Ethanolamine utilization protein EutN/carboxysome structural protein Ccml (IPR004992)
Q8Y7T6	lmo1185	lmo1185	Polyhedral organelle shell protein PduT (IPR011238)
Q8Y7T5	lmo1186	eutH	Ethanolamine utilisation protein EutH (IPR007441)
Q8Y7T4	lmo1187	eutQ	Ethanolamine utilisation EutQ (IPR010424)

**Supplementary Table 2.** Protein profiling of *pdu* induced cells compared to *pdu* non-induced cells (Only list the top 100 rows, the full table with 1447 rows was online in bellowing link; different proteomic measurements with Chapter 2)

log2 Protein abundance ratio( Pdu induced vs Pdu non-induced)	"-Log Student's T-test p-value pdu-induced VS pdu non-induced"			Protein IDs	Protein Annotation	Gene Name
X Axis	Y Axis	change fold $\leq 2$	change fold $> 2$	Pdu		
11.06324211	9.080948755		9.080948755	9.080948755	Q8Y7V9	Phosphate propanoyltransferase Lmo1160
10.33398997	3.393886569		3.393886569	3.393886569	Q8Y7V4	Lmo1165 protein Lmo1165
10.19764503	6.190728658		6.190728658	6.190728658	Q8Y7W7	Lmo1152 protein Lmo1152
9.425119084	2.330679955		2.330679955	2.330679955	Q8Y7V1	Acetate kinase 2 ackA2
9.202652626	7.212200842		7.212200842	7.212200842	Q8Y7V8	Lmo1161 protein Lmo1161
8.850425464	3.976485032		3.976485032	3.976485032	Q8Y7V5	Hyghly similar to Salmonella enterica PduO protein Lmo1164
8.59951531	6.806926793		6.806926793	6.806926793	Q8Y7V6	Lmo1163 protein Lmo1163
8.156435169	3.502941835		3.502941835	3.502941835	Q8Y7W5	Lmo1154 protein Lmo1154
7.623686366	4.162811139		4.162811139	4.162811139	Q8Y7W3	Lmo1156 protein Lmo1156
7.595473936	7.889585055		7.889585055	7.889585055	Q8Y7V7	Lmo1162 protein Lmo1162
7.439521481	5.484115077		5.484115077	5.484115077	Q8Y7X4	Lmo1145 protein Lmo1145
7.065108025	5.505353808		5.505353808	5.505353808	Q8Y7W2	Lmo1157 protein Lmo1157
6.872819236	4.963562713		4.963562713		Q7AP89	Transcriptional regulator CtsR Lmo0229
6.678028226	5.773755411		5.773755411	5.773755411	Q8Y7W4	Lmo1155 protein Lmo1155
6.668858342	5.998110642		5.998110642		Q8YA21	Lmo0345 protein Lmo0345
6.468043836	4.862366876		4.862366876		P66957	Probable transaldolase 2 tal2
6.207201356	5.824745116		5.824745116	5.824745116	Q8Y7X3	Lmo1146 protein Lmo1146
5.977201306	4.722831364		4.722831364		Q8Y943	Lmo0698 protein Lmo0698
5.971846794	4.501645641		4.501645641	4.501645641	Q8Y7W0	Lmo1159 protein Lmo1159
5.854532253	5.435522356		5.435522356	5.435522356	Q8Y7W8	Lmo1151 protein Lmo1151
5.808192841	4.918850722		4.918850722	4.918850722	Q8Y7W1	Lmo1158 protein Lmo1158
5.672013693	6.176363574		6.176363574		Q8YAJ4	Lmo0131 protein Lmo0131
5.652220322	4.368794807		4.368794807	4.368794807	Q8Y7X7	Lmo1142 protein Lmo1142
5.573026249	5.174158402		5.174158402		Q8Y7X2	Lmo1147 protein Lmo1147
5.521721465	4.783392614		4.783392614	4.783392614	Q8Y7W6	Lmo1153 protein Lmo1153
5.481716016	4.59680233		4.59680233		Q8Y7S3	CbiG protein cbiG
5.449628548	1.387929308		1.387929308		Q8Y8G1	DNA protection during starvation protein dps
5.211522545	5.516140179		5.516140179	5.516140179	Q8Y7X6	Lmo1143 protein Lmo1143
5.187865225	6.122915497		6.122915497		Q8Y439	Energy-coupling factor transporter transmembrane protein EcfT ecfT
5.176065341	1.730390912		1.730390912	1.730390912	Q8Y7V3	Lmo1166 protein Lmo1166
5.137191409	7.803467842		7.803467842		Q8Y694	UPF0122 protein Lmo1802
5.124334457	5.465656295		5.465656295		Q8YA19	Lmo0347 protein Lmo0347
5.117233301	1.633278842		1.633278842		Q8YA23	Transketolase Lmo0342
5.009205862	5.57462096		5.57462096		Q8Y844	Transport permease protein Lmo1074

4.859977039	5.592883754	5.592883754		Q8Y8W0	Lmo0782 protein	lmo0782
4.712651679	5.879879258	5.879879258		Q8Y5V4	Segregation and condensation protein A	scpA
4.620386811	4.330151115	4.330151115	4.330151115	Q8Y7X5	Lmo1144 protein	lmo1144
4.604713473	1.404824926	1.404824926		Q8Y4F1	Lmo2493 protein	lmo2493
4.439539918	4.69360523	4.69360523		Q8YA22	Lmo0344 protein	lmo0344
4.432411833	1.013110682	1.013110682		Q7AP75	GbuB protein	gbuB
4.165140877	1.142471087	1.142471087		Q8Y4V7	Gp43 [Bacteriophage A118]	lmo2323
4.119187965	0.934961697	0.934961697		Q8Y4U0	Pseudouridine synthase	lmo2342
4.111262063	1.002658912	1.002658912		Q8Y7X9	Lmo1140 protein	lmo1140
4.10975355	1.175948535	1.175948535		Q8YA64	Lmo0295 protein	lmo0295
3.983963452	0.913293982	0.913293982		Q8Y6E0	Lmo1747 protein	lmo1747
3.936522091	4.354924343	4.354924343		Q8YA18	Lmo0348 protein	lmo0348
3.932810735	5.649734847	5.649734847		Q8Y8S6	Lmo0818 protein	lmo0818
3.834202927	1.04519552	1.04519552		P58724	Blue-light photoreceptor	lmo0799
3.721125109	1.093160603	1.093160603		Q8Y8D1	Lmo0977 protein	lmo0977
3.717183014	0.934467405	0.934467405		Q8Y929	Lmo0713 protein	lmo0713
3.582779551	0.866248595	0.866248595		Q8Y481	Lmo2574 protein	lmo2574
3.518968412	0.73909898	0.73909898		Q8Y4V8	Gp44 [Bacteriophage A118]	lmo2322
3.463308105	0.936456841	0.936456841		Q8YAD9	Lmo0192 protein	lmo0192
3.28009416	0.851808849	0.851808849		Q7AP49	Peptidoglycan lytic protein P45	spl
3.220950595	0.774048974	0.774048974		Q8Y6J3	Deoxyuridine 5-triphosphate nucleotidohydrolase	lmo1691
3.157413491	0.866772952	0.866772952		Q8Y8V5	Lmo0787 protein	lmo0787
3.130340499	0.887778689	0.887778689		Q927T1	Lmo2562 protein	lmo2562
3.12064472	0.782343848	0.782343848		Q8Y507	Lmo2271 protein	lmo2271
2.988969993	0.741676686	0.741676686		Q8Y4Z0	Protein gp14 [Bacteriophage A118]	lmo2289
2.960130292	0.776522813	0.776522813		Q8YAG2	Initiation-control protein YabA	lmo0164
2.952744012	2.827191836	2.827191836		Q929L4	UPF0337 protein	lmo2158
2.92468576	0.628297302	0.628297302		Q8Y7R3	Cobyrinic acid synthase	cobQ
2.922581655	1.034923587	1.034923587		Q8Y4W3	Lmo2316 protein	lmo2316
2.912195244	1.391922695	1.391922695		Q8Y4V4	Lmo2326 protein	lmo2326
2.889536384	0.503652763	0.503652763		Q92AT9	Lmo1719 protein	lmo1719
2.871511307	0.5924775	0.5924775		Q8Y4V2	Lmo2328 protein	lmo2328
2.818026913	0.511131812	0.511131812		Q8Y4Z2	Putative tape-measure [Bacteriophage A118]	lmo2287
2.788295409	0.644962346	0.644962346		Q8YAK4	Lmo0120 protein	lmo0120
2.779238518	1.152468799	1.152468799		Q8Y7S1	Lmo1200 protein	lmo1200
2.751166538	0.921185756	0.921185756		Q8Y5I9	Lmo2073 protein	lmo2073
2.736273066	0.934135686	0.934135686		Q8YAB0	Mini-ribonuclease 3	mrnC
2.688476884	0.933523563	0.933523563		Q8Y7Y7	Lmo1132 protein	lmo1132
2.604273087	0.934965768	0.934965768		Q8Y4G2	Phosphatidylglycerol-prolipoprotein diacylglycerol transferase	lgt

2.599206339	0.668123461	0.668123461	Q8Y624	Formate--tetrahydrofolate ligase	fhs
2.563473516	0.593298326	0.593298326	Q8Y4W2	Lmo2317 protein	lmo2317
2.476898971	0.842802864	0.842802864	Q8Y7S6	CbiE protein	cbiE
2.451147578	0.443784827	0.443784827	Q927H3	Lmo2666 protein	lmo2666
2.45111537	0.647939972	0.647939972	Q8Y5F6	Lmo2108 protein	lmo2108
2.431866902	1.295101481	1.295101481	Q8Y5M9	Lmo2028 protein	lmo2028
2.416438031	0.552269598	0.552269598	Q8YAJ9	Lmo0125 protein	lmo0125
2.402747885	0.933798558	0.933798558	Q8YAQ0	Lmo0067 protein	lmo0067
2.386919314	0.585946543	0.585946543	Q8Y7E9	Lmo1333 protein	lmo1333
2.34791602	0.574348777	0.574348777	Q8Y5W4	Lmo1941 protein	lmo1941
2.342721494	0.934340756	0.934340756	Q8Y7S9	Cobalamin biosynthesis protein CbiD	cobD
2.316008074	2.315128266	2.315128266	Q8Y7S2	CbiH protein	cbiH
2.23863351	3.101679301	3.101679301	Q8Y633	Pyruvate, phosphate dikinase	lmo1867
2.234480213	0.427243412	0.427243412	Q8Y4Z8	Protein gp22 [Bacteriophage A118]	lmo2281
2.219666998	0.574892952	0.574892952	Q8Y4L9	Lmo2418 protein	lmo2418
2.215704839	0.427243412	0.427243412	Q8Y3U2	NAD-dependent protein deacetylase	cobB
2.149999213	0.427243412	0.427243412	Q7AP62	Ribosomal RNA small subunit methyltransferase E	lmo1470
2.134084049	2.169470403	2.169470403	P66503	30S ribosomal protein S20	rpsT
2.127096414	0.371013845	0.371013845	Q8Y4W7	Lmo2312 protein	lmo2312
2.109329531	0.482277612	0.482277612	Q8Y682	Lmo1817 protein	lmo1817
2.085911926	0.674522762	0.674522762	Q8Y3Z4	Permease IIC component	lmo2684
2.074572464	2.925987567	2.925987567	P0DJP1	30S ribosomal protein S21	rpsU
2.030848794	3.580487382	3.580487382	Q8Y634	Putative pyruvate, phosphate dikinase regulatory protein 2	lmo1866
1.971729518	0.514132649	0.514132649	Q8Y726	Lmo1498 protein	lmo1498

**Supplementary Table 3.** Protein profiling of *eut* induced cells compared to *eut* non-induced cells  
Same as Chapter 4 Supplementary Table 2.

**Supplementary Table 4.** Shared induced proteins of *pdu* and *eut* BMC cells.

Significant Upregulated (X>1, changing fold>2)					
Pdu		Eut		Pdu-Eut overlap	
Protein IDs	Gene Name	Protein IDs	Gene Name	Protein IDs	Gene Name
Q8Y7V9	lmo1160	Q8Y7U1	lmo1179	Q8YA21	lmo0345
Q8Y7V4	lmo1165	Q8Y7U3	lmo1177	P66957	tal2

Q8Y7W7	lmo1152	Q92CM7	lmo1180	Q8YA23	lmo0342
Q8Y7V1	pduW	Q8Y7T4	lmo1187	Q8YA22	lmo0344
Q8Y7V8	lmo1161	Q8Y7T9	pduL	Q8Y4V7	lmo2323
Q8Y7V5	lmo1164	Q8Y7U6	eutA	Q8Y8S6	lmo0818
Q8Y7V6	lmo1163	Q8Y7U4	eutC	Q929L4	lmo2158
Q8Y7W5	lmo1154	Q8Y7U2	lmo1178	Q8Y633	lmo1867
Q8Y7W3	lmo1156	Q8Y7U8	pduQ	Q8Y634	lmo1866
Q8Y7V7	lmo1162	Q8Y7U5	eutB	Q8Y9F1	lmo0578
Q8Y7X4	lmo1145	Q8Y7T8	lmo1183	Q8YAN7	lmo0080
Q8Y7W2	lmo1157	Q8Y7T7	lmo1184	Q8Y7V1	pduW
Q7AP89	lmo0229	Q8Y7U0	lmo1181		
Q8Y7W4	lmo1155	Q8Y7T6	lmo1185		
Q8YA21	lmo0345	Q8Y7T5	lmo1186		
P66957	tal2	Q8Y4E7	lmo2499		
Q8Y7X3	lmo1146	P63363	pstB1		
Q8Y943	lmo0698	Q8Y4E9	pstB2		
Q8Y7W0	lmo1159	Q8Y845	lmo1073		
Q8Y7W8	lmo1151	Q8Y7U7	lmo1173		
Q8Y7W1	lmo1158	Q8Y912	lmo0730		
Q8YAJ4	lmo0131	Q8Y9F1	lmo0578		
Q8Y7X7	lmo1142	Q8Y466	lmo2589		
Q8Y7X2	lmo1147	Q8Y6P7	lmo1637		
Q8Y7W6	lmo1153	Q8Y8G5	lmo0939		
Q8Y7S3	cbiG	Q8Y9V8	lmo0412		
Q8Y8G1	dps	Q8Y6H6	lmo1708		
Q8Y7X6	lmo1143	Q8Y6J1	recX		
Q8Y439	ecfT	Q7AP68	opuCD		
Q8Y7V3	lmo1166	Q8Y4G7	lmo2476		
Q8Y694	lmo1802	Q8Y646	lmo1854		
Q8YA19	lmo0347	Q8Y4V7	lmo2323		
Q8YA23	lmo0342	Q8Y9G7	hisE		
Q8Y844	lmo1074	Q8Y3P5	lmo2789		
Q8Y8W0	lmo0782	Q8Y737	lmo1485		
Q8Y5V4	scpA	Q8Y7B1	lmo1375		
Q8Y7X5	lmo1144	Q8Y8H6	lmo0927		
Q8Y4F1	lmo2493	Q8Y608	nth		
Q8YA22	lmo0344	Q8Y523	lmo2254		
Q7AP75	gbuB	Q8Y6Z0	lmo1541		
Q8Y4V7	lmo2323	Q8Y9P7	lmo0477		
Q8Y4U0	lmo2342	Q8Y7E6	lmo1337		
Q8Y7X9	lmo1140	Q8Y686	recG		
Q8YA64	lmo0295	Q8Y6Z1	lmo1539		
Q8Y6E0	lmo1747	Q8Y3K8	lmo2827		
Q8YA18	lmo0348	Q8Y8T4	lmo0810		
Q8Y8S6	lmo0818	Q8Y968	lmo0665		
P58724	lmo0799	Q8Y552	lmo2224		
Q8Y8D1	lmo0977	Q8Y6A1	lmo1794		

## Chapter 6

Q8Y929	lmo0713	Q8Y8F9	lmo0945
Q8Y481	lmo2574	Q8Y913	lmo0729
Q8Y4V8	lmo2322	Q8Y6J8	lmo1686
Q8YAD9	lmo0192	Q8Y9G1	hisD
Q7AP49	spl	Q8Y5I3	lmo2079
Q8Y6J3	lmo1691	Q8Y5Q2	lmo2004
Q8Y8V5	lmo0787	Q8Y8J2	lmo0909
Q927T1	lmo2562	Q8Y5R1	deoC
Q8Y507	lmo2271	Q8Y5S0	ilvC
Q8Y4Z0	lmo2289	Q8Y8S3	lmo0821
Q8YAG2	lmo0164	P58414	cadA
Q929L4	lmo2158	Q8Y8R8	lmo0826
Q8Y7R3	cobQ	Q8Y9T6	lmo0437
Q8Y4W3	lmo2316	Q8Y5J9	lmo2061
Q8Y4V4	lmo2326	Q8Y9R1	lmo0462
Q92AT9	lmo1719	Q8Y5K4	lmo2056
Q8Y4V2	lmo2328	Q8Y878	lmo1039
Q8Y4Z2	lmo2287	Q8Y5N5	lmo2022
Q8YAK4	lmo0120	Q8Y4C9	lmo2521
Q8Y7S1	lmo1200	Q8Y585	hbp1
Q8Y5I9	lmo2073	Q8Y4F0	lmo2494
Q8YAB0	mrnC	Q8Y9V0	lmo0420
Q8Y7Y7	lmo1132	Q926Q9	lmo2850
Q8Y4G2	lgt	Q8Y7K8	lmo1269
Q8Y624	fhs	Q8Y8K1	lmo0900
Q8Y4W2	lmo2317	Q8Y4M1	lmo2416
Q8Y7S6	cbiE	P22262	prfA
Q927H3	lmo2666	Q92CN5	lmo1172
Q8Y5F6	lmo2108	Q8Y735	nadD
Q8Y5M9	lmo2028	Q8Y6Q7	trpA
Q8YAJ9	lmo0125	Q8Y984	lmo0649
Q8YAQ0	lmo0067	Q8Y652	mntC
Q8Y7E9	lmo1333	Q8Y8C7	lmo0981
Q8Y5W4	lmo1941	Q02551	flaA
Q8Y7S9	cobD	Q8Y4H7	lmo2464
Q8Y7S2	cbiH	Q8Y8S8	lmo0816
Q8Y633	lmo1867	Q8Y7M1	lmo1253
Q8Y4Z8	lmo2281	Q8Y6A5	lmo1790
Q8Y4L9	lmo2418	Q8Y5Z0	lmo1913
Q8Y3U2	cobB	Q8Y3Y9	lmo2690
Q7AP62	lmo1470	Q8Y7V2	glpF
P66503	rpsT	Q8Y5K9	lmo2050
Q8Y4W7	lmo2312	Q8Y9G8	lmo0560
Q8Y682	lmo1817	Q8Y5Z9	birA
Q8Y3Z4	lmo2684	Q8Y635	lmo1865
P0DJP1	rpsU	Q8Y9V7	lmo0413
Q8Y634	lmo1866	P60073	lmo0496

Q8Y726	lmo1498	Q8Y5H4	lmo2088
Q8Y5N6	lmo2021	Q8Y7V0	cobD
Q8Y4G3	ppaX	Q8Y662	pyrB
Q8Y9F1	lmo0578	Q8Y8S6	lmo0818
Q8Y6Q1	trpE	Q8Y5T1	lmo1974
Q8Y4Y3	lmo2296	Q8Y7Z8	lmo1121
Q8Y8E1	htpX	Q8YAH3	lmo0153
P58641	pyrF	Q8Y6I2	fosX
Q8Y8L5	lmo0882	Q8Y3T1	lmo2750
Q8Y3Y2	lmo2697	Q8Y882	lmo1035
Q8Y3Y3	lmo2696	P58702	lmo0128
Q8Y4X6	lmo2303	Q8Y8Y7	lmo0755
Q8YAC3	cysK	Q8Y7H1	lmo1309
Q8Y7R9	cbiK	Q8Y3U3	lmo2738
Q8Y7S8	lmo1193	Q8Y6N3	lmo1651
Q8Y985	lmo0648	Q8Y5W3	recS
Q8Y947	lmo0693	Q8Y8F6	lmo0948
Q8YAV3	lmo0010	Q8Y8A6	lmo1004
Q8Y6I9	mprF	Q8Y7K7	lmo1270
Q8Y8I0	coaA	Q8YA31	lmo0334
Q8Y401	lmo2677	Q8YA73	lmo0286
Q8Y3W6	lmo2713	Q8Y622	lmo1880
Q8Y605	lmo1898	Q8Y926	lmo0716
Q8Y6V4	lmo1577	Q8YA27	lmo0338
Q8Y9N2	lmo0493	Q8Y7M2	lmo1252
Q8Y5H2	argG	Q8Y4F8	lmo2486
Q8Y7S0	lmo1201	Q8Y633	lmo1867
Q8Y4I9	lmo2658	Q8Y3T0	lmo2751
Q8Y980	lmo0653	Q8Y6G0	lmo1727
Q8YAD8	lmo0193	Q8Y3S9	lmo2752
Q8Y5U5	fhuC	Q8Y4Q2	lmo2382
Q8Y9I1	lmo0547	Q8YA22	lmo0344
P67288	lmo1306	Q8YA23	lmo0342
Q8Y4S2	lmo2360	Q8Y8Q6	lmo0840
Q8Y424	lmo2651	Q8Y5C4	lmo2141
Q8Y4U8	int	Q8Y8J0	lmo0911
Q8Y4Y2	lmo2297	Q8Y536	lmo2240
Q8Y893	lmo1021	Q8YAH6	lmo0150
Q8Y7S4	cbiF	Q8YAN7	lmo0080
Q8YAN7	lmo0080	Q7AP58	lmo1788
Q8YAE5	lmo0185	P66957	tal2
Q8Y4V6	lmo2324	Q8Y4K5	lmo2433
Q8Y4W4	lmo2315	Q8Y6L3	lmo1671
Q8Y6X8	hemL1	Q8Y8B1	clpE
Q8Y4W1	lmo2318	Q8Y922	lmo0720
Q8Y672	gmk	Q92E21	lmo0636
P0A491	rpmI	Q8Y697	lmo1799

P0DJM4	hrcA	Q8Y667	pyrD
Q8Y427	lmo2648	Q8Y9K5	lmo0522
Q8Y8K6	rsbW	Q8Y634	lmo1866
Q8YAB2	cysE	Q8Y9D2	lmo0600
Q92AU7	lmo1710	Q8Y842	lmo1076
Q8Y4W5	lmo2314	Q8YAR7	lmo0047
Q8Y4W0	lmo2319	Q8Y6B3	lmo1778
Q8Y871	moaC	Q8Y5B9	lmo2146
Q8Y7H7	lexA	Q8YA21	lmo0345
Q8Y7N4	lmo1240	Q8Y8Q5	lmo0841
Q8Y647	lmo1853	Q92C55	glnR
Q8Y854	lmo1064	Q8Y9S1	lmo0452
Q9RQI6	clpP	P13128	hly
Q8Y8N7	lmo0859	Q8Y4F7	lmo2487
Q8Y6J0	lmo1694	Q929L4	lmo2158
Q8Y8W9	lmo0773	Q8Y7V1	pduW
Q8Y4C2	atpC	Q8Y3K6	lmo2829
		Q8Y3M0	lmo2815

**Supplementary Table 5.** Shared repressed proteins of *pdu* and *eut* BMC cells.**Significant Downregulated ( $X > 1$ , , changing fold > 2)**

Pdu		Eut		Pdu-Eut overlap	
Protein IDs	Gene Name	Protein IDs	Gene Name	Protein IDs	Gene Name
Q8Y9T2	lmo0441	Q8Y458	rplM	Q8Y5I5	lmo2077
Q8Y5I5	lmo2077	Q8Y997	lmo0635	P34024	plcA
Q8Y6H7	lmo1707	Q8Y9Z6	lmo0371	Q8Y7G6	uppS
Q8Y6A2	rimM	Q8YAE3	rnmV	P0DJM0	inlA
Q8YAJ6	lmo0129	Q8Y5A8	lmo2160	Q8Y7S7	cbiD
Q8Y470	lmo2585	Q8Y7W8	lmo1151	Q8Y469	lmo2586
Q8Y843	tagH	Q8Y6J7	lmo1687	Q8Y542	lmo2234
Q8Y5X1	folE	Q8Y4Z0	lmo2289	Q92EN6	lmo0399
Q8Y5Z3	lmo1910	Q8Y4Y3	lmo2296	P0A3E6	zurR
Q8Y8J8	lmo0903	Q8Y3Z8	kdpC	Q8Y609	lmo1893
Q8Y829	tagD	Q8YA01	lmo0366	Q8Y556	lmo1979
Q8Y875	lmo1042	Q8Y6Q1	trpE	Q8Y471	fdhD
Q8Y687	fapR	Q8Y411	lmo2667	Q8Y437	lmo2636
P34024	plcA	Q8Y5Y6	pflA	Q7AP60	lmo1518
Q8Y5V6	lmo1949	Q8Y424	lmo2651	Q8Y6J7	lmo1687
P66054	rplK	Q8Y611	recU	Q8Y3L5	lmo2820
Q8Y494	rpoE	Q8Y3L5	lmo2820	Q8YA83	lmo0276
P67234	lmo1796	P66219	rpmG1	Q8Y8J6	lmo0905
Q8Y6Z5	lmo1535	Q8Y894	lmo1020	Q8Y8V8	lmo0784
Q8Y9D5	lmo0595	Q8Y9U4	lmo0426	Q8YAE3	rnmV

Q8Y6X1	dnaI	P58676	ispH	Q8Y792	lmo1400
Q8Y6S7	lmo1606	Q8Y3I7	rhaA	Q8Y9J1	lmo0537
Q8Y3X2	lmo2707	Q8Y6K4	lmo1680	Q8Y8I6	lmo0916
Q9ZIM1	lmo0216	Q8Y469	lmo2586	Q929P4	lmo2125
Q8Y650	lmo1850	Q8Y3U1	lmo2740	Q8Y4M5	lmo2412
Q8Y7E8	lmo1334	Q8Y9L1	lmo0516	Q8Y5E5	lmo2119
Q8Y5M5	ftsZ	Q8YAS4	lmo0039	Q8Y8J9	lmo0902
Q8Y7G6	uppS	Q8Y768	lmo1433	Q8Y6U6	lmo1585
Q8Y8L0	lmo0888	Q8Y417	lmo2660	Q8Y8V2	lmo0790
Q8Y715	lmo1511	Q8Y5G8	lmo2095	Q8Y8U1	lmo0802
Q8Y4K2	lmo2436	Q8Y5F7	lmo2107	Q8Y945	lmo0695
P60357	lmo1503	Q8Y6W2	lmo1569		
Q8Y6L8	lmo1666	Q8YAI5	lmo0141		
Q8Y786	pflB	Q8Y3I8	rhaD		
Q8Y5R1	deoC	Q8Y6C4	purN		
Q8Y4A2	murA2	Q8Y620	rpsN		
Q8YAC4	hslO	Q8Y6I0	lmo1704		
Q8YAG4	lmo0162	P67288	lmo1306		
Q8Y3L2	lmo2823	Q8Y8L9	lmo0878		
Q8Y5C6	lmo2139	Q8Y429	lmo2646		
P0DJM0	inlA	Q8Y935	lmo0706		
Q8Y4B2	glyA	Q8Y413	lmo2664		
Q8Y7S7	cbiD	Q8Y3J3	lmo2842		
Q8Y3R7	lmo2766	Q7AP49	spl		
Q8YAB9	lmo0227	Q8Y537	lmo2239		
Q8Y870	moaA	Q8Y3J1	lmo2844		
Q926Y4	lmo2763	Q8Y8S0	lmo0824		
Q8Y4S9	lmo2353	Q8Y9G9	lmo0559		
Q8Y469	lmo2586	Q8Y9U2	lmo0428		
P0A4J8	rsbV	Q927H3	lmo2666		
Q8Y4A6	thrB	Q8Y4Z4	lmo2285		
Q8Y4V3	lmo2327	Q8Y4J7	lmo2441		
Q8Y5U6	lmo1959	Q8Y3Y8	lmo2691		
Q8YAG1	lmo0165	Q8Y542	lmo2234		
Q8Y5Y7	lmo1916	Q8YAJ8	lmo0126		
Q8YAD2	lmo0212	Q8Y5G6	lmo2097		
Q8Y7C4	xseA	Q8Y914	lmo0728		
Q8Y4U1	lmo2341	Q8Y6E0	lmo1747		
P25145	lmo0432	Q8YA83	lmo0276		
Q8Y542	lmo2234	P66860	smpB		
Q92EN6	lmo0399	Q8Y8T2	lmo0812		
Q8Y5M6	lmo2031	Q8Y4N8	lmo2397		
Q8Y8N8	lmo0858	Q8Y4N5	lmo2400		
Q8Y428	lmo2647	Q8Y4Y2	lmo2297		
P0A3E6	zurR	Q8Y3P6	bvrA		
Q8YAC5	coaX	Q8Y936	flgK		
Q8Y7F8	lmo1323	Q8Y7R2	lmo1209		

Q8Y8A4	lmo1006	Q8Y414	lmo2663
Q8Y644	deoD	Q8Y5K7	coaD
Q8Y5A5	lmo2163	Q8Y5Q8	lmo1998
Q8YA75	metN1	P34024	plcA
Q8Y6A3	trmD	Q8Y947	lmo0693
Q8Y609	lmo1893	Q8Y8V8	lmo0784
Q8Y8R9	lmo0825	Q8Y9B2	lmo0620
Q8Y5D2	lmo2133	Q8Y6Q2	trpG
Q8Y5U0	lmo1965	Q8Y8L1	lmo0887
Q8Y7C2	lmo1363	Q8YA74	lmo0285
Q8Y5S6	lmo1979	Q92EN6	lmo0399
Q8Y833	lmo1085	Q8Y717	recD2
Q8Y8Y2	lmo0760	Q8Y643	lmo1857
Q8Y9J8	lmo0529	Q8Y8V2	lmo0790
Q8Y7J3	plsY	Q8Y5I5	lmo2077
Q8Y471	fdhD	Q8Y8G4	lmo0940
Q8Y4H9	lmo2462	Q8Y476	lmo2579
Q8Y512	lmo2266	Q9XDA6	zurA
Q8Y437	lmo2636	Q8Y426	lmo2649
Q8Y408	lmo2670	Q8Y6F8	lmo1729
Q8Y8W5	lmo0777	Q8Y5X2	lmo1932
Q8Y466	lmo2589	Q8Y9P5	lmo0479
Q8Y4Q2	lmo2382	P0A3E6	zurR
Q8Y6K1	lmo1683	Q92AN7	purS
Q8Y5G5	lmo2098	Q8Y612	lmo1890
Q8Y4K7	lmo2431	Q8Y5E3	lmo2121
Q8Y617	xpt	Q8Y499	lmo2555
Q8Y8G9	lmo0935	Q7AP97	lmo0114
Q8Y9G8	lmo0560	Q8Y3I1	rnplA
Q92CZ9	lmo1023	Q8Y9X4	lmo0394
Q8Y8X8	lmo0764	Q8Y3U2	cobB
Q8Y7F3	truB	Q8Y6X6	lmo1555
Q8Y8K1	lmo0900	Q8Y9X0	lmo0398
Q8Y6P1	lmo1643	Q8Y3Z9	lmo2679
Q8Y9C5	lmo0607	Q8Y9F6	lmo0572
Q8Y3N5	lmo2800	Q8Y5E5	lmo2119
Q7AP60	lmo1518	Q8Y4C8	lmo2522
Q8Y4P9	lmo2386	Q8Y6R7	lmo1616
Q8Y684	lmo1813	Q8Y5I6	lmo2076
Q8Y6J7	lmo1687	Q8Y8J9	lmo0902
Q8Y5K6	lmo2053	Q8Y432	lmo2642
Q8YA57	lmo0304	Q8Y3W6	lmo2713
Q8Y769	lmo1432	Q7AP60	lmo1518
Q8Y410	lmo2668	Q8Y609	lmo1893
Q8Y3L5	lmo2820	Q8Y4H0	whiA
Q8YA83	lmo0276	Q8Y5S2	ilvD
Q8YAT2	lmo0031	Q8YAP0	lmo0077

Q8Y9F3	lmo0575	Q8Y6U6	lmo1585
Q8Y713	lmo1513	Q8Y5R7	leuC
Q8Y9Y2	iolC	Q8Y887	lmo1030
Q8Y3Z6	kdpA	Q8Y3K5	lmo2830
Q8Y9P1	lmo0483	Q92AP5	lmo1763
Q8Y8U5	lmo0797	Q8Y8V5	lmo0787
Q8Y560	lmo2216	Q8Y8P7	lmo0849
Q8Y680	rsgA2	Q8Y4R6	lmo2368
Q8YAE7	lmo0183	Q8Y5I8	lmo2074
Q8Y506	lmo2272	Q8Y6H0	lmo1716
Q8Y3U4	lmo2737	Q8Y879	lmo1038
Q8Y725	mltG	Q8Y5K1	lmo2059
Q8Y5D9	lmo2126	Q8Y7G6	uppS
Q8Y6W9	nrdR	Q8Y4W9	lmo2310
Q8Y3V7	lmo2724	Q8Y752	recO
Q8Y5U9	fur	Q8Y3N9	lmo2796
Q7AP52	lmo2196	Q8Y939	lmo0702
Q8Y3S6	lmo2755	Q8Y746	lmo1466
Q8YA41	lmo0323	Q929P4	lmo2125
Q8Y906	lmo0736	Q8Y471	fdhD
Q8YA95	lmo0260	Q8Y4X5	lmo2304
Q9S389	dltC	Q8Y7E5	lmo1338
Q9RGW9	mecA	Q8Y7I3	miaA
Q8Y828	lmo1090	Q8YA77	lmo0282
Q8Y7Q5	lmo1217	Q8YA39	lmo0325
Q8Y9H2	lmo0556	Q8Y6Q4	trpC
Q8Y4L6	lmo2421	Q8Y7T0	cbiA
Q8Y8J6	lmo0905	Q8Y3P0	lmo2795
Q8Y8V1	lmo0791	Q8Y6W8	coaE
Q8Y668	pyrE	Q8Y7R8	cbiL
Q8Y8V8	lmo0784	P33378	plcB
Q8Y608	nth	Q8YAR0	lmo0056
Q8Y6F0	lmo1737	Q8Y6M3	lmo1661
Q8Y5U3	lmo1962	Q8YAB5	ispD
Q8Y9P7	lmo0477	Q8Y8F2	lmo0952
Q8Y6N8	sbcD	Q8Y773	mntH
Q8Y8P8	lmo0848	Q8Y7S2	cbiH
Q8YAE3	rnmV	Q8Y9B6	lmo0616
Q8Y4K8	lmo2429	Q8Y8J6	lmo0905
Q8Y792	lmo1400	Q8Y9T3	lmo0440
Q8Y627	lmo1873	Q8Y4X8	lmo2301
Q8Y9J1	lmo0537	Q8Y7S4	cbiF
Q8Y8I6	lmo0916	Q8Y7R3	cobQ
P67356	lmo1058	Q8Y8F1	lmo0953
Q8Y728	lmo1495	Q92DY0	lmo0673
Q8Y3Z0	lmo2689	Q8Y7I6	lmo1291
Q8Y941	lmo0700	Q8Y9P0	lmo0485

Q929P4	lmo2125	Q8Y4J9	lmo2439
Q8Y4B1	lmo2540	Q8Y7S6	cbiE
Q8Y457	truA	Q8Y3J2	lmo2843
Q8YAV4	lmo0009	Q8YAL2	lmo0106
Q8Y4M5	lmo2412	Q8YAK7	lmo0111
Q8Y5E5	lmo2119	Q8Y8I6	lmo0916
Q8Y503	lmo2275	Q8Y5H8	lmo2084
Q8Y823	lmo1095	Q8Y5Z8	cca
Q8Y4W8	lmo2311	Q928S1	lmo2361
Q8Y8L4	lmo0883	Q8YA45	lmo0317
Q8Y9T7	lmo0436	Q8Y891	lmo1024
Q8Y9S1	lmo0452	Q8YA85	lmo0274
Q8Y9A4	lmo0628	Q93RD9	dtd
Q8YAR4	lmo0051	Q8Y9J1	lmo0537
Q8YAV2	lmo0011	Q8Y4D3	lmo2517
Q8Y8J9	lmo0902	Q8Y3R4	lmo2769
Q8Y8G2	lmo0942	Q8Y569	lmo2207
Q8Y723	lmo1502	Q8YAE9	lmo0181
Q8Y5X4	ndk	Q8Y6F1	lmo1736
Q8Y4I9	lmo2450	Q8YA46	thiM
Q8YA86	lmo0273	Q8Y7S8	lmo1193
Q8Y3T9	lmo2742	Q8Y7A6	lmo1382
Q8Y9L4	lmo0513	Q7AP56	lmo2164
Q8Y6U6	lmo1585	Q8Y9F8	hisJ
Q8Y4E3	cls	Q8Y7S5	lmo1196
Q8Y4D4	lmo2516	Q8Y719	lmo1507
Q8Y8C6	lmo0982	Q8YA37	lmo0327
Q8Y9V0	lmo0420	P60415	lmo2054
Q8YA24	lmo0341	Q8Y6B5	lmo1776
Q8Y4V1	lmo2329	Q8Y8F3	lmo0951
Q8Y3Y0	lmo2699	Q8Y945	lmo0695
Q8Y922	lmo0720	Q8Y996	lmo0637
Q8Y8V2	lmo0790	Q8Y7S0	lmo1201
Q8Y6Z8	ruvB	Q8Y5R2	lmo1994
Q8Y9X1	lmo0397	Q8Y5S6	lmo1979
Q8Y5F3	lmo2111	Q8Y4H6	lmo2465
Q8Y3X7	recR	Q8Y472	lmo2583
Q8Y4N3	lmo2403	Q8Y8I5	lmo0917
P13128	hly	Q8Y792	lmo1400
Q8Y669	lmo1830	Q7AP96	lmaD
P47762	dnaG	Q8Y5R8	leuB
Q8YAJ2	lmo0133	Q8Y5S3	lmo1982
Q8Y4Q0	lmo2385	Q8Y4M5	lmo2412
Q8Y648	lmo1852	Q8Y9Y4	iolA
Q8Y878	lmo1039	Q8Y7S7	cbiD
Q8Y9W2	lmo0407	Q8Y7S9	cobD
Q8Y8U1	lmo0802	Q8Y5U5	fhuC

Q8Y945	lmo0695	Q8Y415	lmo2662
Q8Y4E5	phoP	Q8Y7Y7	lmo1132
Q8Y3Y7	lmo2692	Q8YAF1	lmo0178
Q8Y7C8	lmo1356	Q8Y8I8	lmo0914
		Q8Y5M3	divlB
		Q8Y5H1	argH
		Q8Y5K5	lmo2055
		Q8Y6F9	lmo1728
		Q8Y5Y2	lmo1921
		Q8Y7S1	lmo1200
		Q8Y3K3	lmo2832
		Q8Y4P7	lmo2388
		P0DJM0	inlA
		Q8Y416	lmo2661
		Q8Y8U1	lmo0802
		Q8Y7R9	cbiK
		Q8Y3T5	lmo2746
		Q8Y7R4	lmo1207
		Q8Y437	lmo2636
		Q8Y7S3	cbiG
		Q8Y7Q7	lmo1215

The table lists UniProt protein ID, X value representing Log2 Protein abundance ratio (eut induced/non-induced in LB), Y value representing -Log10 p-value (induced condition /non-induced condition), NCBI protein Annotation and NCBI Gene ID.

6

**The Supplementary Materials for this chapter can also be found online at:**

<https://www.biorxiv.org/content/10.1101/2021.08.26.457845v1.supplementary-material>

## 6.6. References

1. Radoshevich, L. and P. Cossart, *Listeria monocytogenes: towards a complete picture of its physiology and pathogenesis*. Nature Reviews Microbiology, 2018. **16**(1): p. 32.
2. Gandhi, M. and M.L. Chikindas, *Listeria: a foodborne pathogen that knows how to survive*. International journal of food microbiology, 2007. **113**(1): p. 1-15.

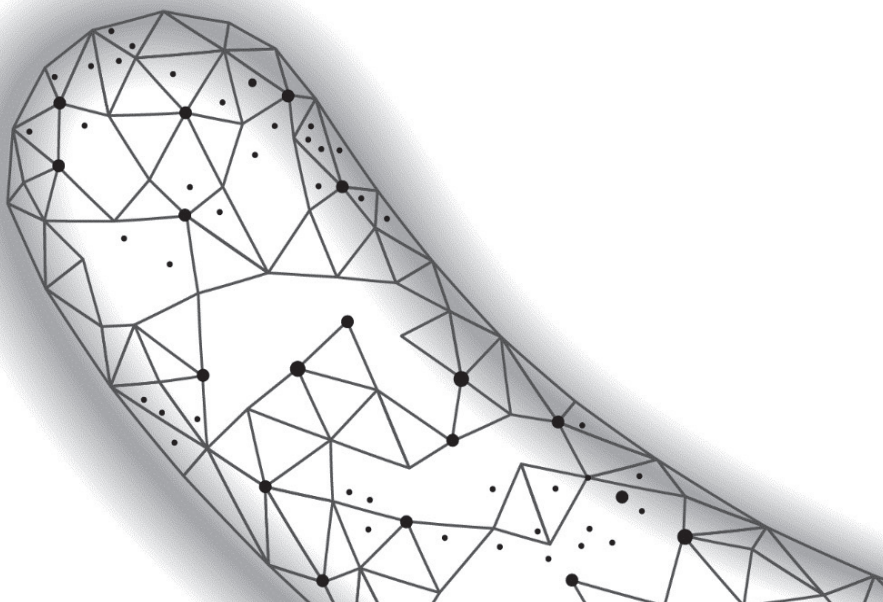
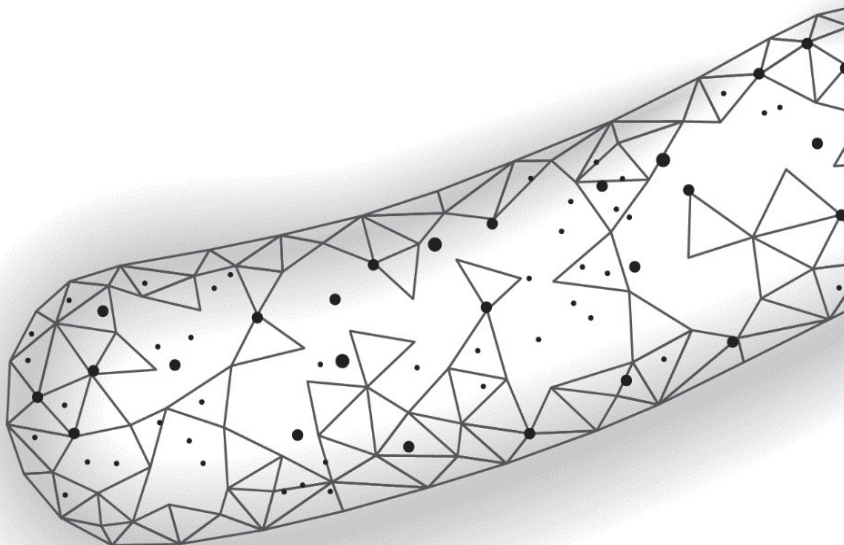
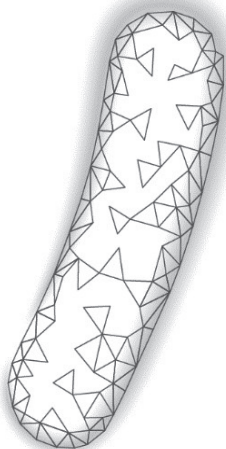
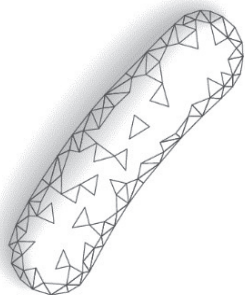
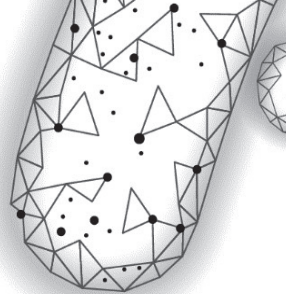
3. Freitag, N.E., G.C. Port, and M.D. Miner, *Listeria monocytogenes—from saprophyte to intracellular pathogen*. Nature Reviews Microbiology, 2009. **7**(9): p. 623-628.
4. Desai, A.N., et al., *Changing epidemiology of Listeria monocytogenes outbreaks, sporadic cases, and recalls globally: A review of ProMED reports from 1996 to 2018*. International Journal of Infectious Diseases, 2019. **84**: p. 48-53.
5. Tasara, T. and R. Stephan, *Cold stress tolerance of Listeria monocytogenes: a review of molecular adaptive mechanisms and food safety implications*. Journal of food protection, 2006. **69**(6): p. 1473-1484.
6. Portnoy, D.A., V. Auerbuch, and I.J. Glomski, *The cell biology of Listeria monocytogenes infection: the intersection of bacterial pathogenesis and cell-mediated immunity*. The Journal of cell biology, 2002. **158**(3): p. 409-414.
7. Ragon, M., et al., *A new perspective on Listeria monocytogenes evolution*. PLoS Pathogens, 2008. **4**(9): p. e1000146.
8. Mengaud, J., et al., *E-cadherin is the receptor for internalin, a surface protein required for entry of L. monocytogenes into epithelial cells*. Cell, 1996. **84**(6): p. 923-932.
9. Tattoli, I., et al., *Listeria phospholipases subvert host autophagic defenses by stalling pre-autophagosomal structures*. The EMBO journal, 2013. **32**(23): p. 3066-3078.
10. Horn, N. and A.K. Bhunia, *Food-associated stress primes foodborne pathogens for the gastrointestinal phase of infection*. Frontiers in microbiology, 2018. **9**: p. 1962.
11. Kim, H. and A.K. Bhunia, *Secreted Listeria adhesion protein (Lap) influences Lap-mediated Listeria monocytogenes paracellular translocation through epithelial barrier*. Gut pathogens, 2013. **5**(1): p. 1-11.
12. Nguyen, B.N., B.N. Peterson, and D.A. Portnoy, *Listeriolysin O: a phagosome-specific cytolysin revisited*. Cellular microbiology, 2019. **21**(3): p. e12988.
13. Jakobson, C.M. and D. Tullman-Ercek, *Dumpster diving in the gut: bacterial microcompartments as part of a host-associated lifestyle*. PLoS Pathogens, 2016. **12**(5): p. e1005558.
14. Kerfeld, C.A., et al., *Bacterial microcompartments*. Nature Reviews Microbiology, 2018. **6**(5): p. 227.
15. Thiennimitr, P., et al., *Intestinal inflammation allows Salmonella to use ethanolamine to compete with the microbiota*. Proceedings of the National Academy of Sciences, 2011. **108**(42): p. 17480-17485.
16. Kerfeld, C.A. and O. Erbilgin, *Bacterial microcompartments and the modular construction of microbial metabolism*. Trends in microbiology, 2015. **23**(1): p. 22-34.
17. Prentice, M.B., *Bacterial microcompartments and their role in pathogenicity*. Current Opinion in Microbiology, 2021. **63**: p. 19-28.

18. Agus, A., K. Clément, and H. Sokol, *Gut microbiota-derived metabolites as central regulators in metabolic disorders*. Gut, 2021. **70**(6): p. 1174-1182.
19. Anast, J.M., T.A. Bobik, and S. Schmitz-Esser, *The Cobalamin-dependent gene cluster of Listeria monocytogenes: implications for virulence, stress response, and food safety*. Frontiers in microbiology, 2020. **11**.
20. Rowley, C.A., C.J. Anderson, and M.M. Kendall, *Ethanolamine influences human commensal Escherichia coli growth, gene expression, and competition with enterohemorrhagic E. coli O157: H7*. mBio, 2018. **9**(5): p. e01429-18.
21. Tang, S., et al., *Transcriptomic analysis of the adaptation of Listeria monocytogenes to growth on vacuum-packed cold smoked salmon*. Appl. Environ. Microbiol., 2015. **81**(19): p. 6812-6824.
22. Schardt, J., et al., *Comparison between Listeria sensu stricto and Listeria sensu lato strains identifies novel determinants involved in infection*. Scientific reports, 2017. **7**(1): p. 17821.
23. Zeng, Z., et al., *Bacterial microcompartment-dependent 1, 2-propanediol utilization stimulates anaerobic growth of Listeria monocytogenes EGDe*. Frontiers in Microbiology, 2019. **10**: p. 2660.
24. Zeng, Z., et al., *Bacterial Microcompartments Coupled with Extracellular Electron Transfer Drive the Anaerobic Utilization of Ethanolamine in Listeria monocytogenes*. mSystems, 2021. **6**(2).
25. Mellin, J., et al., *A riboswitch-regulated antisense RNA in Listeria monocytogenes*. Proceedings of the National Academy of Sciences, 2013. **110**(32): p. 13132-13137.
26. Mellin, J., et al., *Sequestration of a two-component response regulator by a riboswitch-regulated noncoding RNA*. Science, 2014. **345**(6199): p. 940-943.
27. Vizcaino, J.A., et al., *2016 update of the PRIDE database and its related tools (vol 44, pg D447, 2016)*. Nucleic Acids Research, 2016. **44**(22): p. 11033-11033.
28. Mistry, J., et al., *Challenges in homology search: HMMER3 and convergent evolution of coiled-coil regions*. Nucleic acids research, 2013. **41**(12): p. e121-e121.
29. Hulsen, T., J. de Vlieg, and W. Alkema, *BioVenn-a web application for the comparison and visualization of biological lists using area-proportional Venn diagrams*. BMC genomics, 2008. **9**(1): p. 1-6.
30. Szklarczyk, D., et al., *STRING v11: protein-protein association networks with increased coverage, supporting functional discovery in genome-wide experimental datasets*. Nucleic acids research, 2019. **47**(D1): p. D607-D613.
31. Luo, W. and C. Brouwer, *Pathview: an R/Bioconductor package for pathway-based data integration and visualization*. Bioinformatics, 2013. **29**(14): p. 1830-1831.
32. Kragh, M.L. and L.T. Hansen, *Initial Transcriptomic Response and Adaption of Listeria monocytogenes to Desiccation on Food Grade Stainless Steel*. Frontiers in Microbiology, 2020. **10**.



33. Morth, J.P. and K.L. Hein, *Listeria Monocytogenes Lmo0818-Exploring a Putative Ca<sup>2+</sup>-ATPase, to Understand Calcium Ion Specificity*. Biophysical Journal, 2013. **104**(2): p. 300A-300A.
34. Jesse, H.E., I.S. Roberts, and J.S. Cavet, *Metal Ion Homeostasis in Listeria monocytogenes and Importance in Host-Pathogen Interactions*, in *Advances in Microbial Physiology*, Vol 65: *Advances in Bacterial Pathogen Biology*, R.K. Poole, Editor. 2014. p. 83-123.
35. Loessner, M.J., et al., *Complete nucleotide sequence, molecular analysis and genome structure of bacteriophage A118 of Listeria monocytogenes: implications for phage evolution*. Molecular Microbiology, 2000. **35**(2): p. 324-340.
36. Dowd, G.C., et al., *Investigation of the role of ZurR in the physiology and pathogenesis of Listeria monocytogenes*. Fems Microbiology Letters, 2012. **327**(2): p. 118-125.
37. Nair, S., et al., *CtsR controls class III heat shock gene expression in the human pathogen Listeria monocytogenes*. Molecular Microbiology, 2000. **35**(4): p. 800-811.
38. O'Donoghue, B., et al., *Blue-Light Inhibition of Listeria monocytogenes Growth Is Mediated by Reactive Oxygen Species and Is Influenced by sigma(B) and the Blue-Light Sensor Lmo0799*. Applied and Environmental Microbiology, 2016. **82**(13): p. 4017-4027.
39. Guerreiro, D.N., T. Arcari, and C.P. O'Byrne, *The sigma(B)-Mediated General Stress Response of Listeria monocytogenes: Life and Death Decision Making in a Pathogen*. Frontiers in Microbiology, 2020. **11**.
40. Hu, Y., et al., *Transcriptomic and phenotypic analyses suggest a network between the transcriptional regulators HrcA and sigma(B) in Listeria monocytogenes*. Applied and Environmental Microbiology, 2007. **73**(24): p. 7981-7991.
41. Collins, B., et al., *Assessing the Contributions of the LiaS Histidine Kinase to the Innate Resistance of Listeria monocytogenes to Nisin, Cephalosporins, and Disinfectants*. Applied and Environmental Microbiology, 2012. **78**(8): p. 2923-2929.
42. Arolas, J.L., et al., *Expression and purification of integral membrane metalloproteinase HtpX*. Protein Expression and Purification, 2014. **99**: p. 113-118.
43. de las Heras, A., et al., *Regulation of Listeria virulence: PrfA master and commander*. Current opinion in microbiology, 2011. **14**(2): p. 118-127.
44. Scortti, M., et al., *The PrfA virulence regulon*. Microbes and Infection, 2007. **9**(10): p. 1196-1207.
45. dos Santos, P.T., et al., *Listeria monocytogenes Relies on the Heme-Regulated Transporter hrtAB to Resist Heme Toxicity and Uses Heme as a Signal to Induce Transcription of Imo1634, Encoding Listeria Adhesion Protein*. Frontiers in Microbiology, 2018. **9**.
46. Fraser, K.R., et al., *Identification and characterization of an ATP binding cassette L-carnitine transporter in Listeria monocytogenes*. Applied and Environmental Microbiology, 2000. **66**(11): p. 4696-4704.

47. Fillgrove, K.L., et al., *Structure and mechanism of the genomically encoded fosfomycin resistance protein, FosX, from Listeria monocytogenes*. Biochemistry, 2007. **46**(27): p. 8110-8120.
48. Nair, S., E. Milohanic, and P. Berche, *ClpC ATPase is required for cell adhesion and invasion of Listeria monocytogenes*. Infection and Immunity, 2000. **68**(12): p. 7061-7068.
49. Kerfeld, C.A., et al., *Bacterial microcompartments*. Nature Reviews Microbiology, 2018.
50. Dowd, G.C., et al., *Investigation of the role of ZurR in the physiology and pathogenesis of Listeria monocytogenes*. FEMS microbiology letters, 2012. **327**(2): p. 118-125.
51. Chaturongakul, S., et al., *Transcriptomic and Phenotypic Analyses Identify Coregulated, Overlapping Regulons among PrfA, CtsR, HrcA, and the Alternative Sigma Factors sigma(B), sigma(C), sigma(H), and sigma(L) in Listeria monocytogenes*. Applied and Environmental Microbiology, 2011. **77**(1): p. 187-200.
52. van der Veen, S., et al., *The SOS response of Listeria monocytogenes is involved in stress resistance and mutagenesis*. Microbiology-Sgm, 2010. **156**: p. 374-384.
53. van der Veen, S., et al., *The heat-shock response of Listeria monocytogenes comprises genes involved in heat shock, cell division, cell wall synthesis, and the SOS response*. Microbiology-Sgm, 2007. **153**: p. 3593-3607.
54. Rabinovich, L., et al., *Prophage Excision Activates Listeria Competence Genes that Promote Phagosomal Escape and Virulence*. Cell, 2012. **150**(4): p. 792-802.
55. Pasechnek, A., et al., *Active Lysogeny in Listeria Monocytogenes Is a Bacteria-Phage Adaptive Response in the Mammalian Environment*. Cell Reports, 2020. **32**(4).
56. Jesse, H.E., I.S. Roberts, and J.S. Cavet, *Metal ion homeostasis in Listeria monocytogenes and importance in host-pathogen interactions*. Advances in microbial physiology, 2014. **65**: p. 83-123.
57. Gaballa, A., et al., *Characterization of the roles of activated charcoal and Chelex in the induction of PrfA regulon expression in complex medium*. Plos one, 2021. **16**(4): p. e0250989.
58. Nadon, C.A., et al., *Sigma B contributes to PrfA-mediated virulence in Listeria monocytogenes*. Infection and immunity, 2002. **70**(7): p. 3948-3952.



---

## Bacterial microcompartment-dependent 1,2-propanediol utilization of *Propionibacterium freudenreichii*

Published as:

Dank, A. (Co-first author), **Zeng, Z.** (Co-first author), Boeren, S., Notebaart, R. A., Smid, E. J., & Abee, T. (2021). Bacterial microcompartment-dependent 1, 2-propanediol utilization of *Propionibacterium freudenreichii*. *Frontiers in microbiology*, 12.

## Abstract

Bacterial microcompartments (BMCs) are proteinaceous prokaryotic organelles that enable the utilization of substrates such as 1,2-propanediol and ethanolamine. BMCs are mostly linked to the survival of particular pathogenic bacteria by providing a growth advantage through utilization of 1,2-propanediol and ethanolamine which are abundantly present in the human gut. Although a 1,2-propanediol utilization cluster was found in the probiotic bacterium *Propionibacterium freudenreichii*, BMC-mediated metabolism of 1,2-propanediol has not been demonstrated experimentally in *P. freudenreichii*. In this study we show that *Propionibacterium freudenreichii* DSM 20271 metabolizes 1,2-propanediol in anaerobic conditions to propionate and 1-propanol. Furthermore, 1,2-propanediol induced the formation of bacterial microcompartments, which were visualized by transmission electron microscopy and resembled BMCs found in other bacteria. Proteomic analysis of 1,2-propanediol grown cells compared to L-lactate grown cells showed significant upregulation of proteins involved in propanediol-utilization (*pdu*-cluster), DNA repair mechanisms and BMC shell proteins while proteins involved in oxidative phosphorylation were downregulated. 1,2-Propanediol utilizing cells actively produced vitamin B<sub>12</sub> (cobalamin) in similar amounts as cells growing on L-lactate. The ability to metabolize 1,2-propanediol may have implications for human gut colonization and modulation, and can potentially aid in delivering propionate and vitamin B<sub>12</sub> *in situ*.

## 7.1 Introduction

*Propionibacterium freudenreichii* is a Gram-positive, non-spore forming bacterium which has been linked to several potential health promoting effects, such as reducing intestinal inflammation, immunomodulation, modulation of intestinal motility and absorption, reduction of pathogen adhesion and enhancement of bifidobacteria (reviewed by [1]). *P. freudenreichii* is able to cope with a large variety of stresses (oxidative, bile salt, temperature) [2] and consequently has good survival capabilities in the upper intestinal tract [3]. Survival of *P. freudenreichii* in the intestinal environment is supported by expression of pathways involved in the metabolism of substrates present in the intestinal environment, such as propanediol [4].

Propanediol is a major end product from anaerobic degradation of rhamnose or fucose by the human intestinal microbiota and serves as an important carbon source for propanediol utilizing bacteria, which can metabolize 1,2-propanediol into propionate, generating ATP, and into 1-propanol for maintaining redox balance. The metabolism of 1,2-propanediol produces the toxic intermediate propionaldehyde [5]. Some bacteria can protect themselves from toxic intermediates by encapsulating the enzymatic processes in self-assembling proteinaceous organelles called bacterial microcompartments (BMCs) [6]. BMCs are typically about 40-200 nm in diameter and are made of three types of shell proteins: hexamers, pseudohexamers, and pentamers [7]. Based on the highly conserved domain of shell proteins, Axen *et al.* [6] predicted the presence of these organelles in 23 different bacterial phyla, including *Actinobacteria* which includes the species *P. freudenreichii*. However, no experimental evidence of bacterial microcompartment mediated utilization of 1,2-propanediol has been shown in *P. freudenreichii* and its role as carbon source is yet to be elucidated.

BMC-mediated catabolism of substrates involving a toxic aldehyde intermediate is driven by three core enzymes: aldehyde dehydrogenase, alcohol dehydrogenase and phosphotransacylase [6]. The signature enzyme in the propanediol utilization pathway is propanediol dehydratase, a vitamin B<sub>12</sub>-dependent enzyme catalyzing the reaction of 1,2-propanediol to propionaldehyde [6]. Vitamin B<sub>12</sub> is produced in high quantities by *P. freudenreichii* [8] and it also requires vitamin B<sub>12</sub> as a cofactor for a key enzyme in its characteristic Wood-Werkman cycle. It is suggested that *Actinobacteria* such as *P. freudenreichii* obtained the propanediol utilization (*pdu*) cluster through horizontal gene transfer from *Clostridiales* [9], in which acquisition may have been

supported by the ability of *P. freudenreichii* to produce vitamin B<sub>12</sub> *de-novo* [10]. BMCs are also found in some pathogenic bacteria, such as *Salmonella enterica*, *Enterococcus faecalis*, *Listeria monocytogenes*, pathogenic *Escherichia coli* and *Clostridium perfringens* [7]. BMC-mediated utilization of 1,2-propanediol increases competitive fitness of pathogens in the gut and consequently has been linked to virulence [11]. However, symbiotic relationships depending on 1,2-propanediol metabolism have also been shown for beneficial *Lactobacillus reuteri* and *Bifidobacterium breve* [12]. The ability to degrade 1,2-propanediol may have similar implications for the bifidogenic capacity reported for *P. freudenreichii* [13] and consequences for gut modulation and competition with pathogenic bacteria. Furthermore, the active production of vitamin B<sub>12</sub> during metabolism of 1,2-propanediol has not been studied yet in *P. freudenreichii*.

In this study we present evidence for BMC-mediated anaerobic growth of *P. freudenreichii* on 1,2-propanediol, evidenced by substrate utilization, propionate and 1-propanol production, and vitamin B<sub>12</sub> synthesis. Using transmission electron microscopy and proteomics, we confirmed the presence of BMCs, Pdu BMC shell proteins and enzymes in *pdu-induced P. freudenreichii*.

## 7.2 Materials and methods

### 7.2.1 Strains, Culture Conditions, and Growth Measurement

*P. freudenreichii* DSM20271 was grown anaerobically (Anoxomat modified atmosphere, MART; 10% CO<sub>2</sub>, 5% H<sub>2</sub>, 85% N<sub>2</sub>) at 30°C in 50 mL tubes containing 40 mL complex media containing per liter: 10 g tryptone, 5 g yeast extract, 5 g KH<sub>2</sub>PO<sub>4</sub> supplemented with 100 mM L-lactate or 1,2-propanediol. All media was set at pH 7.0 by addition of 5M NaOH and was filter sterilized through 0.2 µm filters into sterile flasks. OD<sub>600</sub> measurements and extracellular metabolite samples were taken daily for a time period of 7 days.

### 7.2.2 Analysis of extracellular metabolites using High Performance Liquid Chromatography

Culture samples were taken at various time intervals and were analyzed for extracellular metabolites by high performance liquid chromatography. 1 mL culture was centrifuged at 17000 × *g* for 1 minute and the supernatant was collected. 0.5 mL supernatant was treated with 0.25 mL Carrez A and 0.25 mL Carrez B, vortexed and centrifuged at 17000 × *g* for 2 minutes. 200 µL supernatant

was stored in HPLC vials at -20 °C upon analysis. HPLC was performed as described by Zeng. Z, et al. [14]. Quantification was performed by addition of a standard curve containing L-lactate, acetate, propionate, 1,2-propanediol and 1-propanol.

### 7.2.3 Transmission Electron Microscopy

*P. freudenreichii* cultures were grown anaerobically at 30°C in 100 mM L-lactate or 1,2-propanediol containing media. Samples were collected after 6 days of incubation (early stationary phase for 1,2-propanediol-grown cells). About 10 µg of dry cell biomass was fixed for 2 h in 2.5% (v/v) glutaraldehyde in 0.1 M sodium cacodylate buffer (pH 7.2). After rinsing in the same buffer, a post-fixation was done in 1% (w/v) OsO<sub>4</sub> for 1 h at room temperature. The samples were dehydrated using ethanol. The dehydrated cell pellets were then embedded in resin (Spurr HM20) for 10 h at 70°C. Thin sections (<100 nm) of polymerized resin samples were obtained with microtomes. After staining with 2% (w/v) aqueous uranyl acetate, the samples were analyzed with a Jeol 1400 plus TEM with 120 kV setting as described by Zeng. Z, et al. [14].

### 7.2.4 Vitamin B12 quantification

After 7 days of incubation the vitamin B<sub>12</sub> (cobalamin) concentration was determined using a microbiological assay (Vitafast vitamin B<sub>12</sub> kit, R-biopharm) for *P. freudenreichii* grown in 66 mM L-lactate and 49 mM 1,2-propanediol medium. Briefly, 1 mL of culture was disrupted by bead beating (lysing matrix B, mp-bio) 2x 1 min at 4.5 m/s with 1 minute on ice in between. Samples were centrifuged and diluted with water to appropriate concentrations for the test kit and were heat-extracted for 30 minutes at 95°C. The samples were cooled to room temperature and vitamin B<sub>12</sub> detection was performed according to the manufacturer protocol.

### 7.2.5 Proteomics

*P. freudenreichii* cells were cultured in media supplemented with 100 mM L-lactate or 100 mM 1,2-propanediol for 7 days. Cell pellets were harvested by centrifugation of 1 mL of sample at 17000 × g for 1 min in table top centrifuges and cell pellets were frozen at -80 degrees. Samples were washed twice with 100 mM Tris (pH 8) and resuspended in 100 µl 100 mM Tris. Samples were lysed by sonication for 45 s twice while cooling 1 min on ice. Protein content was determined using Pierce Coomassie protein assay and samples were diluted to 1

µg/ µl using Tris-HCl pH 8. Samples were prepared according to the filter assisted sample preparation protocol (FASP) [15] with the following steps: reduction with 15 mM dithiothreitol, alkylation with 20 mM acrylamide, and digestion with sequencing grade trypsin overnight. Each prepared peptide sample was analyzed by injecting (18 µl) into a nanoLC-MS/MS (Thermo nLC1000 connected to a LTQ-Orbitrap XL) as described previously (Lu *et al.*, 2011). LCMS data with all MS/MS spectra were analyzed with the MaxQuant quantitative proteomics software package [16] as described before [17, 18].

A protein database with the protein sequence of *P. freudenreichii* DSM 20271 (ID:UP000032238) was downloaded from UniProt. Filtering and further bioinformatics and statistical analysis of the MaxQuant ProteinGroups file were performed with Perseus [19]. Reverse hits and contaminants were filtered out. Protein groups were filtered to contain minimally two peptides for protein identification of which at least one is unique and at least one is unmodified. Also, each group required three valid values in at least one of the two experimental groups. A volcano plot was prepared based on the Student's t-test difference between samples. Volcano plots were produced in Rstudio using EnhancedVolcano [20]. Proteins were considered to be significantly different amongst sample if  $p < 0.05$  and 4-fold change difference was detected. KEGG gene set enrichment analysis was performed using Clusterprofiler [21] and 4-fold change difference amongst proteins. The mass spectrometry proteomics data have been deposited to the ProteomeXchange Consortium via the PRIDE [22] partner repository with the dataset identifier PXD024700.

### 7.2.6 Predicting BMCs shell proteins

The Hidden Markov Models (HMMs) of two BMC shell protein domains listed as Pf00936 and Pf03319 were retrieved from the Pfam database to predict BMC shell proteins as described in [6, 14]. Shell proteins were predicted by a HMM search using the HMMER package and a local protein database of *P. freudenreichii* DSM 20271 genome (CP010341.1 [23]). All hits with an e-value less than or equal to  $1e-05$  that correspond to a genomic record from Genbank, RefSeq, EMBL, or DDBJ databases were accepted as BMC shell protein homologs (Supplementary file 1).

## 7.3 Results

### 7.3.1 Growth performance and metabolite production on 1,2-propanediol and L-lactate

Anaerobic growth of *P. freudenreichii* on 100 mM 1,2-propanediol was monitored for 6 days with daily sampling in triplicate. As a control, *P. freudenreichii* was cultured on 100 mM L-lactate. *P. freudenreichii* was able to completely metabolize 100 mM 1,2-propanediol during a period of 6 days (see Figure 1). This resulted in the production of  $37.5 \pm 0.1$  mM 1-propanol and  $43.2 \pm 0.5$  mM propionate. No production of acetate was observed, and with the current HPLC method used, approximately 28 mM of expected C<sub>3</sub> compounds is missing, conceivably volatile propionaldehyde. In the control cultures, 100 mM L-lactate was consumed within 2 days, resulting in  $65.1 \pm 0.1$  mM propionate and  $30.5 \pm 0.1$  mM acetate, close the expected molar ratio of 2:1 [24]. Growth on 1,2-propanediol resulted in slower growth, with a stationary phase after 120 hours vs 48 hours in L-lactate. Our results clearly demonstrate that *P. freudenreichii* can grow on 1,2-propanediol, metabolizing it to propionate and 1-propanol.

To monitor metabolism of 1,2-propanediol in the presence of other carbon sources *P. freudenreichii* was grown in media containing both L-lactate and 1,2-propanediol. When NAD<sup>+</sup>/NADH pools are shared between the cytosol and the BMC as discussed by Ferlez et al.[25], the highest ATP yield from 1,2-propanediol in the presence of L-lactate can be obtained by co-fermenting 1,2-propanediol and L-lactate solely to propionate (see Supplementary text 1). The expected ATP yield with L-lactate and 1,2-propanediol as mixed substrates is higher compared to cells growing solely on L-lactate (see Supplementary text 1). We found production of  $67.1 \pm 1.5$  mM propionate,  $19.0 \pm 1.0$  mM of acetate and  $28.3 \pm 2.8$  mM 1-propanol in cells growing on the mixed substrates. Assuming 1-propanol:propionate is produced in a 1:1 ratio from 1,2-propanediol and acetate : propionate is produced in a 1:2 ratio from L-lactate, 28 mM of the propionate originates from the 1,2-propanediol metabolism and 38 mM propionate originates from L-lactate metabolism. This matches the total found propionate of  $67.1 \pm 1.5$  mM propionate in the samples. In mixed substrate conditions the amounts of total products formed indicate no apparent loss of C<sub>3</sub> compounds, which may indicate reduced loss of volatile propionaldehyde. Biomass formation with 1:1 L-lactate:1,2-propanediol-grown cells was found to be lower compared to 100 mM L-lactate-grown cells. These results indicate no apparent energetic

benefit from mixed substrate conditions compared to mono substrate conditions, pointing towards independent pathways. Our results show mixed-substrate metabolism influences the total amount of short-chain fatty acid production, but pathway interactions are not apparent.

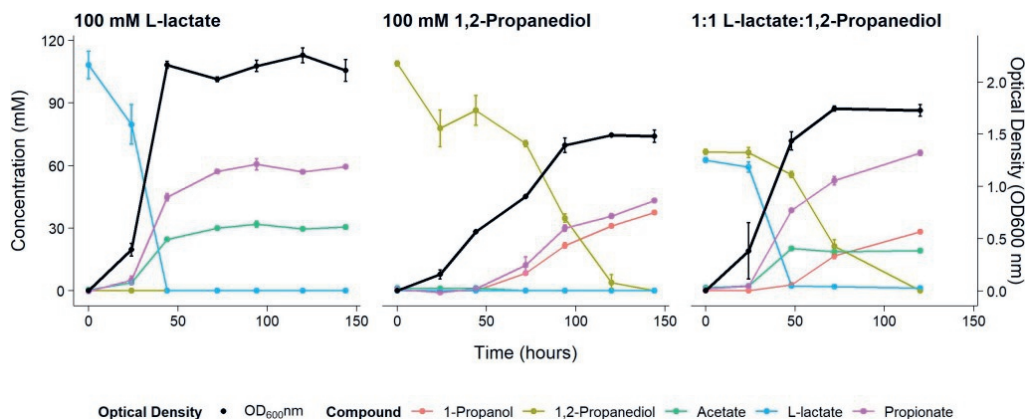


**Figure 1:** Substrate consumption, metabolite production and biomass formation of *P. freudenreichii* grown on 100 mM L-lactate, 100mM 1,2-PD and 1:1 1,2-propanediol:L-lactate for 6 days. Error bars = standard error (n=3 biological replicates).

### 7.3.2 Vitamin B12 production

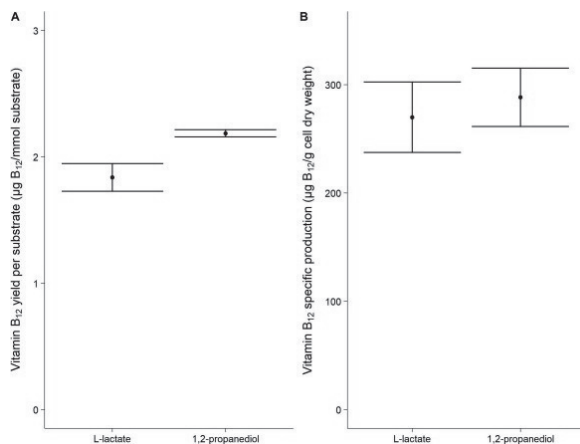


**Figure 2:** Vitamin B<sub>12</sub> formation in cells grown on L-lactate or 1,2-propanediol. **(A)** vitamin B<sub>12</sub> yield in µg/mmol substrate **(B)** Biomass specific vitamin B<sub>12</sub> production in µg/g cell dry weight. Error bars = standard error (n=3 biological replicates).

To demonstrate active vitamin B<sub>12</sub> production under 1,2-propanediol utilizing conditions, *P. freudenreichii* was grown for 7 days in either yeast extract medium supplemented with 66 mM L-lactate or 49 mM 1,2-propanediol. Biomass

formation, substrate utilization and vitamin B<sub>12</sub> production by *P. freudenreichii* was monitored after 7 days of incubation. Incubation vessels were not opened in-between to prevent side effects by oxygen-dependent stimulation of vitamin B<sub>12</sub> production, as has been shown for *P. freudenreichii* [26]. Again, complete utilization of L-lactate and 1,2-propanediol was found (Supplementary file 2).

### 7.3.3 Proteomics and electron microscopy of L-lactate and 1,2-propanediol grown cells

Cells growing in media supplemented with L-lactate (control) and with 1,2-propanediol were visualized using transmission electron microscopy (TEM). Thin sections of cells grown on 1,2-propanediol supplemented media clearly display cellular structures which were not found in the cells grown on L-lactate supplemented media (see Figure 3), and those structures resemble BMC structures found in other bacteria including *L. monocytogenes* [14], *S. enterica* [27] and *E. coli* [28].

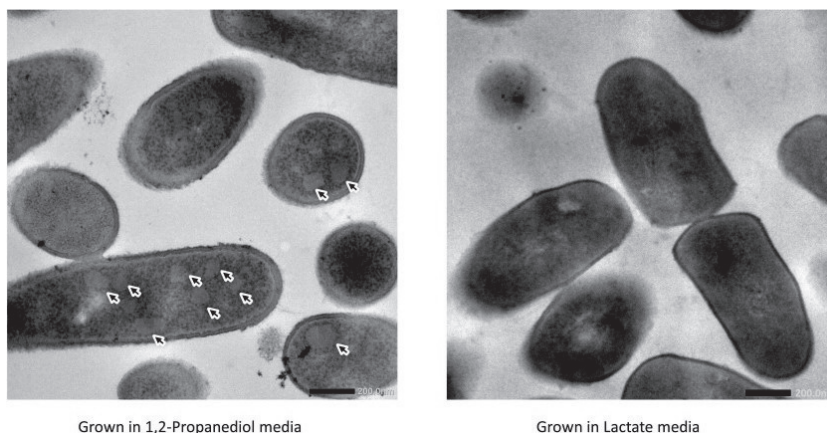
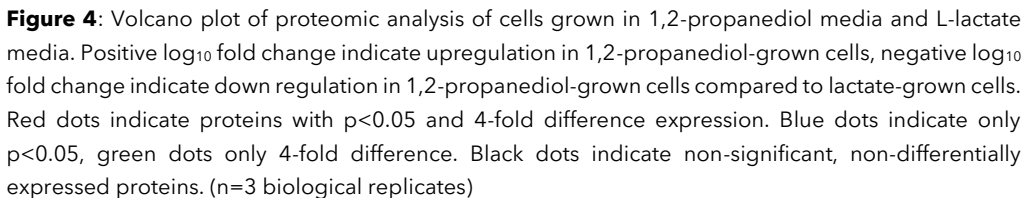


**Figure 3:** Visualization of bacterial microcompartments in propanediol media (left) and absence in lactate media (right).

Proteome analysis revealed that BMC structural shell proteins (PduA, PduB, PduK, PduJ, PduN, PduM) and enzymes involved in 1,2-propanediol utilization (PduL, PduC, PduD, PduE, PduP, PduO, PduQ) were significantly more abundant in cells grown with 1,2-propanediol as a substrate compared to cells grown on L-lactate (Figure 4). Lactate permease (LldP), succinate dehydrogenase subunits A, C1 (SdhA, SdhC1) were found to be significantly more abundant in the L-lactate-grown cells compared to 1,2-propanediol-grown cells, indicating a decrease of proteins in lactate-degradation pathways such as the Wood-Werkman cycle. Gene



### 7.3.4 Overview of BMC-dependent 1,2-propanediol metabolism model in

#### *P. freudenreichii*

Subsequent analysis of the *pdu* cluster in *P. freudenreichii* DSM 20271 identified two distant loci, with locus 1 starting from RM25\_0852 to RM25\_0857 and locus 2 starting from RM25\_1258 to RM25\_1273 (Figure 5A). Locus 1 contains four genes which are *pocR* encoding a transcriptional regulator, *pduQ* encoding 1-propanol dehydrogenase, *pduV* with unknown function and *pduU* encoding BMC shell protein. Locus 2 carries 14 genes including 6 genes encoding BMC shell proteins and 8 genes encoding enzymes for the 1,2-propanediol degradation pathway and is not preceded by any known transcriptional regulators.

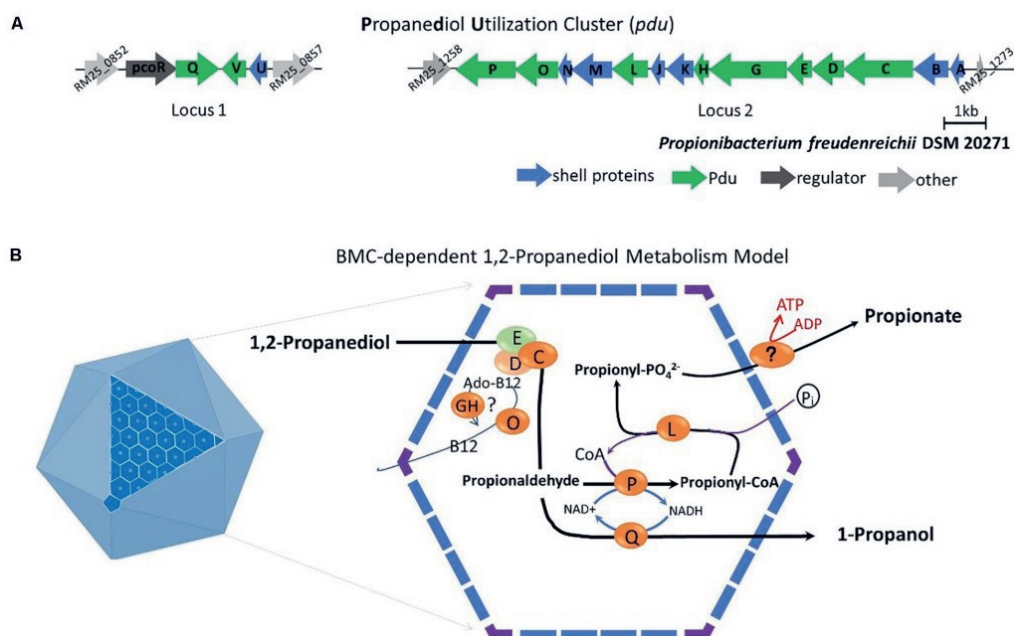


**Figure 5: (A)** Analysis of the *pdu* gene cluster (Details in supplementary file 1). Characters in orange represent Pdu enzymes, in blue represent BMC shell proteins, in dark represent regulator and in grey represent unannotated proteins with gene ID. **(B)** Model of BMC-dependent 1,2-propanediol metabolism. In the left, the icosahedral diagram represent BMC with one surface showing the assembly of shell proteins. In the right, the metabolic pathway of 1,2-propanediol metabolism. PduCDE, B<sub>12</sub>-dependent diol dehydratase; PduP, CoA-dependent propionaldehyde dehydrogenase; PduGH, diol dehydratase reactivase; PduO, corrinoid adenosyltransferase; PduS, Vitamin B<sub>12</sub> reductase; PduL, phosphate propanoyltransferase; PduW, propionate kinase; PduQ, propanol dehydrogenase. See text for details.

Based on the structural studies of BMCs [29, 30] and our understanding of 1,2-propanediol metabolism [5, 7, 14], we propose the model of BMC-dependent 1,2-propanediol metabolism in *P. freudenreichii*, with the predicted BMC shell proteins PduA, PduB, PduK, PduJ, PduM, PduN and PduU constituting the self-organized icosahedral organelle [7, 29]. As illustrated in Figure 5B, the catabolism of 1,2-propanediol starts with the conversion of 1,2-propanediol to propionaldehyde by vitamin B<sub>12</sub>-dependent diol dehydratase PduCDE. The toxic propionaldehyde is then converted to propionate by the enzyme CoA-dependent propionaldehyde dehydrogenase PduP, followed by action of phosphate propanoyltransferase PduL, and potential propionate kinase located in the cytoplasm, resulting in the end product propionate and the production of ATP. The other end product is produced following conversion of propionaldehyde by propanol dehydrogenase PduQ into 1-propanol. The diol dehydratase reactivase PduGH and corrinoid adenosyltransferase PduO are linked to the supply and recycling of vitamin B<sub>12</sub>.

## 7.4 Discussion

*Propionibacterium freudenreichii* is commonly found in the rumen and colon of animals and in the human intestine [31]. In these environments fucose and rhamnose are degraded to 1,2-propanediol by the present microbiota [32]. We showed 1,2-propanediol can be further metabolized into propionate and 1-propanol by *P. freudenreichii*, thereby supporting anaerobic growth. Previously, a locus containing 15 genes involved in propanediol utilization was detected in *P. freudenreichii* [2]. *In vivo* gene expression analysis showed the *pdu* operon to be expressed in *P. freudenreichii* cells contained in the colon environment of a pig [4], pointing towards propanediol utilization in intestinal environments. Interestingly, in this study we identified the *pdu* cluster distributed in two different loci in *P. freudenreichii* DSM 20271. The presence of the *pdu* cluster seems to be species specific in propionic acid bacteria, as blasting the *pdu* cluster of *P. freudenreichii* against *Cutibacterium acnes*, *Acidipropionibacterium acidipropionici*, *A. thoenii* and *A. jensenii* did not result significant hits for key components in the cluster (see Supplementary file 4). Presence of 1,2-propanediol in the medium induced expression of the two loci in *P. freudenreichii* DSM 20271 and resulted in BMC formation, 1,2-propanediol metabolism and consequently propionate and 1-propanol production. Our results show that expression of the *pdu* cluster from two different loci results in effective BMC formation and 1,2-propanediol metabolism. Indeed, BMC genes are split into two or more loci in 40% of the prokaryotic genomes containing BMCs [33]. In *P. freudenreichii* DSM 20271, locus 1 is preceded by transcriptional activator *pocR*, which has been linked to activation of the *pdu* cluster in *Salmonella* [34]. We did not find any annotated transcriptional regulator in the vicinity of locus 2. The presence of two different loci in many prokaryotic genomes suggests expression is controlled by additional regulators next to *PocR*. Indeed heterologous expression of BMCs uncoupled from their cognate transcriptional regulators has been reported previously [35]. The transcriptional regulation and activation of the two *pdu* loci and the role of *pocR* in *P. freudenreichii* requires further attention.

Upregulation of the *pdu* cluster and DNA repair mechanisms clearly indicated the crucial role of BMCs to protect *P. freudenreichii* from the toxic intermediate propionaldehyde produced in the degradation pathway. The ability to utilize substrates producing toxic intermediates upon degradation results in a competitive advantage to other gut microbiota [11], as shown for ethanolamine utilization by *S. enterica* during intestinal inflammation [36]. Interestingly, the

presence of genes encoding metabolosomes for the utilization of ethanolamine and propanediol has been linked to pathogenicity and aids in anaerobic growth and colonization of foodborne pathogens *L. monocytogenes*, *C. perfringens* and *S. typhimurium* [37, 38]. It has been suggested for beneficial bacterium *L. reuteri* that competition for 1,2-propanediol could result in decreased proliferation of pathogens [12]. *P. freudenreichii* is considered to be non-pathogenic and has the generally recognized as safe (GRAS) status [39]. Substrate competition for 1,2-propanediol by *P. freudenreichii* may thus exert similar effects as suggested for *L. reuteri* on growth of pathogenic bacteria. This is in line with reports that *P. freudenreichii* can decrease adhesion of pathogens to human intestinal mucus cells [40]. Furthermore, *P. freudenreichii* stimulates the growth of beneficial bifidobacteria [41, 42] thereby promoting a healthy gut microbiota. The role of BMC-mediated 1,2-propanediol utilization by *P. freudenreichii* and its importance for modulating gut microbiota composition, both by substrate competition and promoting other beneficial microbiota, requires further investigation.

Our study shows the potential of *P. freudenreichii* to substantially contribute to the production of propionate in the human gut. Next to 1,2-propanediol, also lactic acid [43] is a major end-product of microbial fermentation, which consequently can also be fermented by *P. freudenreichii* and additionally contributes to the production of propionate. In mixed substrate conditions both pathways remained active, albeit without apparent interaction based on metabolite formation. However, mixed substrate conditions decreased the loss of C<sub>3</sub>, suggesting less loss of volatile propionaldehyde, thus potentially more efficient BMC assembly. The assembly of BMCs in mixed substrate condition requires further attention. Propionate is linked to many putative health effects (reviewed by [44]) and can further stimulate bifidobacteria [13]. The production of propionate from propanediol further supports the potential of *P. freudenreichii* as a probiotic.

The metabolism of 1,2-propanediol requires propanediol dehydratase, which is vitamin B<sub>12</sub>-dependant [6]. Vitamin B<sub>12</sub> is actively produced by *P. freudenreichii* as it is essential cofactor in a key enzyme in the Wood-Werkman cycle, methylmalonyl-CoA mutase. Synthesis of vitamin B<sub>12</sub> in *P. freudenreichii* follows the anaerobic pathway [10], enabling production of vitamin B<sub>12</sub> for anaerobic metabolism of lactate. Here we show vitamin B<sub>12</sub> is produced in similar amounts in complex medium when cells metabolize 1,2-propanediol or L-lactate as carbon source. In *S. typhimurium* *pocR* mediated expression of vitamin B<sub>12</sub> is induced in the presence of propanediol [45]. We also identified *pocR* upstream of *pdu* loci 1

in *P. freudenreichii* DSM 20271, but as discussed before its exact regulatory role in *P. freudenreichii* remains to be elucidated. Vitamin B<sub>12</sub> production is also regulated by a vitamin B<sub>12</sub> regulated riboswitch in *P. freudenreichii*. In *Propionibacterium* strain UT1 expression of vitamin B<sub>12</sub> biosynthesis occurred at vitamin B<sub>12</sub> concentrations of 750 μM, much higher compared to the vitamin B<sub>12</sub> concentrations found in this study (~90μM). The role of this riboswitch for vitamin B<sub>12</sub> production during metabolism of 1,2-propanediol also remains to be elucidated. Based on our findings, we hypothesize that *P. freudenreichii* occupies a lactate and propanediol-rich niche in the gut environment. Symbiotic relationships have been shown for the production of vitamin B<sub>12</sub> [46, 47], which may be hard-wired in the vitamin B<sub>12</sub> production of *P. freudenreichii*. As next to vitamin B<sub>12</sub>-dependent lactate metabolism, BMC-mediated 1,2-propanediol metabolism supports anaerobic growth of *P. freudenreichii*, thereby contributing to *in situ* vitamin B<sub>12</sub> production in the gut.

This study presents evidence for BMC-mediated vitamin B<sub>12</sub>-dependent utilization of 1,2-propanediol in *P. freudenreichii*. We have shown that 1,2-propanediol supports anaerobic growth of *P. freudenreichii*. It is conceivable that utilization of 1,2-propanediol could aid colonization of propionibacteria in the human gut to exert beneficial effects, such as delivering vitamin B<sub>12</sub> and propionate *in situ*, but these aspects require further study.

## 7.5 Supplementary materials

### Supplementary text 1: Energetics with pathway interactions between bacterial microcompartment (BMC) and Wood-Werkman cycle

The BMC mediated degradation of 1,2-propanediol to propionyl-phosphate and propionate generates one NADH and one ATP. Degradation of lactate to propionate through the Wood-Werkman cycle consumes one NADH and by the anaerobic electron transport from lactate to fumarate translocates 2 H<sup>+</sup>, thereby generating 0.5-0.67 ATP. This means that if lactate and PD are co-metabolised in a 1:1 ratio, the yield obtainable by fermentation of 50 mM Lactate to propionate is 33 mM ATP by fumarate respiration and the total yield of fermentation of 50mM 1,2-Propanediol to propionate is 50 mM ATP by substrate-level phosphorylation. A total yield of 83 mM ATP and sole production of 100 mM propionate would be expected if NAD<sup>+</sup>/NADH pools are shared. If co-factors cannot be shared due to the limitations by shell proteins, the general accepted pathways for both lactate and 1,2-propanediol are expected. Fermentation of 50 mM lactate would result in production of 33 mM propionate + 17 mM acetate, yielding 39 mM ATP (17 mM by substrate level phosphorylation of acetate and 22 mM by fumarate reduction producing propionate). Fermentation of 50 mM PD would result in production of 25 mM propionate and 25 mM 1-propanol, yielding 25 mM ATP. A total production of 58 mM propionate + 17 mM acetate + 25 mM 1-propanol would be expected, yielding a total 64 mM ATP. Hence, sharing NAD<sup>+</sup>/NADH pools would be energetically beneficial. Fermentation of 100 mM Lactate results in 78 mM ATP and fermentation of 100 mM 1,2-PD results in 50 mM ATP. Hence, the biomass formation for 50mM PD:50 mM lactate grown-cells using a shared co-factor pool is expected to be higher compared to 100 mM L-lactate grown-cells, whereas if the co-factor pool is not shared the expected biomass formation is lower compared to 100 mM L-lactate grown cells, but higher compared to 100 mM 1,2-PD grown-cells

### Supplementary file 2: Substrate consumption and biomass production for cells grown for B<sub>12</sub> assay

Sample	mMol substrate utilized	Theoretical yield ATP per mol substrate	Biomass yield (g CDW/L)
L-lactate	65.8	0.78	0.45
1,2-Propanediol	49.1	0.50	0.38

**The Supplementary Materials for this chapter can also be found online at:**

<https://www.frontiersin.org/articles/10.3389/fmicb.2021.679827/full#supplementary-material>

## 7.6 References

1. Cousin, F.J., et al., *Dairy propionibacteria as human probiotics: A review of recent evidence*. Dairy Science & Technology, 2011. **91**(1): p. 1-26.
2. Falentin, H., et al., *The Complete Genome of Propionibacterium freudenreichii CIRM-BIA1(T), a Hardy Actinobacterium with Food and Probiotic Applications*. Plos One, 2010. **5**(7).
3. Huang, Y. and M.C. Adams, *In vitro assessment of the upper gastrointestinal tolerance of potential probiotic dairy propionibacteria*. International Journal of Food Microbiology, 2004. **91**(3): p. 253-260.
4. Saraoui, T., et al., *A unique in vivo experimental approach reveals metabolic adaptation of the probiotic Propionibacterium freudenreichii to the colon environment*. BMC Genomics, 2013. **14**.
5. Sampson, E.M. and T.A. Bobik, *Microcompartments for B-12-dependent 1,2-propanediol degradation provide protection from DNA and cellular damage by a reactive metabolic intermediate*. Journal of Bacteriology, 2008. **190**(8): p. 2966-2971.
6. Axen, S.D., O. Erbilgin, and C.A. Kerfeld, *A Taxonomy of Bacterial Microcompartment Loci Constructed by a Novel Scoring Method*. Plos Computational Biology, 2014. **10**(10).
7. Kerfeld, C.A., et al., *Bacterial microcompartments*. Nature Reviews Microbiology, 2018. **16**(5): p. 277-290.
8. Burgess, C.M., E.J. Smid, and D. van Sinderen, *Bacterial vitamin B2, B11 and B12 overproduction: An overview*. International Journal of Food Microbiology, 2009. **133**(1-2): p. 1-7.
9. Ravcheev, D.A., et al., *Comparative Genomic Analysis Reveals Novel Microcompartment-Associated Metabolic Pathways in the Human Gut Microbiome*. Frontiers in Genetics, 2019. **10**.
10. Roessner, C.A., et al., *Isolation and characterization of 14 additional genes specifying the anaerobic biosynthesis of cobalamin (vitamin B-12) in Propionibacterium freudenreichii (P-shermanii)*. Microbiology-Sgm, 2002. **148**: p. 1845-1853.
11. Jakobson, C.M. and D. Tullman-Ercek, *Dumpster Diving in the Gut: Bacterial Microcompartments as Part of a Host-Associated Lifestyle*. Plos Pathogens, 2016. **12**(5).
12. Cheng, C.C., et al., *Ecological Importance of Cross-Feeding of the Intermediate Metabolite 1,2-Propanediol between Bacterial Gut Symbionts*. Applied and Environmental Microbiology, 2020. **86**(11).
13. Kaneko, T., et al., *GROWTH STIMULATOR FOR BIFIDOBACTERIA PRODUCED BY PROPIONIBACTERIUM-FREUDENREICHII AND SEVERAL INTESTINAL BACTERIA*. Journal of Dairy Science, 1994. **77**(2): p. 393-404.
14. Zeng, Z., et al., *Bacterial Microcompartment-Dependent 1,2-Propanediol Utilization Stimulates Anaerobic Growth of Listeria monocytogenes EGDe*. Frontiers in Microbiology, 2019. **10**.
15. Wisniewski, J.R., et al., *Universal sample preparation method for proteome analysis*. Nature Methods, 2009. **6**(5): p. 359-U60.

16. Cox, J., et al., *Accurate Proteome-wide Label-free Quantification by Delayed Normalization and Maximal Peptide Ratio Extraction, Termed MaxLFQ*. Molecular & Cellular Proteomics, 2014. **13**(9): p. 2513-2526.
17. Wendrich, J.R., et al., *In Vivo Identification of Plant Protein Complexes Using IP-MS/MS*, in *Plant Hormones: Methods and Protocols*, 3rd Edition, J. KleineVehn and M. Sauer, Editors. 2017. p. 147-158.
18. Smaczniak, C., et al., *Proteomics-based identification of low-abundance signaling and regulatory protein complexes in native plant tissues*. Nature Protocols, 2012. **7**(12): p. 2144-2158.
19. Tyanova, S., et al., *The Perseus computational platform for comprehensive analysis of (prote)omics data*. Nature Methods, 2016. **13**(9): p. 731-740.
20. Blighe, K., S. Rana, and M. Lewis, *EnhancedVolcano: Publication-ready volcano plots with enhanced colouring and labeling*. R package version, 2019. **1**(0).
21. Yu, G.C., et al., *clusterProfiler: an R Package for Comparing Biological Themes Among Gene Clusters*. Omics-a Journal of Integrative Biology, 2012. **16**(5): p. 284-287.
22. Vizcaino, J.A., et al., *2016 update of the PRIDE database and its related tools*. Nucleic Acids Research, 2016. **44**(D1): p. D447-D456.
23. Deptula, P., et al., *De novo assembly of genomes from long sequence reads reveals uncharted territories of Propionibacterium freudenreichii*. BMC Genomics, 2017. **18**.
24. Seeliger, S., P.H. Janssen, and B. Schink, *Energetics and kinetics of lactate fermentation to acetate and propionate via methylmalonyl-CoA or acrylyl-CoA*. FEMS Microbiology Letters, 2002. **211**(1): p. 65-70.
25. Ferlez, B., M. Sutter, and C.A. Kerfeld, *Glycyl Radical Enzyme-Associated Microcompartments: Redox-Replete Bacterial Organelles*. Mbio, 2019. **10**(1).
26. Quesada-Chanto, A., et al., *Effect of oxygen supply on biomass, organic acids and vitamin B-12 production by Propionibacterium shermanii*. World Journal of Microbiology & Biotechnology, 1998. **14**(6): p. 843-846.
27. Crowley, C.S., et al., *Structure of the PduU shell protein from the Pdu microcompartment of Salmonella*. Structure, 2008. **16**(9): p. 1324-1332.
28. Herring, T.I., et al., *A bacterial microcompartment is used for choline fermentation by Escherichia coli 536*. Journal of bacteriology, 2018. **200**(10): p. e00764-17.
29. Greening, C. and T. Lithgow, *Formation and function of bacterial organelles*. Nature Reviews Microbiology, 2020. **18**(12): p. 677-689.
30. Sutter, M., et al., *Assembly principles and structure of a 6.5-MDa bacterial microcompartment shell*. Science, 2017. **356**(6344): p. 1293-1297.
31. Bryant, M.P., *BACTERIAL SPECIES OF THE RUMEN*. Bacteriological Reviews, 1959. **23**(3): p. 125-153.
32. Xue, J.F., et al., *Exogenous or L-Rhamnose-Derived 1,2-Propanediol Is Metabolized via a pduD-Dependent Pathway in Listeria innocua*. Applied and Environmental Microbiology, 2008. **74**(22): p. 7073-7079.

33. Abdul-Rahman, F., E. Petit, and J.L. Blanchard, *The distribution of polyhedral bacterial microcompartments suggests frequent horizontal transfer and operon reassembly*. Journal of Phylogenetics & Evolutionary Biology, 2013: p. 1-7.
34. Chen, P., D.I. Andersson, and J.R. Roth, *THE CONTROL REGION OF THE PDU/COB REGULON IN SALMONELLA-TYPHIMURIUM*. Journal of Bacteriology, 1994. **176**(17): p. 5474-5482.
35. Wilson, J.W., *Manipulating microcompartment operons to study mechanism and function*. Current Opinion in Microbiology, 2021. **60**: p. 66-72.
36. Thiennimitr, P., et al., *Intestinal inflammation allows Salmonella to use ethanolamine to compete with the microbiota*. Proceedings of the National Academy of Sciences of the United States of America, 2011. **108**(42): p. 17480-17485.
37. De Weirtdt, R., et al., *Glycerol Supplementation Enhances L. reuteri's Protective Effect against S. Typhimurium Colonization in a 3-D Model of Colonic Epithelium*. Plos One, 2012. **7**(5).
38. Korbøl, J.O., et al., *Systematic association of genes to phenotypes by genome and literature mining*. Plos Biology, 2005. **3**(5): p. 815-825.
39. Meile, L., G. Le Blay, and A. Thierry, *Safety assessment of dairy microorganisms: Propionibacterium and Bifidobacterium*. International Journal of Food Microbiology, 2008. **126**(3): p. 316-320.
40. Collado, M.C., J. Meriluoto, and S. Salminen, *In vitro analysis of probiotic strain combinations to inhibit pathogen adhesion to human intestinal mucus*. Food Research International, 2007. **40**(5): p. 629-636.
41. HoJo, K., et al., *Effect of ingested culture of Propionibacterium freudenreichii ET-3 on fecal microflora and stool frequency in healthy females*. Bioscience and microflora, 2002. **21**(2): p. 115-120.
42. Satomi, K., et al., *Effects of culture-powder of Propionibacterium freudenreichii ET-3 on fecal microflora of normal adults*. Bioscience and microflora, 1999. **18**(1): p. 27-30.
43. Macfarlane, G.T. and G.R. Gibson, *Carbohydrate fermentation, energy transduction and gas metabolism in the human large intestine, in Gastrointestinal microbiology*. 1997, Springer. p. 269-318.
44. Hosseini, E., et al., *Propionate as a health-promoting microbial metabolite in the human gut*. Nutrition Reviews, 2011. **69**(5): p. 245-258.
45. RichterdaHlfors, A.A., S. Ravnum, and D.I. Andersson, *VITAMIN-B-12 REPRESSION OF THE COB OPERON IN SALMONELLA-TYPHIMURIUM - TRANSLATIONAL CONTROL OF THE CBIA GENE*. Molecular Microbiology, 1994. **13**(3): p. 541-553.
46. Sokolovskaya, O.M., A.N. Shelton, and M.E. Taga, *Sharing vitamins: Cobamides unveil microbial interactions*. Science, 2020. **369**(6499): p. 48-+.
47. Belzer, C., et al., *Microbial Metabolic Networks at the Mucus Layer Lead to Diet-Independent Butyrate and Vitamin B-12 Production by Intestinal Symbionts*. Mbio, 2017. **8**(5).



# 8

---

## General Discussion

Part of this chapter was submitted for publication:

**Zeng, Z.<sup>#</sup>**, Dank, A<sup>#</sup>, Smid, E. J., Notebaart, R. A., & Abee, T. Bacterial microcompartments in food-related microbes, *Current Opinion in Food Science* (Accepted for publication)

*Listeria monocytogenes* is a facultative anaerobe responsible for a severe infection called listeriosis, which primarily affects immunocompromised individuals [1, 2]. This foodborne pathogen can activate adaptive stress responses supporting its survival in a range of stress conditions encountered in food production and host environments [3-5]. The capacity to utilize alternative substrates for growth is crucial for *L. monocytogenes* to survive in environments when common nutrients such as glucose are unavailable [4-6]. In recent years more and more evidence has been presented that so-called Bacterial Microcompartments (BMCs) play an essential role in the utilization of such alternative substrates. These substrates include specific host-derived substrates by enteric pathogens that result from degradation of phospholipids and metabolism of mucus-derived saccharides, including ethanolamine and 1,2-propanediol. Notably, these compounds are also encountered in a wide range of food products [6-9], and could therefore also contribute to transmission of pathogens to the host [7]. It has been suggested that BMCs also play a role in *L. monocytogenes* ecophysiology and pathogenicity [5-7, 10-15], but experimental evidence supporting these claims are very scarce. Therefore, this thesis aims to unveil the role of BMC-dependent 1,2-propanediol and ethanolamine utilization in *L. monocytogenes* growth performance in anaerobic conditions, and to obtain insights into possible impacts on stress response and virulence of this foodborne pathogen.

### 8.1 Bacterial fitness and food safety

A number of studies suggest that BMC-dependent metabolism contributes to the survival of foodborne pathogens in food and food production environments [6, 7, 16, 17] (Figure 1). A functional ethanolamine (*eut*) BMC confers growth benefits for pathogenic Enterohaemorrhagic *Escherichia coli* in GI tract with mucus [18], and *Salmonella* Typhimurium in food environments such as egg yolk or milk [19]. Previous RNAseq studies on *L. monocytogenes* grown on vacuum-packed cold smoked salmon (CSS) stored at refrigeration temperature, showed increased expression of the propanediol (*pdu*) and *eut* genes which point to the contribution of *pdu* and *eut* to *L. monocytogenes* growth and/or survival in this food product [10]. CSS is rich in lipids including phosphatidylethanolamine (PE), which can be degraded by some spoilage lactic acid bacteria (LAB), with ethanolamine (EA) as one of the products [20]. Notably, enhanced growth of *L. monocytogenes* during prolonged storage of CSS was linked to increased growth of spoilage LAB [21-23], conceivably due to supply of *eut* and *pdu* BMC substrates following degradation of phospholipids by LAB. Another study showed increased expression of 17

genes of the *eut* pathway in *L. monocytogenes* grown at 4°C [24]. In line with this observation, deletion of *eutV*, that together with *eutW* constitute the two-component regulator system of the *eut* operon, also resulted in reduced growth of *L. monocytogenes* at 4°C [14]. Furthermore, a study about the regulators of *pdu/eut* found that *pocR* and *eutV/eutW* were highly induced during lactic acid exposure at pH 3.4 [25]. All of the studies mentioned here emphasized the importance of *pdu* and *eut* BMCs for fitness of *L. monocytogenes* and consequently possible food safety issues.

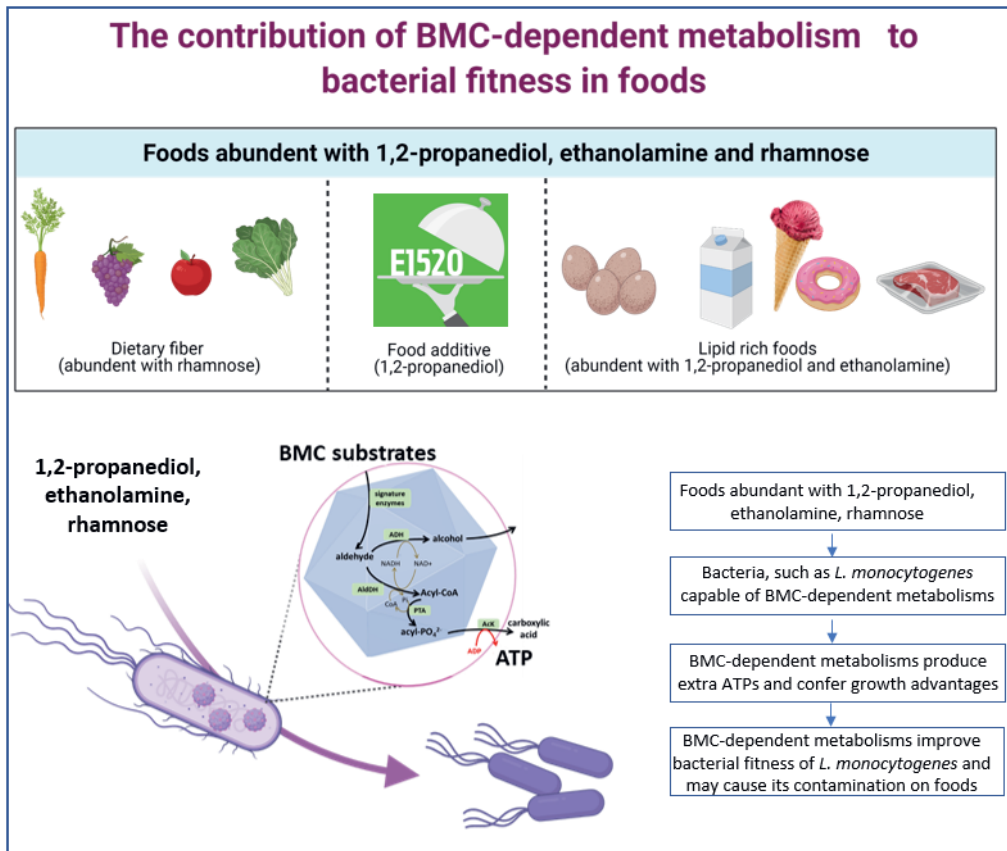


**Figure 8.1 The contribution of BMC-dependent metabolism to bacterial fitness in foods**, details in text

Our studies in chapter 2 and chapter 4 firstly examined the utilization of 1,2-propanediol and ethanolamine, and verified the formation of BMCs for 1,2-propanediol and ethanolamine utilization of *L. monocytogenes* anaerobic growth [26, 27]. The main conclusion in chapter 2 and chapter 4 is that the utilization of 1,2-propanediol and ethanolamine indeed stimulate the anaerobic growth of *L.*

*monocytogenes* which will confer an increased fitness of *L. monocytogenes* in food environments containing 1,2-propanediol and ethanolamine. Studies in defined minimal medium with 1,2-propanediol as an energy source show that the improved anaerobic growth was supported by the extra generation of ATP in the conversion of propionyl-phosphate to the end product propionate [26]. Similar to 1,2-propanediol metabolism, the improved anaerobic growth of *L. monocytogenes* grown on ethanolamine was supported by the extra generation of ATP via the oxidative ATP-producing branch to the end product acetate [27].

Notably, 1,2-propanediol is present in various foods, as it is used as a solvent carrier, humectant, thickener, emulsifier and stabilizer in food with the European food additive number E1520, in biscuits, cakes and flavored drinks [9]. Moreover 1,2-propanediol is abundant in the human GI tract where it is derived from anaerobic degradation of rhamnose or fucose by the human intestinal microbiota [7], including *Bacteroides thetaiotamicron* [28], *Anaerostipes rhamnosivorans* [29], *Bifidobacterium longum* [30] and mucus-colonizing *Akkermansia mucinophila* [31]. Ethanolamine is a product of the breakdown of phosphatidylethanolamine from bacterial and eukaryotic cell membranes and is therefore abundant in the human GI tract [16, 32]. Lipid rich foods such as egg yolk and milk including human milk contain large amounts of phosphatidylethanolamine [7]. Recent studies showed that BMC dependent substrate utilization pathways can affect composition of bacterial communities in natural environments, enabling BMC containing microbes to use a selection of carbon and/or nitrogen sources that are niche specific [33-37]. For example, corrosion by *Halanaerobium* bacteria in hydraulically fractured shales is facilitated via utilization of ethanolamine and trimethylamine (TMA) and then ethanolamine is taken up by *Methanohalophilus* bacteria which determines composition of this subterranean bacterial community [38, 39]. Regarding impact of BMC on GI microbiota, it has been reported that pathogenic *E. coli* encoding *eut* BMC, gained a competitive advantage over commensal microbiota by using ethanolamine as a nitrogen source in the bovine intestinal content [18]. This can distort the bacterial community in the GI tract resulting in overgrowth of pathogens [37]. A similar competitive advantage was found with pathogenic *S. Typhimurium* containing *eut* BMC [93] and pathogenic *E. coli* containing choline-utilizing BMC [40]. Data presented in this thesis also strongly support that BMC-dependent metabolism in *L. monocytogenes* confer a growth advantage that may contribute to its competitive fitness in the human GI tract as discussed in the next section.

Next to our studies of *pdu* BMC in propanediol grown cells, we studied rhamnose metabolism and rhamnose-derived 1,2-propanediol utilization of *L. monocytogenes* in anaerobic conditions. Our data provide evidence for another extension of the BMC-dependent metabolic repertoire of *L. monocytogenes* in anaerobic conditions, that now includes *pdu* BMC [26], *eut* BMC [27], and *pdu* BMC-stimulated rhamnose metabolism (Figure 8.1) [41]. The indicated substrates (1,2-propanediol, ethanolamine and rhamnose) can be found in a wide range of environments including foods and human GI tract [6, 7, 17, 42]. Compartmentalized metabolic pathway may confer a competitive advantage to bacteria capable of BMC-dependent metabolisms over the existing gut microbiota, which typically lack microcompartment operons and thus are unable to utilize the substrates metabolized in the microcompartments [37]. For example, the competitive fitness of *L. monocytogenes* may be enhanced by encoding BMC to metabolize these BMC substrates that are supplied by enzymatic activities of gut microbiota, such as release of ethanolamine following membrane phospholipid degradation and release of rhamnose following mucus glycan hydrolysis activity of for example *Bacteriodes* spp, and by supply of propanediol as a fermentation product, for example derived from fucose metabolism [6, 7, 16, 17, 37].

## 8.2 Stress responses and pathogenicity

The *pdu* and *eut* operons have recently been highlighted to contribute to stress response and pathogenicity of *L. monocytogenes* [5-7]. Activation of virulence factors in *L. monocytogenes* involves various proteins that are primarily regulated through transcription regulator PrfA (positive regulatory factor A) [4, 5, 43]. The activity of PrfA is modulated by certain environmental signals at the transcriptional and post-transcriptional level, which include temperature and the availability of nutrients [5, 43].

The pathogenic contributions of *pdu* and *eut* operons have been mostly studied in *Salmonella* spp. (recently reviewed in [7]). Using animal models, evidence for functionality of *pdu* and *eut* operons in *S. Typhimurium* pathogenesis was presented [7]. The upregulation of *pdu* and *eut* operon was demonstrated to enhance the *S. Typhimurium* colonisation of the chicken caecum [44]. *S. Enteritidis* grown in *eut* operon-inducing egg yolk medium also showed increased colonisation in a mouse colitis model [45]. Deletion mutants of the *eutR* regulator for *eut* operon and *pocR* regulator for *pdu* operon

attenuated *S. Typhimurium* replication in a *Caenorhabditis elegans* model [19]. Contribution of BMC-dependent metabolism to pathogenicity has been linked eut BMC conferred intraluminal growth advantage for *S. Typhimurium* in a mouse colitis model via triggering the SPI-2 pathogenicity island encoding tetrathionate reductase. [7, 46, 47]. During colonization, effector molecules cause inflammation of the intestine subsequently forming tetrathionate [48]. Tetrathionate is utilized as the electron acceptor by selected tetrathionate reductase positive, *eut* operon-containing organisms, conferring a distinct competitive advantage, in conjunction with 1,2-propanediol, also found in the gut [37, 46]. Notably, *L. monocytogenes* lacks tetrathionate reductase, but anaerobic electron transfer with fumarate reduction via membrane-bound fumarate reductase [49] and recently described flavin-based extracellular electron transfer (EET) with  $\text{Fe}^{3+}$  as an electron acceptor [50], could act as substitutes in BMC-dependent EA catabolism. In chapter 4, we provide evidence that *L. monocytogenes* copes with this by linking eut BMC activity to flavin-based extracellular electron transfer (EET) using iron as an electron acceptor [27]. Use of EET increases flux and ATP generation in the oxidative branch of *eut* and *pdu* BMC, and this conceivably enhances growth and competitive fitness of opportunistic pathogens such as *Salmonella* and *L. monocytogenes* in anaerobic conditions such as encountered in the (inflamed) GI tract [37].

Evidence for a role of BMC in *L. monocytogenes* pathogenicity, was obtained in studies using a *pduD* deletion mutant, that showed attenuated virulence and faster clearing of *L. monocytogenes* in the GI tract which indicates the importance of *pdu* for the fitness of *L. monocytogenes* during infection in the GI tract [15]. *L. monocytogenes* EGDe virulence in a mouse infection model is also reduced by knocking out *eutB* (encoding the ethanolamine ammonia-lyase subunit) [13]. The importance of *eut* and *pdu* activation in stress survival and virulence of *L. monocytogenes* was highlighted in recent reviews [6]. Next to the experimental evidence including metabolic and proteomic analysis, combined with transmission electron microscopy, for activation of *L. monocytogenes pdu* and *eut* BMCs and corresponding growth stimulation in anaerobic conditions (Chapter 6, [26, 27]), Chapter 6 provides evidence for shared and specific metabolic, stress resistance and virulence associated responses at proteome level in *pdu* and *eut* BMC primed *L. monocytogenes* cells. Shared stress responses include activation of stress defense proteins and SOS DNA damage repair enzymes [51, 52], conceivably linked to activation and selected expression of previously described

lysogenic prophage A118 gene cluster. Majority of *L. monocytogenes* strains have prophages in their genome, including A118 and A118-like prophages such as those found in *L. monocytogenes* 10403S [53-55]. Pasechnik et al. [55] recently provided evidence for temperature-dependent activation of lysogeny as a bacteria-phage adaptive response in the mammalian environment. Since in our studies we used *L. monocytogenes* EGDe grown at 30°C, mimicking priming of *pdu* and *eut* BMCs before entering the human host for example during transmission in foods, future experiments should also include cells primed at 37°C to mimic activation of BMCs inside the mammalian host [56]. Inclusion of multiple *L. monocytogenes* strains, without and with lysogenic prophages, will further add to our understanding of mechanisms underlying production and functionality of *pdu* and *eut* BMCs in *L. monocytogenes* competitive fitness and survival during transmission in the food chain and inside the mammalian host. In chapter 5, our data showing utilization of rhamnose-derived 1,2-propanediol with vitamin B12, may suggest that rhamnose *pdu* BMC activation in the GI tract can increase competitive fitness of *L. monocytogenes* and increase the likelihood of successful invasion into the intestinal epithelium [6]. In chapter 5, presented results show that rhamnose *pdu* BMC induced cells similar to *eut* and *pdu* BMC induced cells, showed significantly higher Caco-2 translocation efficacy, while adhesion and invasion were similar to that of non-induced rhamnose grown cells. Proteomics analysis showed significantly upregulated proteins of *pdu* BMC on rhamnose indicating ribosomal regulation and activation of glutathione synthase GshF. The later enzyme GshF was recently shown to play an important role in the production of intracellular glutathione that acts in redox stress defense and as the allosteric activator of PrfA [57]. Insights obtained in chapters 5 and 6, indicate that *eut* and (rhamnose) *pdu* BMC activation is associated with enhanced Caco-2 cell translocation efficacy, but virulence factors involved and underlying mechanisms of presumed transcellular and/or paracellular transport of *L. monocytogenes* cells remain to be elucidated [56].

### 8.3 Recent structural insights of BMC shell proteins

Bacterial microcompartments (BMCs) are self-assembling prokaryotic organelles consisting of a polyhedral proteinaceous shell and encapsulated enzymes [17, 58-60]. The homologous hexameric shell proteins form facets of BMC while pentameric proteins form the vertices of a polyhedral shell [60, 61]. Recent structural data have highlighted small variations in the sequence and topology of BMC shell proteins, emphasizing how variation and specialization enable the

construction of complex molecular devices. BMCs are typically about 40–200 nm in diameter and are made of three types of shell proteins: hexamers (BMC-H), pseudo-hexamers (BMC-T), and pentamers (BMC-P) [59, 61, 62]. Hexamers and pseudo-hexamers are formed by the classical BMC shell proteins containing the Pf00936 domain, while pentamers are formed by the non-classical BMC shell proteins containing the Pf03319 domain [26, 63]. Whereas BMC-H and BMC-T proteins constitute the facets of the shells, pentameric proteins are required to cap the vertices of the polyhedral shell [59, 61, 62, 64]. The third conserved building block, the BMC-P proteins, contains a single Pfam03319 domain and assembles into cyclical pentamers [59, 61, 62, 64]. All BMCs exhibit some common building principles: self-assembly, encapsulation, modularity, shell permeability, and structural plasticity [59].

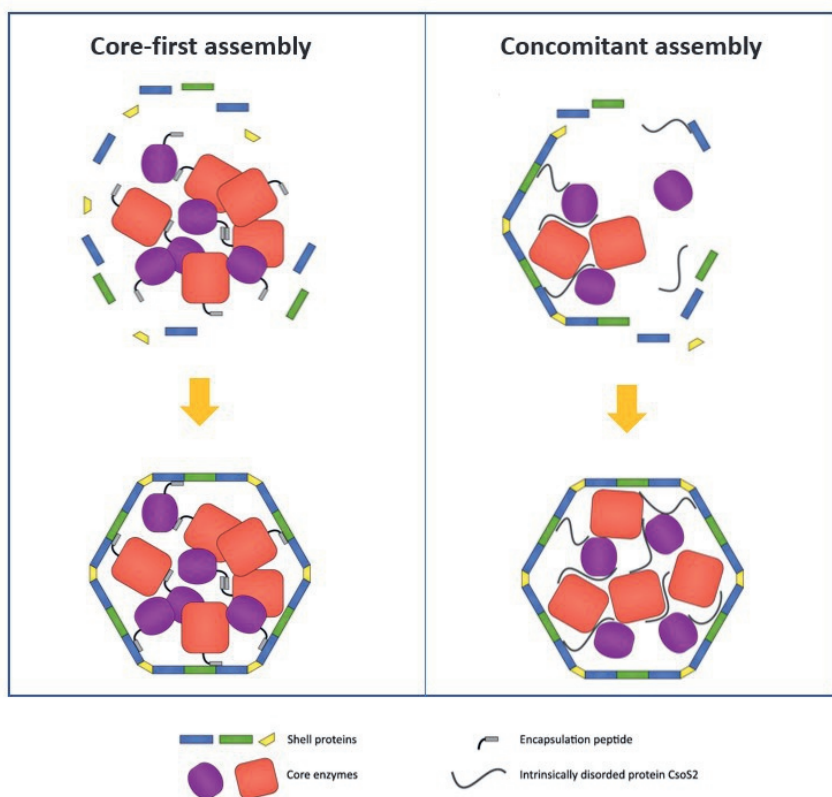


**Figure 8.2 Assembly process of BMCs. Core-first assembly** (Adapted from Kirst and Kerfeld [36]): Aggregation of the core enzymes is facilitated by the encapsulation peptide in combination with other assembly proteins. After aggregation the encapsulation peptide interacts with the shell proteins to form a complete BMC. **Concomitant assembly**: simultaneous core aggregation and shell protein recruitment is enabled by the intrinsically disordered protein such as CsoS2 in alpha carboxysomes.

Based on the structural studies of carboxysomes, the self-assembly mechanism of BMC is postulated in two ways, one where enzymatic cargo coalesces and then is encapsulated by the shell proteins (Core-first assembly) [65], and the other, where cargo and shell assemble simultaneously (Concomitant assembly) [66]. In the core-first assembly, aggregation of the core enzymes is facilitated by the encapsulation peptide in combination with other assembly proteins. After aggregation the encapsulation peptide interacts with the shell proteins to form a complete BMC. In the concomitant assembly, simultaneous core aggregation and shell protein are recruited by the intrinsically disordered protein. In the formation of BMCs, a key role is played by encapsulation peptide (EP) sequences [67, 68]. EPs are small, 10–20 residue-long amphipathic  $\alpha$ -helices that are attached to the core enzymes N- or C-terminally or inside the flexible surface loops [69, 70]. Based on the amphipathic  $\alpha$ -helices features of EP, we predicted and identified the specific hydrophobic  $\alpha$ -helix in the N terminus of the encapsulated enzyme PduD, PduQ and PduP in *pdu* BMC of *L. monocytogenes*. Similar to *pdu* BMC, the specific hydrophobic  $\alpha$ -helix in the N terminus of the encapsulated enzymes EutC, EutD, and EutE are predicted as EPs, aligned with those of the previously described BMC-encapsulated proteins in *S. Typhimurium* [60, 67, 70]. Computational modelling unveiled that shell size depends on interaction strengths, subunit stoichiometry, and initial conditions [70]. The central pores of BMC shell proteins provide routes for the diffusion of molecules including cofactors and electron across the BMC shell [60]. The identified *L. monocytogenes* *eut* lmo1185 shell protein belongs to the class of trimeric shell proteins (BMC-T) with two fused Pfam00936 domains. We hypothesize that this predicted PduT-like shell protein with a [4Fe-4S] cluster [71] acts as a redox carrier in this process. Further studies are required to elucidate the role of this *eut* BMC shell protein as a redox carrier [27]. BMC shell proteins display a surprising degree of flexibility which is particularly caused by permuted BMC shell proteins [60]. The structural variations of BMCs and flexible protein-protein interactions may enable fine tuning of BMC assembly and shell permeability in response to a varying environment [59].

A great deal of structural studies focused on the BMC shell proteins assembly and BMC flexibility [33–35, 58–60, 72], the encapsulation mechanism of encapsulated enzymes into BMC shell remains murky (as indicated in Figure 8.2). We have designed experiments to investigate the potential encapsulation mediated by encapsulation peptide (EP) (data are not included in this thesis). The enzyme EutE

with predicted EP and the enzyme EutQ without EP are purified to test their *in vitro* binding with three types of shell proteins as shown in Table 8.1. Our ongoing study involves X-ray crystallography to unveil the structures of the protein interaction between encapsulated enzymes and shell proteins.

**Table 8.1 Purified Proteins to test the proteins interaction between encapsulated enzymes and shell proteins**

Purified Proteins	Proteins Annotation
EutK	shell protein, BMC-H type,
Lmo1185	shell protein, BMC-T type,
EutN	shell protein, BMC-P type,
EutE	enzyme with encapsulation peptide
EutQ	enzyme without encapsulation peptide

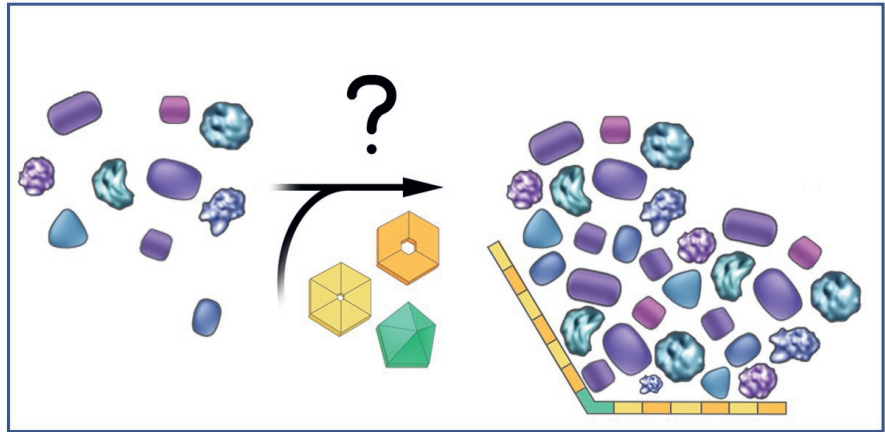


**Figure 8.2 Question about how to encapsulate enzymes into BMC,** adapted from Thom Graves, details in text

8.4 Bioengineering application

Recombineering, DNA synthesis technology, and advanced cloning techniques have all been applied in creative ways to study the nature of BMC mechanism and function. BMCs have been engineered and applied in serving as nano-factories for biochemical production or as novel drug delivery devices [17, 33, 36, 58, 73]. The bioengineering of BMCs was firstly reported in transplanting the *pdu* BMC locus from *Citrobacter freundii* to *E. coli* which enable *E. coli* to grow on propanediol [74]. Taking advantage of the self-assembly process, many recent efforts have emphasized the engineering of BMCs to encapsulate new pathways

for improved function of heterologous metabolic production [33, 36, 58, 73, 75-77].

The methods to manipulate BMC need to be developed enable the modification of BMC locus and BMC structures, such as loading heterologous cargo, engineering the permeability of the pores, and controlling the assembly process. To encapsulate the non-endogenous cargo enzymes, native encapsulation peptides have been fused to heterologous cargo in order to target them into the lumen of the shells [36, 73, 75, 78, 79]. The signal sequences of encapsulation peptide have been identified and characterized for the Pdu enzymes PduD [80], PduL [81], and PduP [68]; and the Eut enzymes EutC and EutE [82], among other putative tags. These signal sequences largely follow a common motif, which has informed the design of de novo signal sequences [58]. Danielle Tullman-Ercek et. al, expanded a novel leucine-zipper motif can function as a signal sequence for microcompartment localization [79]. To construct effective synthetic BMCs, the shell permeability would need to be tuned to fit its catalytic function [36]. To enhance the shell proteins' selectivity; a redox active [4Fe-4S] cluster has been incorporated into a BMC-T pore to enable electron flow across the shell [71, 83], which is aligned with our predicted electron transfer pore of shell protein Lmo1185 [27]. Recent efforts to assemble BMC shells *in vitro* will facilitate the understanding of BMC assembly mechanism and then apply to the control of BMC assembly [84].

The potential to form such functional architectures from a single, modulated building block can be applied as a powerful tool for the future of metabolic engineering. The modular metabolisms in compartmentalized BMCs will provide unique advantages, such as increasing pathway efficiency, avoiding metabolite cross-talk, improving enzyme kinetics through creating a private pool and maximizing substrate specificity and minimizing metabolite damage [36]. Targeting the genetically fused cargo to the lumen of BMC shell is a predominate strategy used in several studies [58, 68, 85, 86]. Significantly, the *Citrobacter freundii pdu* BMC can be produced as an empty compartment through the coordinated production of only the shell proteins [86]. Enzymes can then be targeted so that they are incorporated into the BMC through the fusion of peptide sequences that are found at the N-terminus of proteins such as PduD (D18) and PduP (P18) [67, 80]. Targeting of the *Zymomonas mobilis* pyruvate decarboxylase and alcohol dehydrogenase resulted in the conversion of the Pdu BMC into an ethanol bioreactor [68]. Matthew J. L et al, redesigned *pdu* BMC into a 1,2-

propanediol synthesising factory using glycerol as the starting material and added N-terminal targeting peptides to glycerol dehydrogenase, dihydroxyacetone kinase, methylglyoxal synthase and 1,2-propanediol oxidoreductase [85]. Further development of these hexamer-based BMCs will not only benefit metabolic engineering efforts towards bioproduction of small molecule products, but also enable detailed study of how encapsulation versus colocalization impacts pathway performance [58].

BMC shells also have the potential to function as nanocarrier for biomedicine. Nanomedicine includes the development of nanoparticles to serve as drug-delivery systems and platforms for designer vaccines [36, 87, 88]. For example, shell proteins could be engineered to incorporate an array of suitable peptides already developed for existing nanoparticles to facilitate active targeting of the shell to pathogens or cancer cells, tumour and cell penetration, and endosomal escape [36, 58]. BMC shells are geometrically similar to icosahedral viruses and also have roughly the same size, ranging from 40 to 200 nm in diameter depending on the type of BMC [17, 33, 60]. The BMC structures we observed in *L. monocytogenes* aligned with previous BMC structures in *Salmonella* species and *Haliangium ochraceum* are formed in homogeneous particles of 40 nm diameter, which is very similar to virus-like particles currently used as scaffolds in biomedical engineering [36]. The *Haliangium ochraceum* BMC shell can tolerate peptide fusions to its constituent proteins, allowing for its efficient assembly, and permitting the presentation of a diverse set of antigens [84, 89]. This flexibility in modifying different shell proteins in combination with the *in vitro* assembly method would allow high throughput screening of different combinations and densities of antigens for the most potent immune response [36]. While there are still challenges and open questions regarding antigenicity of BMC, BMC assembly, encapsulation mechanism, and permeability, scientists are poised to address them and put these exciting organelles to apply BMC as nanocarrier for biomedicine.

### 8.5 Future perspectives

**Role of BMCs in *L. monocytogenes* growth in foods.** This thesis demonstrates that BMC-dependent metabolism including the utilization of 1,2-propanediol, ethanolamine and rhamnose can stimulate the anaerobic growth of *L. monocytogenes* [26, 27, 41]. Further research is required to unveil the molecular mechanisms and significance of *eut* and (rhamnose) *pdu* BMC in *L.*

*monocytogenes* transmission in foods, including impact on growth and survival in different food matrixes, and interactions with co-microbiota, especially other food spoilage bacteria. Cold smoked salmon is of special interest due to the large number of listeriosis cases associated with this food product [90-93]. Previous studies describing activation of *L. monocytogenes eut* and *pdu* gene expression in vacuum-packed cold smoked salmon [10, 21, 92], could be extended with studies in filter-sterilized cold smoked salmon-based medium derived following stomacher treatment. Such studies can shed light on roles of *L. monocytogenes pdu* and *eut* BMC in anaerobic growth on cold smoked salmon, and whether LAB can supply phospholipid degradation products as substrates for this pathogen. *L. monocytogenes* also increased expression of the *pdu* gene cluster in co-culture biofilm with *Bacillus subtilis* as well as in co-culture with *Brevibacterium* spp. isolated from cheese [94, 95]. All these observations point to a possible role of *eut* and *pdu* BMC in *L. monocytogenes* growth and survival in food matrixes, that can affect contamination levels reached by this foodborne pathogen. A thorough study of the role of co-microbiota in selected foods, may reveal whether and how these affect *L. monocytogenes* performance in foods, and consequently affect food quality and safety issues.

**Role of BMCs in *L. monocytogenes* interaction with the host.** Most of the known BMC substrates including 1,2-propanediol, ethanolamine and rhamnose are constantly produced in the human intestine by bacterial metabolism of food or host cell components [7]. In Chapter 5 and 6 we present evidence that the activation of BMC-dependent metabolism in *L. monocytogenes* significantly improved its translocation efficiency across Caco-2 human intestinal epithelial cell line compared to BMC non-induced *L. monocytogenes* cells. Our studies based on the *in vitro* assay of *L. monocytogenes* interaction with Caco-2 cells are not sufficient to understand the potential of BMC-dependent metabolisms on *L. monocytogenes* intestinal fitness and even its competition against gut microbiota. As mentioned before, the main reported evidence for contribution of BMC-dependent metabolism to microbial pathogenicity was the demonstration that a functional *eut* operon conferred an intraluminal growth advantage for *S. Typhimurium* in a mouse colitis model in combination with triggering of SPI-2 pathogenicity island encoding tetrathionate reductase [7, 46, 47]. To understand the mechanisms underlying conceivable impact of BMC-dependent substrate metabolism on *L. monocytogenes* intestinal (competitive) fitness, additional studies are required, for example using *pdu* and *eut* BMC-induced cells, in

combination with selected deletion mutants, and assess their performance in different mouse models. Additional parameters can be included, such as the impact of a high fat diet on *L. monocytogenes* infection capacity, as recently reported by las Heras et al. [96]. These authors investigated the influence of a high-fat diet upon parameters that influence *L. monocytogenes* infection in mice. Their results showed that short-term consumption of a westernized diet has the capacity to significantly alter host susceptibility to *L. monocytogenes* infection concomitant with changes to the host intestinal microbiota and physiological landscape. Based on their findings they suggest that diet should be a consideration when developing models that reflect human infectious disease. In addition, availability of micronutrients and divalent metals, especially iron, may affect competitive fitness of microbiota. In chapter 4, we provide evidence that *L. monocytogenes* *eut* BMC dependent metabolism via the oxidative ATP generating acetate branch is two-fold higher than via the NADH regenerating ethanol producing branch, by linking BMC activity to flavin-based extracellular electron transfer (EET) using iron as an electron acceptor [27]. This suggests that EET-linked BMC-dependent metabolism may further enhance competitive fitness and survival of *L. monocytogenes* in anaerobic conditions in the disbalanced/inflamed GI tract [37].

***L. monocytogenes* BMC structures and functionality.** The *pdu* and *eut* operon in *L. monocytogenes* can be used in further studies in synthetic biology, to design and engineer BMCs with specialized functions. As we mentioned before, the *pdu* and *eut* operon are strictly controlled by a complex regulation network involved with RNA-mediated regulation (B12-dependent riboswitch) and protein-mediated regulation (two-component regulation system) [97-99]. The *pdu* and *eut* operon in *L. monocytogenes* is just about 39 Kilobase in size (from *lmo1142* to *lmo1187*) which is very condensed taken into account the number of encoded shell proteins and encapsulated enzymes [26, 100]. Recently developed Cas9-assisted cloning of large gene cluster will allow to manipulate BMC operon to study assembly mechanism and test functionality *in vitro* [101]. All these unique features of the *pdu* and *eut* operon in *L. monocytogenes* meet the engineering need to re-design BMC. It has been clearly demonstrated that heterologous proteins can be specifically targeted to BMCs, thus opening the possibility of designing BMCs for desired applications involving tailored metabolic pathways, sequestration of specific target proteins, and purification of compartmentalized protein collections [33]. Further understanding of protein-protein interactions of

shell proteins and encapsulated enzymes via X-ray crystallography, will add to our understanding of BMC synthesis and organisation, and can facilitate loading heterologous cargo into BMC lumen. Furthermore, the isolation of the native BMC particles from BMC-induced *L. monocytogenes* cells via sucrose gradient ultracentrifugation as previously reported for carboxysomes [102] will increase our understanding of BMC structure, protein stoichiometry and enzymatic activity.

All these aspects highlight the relevance and need to further study the diversity and functionality of BMCs, and to define in more detail their roles in health and disease.

## 8.7 References

1. Radoshevich, L. and P. Cossart, *Listeria monocytogenes: towards a complete picture of its physiology and pathogenesis*. Nature Reviews Microbiology, 2018. **16**(1): p. 32.
2. Farber, J. and P. Peterkin, *Listeria monocytogenes, a food-borne pathogen*. Microbiology and Molecular Biology Reviews, 1991. **55**(3): p. 476-511.
3. NicAogáin, K. and C.P. O'Byrne, *The role of stress and stress adaptations in determining the fate of the bacterial pathogen Listeria monocytogenes in the food chain*. Frontiers in microbiology, 2016. **7**: p. 1865.
4. Freitag, N.E., G.C. Port, and M.D. Miner, *Listeria monocytogenes—from saprophyte to intracellular pathogen*. Nature Reviews Microbiology, 2009. **7**(9): p. 623-628.
5. Radoshevich, L. and P. Cossart, *Listeria monocytogenes: towards a complete picture of its physiology and pathogenesis*. Nature Reviews Microbiology, 2018. **16**(1): p. 32-46.
6. Anast, J.M., T.A. Bobik, and S. Schmitz-Esser, *The Cobalamin-dependent gene cluster of Listeria monocytogenes: implications for virulence, stress response, and food safety*. Frontiers in microbiology, 2020. **11**.
7. Prentice, M.B., *Bacterial microcompartments and their role in pathogenicity*. Current Opinion in Microbiology, 2021. **63**: p. 19-28.
8. Authority, E.F.S., E.C.f.D. Prevention, and Control, *The European Union summary report on trends and sources of zoonoses, zoonotic agents and food-borne outbreaks in 2017*. EFSA Journal, 2018. **16**(12): p. e05500.
9. Younes, M., et al., *Re-evaluation of propane-1,2-diol alginate (E 405) as a food additive*. Efsa Journal, 2018. **16**(7).
10. Tang, S., et al., *Transcriptomic analysis of the adaptation of Listeria monocytogenes to growth on vacuum-packed cold smoked salmon*. Appl. Environ. Microbiol., 2015. **81**(19): p. 6812-6824.
11. Schmid, B., et al., *Role of cold shock proteins in growth of Listeria monocytogenes under cold and osmotic stress conditions*. Applied and environmental microbiology, 2009. **75**(6): p. 1621-1627.

12. Chiara, M., et al., *Comparative genomics of Listeria sensu lato: genus-wide differences in evolutionary dynamics and the progressive gain of complex, potentially pathogenicity-related traits through lateral gene transfer*. Genome biology and evolution, 2015. **7**(8): p. 2154-2172.
13. Joseph, B., et al., *Identification of Listeria monocytogenes genes contributing to intracellular replication by expression profiling and mutant screening*. Journal of bacteriology, 2006. **188**(2): p. 556-568.
14. Chan, Y.C., et al., *Contributions of two-component regulatory systems, alternative  $\sigma$  factors, and negative regulators to Listeria monocytogenes cold adaptation and cold growth*. Journal of food protection, 2008. **71**(2): p. 420-425.
15. Schardt, J., et al., *Comparison between Listeria sensu stricto and Listeria sensu lato strains identifies novel determinants involved in infection*. Scientific reports, 2017. **7**(1): p. 17821.
16. Kaval, K.G. and D.A. Garsin, *Ethanolamine utilization in bacteria*. mBio, 2018. **9**(1): p. e00066-18.
17. Kerfeld, C.A., et al., *Bacterial microcompartments*. Nature Reviews Microbiology, 2018.
18. Bertin, Y., et al., *Enterohaemorrhagic Escherichia coli gains a competitive advantage by using ethanolamine as a nitrogen source in the bovine intestinal content*. Environmental microbiology, 2011. **13**(2): p. 365-377.
19. Srikumar, S. and T.M. Fuchs, *Ethanolamine utilization contributes to proliferation of Salmonella enterica serovar Typhimurium in food and in nematodes*. Applied and environmental microbiology, 2011. **77**(1): p. 281-290.
20. Gänzle, M.G., N. Vermeulen, and R.F. Vogel, *Carbohydrate, peptide and lipid metabolism of lactic acid bacteria in sourdough*. Food microbiology, 2007. **24**(2): p. 128-138.
21. Gimenez, B. and P. Dalgaard, *Modelling and predicting the simultaneous growth of Listeria monocytogenes and spoilage micro-organisms in cold-smoked salmon*. Journal of applied microbiology, 2004. **96**(1): p. 96-109.
22. Lappi, V.R., et al., *Prevalence and growth of Listeria on naturally contaminated smoked salmon over 28 days of storage at 4 C*. Journal of food protection, 2004. **67**(5): p. 1022-1026.
23. Løvdal, T., *The microbiology of cold smoked salmon*. Food Control, 2015. **54**: p. 360-373.
24. Hingston, P., et al., *Strand specific RNA-sequencing and membrane lipid profiling reveals growth phase-dependent cold stress response mechanisms in Listeria monocytogenes*. PLoS One, 2017. **12**(6): p. e0180123.
25. Cortes, B.W., et al., *Transcriptome sequencing of Listeria monocytogenes reveals major gene expression changes in response to lactic acid stress exposure but a less pronounced response to oxidative stress*. Frontiers in microbiology, 2020. **10**: p. 3110.

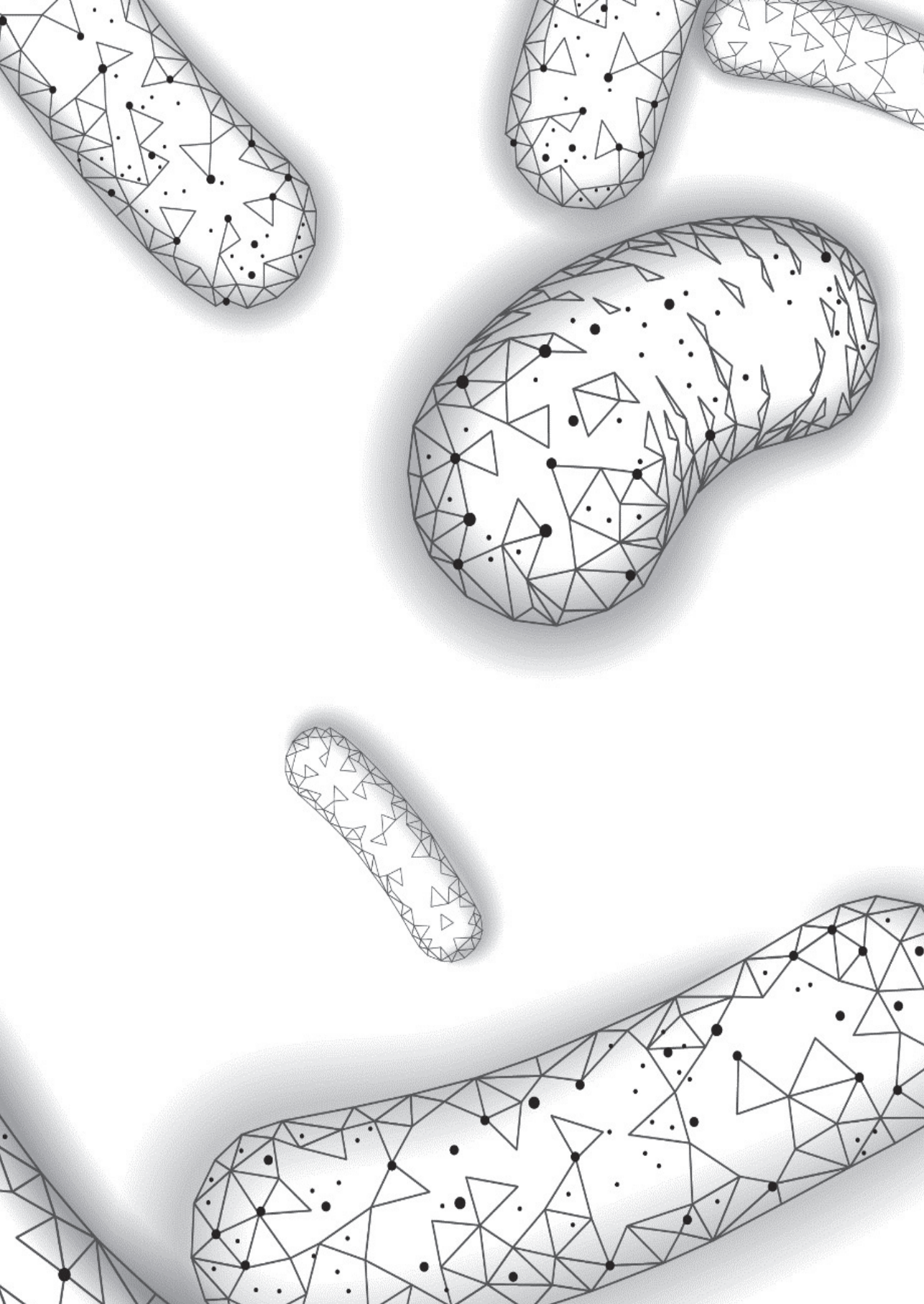
26. Zeng, Z., et al., *Bacterial microcompartment-dependent 1, 2-propanediol utilization stimulates anaerobic growth of Listeria monocytogenes* EGDe. *Frontiers in Microbiology*, 2019. **10**: p. 2660.
27. Zeng, Z., et al., *Bacterial Microcompartments Coupled with Extracellular Electron Transfer Drive the Anaerobic Utilization of Ethanolamine in Listeria monocytogenes*. *mSystems*, 2021. **6**(2).
28. Ng, K.M., et al., *Microbiota-liberated host sugars facilitate post-antibiotic expansion of enteric pathogens*. *Nature*, 2013. **502**(7469): p. 96-+.
29. Louis, P. and H.J. Flint, *Formation of propionate and butyrate by the human colonic microbiota*. *Environmental Microbiology*, 2017. **19**(1): p. 29-41.
30. Bunesova, V., C. Lacroix, and C. Schwab, *Fucosyllactose and L-fucose utilization of infant Bifidobacterium longum and Bifidobacterium kashiwanohense*. *Bmc Microbiology*, 2016. **16**.
31. Belzer, C., et al., *Microbial Metabolic Networks at the Mucus Layer Lead to Diet-Independent Butyrate and Vitamin B-12 Production by Intestinal Symbionts*. *Mbio*, 2017. **8**(5).
32. Garsin, D.A., *Ethanolamine utilization in bacterial pathogens: roles and regulation*. *Nature Reviews Microbiology*, 2010. **8**(4): p. 290-295.
33. Wilson, J.W., *Manipulating microcompartment operons to study mechanism and function*. *Current Opinion in Microbiology*, 2021. **60**: p. 66-72.
34. Sutter, M., et al., *A catalog of the diversity and ubiquity of bacterial microcompartments*. *Nature Communications*, 2021. **12**(1): p. 1-12.
35. Stewart, A.M., et al., *Advances in the World of Bacterial Microcompartments*. *Trends in Biochemical Sciences*, 2021.
36. Kirst, H. and C.A. Kerfeld, *Bacterial microcompartments: catalysis-enhancing metabolic modules for next generation metabolic and biomedical engineering*. *BMC biology*, 2019. **17**(1): p. 1-11.
37. Jakobson, C.M. and D. Tullman-Ercek, *Dumpster diving in the gut: bacterial microcompartments as part of a host-associated lifestyle*. *PLoS pathogens*, 2016. **12**(5): p. e1005558.
38. Borton, M.A., et al., *Coupled laboratory and field investigations resolve microbial interactions that underpin persistence in hydraulically fractured shales*. *Proceedings of the National Academy of Sciences*, 2018. **115**(28): p. E6585-E6594.
39. Mouser, P.J., et al., *Hydraulic fracturing offers view of microbial life in the deep terrestrial subsurface*. *FEMS microbiology ecology*, 2016. **92**(11).
40. Herring, T.I., et al., *A bacterial microcompartment is used for choline fermentation by Escherichia coli 536*. *Journal of bacteriology*, 2018. **200**(10): p. e00764-17.
41. Zeng, Z., et al., *Anaerobic Growth of Listeria monocytogenes on Rhamnose Is Stimulated by Vitamin B(12) and Bacterial Microcompartment-Dependent 1,2-Propanediol Utilization*. *mSphere*, 2021: p. e0043421.
42. Yeates, T.O., et al., *Protein-based organelles in bacteria: carboxysomes and related microcompartments*. *Nature Reviews Microbiology*, 2008. **6**(9): p. 681.

43. de las Heras, A., et al., *Regulation of Listeria virulence: PrfA master and commander*. Current opinion in microbiology, 2011. **14**(2): p. 118-127.
44. Harvey, P., et al., *Salmonella enterica serovar Typhimurium colonizing the lumen of the chicken intestine grows slowly and upregulates a unique set of virulence and metabolism genes*. Infection and immunity, 2011. **79**(10): p. 4105-4121.
45. Moreau, M.R., et al., *Growth in egg yolk enhances Salmonella Enteritidis colonization and virulence in a mouse model of human colitis*. PLoS One, 2016. **11**(3): p. e0150258.
46. Thiennimitr, P., et al., *Intestinal inflammation allows Salmonella to use ethanolamine to compete with the microbiota*. Proceedings of the National Academy of Sciences, 2011. **108**(42): p. 17480-17485.
47. Bruno, V.M., et al., *Salmonella Typhimurium type III secretion effectors stimulate innate immune responses in cultured epithelial cells*. PLoS pathogens, 2009. **5**(8): p. e1000538.
48. Chowdhury, C., et al., *Diverse bacterial microcompartment organelles*. Microbiology and Molecular Biology Reviews, 2014. **78**(3): p. 438-468.
49. Light, S.H., et al., *Extracellular electron transfer powers flavinylated extracellular reductases in Gram-positive bacteria*. Proceedings of the National Academy of Sciences, 2019. **116**(52): p. 26892-26899.
50. Light, S.H., et al., *A flavin-based extracellular electron transfer mechanism in diverse Gram-positive bacteria*. Nature, 2018. **562**(7725): p. 140.
51. van der Veen, S., et al., *The SOS response of Listeria monocytogenes is involved in stress resistance and mutagenesis*. Microbiology-Sgm, 2010. **156**: p. 374-384.
52. van der Veen, S., et al., *The heat-shock response of Listeria monocytogenes comprises genes involved in heat shock, cell division, cell wall synthesis, and the SOS response*. Microbiology-Sgm, 2007. **153**: p. 3593-3607.
53. Loessner, M.J., et al., *Complete nucleotide sequence, molecular analysis and genome structure of bacteriophage A118 of Listeria monocytogenes: implications for phage evolution*. Molecular Microbiology, 2000. **35**(2): p. 324-340.
54. Rabinovich, L., et al., *Prophage Excision Activates Listeria Competence Genes that Promote Phagosomal Escape and Virulence*. Cell, 2012. **150**(4): p. 792-802.
55. Pasechnik, A., et al., *Active Lysogeny in Listeria Monocytogenes Is a Bacteria-Phage Adaptive Response in the Mammalian Environment*. Cell Reports, 2020. **32**(4).
56. Gahan, C. and C. Hill, *Gastrointestinal phase of Listeria monocytogenes infection*. Journal of Applied Microbiology, 2005. **98**(6): p. 1345-1353.
57. Reniere, M.L., A.T. Whiteley, and D.A. Portnoy, *An in vivo selection identifies Listeria monocytogenes genes required to sense the intracellular environment and activate virulence factor expression*. PLoS pathogens, 2016. **12**(7): p. e1005741.

58. Kennedy, N.W., et al., *Bacterial microcompartments: tiny organelles with big potential*. Current Opinion in Microbiology, 2021. **63**: p. 36-42.
59. Liu, L.-N., et al., *Protein stoichiometry, structural plasticity and regulation of bacterial microcompartments*. Current Opinion in Microbiology, 2021. **63**: p. 133-141.
60. Ochoa, J.M. and T.O. Yeates, *Recent structural insights into bacterial microcompartment shells*. Current Opinion in Microbiology, 2021. **62**: p. 51-60.
61. Sutter, M., et al., *Assembly principles and structure of a 6.5-MDa bacterial microcompartment shell*. Science, 2017. **356**(6344): p. 1293-1297.
62. Kerfeld, C.A., et al., *Protein structures forming the shell of primitive bacterial organelles*. Science, 2005. **309**(5736): p. 936-938.
63. Axen, S.D., O. Erbilgin, and C.A. Kerfeld, *A taxonomy of bacterial microcompartment loci constructed by a novel scoring method*. PLoS computational biology, 2014. **10**(10): p. e1003898.
64. Tanaka, S., et al., *Atomic-level models of the bacterial carboxysome shell*. Science, 2008. **319**(5866): p. 1083-1086.
65. Cameron, J.C., et al., *Biogenesis of a bacterial organelle: the carboxysome assembly pathway*. Cell, 2013. **155**(5): p. 1131-1140.
66. Iancu, C.V., et al., *Organization, structure, and assembly of  $\alpha$ -carboxysomes determined by electron cryotomography of intact cells*. Journal of molecular biology, 2010. **396**(1): p. 105-117.
67. Fan, C., et al., *Short N-terminal sequences package proteins into bacterial microcompartments*. Proceedings of the National Academy of Sciences, 2010. **107**(16): p. 7509-7514.
68. Lawrence, A.D., et al., *Solution structure of a bacterial microcompartment targeting peptide and its application in the construction of an ethanol bioreactor*. ACS synthetic biology, 2014. **3**(7): p. 454-465.
69. Kalnins, G., et al., *Encapsulation mechanisms and structural studies of GRM2 bacterial microcompartment particles*. Nature communications, 2020. **11**(1): p. 1-13.
70. Mohajerani, F. and M.F. Hagan, *The role of the encapsulated cargo in microcompartment assembly*. PLoS computational biology, 2018. **14**(7): p. e1006351.
71. Pang, A., M.J. Warren, and R.W. Pickersgill, *Structure of PduT, a trimeric bacterial microcompartment protein with a 4Fe-4S cluster-binding site*. Acta Crystallographica Section D: Biological Crystallography, 2011. **67**(2): p. 91-96.
72. Kennedy, N.W., et al., *Self-assembling shell proteins PduA and PduJ have essential and redundant roles in bacterial microcompartment assembly*. Journal of Molecular Biology, 2021. **433**(2): p. 166721.
73. Young, E.J., et al., *Engineering the bacterial microcompartment domain for molecular scaffolding applications*. Frontiers in microbiology, 2017. **8**: p. 1441.

74. Parsons, J.B., et al., *Biochemical and structural insights into bacterial organelle form and biogenesis*. Journal of biological chemistry, 2008. **283**(21): p. 14366-14375.
75. Slininger Lee, M.F., C.M. Jakobson, and D. Tullman-Ercek, *Evidence for improved encapsulated pathway behavior in a bacterial microcompartment through shell protein engineering*. ACS synthetic biology, 2017. **6**(10): p. 1880-1891.
76. Wagner, H.J., et al., *Engineering bacterial microcompartments with heterologous enzyme cargos*. Engineering in Life Sciences, 2017. **17**(1): p. 36-46.
77. Liang, M., et al., *Bacterial microcompartment-directed polyphosphate kinase promotes stable polyphosphate accumulation in E. coli*. Biotechnology journal, 2017. **12**(3): p. 1600415.
78. Lassila, J.K., et al., *Assembly of robust bacterial microcompartment shells using building blocks from an organelle of unknown function*. Journal of Molecular Biology, 2014. **426**(11): p. 2217-2228.
79. Jakobson, C.M., M.F. Slininger Lee, and D. Tullman-Ercek, *De novo design of signal sequences to localize cargo to the 1, 2-propanediol utilization microcompartment*. Protein Science, 2017. **26**(5): p. 1086-1092.
80. Fan, C. and T.A. Bobik, *The N-terminal region of the medium subunit (PduD) packages adenosylcobalamin-dependent diol dehydratase (PduCDE) into the Pdu microcompartment*. Journal of bacteriology, 2011. **193**(20): p. 5623-5628.
81. Liu, Y., et al., *The PduL phosphotransacylase is used to recycle coenzyme A within the Pdu microcompartment*. Journal of bacteriology, 2015. **197**(14): p. 2392-2399.
82. Quin, M.B., et al., *Encapsulation of multiple cargo proteins within recombinant Eut nanocompartments*. Applied microbiology and biotechnology, 2016. **100**(21): p. 9187-9200.
83. Aussignargues, C., et al., *Structure and function of a bacterial microcompartment shell protein engineered to bind a [4Fe-4S] cluster*. Journal of the American Chemical Society, 2016. **138**(16): p. 5262-5270.
84. Hagen, A.R., et al., *In vitro assembly of diverse bacterial microcompartment shell architectures*. Nano letters, 2018. **18**(11): p. 7030-7037.
85. Lee, M.J., et al., *Employing bacterial microcompartment technology to engineer a shell-free enzyme-aggregate for enhanced 1, 2-propanediol production in Escherichia coli*. Metabolic engineering, 2016. **36**: p. 48-56.
86. Parsons, J.B., et al., *Synthesis of empty bacterial microcompartments, directed organelle protein incorporation, and evidence of filament-associated organelle movement*. Molecular cell, 2010. **38**(2): p. 305-315.
87. Shen, Y., et al., *Applications and perspectives of nanomaterials in novel vaccine development*. MedChemComm, 2018. **9**(2): p. 226-238.
88. Steele, J.F., et al., *Synthetic plant virology for nanobiotechnology and nanomedicine*. Wiley Interdisciplinary Reviews: Nanomedicine and Nanobiotechnology, 2017. **9**(4): p. e1447.

89. Hagen, A., et al., *Programmed loading and rapid purification of engineered bacterial microcompartment shells*. Nature communications, 2018. **9**(1): p. 1-10.
90. Rorvik, L.M., *Listeria monocytogenes in the smoked salmon industry*. International Journal of Food Microbiology, 2000. **62**(3): p. 183-190.
91. Shi, Y.G., et al., *Pasteurizing Cold Smoked Salmon (Oncorhynchus nerka): Thermal Inactivation Kinetics of Listeria monocytogenes and Listeria innocua*. Journal of Aquatic Food Product Technology, 2015. **24**(7): p. 712-722.
92. Cheng, C., F. Arritt, and C. Stevenson, *Controlling Listeria monocytogenes in Cold Smoked Salmon with the Antimicrobial Peptide Salmine*. Journal of Food Science, 2015. **80**(6): p. M1314-M1318.
93. Beaufort, A., et al., *Prevalence and growth of Listeria monocytogenes in naturally contaminated cold-smoked salmon*. Letters in Applied Microbiology, 2007. **44**(4): p. 406-411.
94. Anast, J.M. and S. Schmitz-Esser, *The transcriptome of Listeria monocytogenes during co-cultivation with cheese rind bacteria suggests adaptation by induction of ethanolamine and 1, 2-propanediol catabolism pathway genes*. PloS one, 2020. **15**(7): p. e0233945.
95. Tirumalai, P.S., *Metabolic gene expression shift by Listeria monocytogenes in coculture biofilms*. Canadian journal of microbiology, 2015. **61**(5): p. 327-334.
96. Las Heras, V., et al., *Short-term consumption of a high-fat diet increases host susceptibility to Listeria monocytogenes infection*. Microbiome, 2019. **7**(1): p. 1-12.
97. Mellin, J., et al., *A riboswitch-regulated antisense RNA in Listeria monocytogenes*. Proceedings of the National Academy of Sciences, 2013. **110**(32): p. 13132-13137.
98. Lebreton, A. and P. Cossart, *RNA-and protein-mediated control of Listeria monocytogenes virulence gene expression*. RNA biology, 2017. **14**(5): p. 460-470.
99. Mellin, J., et al., *Sequestration of a two-component response regulator by a riboswitch-regulated noncoding RNA*. Science, 2014. **345**(6199): p. 940-943.
100. Toledo-Arana, A., et al., *The Listeria transcriptional landscape from saprophytism to virulence*. Nature, 2009. **459**(7249): p. 950-956.
101. Jiang, W., et al., *Cas9-Assisted Targeting of CHromosome segments CATCH enables one-step targeted cloning of large gene clusters*. Nature communications, 2015. **6**(1): p. 1-8.
102. Chaijarasphong, T., et al., *Programmed ribosomal frameshifting mediates expression of the  $\alpha$ -carboxysome*. Journal of molecular biology, 2016. **428**(1): p. 153-164.



# Appendix

---

**Summary**

**Acknowledgements**

**About the author**

**Affiliation of co-authors**

**List of publications**

**Overview of completed training activities**



## Summary

*Listeria monocytogenes* is a facultative anaerobe responsible for a severe infection called listeriosis, which primarily affects immunocompromised individuals. This foodborne pathogen can activate adaptive stress responses supporting its survival in a range of stress conditions encountered in food production and host environments. The capacity to utilize alternative substrates for growth is crucial for the survival of *L. monocytogenes* when other efficient nutrients such as glucose are unavailable. In recent years more and more evidence has been presented that so-called Bacterial Microcompartments (BMCs) play an essential role in the utilization of specific host-derived substrates by enteric pathogens that result from degradation of phospholipids and metabolism of mucus-derived saccharides, including ethanolamine and 1,2-propanediol. Notably, these compounds are also encountered in a wide range of food products, and could therefore also contribute to transmission of pathogens to the host. It has been suggested that BMCs also play a role in *L. monocytogenes* ecophysiology and pathogenicity, but experimental evidence supporting these claims are very scarce. More details are mentioned in **Chapter 1** general introduction. Therefore, this thesis aims to unveil the role of BMC-dependent 1,2-propanediol and ethanolamine utilization in *L. monocytogenes* growth performance in anaerobic conditions, and to obtain insight in possible impacts on stress response and virulence of this foodborne pathogen.

The utilization of 1,2-propanediol and corresponding BMC structures were examined in **Chapter 2**. In *L. monocytogenes*, we demonstrate efficient utilization of 1,2-propanediol with concomitant production of 1-propanol and propionate after 24 hours of anaerobic growth, while the utilization was significantly reduced in aerobic conditions. In line with this, expression of genes encoding predicted shell proteins and the signature enzyme propanediol dehydratase is upregulated more than 20-fold in cells anaerobically grown in *pdu*-induced versus *pdu* non-induced control conditions. Additional proteomics analysis confirmed the presence of BMC shell proteins and Pdu enzymes in cells that show active degradation of 1,2-propanediol. Furthermore, using transmission electron microscopy (TEM), BMC structures have been detected in these cells linking gene expression, protein composition and BMCs to activation of the *pdu* cluster in anaerobic growth of *L. monocytogenes*. Studies in defined minimal medium with 1,2-propanediol as an energy source showed a significant increase

in cell numbers, indicating that 1,2-propanediol metabolism and the predicted generation of ATP in the conversion of propionyl-phosphate to the end product propionate can support anaerobic growth of *L. monocytogenes*.

In **Chapter 3**, we extend this study to analyse anaerobic rhamnose metabolism and rhamnose-derived 1,2-propanediol utilization of *L. monocytogenes* and the role of BMCs in this process. We unveil that the vitamin B12-dependent activation of *pdu* stimulates metabolism and anaerobic growth of *L. monocytogenes* EGDe on rhamnose via 1,2-propanediol degradation into 1-propanol and propionate. TEM observation of *pdu*-induced cells shows that BMCs are formed and additional proteomics experiments confirm expression of *pdu* BMC shell proteins and enzymes. Furthermore, we discuss physiological effects and energy efficiency of *L. monocytogenes pdu* BMC-driven anaerobic rhamnose metabolism and impact on competitive fitness in environments such as the human intestine.

The utilization of ethanolamine, corresponding BMC structures and physiological functionality of *eut* were examined in **Chapter 4**. We demonstrate B12-induced activation of the *eut* operon in *L. monocytogenes* coupled to the utilization of ethanolamine thereby enabling growth. BMC-dependent ethanolamine metabolism is found to produce acetate and ethanol in a molar ratio of 2:1. Flux via the ATP generating acetate branch causes an apparent redox imbalance due to reduced regeneration of NAD<sup>+</sup> in the ethanol branch resulting in a surplus of NADH. The redox imbalance is hypothesized to be compensated by linking *eut* BMC to anaerobic flavin-based extracellular electron transfer (EET). Using *L. monocytogenes* wild type, a BMC mutant and an EET mutant, we could indeed demonstrate an interaction between BMC and EET which provide evidence for a role of Fe<sup>3+</sup> as an electron acceptor. Taken together, our results suggest an important role of BMC-dependent ethanolamine metabolism in *L. monocytogenes* anaerobic growth with a crucial role for the flavin-based EET system in redox balancing.

Regarding the potential effects of BMC-dependent metabolism on *L. monocytogenes* virulence, **Chapter 5** and **Chapter 6** examine in-vitro Caco-2 virulence ability of BMC-induced *L. monocytogenes* cells compared to BMC non-induced cells aligned with systematic proteomics analyses. In **Chapter 5**, we investigate the impact of B12 on aerobic and anaerobic growth of *L. monocytogenes* on rhamnose, and observed growth stimulation and *pdu* BMC activation only in anaerobically grown cells with B12 added to the medium.

Comparative Caco-2 virulence assays, showed that these *pdu* BMC induced cells had significantly higher translocation efficiency compared to aerobically grown cells (without and with added B12) and non-induced anaerobically grown cells, while adhesion and invasion capacity was similar for all cells. Comparative proteomics analysis showed specific and overlapping responses linked to metabolic shifts, activation of stress defense proteins and virulence factors in *L. monocytogenes*, uniquely upregulated in anaerobically rhamnose grown *pdu* BMC induced cells. In **Chapter 6**, we present evidence that metabolically primed *L. monocytogenes* with active *eut* and *pdu* BMCs, as confirmed by metabolic analysis, TEM and proteomics, show significantly enhanced translocation efficacy compared to non-induced cells in a trans-well assay using Caco-2 cells. Taken together, the presented results in chapter 5 and chapter 6, provide insights into potential impact of *eut* and (rhamnose) *pdu* BMC-dependent metabolism on *L. monocytogenes* competitive fitness and virulence.

In connection to our findings on *pdu* BMC in pathogenic *L. monocytogenes*, we screened whole genome sequences of beneficial bacteria including *Propionibacterium freudenreichii*, for presence of *pdu* genes, and following identification of these genes (distributed in two genetic loci), we decided to study the functionality of *pdu* BMC in this bacterium (**Chapter 7**). We provided evidence that *P. freudenreichii* DSM 20271 metabolizes 1,2-propanediol in anaerobic conditions to propionate and 1-propanol, which align with the formation of BMCs evidenced by proteomics and TEM. 1,2-Propanediol utilizing cells actively produced vitamin B12 in similar amounts as cells growing on L-lactate. The ability to metabolize 1,2-propanediol may have implications for human gut colonization and modulation, and can potentially aid in delivering propionate and vitamin B12 in situ.

The results of the experimental chapters (chapter 2-7) are further discussed in **Chapter 8** with the emphasis on roles of BMCs in *L. monocytogenes* growth in foods, *L. monocytogenes* interaction with the host and its bioengineering application. Insights obtained in this study, highlight the relevance of BMC in microbial ecology and performance in foods and during interactions with the host. There is still a lot to discover in diversity and functionality of BMCs, and further studies are required to define in more detail their roles in health and disease.

## Acknowledgements

When I look back my PhD journey in WUR, so many pictures flash on the screen on my memory. I see smiles, strength, encouragement, achievements as well as pains and failures. I am so lucky to have all of your supports to finalize my dissertation along these four years. Here I express my gratitude from the bottom of my heart.

Firstly I am profoundly grateful to my promoter Tjakko Abee. During my PhD journey here, I am impressed by your continued passion, great patience and immense knowledge, which are indispensable for the completion of my PhD research. Your valuable comment to examine the BMC-dependent metabolisms in the anaerobic environments is exactly the key to open this nice discovery. Your responsible guidance helped me in all the time of my PhD research and writing of this thesis. Thank you. Tjakko.

My sincere thanks also go to my promoter Eddy J. Smid. It is Eddy who replied my application to do a PhD research in WUR and then arranged the interview for me. I appreciate a lot for insightful comments and warm encouragement from Eddy. You encouraged me to explore some other beautiful things in life and keep a good balance of life and work, which will be a piece of lifelong advice to me. Thanks for sharing your insightful suggestions about career development.

I sincerely thank my co-promoter Richard A. Notebaart for the continuous support of my PhD study and related bioinformatic analysis, for your patience and expertise. I appreciate the challenging questions raised by you which inspire me to think beyond my PhD research. During the 4 years, our biweekly BMC meetings ensured our excellent discussions on my PhD research. Thanks for all your thoughtful suggestions and supports for this dissertation.

Besides my supervisors, I would like to thank the rest of my thesis committee: Prof. Dr H. Smidt from WUR; Prof. Dr C. Gahan from UCC, Ireland; Dr M. H. J Wells-Bennik, NIZO Food Research; Dr A. M. López Contreras from WUR.

I am also so lucky to have excellent technical supports from other research groups. My tremendous appreciations go to: Sjef in Biochemistry WUR for your excellent help of proteomics, Jan van Lent and Marcel G. in WEMC for your guidance and detailed instruction for my TEM experiments, Lucas M. W. in RIVM for assisting me perform the Caco-2 experiments, Samuel L. from Chicago and Varaang from UC Berkeley for your contribution to chapter 4. Although the BMC structure project

was not included in this thesis and may be challenging to finalize, I want to thank you for your efforts to setup the experiments: Daan and Adrie from Biochemistry WUR and Arjen from TU Delft.

To all my current and former colleagues in FHM, I am thankful for our coffee break, lab outing, summer BBQ, PhD weekend, PhD trip to China, Thursday running, discussion and your supports during my four years in the department. Thanks for creating a warm environment. Marcel Z for your excellent leadership of FHM and hosting summer BBQ. Gerda, Denja, Dennis, Heidy, Gamze, Wilma, Ingrid, Gerrieke, Martine, Mark, Marcel T, Judith, Anneloes, Jasper B., Oscar, James, Alberto G, Esther, Natalie B. To all my dear PhD colleagues, Jeroen, Natalia C., Yue, Frank, Claire, Evelien, Bernard, Angela, Diego (RIP, You are always in my heart), Anneloes, Maren, Jasper B, Pjotr, Alberto B, Rebecca, Linda, Xuchuan, Alexander D, Sylviani, Tamara, George, Domiziana, Alexandra, William, Lise.

Many thanks to all the MSc. Student who worked with me on the BMC research: Siming Li, James Jonathan, Zihao Wang, Reinder Droppers, Ritika Shanker. I am pleased to have the opportunity to supervise all of you. All of you are very enjoyable to work with. I learned a lot from your different personalities. Thanks for contributing experimental data to this dissertation and wish you all the best in the future.

A big hug to my paranympths Yue Liu and Alexander Dachev. Thanks for standing with me on the defense day. Yue, I appreciate a lot your listening to my complaint when I was down with the experiments. Your encouragement always make me calm down and think in a positive way. Alexander, you are my brother from Bulgaria. We had some many fun together, drinking, cooking, running and outings, which are unforgettable moments in my heart. Thanks for your great supports as well as our insightful discussions.

Furthermore, I will like to thanks all of my Chinese friends I met in Netherlands who make my study and life a wonderful time. Thanks for all the beautiful memories: Wenjie Xia (My DF), Bin Jiang, Xilong Zhou, Taojun Wang, Denke Hua, Yifan Zhu, Jie Lian, Chen Zhang, Xiulu Sun, Zhihong Lv, Yan Liu, Hui Cao, Zhe Cheng, Qinhui Xing, Na Wang, Yanjun Song, Shanshan Yang, Qiuhong Miao, Min Xu, Yidong Wang, Weizhao Sun, Caifang Wen, Wenyu Zhao, Ningjin Liu, Zhaojun Wang, Fahui Liu, Ya Gao, Sibao Wang, Xinyu Chang, Shuxuan Zhang, Zhi Lei, Fengyang Sui, Junfang Wang, Jialun Wu, Jin Li, Xiaofei Yu, Chunzhe Lu, Jiali Meng, Yijun Chen, Jilu Feng, Wei Yang, Sydney, Badr Roui, Karla, Fabian, Jimmy, Anurag

Pandey, Fausto A, Rense, Nicola C, Fanny Thien, Jac N. and Julianne L. Also thanks to my corridor mates and friends in Asserpark, Janella, Rosemarijn, Ivan, Pia, Olga, Luis, Livia, Jessica, Linda J, Chrisom, Mathieu, Dimitris Liolios (My Greek brother) and Alexander Dachev (My Bulgarian brother).

Last but most important, I would like to express my deepest gratitude to my beloved family for your endless love and supports. To my dad Shunhe and my mom Huiluan, thank you for encouraging me, supporting me and making me believed that I should never let difficulties hold me back from what I want to do. To my wife Zhou (舟妹), you're the love of my life and I can't imagine completing this thesis without you. Your unending love is my vision, my hope, my goal, and my soul. Thank you for being with me, my heart will always belong to you. No matter how many challenges come in my life, I will face them without difficulty because of unending supports from my beloved family. I love you. My family.

## About the author

**Name:** Zhe Zeng

**Date of birth:** 27 April 1991

**Place of birth:** Chaozhou, Guangdong Province, China

### Educational background:

**Wageningen University and Research**

(The Netherlands)  
Food Microbiology

Ph.D. 2017-2021

**Shanghai Institutes for Biological Sciences,  
Chinese Academy of Sciences** (China)

Industrial microbiology and biotechnology

MSc. 2014-2017

**Nanchang University** (China)

Bioengineering

BSc. 2010-2014

### Contact information:

[zengzhe2010@outlook.com](mailto:zengzhe2010@outlook.com)

## **Affiliation of co-authors**

**Alexander Dank, Siming Li, Eddy J. Smid, Richard A. Notebaart, Tjakko Abee**

Laboratory of Food Microbiology, Wageningen University & Research, The Netherlands

**Sjef Boeren**

Laboratory of biochemistry, Wageningen University & Research, The Netherlands

**Lucas M Wijnands**

Centre for Infectious Disease Control, National Institute for Public Health and the Environment (RIVM), Bilthoven, The Netherlands

**Varaang Bhandula**

Department of Molecular and Cell Biology, University of California, Berkeley, Berkeley, California, USA.

**Samuel H. Light**

Department of Microbiology, The University of Chicago, Chicago, Illinois, USA.

## List of publications

(This dissertation)

**Zeng, Z.**, Smid, E. J., Boeren, S., Notebaart, R. A., & Abee, T. (2019). Bacterial microcompartment-dependent 1, 2-propanediol utilization stimulates anaerobic growth of *Listeria monocytogenes* EGDe. *Frontiers in microbiology*, 10, 2660.

**Zeng Z**, Li S, Boeren S, Smid E. J., Notebaart R. A., Abee T. Anaerobic Growth of *Listeria monocytogenes* on Rhamnose Is Stimulated by Vitamin B12 and Bacterial Microcompartment-Dependent 1,2-Propanediol Utilization. *mSphere*. 2021 Jul 21:e0043421.

**Zeng, Z.**, Boeren, S., Bhandula, V., Light, S. H., Smid, E. J., Notebaart, R. A., & Abee, T. (2021). Bacterial microcompartments coupled with extracellular electron transfer drive the anaerobic utilization of ethanolamine in *Listeria monocytogenes*. *mSystems*, 6(2), e01349-20.

Dank, A.<sup>#</sup> (Co-first author), **Zeng, Z.**<sup>#</sup> (Co-first author), Boeren, S., Notebaart, R. A., Smid, E. J., & Abee, T. (2021). Bacterial microcompartment-dependent 1, 2-propanediol utilization of *Propionibacterium freudenreichii*. *Frontiers in microbiology*, 12.

**Zeng, Z.**, Wijnands, L. M, Boeren, S, Smid, E. J., Notebaart, R. A., & Abee, T. Impact of vitamin B12 on rhamnose metabolism, stress defense and in-vitro virulence of *Listeria monocytogenes* (Preprint in bioRxiv: doi: <https://doi.org/10.1101/2021.08.26.457850>; Under review)

**Zeng, Z.**, Wijnands, L. M, Boeren, S, Smid, E. J., Notebaart, R. A., & Abee, T. Impact of bacterial microcompartment-dependent ethanolamine and propanediol metabolism on *Listeria monocytogenes* interactions with Caco-2 cells (Preprint in bioRxiv: doi: <https://doi.org/10.1101/2021.08.26.457845>, Under review)

**Zeng, Z.**<sup>#</sup>, Dank, A<sup>#</sup>, Smid, E. J., Notebaart, R. A., & Abee, T. Bacterial microcompartments in food-related microbes, *Current Opinion in Food Science* (2021, Accepted for publication)

# Overview of completed training activities

## A. Discipline specific activities

<i>Name of the course/meeting</i>	<i>Organizers</i>	<i>City</i>	<i>Year</i>
Advanced Course Bioprocess Design	BioTech Delft	Wageningen	2017
Microscopy and Spectroscopy in Food and Plant Sciences	VLAG & EPS	Wageningen	2018
Pujiang Innovation Forum *	CAS	Shanghai, CN	2019
20th ISOPOL *	ISOPOL	Toronto, CA	2019
Electron Microscopy course	WEMC	Wageningen	2019
Constraint-based modelling *	BioSB	Leiden	2019
In situ Structural Biology	EMBO	Online	2020
5th Food Science Frontiers Research Forum *	ZJSU	Online	2020
The 1st International BioDesign Research Conference	BioDesign Research	Online	2020
LAS-ICMSF	ICMSF	Online	2021
Annual Conference Online 2021 *	Microbiology Society	Online	2021
43rd Symposium on Biomaterials, Fuels and Chemicals	SBFC	Online	2021
World Microbe Forum 2021 *	AMS & FEMS	Online	2021

## B. General courses

VLAG PhD week	VLAG	Baarlo	2017
Scientific Writing	WGS	Wageningen	2018
PhD Workshop Carousel	WGS	Wageningen	2018
Speaking and Pronunciation 1&2	WUR	Wageningen	2019
Reviewing a Scientific Manuscript	WGS	Wageningen	2019
Scientific Publishing	WGS	Wageningen	2020
How to present online	WUR	Online	2021
Writing Grant Proposals	WGS	Online	2021
Career Perspectives	WGS	Online	2021

## C. Other activities

Preparation of research proposal	FHM	Wageningen	2017
PhD study tour to China **	FHM	China	2019
Annual Fall KNVM Microbial Ecology Symposium	KNVM & NIOO	Wageningen	2019
Food Microbiology department seminars **	FHM	Wageningen	2017-2021
22nd EMBL PhD Symposium **	EMBL	Online	2020
mSystems Thinking Series Microbiology	mSystems	Online	2021
VLAG course Ecophysiology of food-associated micro-organisms (lecturer) **	VLAG	Wageningen	2021

\* Poster Presentation; \*\* Oral Presentation



The research described in this thesis was performed at the Laboratory of Food Microbiology, Wageningen University & Research. And Zhe Zeng was sponsored by a PhD fellowship from the China Scholarship Council (No. 201704910823).

Financial support from Wageningen University for printing this thesis is gratefully acknowledged.

Cover design and thesis layout by Zhe Zeng.

Printed by Proefschrifmaken.



